NON-INVASIVE OPTICAL MONITORING OF BRAIN HAEMODYNAMICS AND METABOLISM FOLLOWING ACUTE BRAIN INJURY

ARNAB GHOSH
BSc(Hons) MB,ChB MRCS

Thesis for award of degree of PhD

Department of Brain Repair & Rehabilitation
Institute of Neurology
UCL

March 2017

DECLARATION

I, Arnab Ghosh, confirm that the work presented in this thesis is my own. Where information has been derived from other sources, I confirm that this has been indicated in the thesis.

London, March 2017

Arnab Ghosh

2difference in arterial:venous oxygen concentration

ABSTRACT

Following acute brain injury (ABI), cellular hypoxia-ischaemia (CH-I) is central to the pathophysiological cascades that lead to death and neurological disability. Thus, a key tenet of neurocritical care is the avoidance of CH-I, and a key prerequisite to doing so is the availability of a bedside clinical monitor that can identify CH-I as it occurs.

This thesis describes normal cerebral physiology, how this is deranged and clinically manipulated following ABI, and the use of near infrared spectroscopy (NIRS), a non-invasive optical technique, to monitor for CH-I in a variety of clinical contexts. I then present my work investigating the use of NIRS, with an emphasis on the measurement of the oxidation state of cytochrome *c* oxidase (CCO), in healthy volunteers who are subjected to a variety of challenges designed to manipulate cerebral oxygen delivery with both isovolaemic and hyper/hypovolaemic challenges.

Finally, I describe experiments in a cohort of a patients who have suffered from ABI, manipulating cerebral oxygen delivery by means of normobaric hyperoxia. The results suggest that the measurement of CCO with NIRS in patients with ABI provides a useful adjunct to established monitors of cerebral haemodynamics and metabolism; an in-depth discussion of the observed changes in different haemodynamic and metabolic parameters, and their relevance to normal physiology and pathophysiology of ABI is carried out.

PUBLICATIONS

The following publications have arisen from this work:

[1] Tachtsidis, I, Leung, T, Elwell, CE, Ghosh, A, Smith, M & Cooper, CE. Multi-Wavelength, Depth Resolved, Scattering and Pathlength Corrected in vivo Near-Infrared Spectroscopy of Brain Tissue. *Biomedical Optics (BIOMED), OSA Technical Digest*, p. BTuB, 2010.

[2] Tachtsidis, I, Tisdall, MM, Pritchard, C, Leung, TS, Ghosh, A, Elwell, CE & Smith, M. Analysis of the changes in the oxidation of brain tissue cytochrome-c-oxidase in traumatic brain injury patients during hypercapnoea: a broadband NIRS study. *Advances in Experimental Medicine and Biology*, 701:9–14, 2011.

[3] Ghosh, A, Tachtsidis, I, Kolyva, C, Cooper, CE, Smith, M & Elwell, CE. Use of a hybrid optical spectrometer for the measurement of changes in oxidized cytochrome c oxidase concentration and tissue scattering during functional activation. *Advances in Experimental Medicine and Biology*, 737:119–124, 2012.

[4] Kolyva, C, Tachtsidis, I, Ghosh, A, Moroz, T, Cooper, CE, Smith, M & Elwell, CE. Systematic investigation of changes in oxidized cerebral cytochrome c oxidase concentration during frontal lobe activation in healthy adults. *Biomedical optics express*, 3(10):2550–2566, 2012.

[5] Ghosh, A, Elwell, C & Smith, M. Cerebral near-infrared spectroscopy in adults: a work in progress. *Anesthesia & Analgesia*, 115(6):1373–1383, 2012.

[6] Kolyva, C, Ghosh, A, Tachtsidis, I, Highton, D, Smith, M & Elwell, CE. Dependence on NIRS Source-Detector Spacing of Cytochrome C Oxidase Response to Hpoxia and Hypercapnia in the Adult Brain. *Advances in Experimental Medicine and Biology*, 789(353-9), 2013.

[7] Ghosh, A, Tachtsidis, I, Kolyva, C, Highton, D, Elwell, C & Smith, M. Normobaric hyperoxia does not change optical scattering or pathlength but does increase oxidised cytochrome C oxidase concentration in patients with brain injury. *Advances in Experimental Medicine and Biology*, 765:67–72, 2013.

[8] Ghosh, A, Kolyva, C, Highton, D, Tachtsidis, I, Elwell, CE & Smith, M. Reduction of Cytochrome c Oxidase During Vasovagal Hypoxia-Ischaemia in Human Adult Brain: a Case Study. *Advances in Experimental Medicine and Biology*, 789:21–27, 2013.

[9] Kolyva, C, Ghosh, A, Tachtsidis, I, Highton, D, Cooper, CE, Smith, M & Elwell, CE. Cytochrome c oxidase response to changes in cerebral oxygen delivery in the adult brain shows higher brain-specificity than haemoglobin. *NeuroImage*, 85(1):234–244, 2014.

[10] Robertson, JL, Ghosh, A, Correia, T, Highton, D, Smith, M, Elwell, CE & Leung, TS. Effect of blood in the cerebrospinal fluid on the accuracy of cerebral oxygenation measured by near infrared spectroscopy. *Advances in Experimental Medicine and Biology*, 812:233–240, 2014.

[11] Highton, D, Ghosh, A, Tachtsidis, I, Panovska-Griffiths, J, Elwell, CE & Smith, M. Monitoring Cerebral Autoregulation After Brain Injury: Multimodal Assessment of Cerebral Slow-Wave Oscillations Using Near-Infrared Spectroscopy. *Anesthesia & Analgesia*, 121(1):198–205, 2015.

[12] Ghosh, A, Highton, D, Kolyva, C, Tachtsidis, I, Elwell, CE & Smith, M. Hyperoxia results in increased aerobic metabolism following acute brain injury. *Journal of cerebral blood flow and metabolism*, p. 271678X16679171, 2016.

"Genius depends ... on rapid metabolism, on the possibility of drawing again and again on great, even tremendous quantities of strength"

— Friedrich Nietsche

ACKNOWLEDGMENTS

It is no exaggeration to say that undertaking the work described in this thesis and preparing the thesis itself has been the greatest challenge I have ever faced. Fortunately, it is not a challenge that I have faced alone; I am deeply indebted to many people who have supported me in completing this work.

Martin Smith, my primary supervisor, has been unfailingly encouraging, whilst also insisting on a degree of rigour that has improved this work to no end, for which I am very grateful. David Highton, with whom I have shared a lab, has been a constant aid in both conceiving, performing and understanding the experiments that are described here.

In the Department of Medical Physics and Bioengineering, Clare Elwell, my secondary supervisor, has showed great patience in tutoring me in the subject of medical optics, and has shown an infectious enthusiasm in taking this work in to the clinical setting. Her colleague Ilias Tachtsidis is the creator of the primary apparatus used for the experiments in this thesis, and is responsible for training me in the operation and maintenance of optical spectrometers to the extent that he has kindly described me to be as capable as any engineering doctoral candidate! Christina Kolyva has undertaken an enormous amount of data analysis, in particular on the data described in Chapter 4; without her unfailingly meticulous work in this, as well as revising the many papers we have co-authored, I could easily have been overwhelmed.

I am also indebted to the many nursing and medical staff of the Departments of Neurosurgery, Neurocritical Care and Neuroanaesthesia in the National Hospital for Neurology and Neurosurgery at Queen Square. There is no doubt that my experiments were an imposition on their time and space, and I am grateful for their accommodations. I am also grateful to the very many of them who volunteered (often after busy nightshifts) to undergo the experiments described in Chapter 4.

My girlfriend Tessa has been a constant source of (occasionally badgering) encouragement, and for her support and understanding in allowing me to complete this work, I owe her much.

Finally, I am grateful to the families of the patients who provided assent for their relatives to be included in the experiment described in Chapter 5. In a time of great fear and apprehension, they have shown great generosity in allowing their loved ones to be included in these studies.

And to the Pea.

CONTENTS

LIST OF FIGURES

LIST OF TABLES

μ_a	optical absorption coefficient
μ_s	optical scattering coefficient
μ_s'	reduced optical scattering coefficient
A:V ratio	arterial:venous blood volume ratio
ABG	arterial blood gas
ABI	acute brain injury
ABP	arterial blood pressure
AC	average wave amplitude
ac-CoA	acetyl coenzyme A
ACA	anterior cerebral artery
AComm	anterior communicating artery
ADC	analogue-to-digital convertor
ADP	adenosine 5′-diphosphate
AMPA	α-amino-3-hydroxy-5-methyl-4-isoxazolepropionic acid
ANLSH	astrocyte–neurone lactate shuttle hypothesis
ANOVA	analysis of variance
aSAH	aneurysmal subarachnoid haemorrhage
ATP	adenosine 5′-triphosphate
$AVDO_2$	arterio-venous oxygen concentration difference
BBB	blood–brain barrier
BBS	broadband spectroscopy
BLL	Beer-Lambert Law
BP	blood pressure
BPM	beats per minute
BTH	brain tissue hypoxia
CA	cerebrovascular autoregulation
Ca^{2+}	calcium ions

CBF	cerebral blood flow
CBV	cerebral blood volume
CCD	charge-coupled device
CCO	cytochrome c oxidase
cDO_2	cerebral oxygen delivery
CEA	carotid endarterectomy
CH-I	cellular hypoxia-ischaemia
CMD	cerebral microdialysis
CMRO	
CNS	central nervous system
CO_2	carbon dioxide
CoA	coenzyme A
COS	CCO oxygen saturation
CPB	cardiopulmonary bypass
CPP	cerebral perfusion pressure
CSF	cerebrospinal fluid
CT	computed tomography
Cu_A	copper A
Cu_B	copper B
DAI	diffuse axonal injury
DC	average light intensity
DCI	delayed cerebral ischaemia
DNA	deoxyribonucleic acid
DND	delayed neurological deficit
DO_2	oxygen delivery
DPF	differential pathlength factor
DPG	2,3-diphosphoglycerate
DSA	digital subtraction angiography
EAA	excitatory amino acid
$ecDO_2$	estimated cerebral oxygen delivery
ECF	extracellular fluid
ETC	electron transport chain
$etCO_2$	end tidal CO_2

etO_2	end tidal O_2
$FADH_2$	flavin adenine dinucleotide hydride
FiO_2	inspired fraction of oxygen
GCS	Glasgow Coma Score
GLUT	glucose transporter
GOS	Glasgow Outcome Score
GTP	guanosine triphosphate
[HbDiff]	haemoglobin difference concentration
$[HbO_2]$	oxyhaemoglobin concentration
[HbT]	total haemoglobin concentration
HCO_3^-	bicarbonate ion
[HHb]	deoxyhaemoglobin concentration
HIF-1α	hypoxia-inducible factor 1α
HR	heart rate
ICH	intracerebral haemorrhage
ICP	intracranial pressure
IQR	interquartile range
K_m	Michaelis-Menton constant
LDH	lactate dehydrogenase
LED	light-emitting diode
LPR	lactate:pyruvate ratio
LRT	Likelihood Ratio Test
MAP	mean arterial pressure
mBLL	modified Beer-Lambert Law
MCA	middle cerebral artery
MCT-1	monocarboxylate transporter 1
MD	microdialysis
MDBBS	multidistance broadband spectrometer
MDFD	multidistance frequency domain spectrometer
$Na^{+\ddot{}}/K^{+\ddot{}}Na^+/K^+$ ATPase	sodium potassium ATPase pump
NAD^+	nicotinamide adenine dinucleotide
NADH	nicotinamide adenine dinucleotide hydride
NBH	normobaric hyperoxia

NCCU	neurocritical care unit
NIR	near infrared
NIRS	near infrared spectroscopy
NMDA	N-methyl-D-aspartate
NO·	nitric oxide
NO_2^-	nitrite
O_2	oxygen
O_2·	superoxide
OEF	oxygen extraction fraction
oxCCO	oxidised-reduced cytochrome *c* oxidase
[oxCCO]	concentration of oxidised-reduced cytochrome *c* oxidase
P_aCO_2	arterial partial pressure of carbon dioxide
P_aO_2	arterial partial pressure of oxygen
$P_{br}O_2$	brain partial pressure of oxygen
PCA	posterior cerebral artery
PCO_2	partial pressure of carbon dioxide
PComm	posterior communicating artery
PDHC	pyruvate dehydrogenase complex
PET	positron emission tomography
PFK-1	phosphofructokinase-1
pHOS	hybrid optical spectrometer
pO_2	partial pressure of oxygen
PRx	pressure reactivity index
RCT	randomised, controlled trial
RLRT	restricted likelihood ratio test
ROS	reactive oxygen species
rsO_2	regional oxygen saturation
SAH	subarachnoid haemorrhage
SEM	standard error of mean
$SjvO_2$	jugular venous haemoglobin saturation
SPECT	single photon emission computed tomography
SpO_2	pulse haemoglobin oxygen saturation

SRS	spatially-resolved spectroscopy
sTBI	severe traumatic brain injury
TBI	traumatic brain injury
TCA	tricarboxylic acid
TCD	transcranial Doppler
THI	total haemoglobin index
THx	total haemoglobin reactivity index
TOI	tissue oxygenation index
TOS	tissue oxygen saturation
TPSF	temporal point spread function
TRS	time-resolved spectroscopy
UCLn	University College London *n*-wavelength
UV	ultraviolet
V_{MCA}	middle cerebral artery flow velocity

Part I

BACKGROUND AND PRINCIPLES

1

REVIEW OF CEREBRAL PHYSIOLOGY

This thesis concerns the monitoring of brain haemodynamic & metabolic function and dysfunction – during a number of functional and physiological challenges — in healthy volunteers and ultimately in a cohort of patients who have suffered from acute brain injury (ABI). In order to understand the nature of brain haemodynamic and metabolic dysfunction following ABI and interpret the data collected during experiments in healthy volunteers and brain-injured patients, an understanding of the normal mechanisms of the supply and utilisation of substrate to yield the primary product of adenosine 5′-triphosphate (ATP), as well as additional by-products of cellular metabolism, is crucial. In this chapter, I describe these mechanisms that are central to brain tissue survival and function.

1.1 GROSS ANATOMICAL AND PHYSIOLOGICAL PERSPECTIVE

The adult human brain is a 1.5 kilogram organ contained within the cranial vault comprising $2x10^{10}$ neurons and $4x10^{10}$ glial cells arranged in a highly organised fashion, with an estimated $15x10^{10}$ synapses formed between neurons [1, 2]. The human central nervous system (CNS) is responsible for the generation of signals that lead to locomotor activity in response to stimuli in the surrounding environment – it is the anatomical and physiological substrate that co-ordinates behaviour. The evolutionary advantage conferred on humans through the development of this highly specialised and intricate organ – and thus complex behaviour – is undeniable. Yet this ability comes at a cost: neural tissue is exquisitely fragile as a consequence of the extraordinary amount of energy that is required to sustain it.

1.1.1 *Electrochemical basis of neuronal function – the resting and action potentials*

The resting potential, an electrostatic potential across cell membranes that is maintained through the action of an ATP-consuming membrane pump, the sodium potassium ATPase pump (Na^+/K^+ ATPase), exists across the membranes of mammalian cells. It is the result from the differences in ion concentration across the membrane, generated by the Na^+/K^+ ATPase. At rest, the isostatic balance between electrostatic force and ion diffusion determines the flow of ions across leakage channels in the neuronal membrane, thus generating the potential [3].

The resting potential is exploited in a number of ways; one of its significant roles is as a useable store of energy, which membrane-bound pumps can utilise to perform secondary active transport of molecules across membranes. In neuronal cells, the resting potential gives rise to the possibility of communication – through the action potential and the excitatory and inhibitory postsynaptic potentials. However, this carries a high metabolic price: at least half the oxygen consumed in the brain is utilised in maintaining the resting potential [4].

1.1.2 *Biochemical basis of energy generation*

The survival and function of neural tissue is thus predicated on the ability of cells to generate energy. For the purposes of this thesis, the term *cellular energy generation* is taken to be synonymous with *ATP synthesis*. Each endothermic metabolic process – that is, each that must be driven 'thermodynamically uphill' – must be coupled to an exothermic process, or an 'engine'. ATP acts as that driver, and the hydrolysis one inorganic phosphate ion, given by the equation

$$\mathrm{ATP} + \mathrm{H_2O} \longrightarrow \mathrm{ADP} + \mathrm{P_i} (\Delta G^{0\prime} = -30.5 \mathrm{kJ.mol}^{-1}),$$

or two phosphate ions, given by the equation

$$\mathrm{ATP} + 2\mathrm{H_2O} \longrightarrow \mathrm{AMP} + 2\mathrm{P_i} (\Delta G^{0\prime} = -45.0 \mathrm{kJ.mol}^{-1}). \tag{1.1}$$

ATP can be synthesised from the oxidation of carbohydrate via a combination of glycolysis followed by either anaerobic respiration or aerobic respiration. ATP synthesis is also possible by the beta-oxidation of fatty acids. ATP synthesis by glycolysis and aerobic respiration is summarised by the equation

$$\mathrm{C_6H_{12}O_6} + 6\,\mathrm{O_2} + 38\,\mathrm{ADP} + 38\,\mathrm{P_i} \longrightarrow 6\,\mathrm{CO_2} + 6\,\mathrm{H_2O} + 38\,\mathrm{ATP}; \tag{1.2}$$

anaerobic respiration can be summarised by the equation

$$\mathrm{C_6H_{12}O_6} + 6\,\mathrm{O_2} + 2\,\mathrm{ADP} + 2\,\mathrm{P_i} \longrightarrow 2\,\mathrm{C_2H_5COOH} + 2\,\mathrm{ATP}. \tag{1.3}$$

The process of aerobic respiration is summarised in Figure 1.5.

Whilst these processes are described in detail below, a gross comparison highlights points of physiological and clinical importance:

- glucose is a primary substrate for both anaerobic and aerobic respiration;
- aerobic respiration requires the presence of oxygen to act as an electron acceptor;
- the complete oxidation of glucose during aerobic respiration yields carbon dioxide (CO_2) as a waste product;

- the incomplete oxidation of glucose during anaerobic respiration yields lactate;
- the amount of ATP generated by the oxidation of glucose is an order of magnitude higher when performed by aerobic rather than anaerobic respiration.

The important stages in cellular energy generation – supply of metabolic substrate to neural tissue, glycolysis, Kreb's cycle, fermentation, and mitochondrial oxidative phosphorylation – are described below.

1.2 SUPPLY OF METABOLIC SUBSTRATE TO TISSUE

Oxygen and glucose are the key substrates required for cellular energy generation. The brain can use alternative fuels – namely ketone bodies and lactate, the latter of which is discussed below – and does so in disease states, but glucose remains the primary substrate for oxidation for the purposes of brain cellular energy generation [5].

Glucose supply is achieved by means of nutrition (typically 350g/day) with further stores of 400g in the liver as glycogen. Plasma glucose levels are subject to homeostatic control primarily via the pancreatic hormones insulin and glucagon, which maintain plasma glucose levels in the range 4.0–6.0 mM.

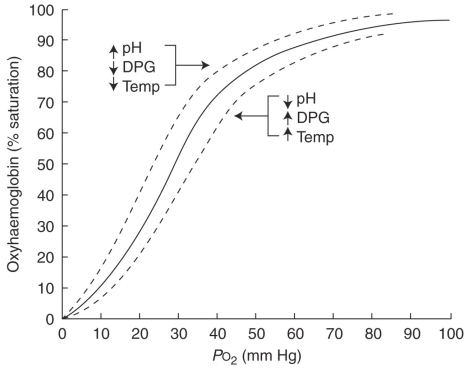

Figure 1.1 – The haemoglobin–oxygen dissociation curve. From [6].

The presence of oxygen (O_2) is prerequisite to aerobic respiration. Ambient air contains 21% O_2 by volume, which equates to a arterial partial pressure of oxygen (P_aO_2) of 19.8 kPa. Oxygen diffuses from alveolar air to pulmonary blood, is pumped by the heart to the cerebral circulation, and then diffuses freely across the blood–brain barrier (BBB) to neural cells and ultimately to mitochondria. Diffusion gradients and barriers are present at each stage.

At the pulmonary level, oxygen diffuses across the alveolar membrane into pulmonary blood, where a small proportion, corresponding to roughly 1.5 percent of the total oxygen carrying capacity of blood, is transported as simply dissolved oxygen.

The remaining 98.5% of oxygen is transported by reversible binding to haemoglobin, a tetrameric erythrocytic protein that has a characteristic sigmoidal saturation curve (shown in Figure 1.1), with a high affinity for oxygen at lower partial pressures, and a lower affinity at higher concentrations. The affinity of haemoglobin for oxygen, is also influenced by other factors such as tissue/capillary pH, arterial partial pressure of carbon dioxide (P_aCO_2), temperature and allosteric binding by co-factors such as 2,3-diphosphoglycerate (DPG) [6,7]. These factors, combined, result in haemoglobin being an effective transporter of oxygen from the lungs (neutral pH, low P_aCO_2, high P_aO_2) to the tissues, particularly cerebral tissue (where the converse conditions exist).

1.2.1 *Cerebrovascular supply*

GROSS ANATOMY After being pumped through the left side of the heart and the extracranial circulation, oxygenated blood is transported through the cerebrovascular system to neural tissue. The arterial system, depicted in Figure 1.2, is grossly divided in to anterior and posterior circulations based on the extracranial origins of these systems: the anterior circulation is derived from the bifurcation of the internal carotid arteries, and the posterior circulation derived from the vertebrobasilar system, which refers to the two vertebral arteries and the basilar artery formed where they fuse.

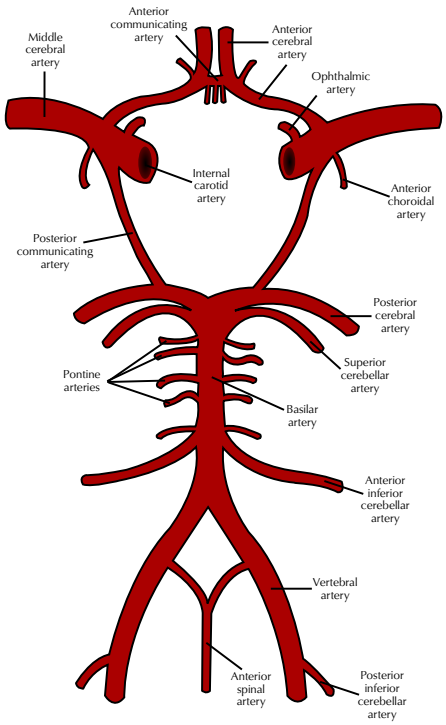

Figure 1.2 – The circle of Willis. From [8].

The anterior and posterior circulations meet in an anastamotic circle, the circle of Willis, in the midline of the skull base. Though incomplete in up to 40% of individuals, this structure provides a degree of vascular redundancy, and acts as a partial guard against ischaemia resulting from the stenosis or occlusion of a parent vessel. The anterior circulation comprises the two anterior cerebral arteries (ACAs), which are joined in the midline by the anterior communicating artery (AComm), the middle cerebral arteries (MCAs). Each MCA is joined by a posterior communicating artery (PComm) to the ipsilateral posterior cerebral artery (PCA). The PCAs are the major arteries of the posterior circulation, and are formed by the bifurcation of the basilar artery at its terminal tip. In both anterior and posterior circulations, arteries display a variable pattern of arborisation, with cortical arterioles originating along the length of the vessels. Deeper structures in the midbrain – such as the basal ganglia and thalamus – are supplied by small lenticulostriate arteries that originate from the ACA and MCA. The cortical arterial networks terminate in anastamotic plexuses – with the extracranial circulation in the leptomeningial plexus, and in the 'watershed areas' at the borders between the territories served by the anterior, middle and posterior cerebral arteries [9].

The flow of blood through the cerebral vasculature is subject to tight, active regulation. The two most important components of this regulation are neurovascular coupling and cerebrovascular autoregulation (CA).

CEREBRAL AUTOREGULATION CA describes the ability of the brain to maintain cerebral blood flow (CBF) within a relatively stable range across a wide range of mean arterial pressures. The current concept of CA was formulated by Lassen, who

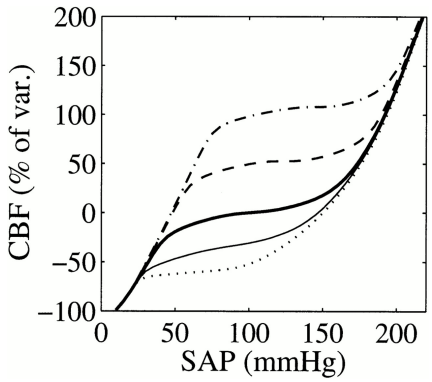

Figure 1.3 – Lassen curves depicting the relationship between CBF and arterial blood pressure at different levels of P_aCO_2. SAP – systolic arterial pressure. From [10].

first plotted CBF against arterial blood pressure (ABP), giving the classic autoregulatory curve that bears his name, depicted in Figure 1.3 [11]. Ironically, the phenomena underlying this pressure-flow relationship – where pial blood vessels dilate in response

to hypotension and constrict in response to hypertension – were directly observed via a cranial window by Fog in the 1930s [12,13], but elude simple measurement in the adult human in the clinical setting. A variety of methods are currently used to measure CBF and characterise CA, including transcranial Doppler (TCD) ultrasonography and near infrared spectroscopy (NIRS). CA is disturbed in a variety of diseases, both neurological and systemic (discussed in Chapter 2.2.2) and there is burgeoning interest in the potential to use knowledge of CA to guide treatment following ABI [14].

NEUROVASCULAR COUPLING Whilst the process of CA acts to maintain constant CBF in the face of potential *extracranial* variability (in the form of variations in ABP), there also a need to vary CBF in order to meet variations in metabolic demand. Neuronal activation induces an increase in metabolic demand, as the resting membrane potential is re-established after the depolarising action potentials and post-synaptic potentials. Neurovascular coupling is the phenomenon by which brain activation is accompanied by a *functional hyperaemia*, thus ensuring that the increase in metabolic demand that is induced by activation is met by increased CBF [15].

Mediators of neurovascular coupling include vasoactive ions, substrates and products of metabolism and vasoactive neurotransmitters. Some of these factors (for example, blood and interstitial K^+ concentrations or glutamate concentrations) are subject to intense homeostatic control and show transient changes that correlate closely with neuronal activation. Other factors, such as interstitial CO_2 levels, vary not only with regional activation metabolic activity, but also as a result of extra- and intra-cranial factors. Thus, changes in extracellular CO_2 concentrations can act to modulate regional CBF in response to functional activation, but can also modulate regional or global CBF as a result of systemic changes in P_aCO_2. There is thus a complex and non-linear interplay between neurovascular coupling and cerebral autoregulation, one aspect of which is illustrated in Figure 1.3. Similarly, hypoxia reliably produces cerebral vasodilatation, and this effect is thought to be primarily mediated by nitric oxide (NO·) [16].

BLOOD–BRAIN BARRIER The final stage of delivery of metabolic substrate to tissue is traversal of the BBB. Rather than being a discernible physical entity, the BBB is a functional barrier that acts to facilitate the influx and efflux of metabolic substrates and products. It regulates ion balance and protects from potentially harmful circulating molecules [17].

The physical basis of the BBB is a complex of cells, termed the neurovascular unit, comprising endothelial cells, astrocytes, pericytes, neurons, and extracellular matrix around the vessels; the neurovascular unit is also responsible for mediating some of the CBF regulation described above, such as neurovascular coupling, on the microvascular level. Segregation of blood from brain extracellular fluid (ECF) is achieved through the presence of adherens junctions and tight junctions. The former refer to the

structures between adjacent endothelial cells within the capillary bed, across which scant diffusion/transport of substrate occurs. Tight junctions are formed at the point where circumferential endothelial cells 'complete the circle' and an endothelial cell's membrane apposes itself; this is depicted schematically in figure 1.4a. These tight junctions are made impermeable to polar molecules by the presence of proteins such as occludin [17].

Traversal of the BBB can occur by a number of mechanisms, summarised in figure 1.4b. Whilst the vasoactive product of metabolism CO_2, being lipophilic, can diffuse freely across the BBB, other small charged molecules – including glucose, lactate, pyruvate, H^+ ions and bicarbonate ion (HCO_3^-), must undergo active or facilitated transport through endothelial cells and astrocytes in order to reach the brain ECF. Glucose enters brain ECF through facilitated diffusion through glucose transporter (GLUT)-1 channels, and lactate-pyruvate can undergo bidirectional flux through the monocarboxylate transporter 1 (MCT-1) channel [18].

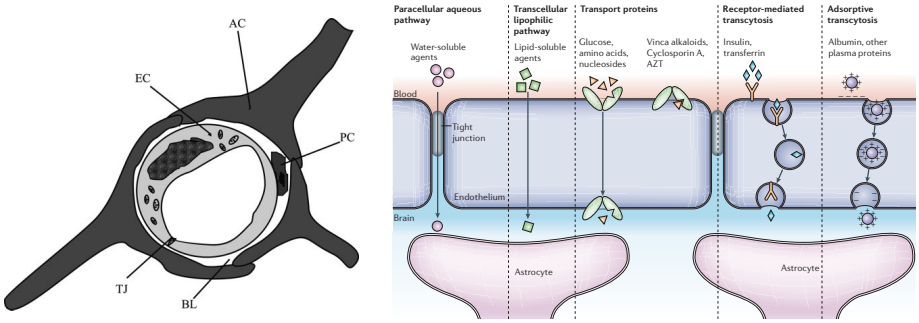

(a) Schematic depiction of the BBB. From [17].

(b) Transport across the BBB. From [19].

Figure 1.4 – Schematic depiction of blood–brain barfrier structure and transport routes across it. AC – astrocyte; BL – basal lamina; EC – endothelial cell; PC – pericyte; TJ – tight junction.

1.3 CELLULAR RESPIRATION

Cellular respiration is the process by which cellular energy generation (considered, for the purposes of this thesis, to be synonymous with ATP synthesis) occurs. The preceding section describes the delivery of metabolic substrate to brain parenchymal ECF. Here, we consider the steps in neuronal and glial cellular energy generation, starting from substrate that situated in the ECF.

After the facilitated transport of glucose (via GLUT-1 to astrocytic cytosol and GLUT-3 in to neuronal cytosol), the process of cellular respiration takes place in two stages. The first stage is glycolysis, which takes place in the cytosol, and yields the intermediate metabolite *pyruvate*. The second stage of cellular respiration depends on the presence of oxygen – i. e. whether metabolism is aerobic or anaerobic. In the presence of

oxygen, aerobic respiration occurs within the mitochondria. This process, termed *oxidative phosphorylation*, depends on the generation of a proton gradient across the inner membrane of the mitochondrion, which is then harnessed to phosphorylate adenosine 5′-diphosphate (ADP), in the reverse of the reaction shown in Equation 1.1. In the absence of oxygen, pyruvate undergoes anaerobic fermentation to yield the monocarboxyl acid lactate [3].

1.3.1 *Glycolysis*

The process of glycolysis, summarised in Equation 1.4, takes place in multiple stages and acts to convert a single glucose molecule in to two pyruvate molecules, also resulting

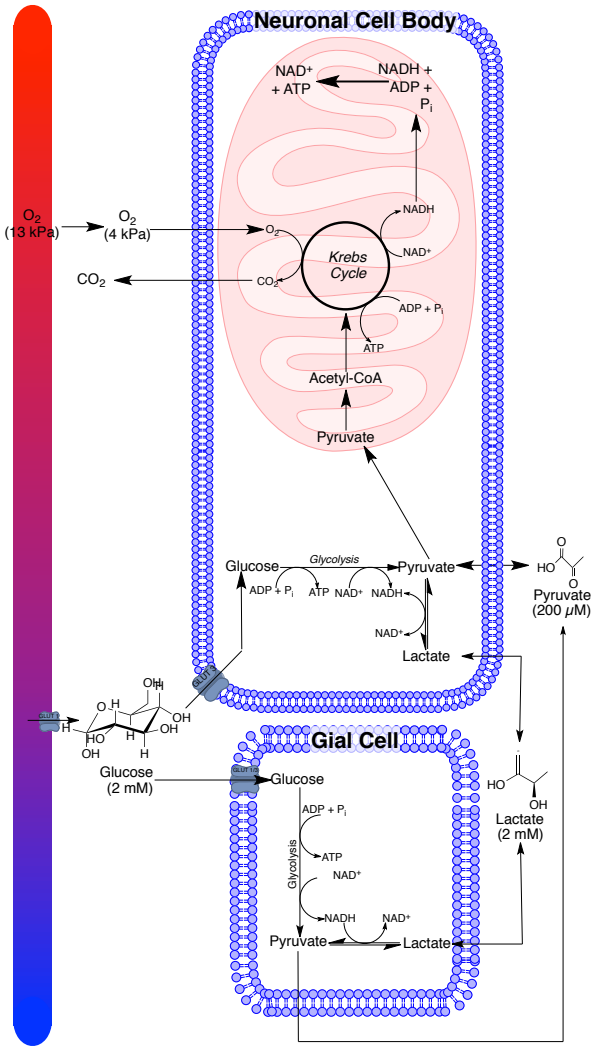

Figure 1.5 – Schematic summary of cerebral aerobic respiration. Adapted from [20].

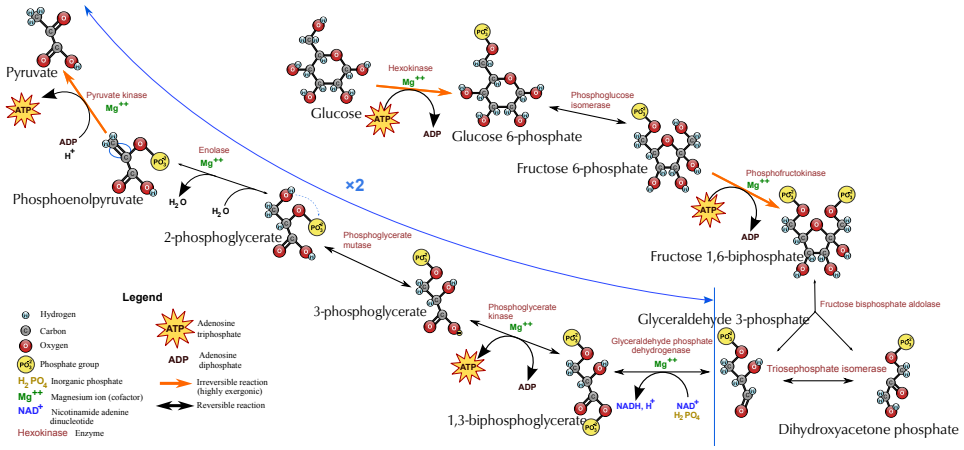

Figure 1.6 – Stages in classical model of glycolysis. Modified from [22].

in the phosphorylation of two molecules of ADP to yield ATP and the oxidation of two molecules of nicotinamide adenine dinucleotide hydride (NADH), and is given by the equation

$$\begin{aligned} &C_6H_{12}O_6 + 2\,ADP^+ 2\,P_i + 2\,NAD^+ \\ &\longrightarrow 2\,CH_3COCOOH + 2\,ATP + 2\,NADH + 2\,H^+. \end{aligned} \tag{1.4}$$

The individual steps of glycolysis are illustrated in figure 1.6. Of these stages, a crucial regulatory step is that of phosphorylation of phosphofructose by phosphofructokinase-1 (PFK-1), the third stage in the pathway. Counterintuitively (ATP is a substrate and ADP is a product of the PFK-1-catalysed reaction), ATP acts as an allosteric inhibitor and ADP as a facilitating co-factor of the reaction. Thus the rate of glycolysis, and so the rate of pyruvate generation, is directly coupled to intracellular ATP levels [21].

1.3.2 *Anaerobic fermentation*

The pyruvate generated by glycolysis can meet two fates, depending on the presence or absence of adequate mitochondrial oxygen. In the presence of adequate mitochondrial oxygenation (and absence of any other disordered mitochondrial function), adequate intracellular ATP levels prevent pyruvate accumulation by the PFK-1 coupling described above. In the *absence* of adequate mitochondrial oxygen, ATP levels fall with a concommitant rise in cytosolic NADH and flavin adenine dinucleotide hydride ($FADH_2$) levels (as mitochondrial oxidative phosphorylation fails to consume the reduced coenzymes). These conditions combine to drive the reaction catalysed by lactate dehydrogenase (LDH) towards lactate (i. e. to the right), as given by the equation

$$CH_3COCOOH + NADH + H^+ \overset{LDH}{\rightleftharpoons} CH_3CHOHCOOH + NAD^+. \tag{1.5}$$

Lactate is clasically described as a metabolically inactive waste product of anaerobic metabolism [23]. However, there is an increasing body of work suggesting that lactate, far from being a toxic and metabolically inactive by-product of anaerobic metabolism, is in fact closely involved with aerobic metabolism under normal resting conditions in brain tissue.

In the brain, a growing body of evidence points to lactate as a key intermediary in normal metabolism with potential neuroprotective effects [24]. Lines of evidence suggesting this include that:

- astrocytes are a major source of lactate production, in particular in response to glutamate, the primary excitatory neurotransmitter in the central nervous system [25];
- lactate may be a preferred fuel for neurons, in particular after traumatic or hypoxic brain injury [24];
- brain tissue can rely on lactate produced elsewhere in the body [26].

The astrocyte–neurone lactate shuttle hypothesis (ANLSH) unifies a number of these findings to yield an integrated model of the role of lactate in brain energy metabolism [27]. Central to the hypothesis is that the primary site of aerobic glycolysis is within astrocytes, and that the end-product of glycolysis, lactate, is shuttled to neuronal mitochondria by mono-carboxylate transporters, where they are converted back to pyruvate and undergo oxidation in the TCA cycle. A more radical hypothesis, where lactate does not only act as an additional energy substrate during times of metabolic distress, but is actually the primary substrate for the TCA cycle in health and pathology, has also been posited [28,29].

Whilst there are compelling arguments in favour of both the ANLSH and Schurr's obligatory fermentation hypothesis, the crucial underlying premise in both theories is that lactate is a normal intermediary in cerebral energy generation in both healthy and pathological states.

1.3.3 *Aerobic metabolism*

PYRUVATE DECARBOXYLATION Regardless of the role of lactate as a metabolic substrate, the fact remains that it is readily converted to pyruvate by various isoforms of lactate dehydrogenase (LDH). In the mitochondrial matrix, this pyruvate is bound to coenzyme A (CoA) as it is irreversibly converted to acetyl coenzyme A (ac-CoA) by the pyruvate dehydrogenase complex (PDHC), as given by the equation

$$CH_3CHOHCOOH + NAD^+ + CoA \xrightarrow{PDHC} Ac\text{-}CoA + NADH + H^+. \qquad (1.6)$$

This reaction takes place under strict regulation to couple acetyl CoA generation to the availability of ATP and nicotinamide adenine dinucleotide (NAD^+). Ac-CoA is used in

several different pathways, including the generation of fatty acids, steroids and ketone bodies. With respect to energy generation in the brain, it is complete oxidation of ac-CoA through the tricarboxylic acid (TCA) cycle which is of crucial importance [23].

TRICABOXYLIC ACID CYCLE The TCA cycle involves the complete oxidation of ac-CoA in order to yield reduced coenzymes (predominantly NADH) to fuel oxidative phosphorylation and the generation of ATP. Ac-CoA can be generated from many sources, but in the brain the main supply is derived from pyruvate; in alternative circumstances such as those seen during prolonged starvation, ac-CoA can also be derived from ketone bodies generated in the liver.

The TCA cycle consists of a cyclic series of reactions which take place within the mitochondrial matrix. The cycle itself begins with the acetylation of oxaloacetate followed by a series of eight reactions, of which three are oxidation reaction which yield the reduced coenzymes NADH or $FADH_2$. The net reaction of one cycle of the TCA cycle is shown in Figure 1.7 and given by the equation

$$\begin{aligned} &\text{Ac-CoA} + 3\,\text{NAD}^+ + \text{FAD} + \text{GDP} + \text{P}_\text{i} \\ &\longrightarrow \text{CoA} + 3\,\text{CO}_2 + 3\,\text{NADH} + \text{FADH}_2 + \text{GTP} + 3\,\text{H}^+. \end{aligned} \tag{1.7}$$

Aside from the production of the reduced coenzymes FADH2 and NADH, the TCA cycle is also responsible for the generation of guanosine triphosphate (GTP), an ATP-like phosphorylated nucleotide which can be hydrolyzed like ATP for energy [7,23].

MITOCHONDRIAL OXIDATIVE PHOSPHORYLATION Thus far, the oxidation of one molecule of glucose has been responsible for the generation of 10 molecules of NADH, 2 molecules of $FADH_2$, 2 molecules of GTP and 2 molecules of ATP, all 'carrier molecules' which contain energy released by glucose oxidation. However, whilst the reduced coenzymes NADH and $FADH_2$ are able to supply the energy to facilitate a minority of cellular processes, ATP is by far the predominant carrier molecule used in cellular metabolism.

Oxidative phosphorylation is the process by which the reduced coenzymes are oxidised, and the free energy harnessed to phosphorylate ADP, in the reverse of Equation 1.1. This process is carried out by a collection of four protein complexes (I-IV) embedded within the inner mitochondrial membrane, termed the electron transport chain. Complexes I, III and IV are responsible for the sequential oxidation of NADH and $FADH_2$, harnessing the resultant free energy to pump protons against their concentration from the mitochondrial matrix in to the intermembrane space. In doing so, they generate a *proton motive force*. This is harnessed by ATP synthase (also known as complex

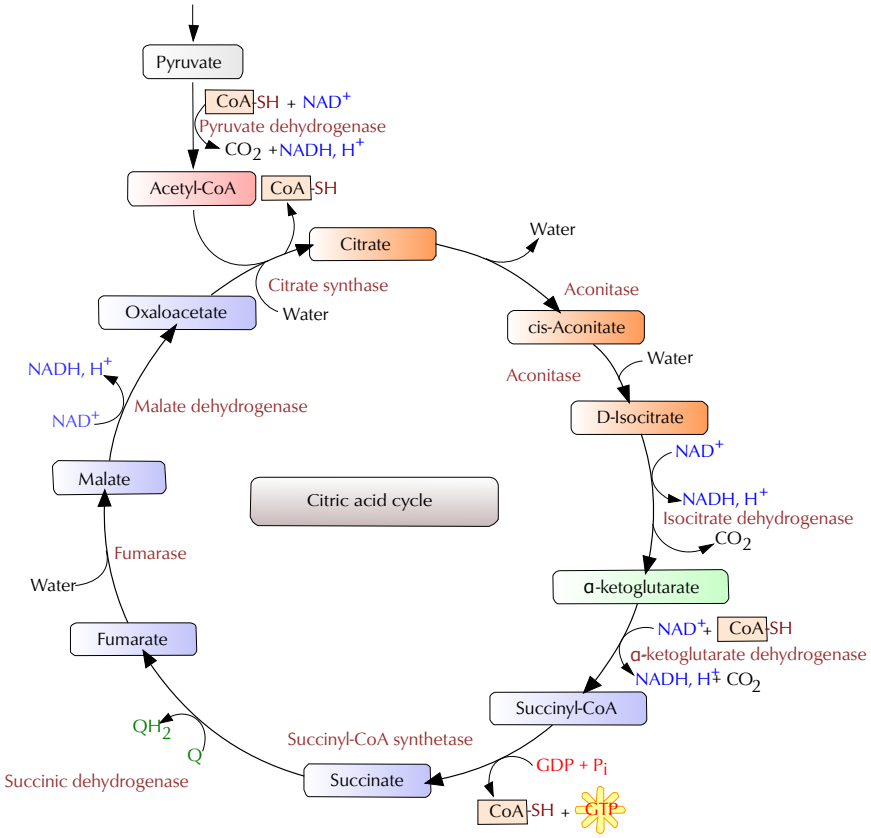

Figure 1.7 – Stages in TCA cycle. Modified from [30].

V), which allows protons to flow along their electrochemical gradient, utilizing the liberated free energy to phosphorylate ADP [31], given by the equation

$$\mathrm{NADH} + \tfrac{1}{2}\,\mathrm{O_2} + \mathrm{H^+} \longrightarrow \mathrm{NAD^+} + \mathrm{H_2O}. \tag{1.8}$$

Thus, the oxidation of NAD, as shown in Equation 1.8 releases the free energy required for the generation of ATP, in the reverse of the process depicted in Equation 1.1. The components of the chain and a schematic diagram of its function are shown in Table 1.1 and Figure 1.8.

CYTOCHROME C OXIDASE Cytochrome c oxidase (CCO) is the final electron acceptor in the electron transport chain. It is considered here in more detail as it is a key subject of study of this thesis.

Cytochrome c oxidases of the aa_3 variety are found in a multitude of organisms encompassing all cellular phylogenetic kingdoms. Although the variants cytochrome c oxidase (CCO) comprising 3, 4 and 13 subunits have been described, the metabolic

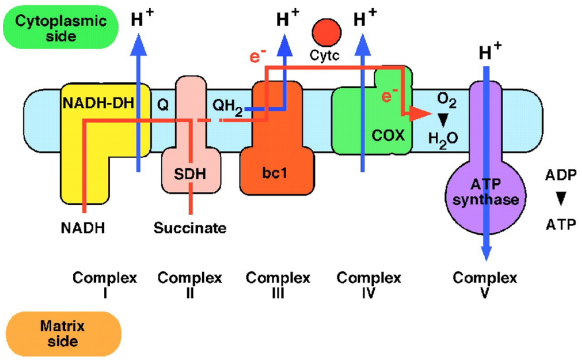

Figure 1.8 – Schematic depiction of electron transport chain. From [32]

functions of CCO are performed by three core subunits (I, II and III), which are well-conserved across species. Subunit I is the best conserved subunit and contains two haem groups – one haem *a* and one haem a_3 in mammalian mitochondrial forms – and a copper atom, copper B (Cu_B). Subunit II contains a binuclear copper centre, copper A (Cu_A) [33].

CCO carries out two main metabolic functions within mitochondria: the translocation of one proton from the mitochondrial matrix in to the intermembrane space, and reduction of oxygen. The latter processoccurs by the binding of two protons (from the matrix side of the membrane), two electrons to half a dioxygen molecule, as given by the equation

$$\tfrac{1}{2}O_2 + 2\,H^+ + 2\,e^- \xrightarrow{CCO} H_2O. \tag{1.9}$$

The Cu_A centre of subunit II is the likely binding site of cytochrome *c*. The electron is then transferred to the haem a_3–Cu_B complex via haem *a*. The electron is then passed from Cu_B to oxygen, which is then bound to a proton to yield water. The precise mechanism by which two protons – one as a charged particle, one as a substrate to yield water – are transferred across the mitochondrial inner membrane are unclear. However, it is apparent that the transfer of an electron to haem *A* causes the uptake of a proton from an unidentified 'pump site' and the subsequent transfer of that electron to the haem a_3–Cu_B complex leads to the release of the proton in to the intermembrane space [33–35]. The key catalytic centre, and a major regulatory site, is the haem a_3-Cu_B core. The iron contained within haem a_3 cycles between $+2$, $+3$ and $+4$ oxidation states, with the pH on each side of the mitochondrial membrane as well as the supply of electrons (in the form of reduced NADH and $FADH_2$) acting to regulate the rate of reaction via effects on the haem a_3-Cu_B core. Meanwhile, the copper ion in Cu_B alternates between the $+1$ and $+2$ oxidation state. Aside from the two roles of oxygen reduction and proton translocation, there is an increasing body of evidence suggesting

COMPONENT	NOTES
Complex I	NADH:ubiquinone oxidoreductase. Oxidises NADH and translocates one proton across mitochondrial membrane.
Complex II	Succinate:ubiquinone reductase. Participates in electron transport but does not translocate protons across mitochondrial membrane. Participates in TCA and transfers electrons from complex I to coenzyme Q.
Complex III	Cytochrome bc_1 Delivers electrons from coenzyme Q to cytochrome c. translocates one proton across mitochondrial membrane.
Complex IV	Cytochrome *c* oxidase Oxidises cytochrome *c* and translocates one proton proton across mitochondrial membrane and oxidises half dioxygen molecule per cycle.
Coenzyme Q	Ubiquinone Small coenzyme able to diffuse along mitochondrial membrane. Acts as electron shuttle between Complexes II & III.
Cytochrome c	Membrane-anchored protein that acts as electron carrier between complexes III & IV.

Table 1.1 – Components of electron transport chain

that CCO in has a role in the inactivation of NO·. NO· is a substance that has a multitude of physiological and pathological roles. In health, NO· acts as an intercellular and second messenger, and contributes to the control of cerebral vascular tone; it also acts as a neurotransmitter. Following brain injury, overproduction of NO· can trigger deleterious cascades [36]. The interaction between NO· and CCO is complex, and depends on the oxidation state of the Cu_B subunit; NO· can also bind the haem a_3 subunit of CCO, and in doing so inhibit the flow of electrons through CCO [37]. These complex interactions may also form the basis of the characteristic cerebral vasodilation observed during hypoxia [16,38].

1.4 CONCLUSION

This chapter has described the process of cellular respiration, by which ATP is generated from the primary metabolic substrates glucose and oxygen as well as the stages in and regulation of supply of these substrates to neural tissue. The description of these physiological processes is not exhaustive; the level of detail in which they are discussed is tailored to its relevance to the remainder of the thesis. Having established how these

processes occur in health, the next chapter describes their malfunction following acute brain injury.

REFERENCES

[1] Pakkenberg, B & Gundersen, HJ. Neocortical neuron number in humans: effect of sex and age. *The Journal of comparative neurology*, 384(2):312–320, 1997.

[2] Pakkenberg, B, Pelvig, D, Marner, L, Bundgaard, MJ, Gundersen, HJG, Nyengaard, JR & Regeur, L. Aging and the human neocortex. *Experimental gerontology*, 38(1-2):95–99, 2003.

[3] Alberts, B, Johnson, A, Julian, L, Raff, M, Keith, R, Johnson, A, Lewis, J, Raff, M, Roberts, K & Walter, P. *Molecular Biology of the Cell*. 4th ed. Garland Science, 2002.

[4] Clausen, T, Van Hardeveld, C & Everts, ME. Significance of cation transport in control of energy metabolism and thermogenesis. *Physiological reviews*, 71(3):733–774, 1991.

[5] Prins, ML. Cerebral metabolic adaptation and ketone metabolism after brain injury. *Journal of Cerebral Blood Flow & Metabolism*, 28(1):1–16, 2008.

[6] Walsh, TS & Saleh, EED. Anaemia during critical illness. *British Journal of Anaesthesia*, 97(3):278–291, 2006.

[7] Zauner, A, Daugherty, WP, Bullock, MR & Warner, DS. Brain oxygenation and energy metabolism: part I-biological function and pathophysiology. *Neurosurgery*, 51(2):289–301; discussion 302, 2002.

[8] Castilhos, R. File:circle of willis en.svg. `http://commons.wikimedia.org/wiki/File:Circle_of_Willis_en.svg`, 2007.

[9] Scremin, OU. Cerebral Vascular System. In *The Human Nervous System, Second Edition*, pp. 1325–1348. Academic Press, 2004.

[10] Ursino, M & Lodi, CA. Interaction among autoregulation, CO2 reactivity, and intracranial pressure: a mathematical model. *The American journal of physiology*, 274(5Pt2):H1715–28, 1998.

[11] Lassen, NA. Control of cerebral circulation in health and disease. *Circulation research*, 34(6):749–760, 1974.

[12] Fog, M. Cerebral Circulation: I. Reaction of Pial Arteries to Epinephrine by Direct Application and by Intravenous Injection. *Archives of Neurology and Psychiatry*, 41(1):109–118, 1939.

[13] Fog, M. Cerebal Circulation: II. Reaction of Pial Arteries to Increase in Blood Pressure. *Archives of Neurology and Psychiatry*, 41(2):260–268, 1939.

[14] Czosnyka, M, Brady, K, Reinhard, M, Smielewski, P & Steiner, LA. Monitoring of cerebrovascular autoregulation: facts, myths, and missing links. *Neurocritical Care*, 10(3):373–386, 2009.

[15] Iadecola, C. Neurovascular regulation in the normal brain and in Alzheimer's disease. *Nature reviews Neuroscience*, 5(5):347–360, 2004.

[16] Van Mil, AHM, Spilt, A, Van Buchem, MA, Bollen, ELEM, Teppema, L, Westendorp, RGJ & Blauw, GJ. Nitric oxide mediates hypoxia-induced cerebral vasodilation in humans. *Journal of Applied Physiology*, 92(3):962–966, 2002.

[17] Hawkins, BT & Davis, TP. The blood-brain barrier/neurovascular unit in health and disease. *Pharmacological reviews*, 57(2):173–185, 2005.

[18] Ohtsuki, S & Terasaki, T. Contribution of carrier-mediated transport systems to the blood-brain barrier as a supporting and protecting interface for the brain; importance for CNS drug discovery and development. *Pharmaceutical research*, 24(9):1745–1758, 2007.

[19] Abbott, NJ, Rönnbäck, L & Hansson, E. Astrocyte-endothelial interactions at the blood-brain barrier. *Nature reviews Neuroscience*, 7(1):41–53, 2006.

[20] Ghosh, A & Smith, M. Brain Tissue Biochemistry. In Matta, BF, Menon, DK & Smith, M, eds., *Core Topics in Neuroanaesthesia and Neurointensive Care*, pp. 85–100. Cambridge University Press, 2011.

[21] Passonneau, JV & Lowry, OH. The role of phosphofructokinase in metabolic regulation. *Advances in enzyme regulation*, 2:265–274, 1964.

[22] Mrabet, Y. File:glycolysis.svg. `http://commons.wikimedia.org/wiki/File:Glycolysis.svg`, 2011.

[23] Harris, RA. Carbohydrate metabolism i: Major metabolic pathways and their control. In Devlin, TM, ed., *Textbook of Biochemistry with Clinical Correlations,*, 4th ed. Wiley-Liss, 2007.

[24] Pellerin, L. Lactate as a pivotal element in neuron-glia metabolic cooperation. *Neurochemistry international*, 43(4-5):331–338, 2003.

[25] Kasischke, KA, Vishwasrao, HD, Fisher, PJ, Zipfel, WR & Webb, WW. Neural activity triggers neuronal oxidative metabolism followed by astrocytic glycolysis. *Science*, 305(5680):99–103, 2004.

[26] Dalsgaard, MK, Quistorff, B, Danielsen, ER, Selmer, C, Vogelsang, T & Secher, NH. A reduced cerebral metabolic ratio in exercise reflects metabolism and not

accumulation of lactate within the human brain. *The Journal of Physiology*, 554(Pt 2):571–578, 2004.

[27] Pellerin, L & Magistretti, PJ. Neuroscience. Let there be (NADH) light. *Science*, 305(5680):50–52, 2004.

[28] Schurr, A, Payne, RS, Miller, JJ & Rigor, BM. Brain lactate is an obligatory aerobic energy substrate for functional recovery after hypoxia: further in vitro validation. *Journal of Neurochemistry*, 69(1):423–426, 1997.

[29] Schurr, A. Lactate: the ultimate cerebral oxidative energy substrate? *Journal of cerebral blood flow and metabolism*, 26(1):142–152, 2006.

[30] Ramsköld, D, Anonymous, S, Anonymous & Mrabet, Y. File:circle of willis en.svg. `http://commons.wikimedia.org/wiki/File:Citric_acid_cycle_with_aconitate_2.svg`, 2007.

[31] Hatefi, Y. The mitochondrial electron transport and oxidative phosphorylation system. *Annual review of biochemistry*, 54:1015–1069, 1985.

[32] Saraste, M. Oxidative phosphorylation at the fin de siècle. *Science*, 283(5407):1488–1493, 1999.

[33] Michel, H, Behr, J, Harrenga, A & Kannt, A. Cytochrome c oxidase: structure and spectroscopy. *Annual review of biophysics and biomolecular structure*, 27:329–356, 1998.

[34] Wikström, M. Cytochrome c oxidase: 25 years of the elusive proton pump. *Biochimica et biophysica acta*, 1655(1-3):241–247, 2004.

[35] Brzezinski, P & Gennis, RB. Cytochrome c oxidase: exciting progress and remaining mysteries. *Journal of Bioenergetics and Biomembranes*, 40(5):521–531, 2008.

[36] Pacher, P, Beckman, JS & Liaudet, L. Nitric oxide and peroxynitrite in health and disease. *Physiological reviews*, 87(1):315–424, 2007.

[37] Brunori, M, Giuffrè, A, Forte, E, Mastronicola, D, Barone, MC & Sarti, P. Control of cytochrome c oxidase activity by nitric oxide. *Biochimica et biophysica acta*, 1655(1-3):365–371, 2004.

[38] Palacios-Callender, M, Hollis, V, Mitchison, M, Frakich, N, Unitt, D & Moncada, S. Cytochrome c oxidase regulates endogenous nitric oxide availability in respiring cells: a possible explanation for hypoxic vasodilation. *Proceedings of the National Academy of Sciences of the United States of America*, 104(47):18508–18513, 2007.

2

ACUTE BRAIN INJURY

This chapter describes the epidemiology, pathophysiology and tenets of clinical management of ABI. Whilst the diseases that comprise this grouping – subarachnoid haemorrhage (SAH), traumatic brain injury (TBI), ischaemic stroke and intracerebral haemorrhage (ICH) – are distinct pathological entities, there are significant commonalities in their pathophysiology, and thus their clinical management. Thus, while the clinical studies in this thesis focus primarily on patients with SAH and TBI, the focused review in this chapter draws on evidence from all subtypes of ABI, with particular reference to the pivotal role of cerebral cellular hypoxia-ischaemia (CH-I) in the pathophysiology of ABI and the clinical monitoring modalities and strategies used to detect and prevent it.

2.1 DEFINITIONS & EPIDEMIOLOGY

2.1.1 *Traumatic brain injury*

TBI is common, with an incidence of 229/100,000 people/year in England, which is consistent with the European average of 235/100,000 in Europe but markedly lower than the incidence of 579/100,000 observed in the USA [1–3]. TBI comprises 1.4% of Emergency Department attendances in the USA [3], and was found to account for 3.4% of attendances in the Emergency Department in one western English district general hospital [4]. Ninety percent of TBI is classified as 'mild' [2]; the data regarding such injuries are complex and controversial, but in general, mild TBI is associated with negligible mortality and carries a good prognosis for recovery, although the period of recovery and rehabilitation incurs significant personal and societal cost. The remaining moderate and severe TBI – typically defined by an admission Glasgow Coma Score (GCS) of 9–12 and 3–8, respectively – exacts a more apparent heavy toll on both the individual and society: a mortality rate of 40% has been observed in both British and pan-European multicentre studies following severe TBI [5,6]. Furthermore, disability is common amongst TBI survivors: TBI is the leading cause of injury-related long-term disability, with up to 60% of survivors suffering from impairments leading to limitations in cognition, major activity, and recreation [7,8]. The patients described in the clinical studies of this thesis are patients who require admission to a neurocritical care unit (NCCU) with invasive intracranial monitoring, and thus have invariably suffered from severe TBI.

2.1.2 *Subarachnoid haemorrhage*

SAH is a form of stroke characterised by haemorrhage in to the subarachnoid space, the cerebrospinal fluid (CSF) space between the arachnoid and pial membranes of the meninges. SAH has an incidence of 9/100,000 people/year and a female preponderance [9]. A poor outcome (death or severe disability) is seen in 20–30% of patients suffering SAH [10,11]. SAH occurs in a relatively young population (albeit somewhat higher than that of TBI); as a result, the loss of productive life years in the general population is the same for SAH as it is from ischaemic stroke, even though ischaemic stroke is as much as 50 times higher in incidence [9,12–14].

Whilst traumatic SAH can be observed as a feature of TBI (where it is a feature of a high energy impact and associated with poor outcome [15]), *spontaneous* SAH can be attributed to the rupture of an intracranial aneurysm in over 85% of cases [13]. A number of grading scales exist for aneurysmal subarachnoid haemorrhage (aSAH), which aim to prognosticate based variously on clinical features, radiological features and combinations of the two, although none has proved definitely superior to the others [16]. The patients described in the clinical portions of this thesis, like those with TBI, are patients who require admission to a NCCU with invasive intracranial monitoring, and thus fall at the 'poor-grade' end of classification spectra, regardless of scale used.

2.2 PATHOPHYSIOLOGY OF ACUTE BRAIN INJURY

Pathophysiological processes contributing to ABI are widely considered in terms of *primary* and *secondary* injury processes. The term primary injury has historically referred to that cellular death and dysfunction which occurs at the ictus of injury and is "instantaneous and irreversible" [17], whereas the term secondary injury referred to potentially avoidable, delayed cell death occurring as a result of subsequent insults to tissue rendered susceptible to injury as a consequence of pathophysiological cascades set in motion at ictus. This framework has gained currency in a number brain pathologies, including TBI, SAH, ICH and ischaemic stroke, as well as extracranial diseases such as spinal cord injury [18–22]. However, it is increasingly recognised that primary injuries evolve in the hours following ictus, and the cascades that lead to cell death may be modifiable. Thus, whilst the terms 'primary' and 'secondary' injury are still widely employed in the literature, there is an overlap in their timescales – depicted schematically in Figure 2.1 – and so a more precise way of distinguishing the two types of injury may be on the basis of time course, where primary injury occurs in the immediate aftermath of ictus, and secondary injury processes exert their effects over the following days [17]; some authors underline this point by referring to primary brain injury as 'early brain injury' [23].

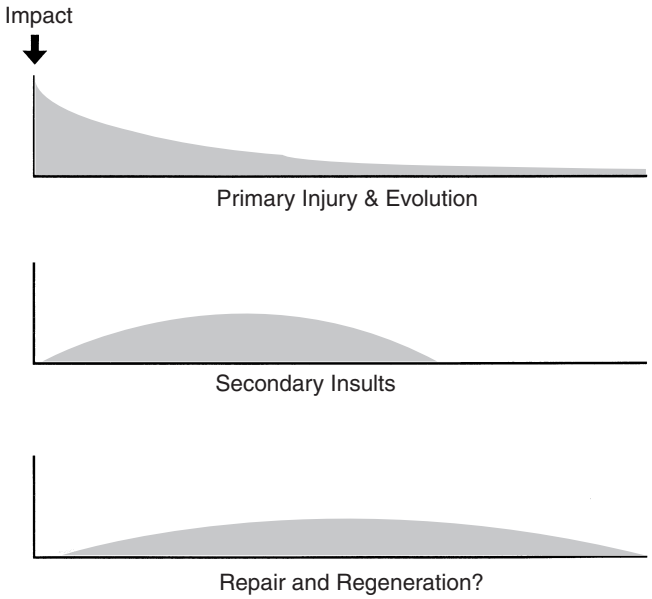

Figure 2.1 – Schematic depiction of the time-courses of primary and secondary injury, from [17].

Following both TBI and SAH, an enormous array of interacting processes conspire to cause cell death and dysfunction; a complete review of these processes and their interactions is beyond the scope of this thesis. However, the aggressive avoidance of secondary injury has seen a concomitant improvement in outcomes following ABI in the last two decades, and forms a central tenet to contemporary critical care management of these diseases [24]. In order to aid in understanding of these tenets (described in Section 2.3 below), the most important primary and secondary injury processes are considered here.

2.2.1 *Mechanisms of primary/early brain injury*

TRAUMATIC BRAIN INJURY In TBI, injury is a result of the impartation of kinetic injury to the tissue of the brain as a consequence of blunt, or more rarely penetrating, trauma. Intracranial contents have heterogeneous density and viscoelastic properties; consequently the acceleration/deceleration forces at impact result in a complex pattern of tensile, compressive and shearing strains [25]. On a macroscopic level, damage resulting from these strains includes the formation of haematomas (both intraparenchymal and extracerebral), focal cerebral contusions and widespread disruption of white matter tracts by shearing forces with diffuse swelling, which is termed diffuse axonal injury (DAI).

On a cellular level, these macroscopic events lead to cellular death through direct cellular disruption, resulting in membrane microporation, loss of cellular ion homeostasis (which, as discussed in Section 1.1.1, is crucial to cellular survival), and changes

in protein conformation. Furthermore, acute critical ischaemia – discussed below – can occur shortly after injury ictus, as a result of locally raised intraparenchymal pressure (for example, in peri-contusional tissue) and focal microvascular disruption by injury [26].

SUBARACHNOID HAEMORRHAGE Primary injury in aSAH is related to the immediate effects of aneurysm rupture. Rupture and the subsequent extravasation of blood, with consequent 'mass effect', results in the rapid development of severe intracranial hypertension – intracranial pressure (ICP) can reach the level of diastolic arterial pressure within one minute – with concomitant cerebral circulatory arrest [27]. Thus, global acute ischaemia is the predominant primary injury process that occurs in subarachnoid haemorrhage. In addition to this acute ischaemic insult, there may be direct tissue damage as a consequence of intraparenchymal haemorrhage associated with aneurysm rupture [13].

Following ABI ictus, cells that survive these insults do not simply return to normal function; rather, the effect of these primary insults is to put in motion a series of pathophysiological cascades that render neural tissue vulnerable to further damage by secondary injury processes.

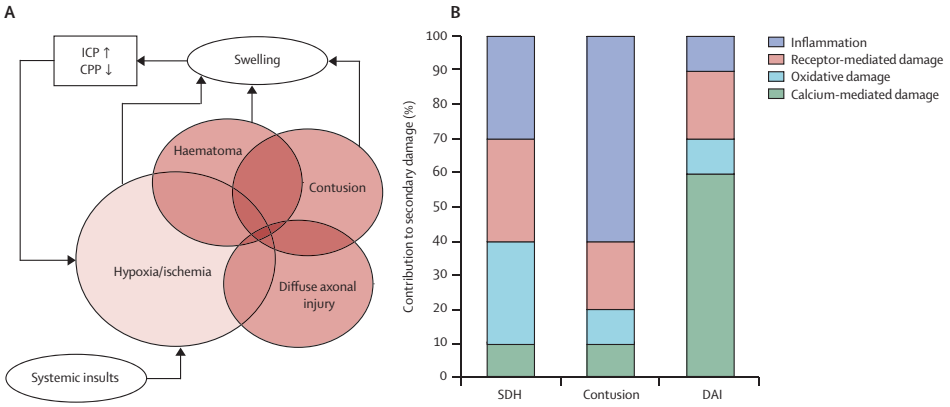

Figure 2.2 – A – interplay between primary injury processes and mechanism resulting development of secondary ischaemia; B – predominant contributing factors that lead to secondary cell death following different forms of traumatic brain injury. From [26].

2.2.2 *Processes of secondary brain injury*

Primary injuries in both TBI and SAH set in motion a series of concurrent cascades which can conspire to cause cell death beyond that incurred during the primary injury, and thus lead to further mortality and morbidity following ABI. Although the nature of the primary insult varies in different forms of ABI, there are substantial similarities

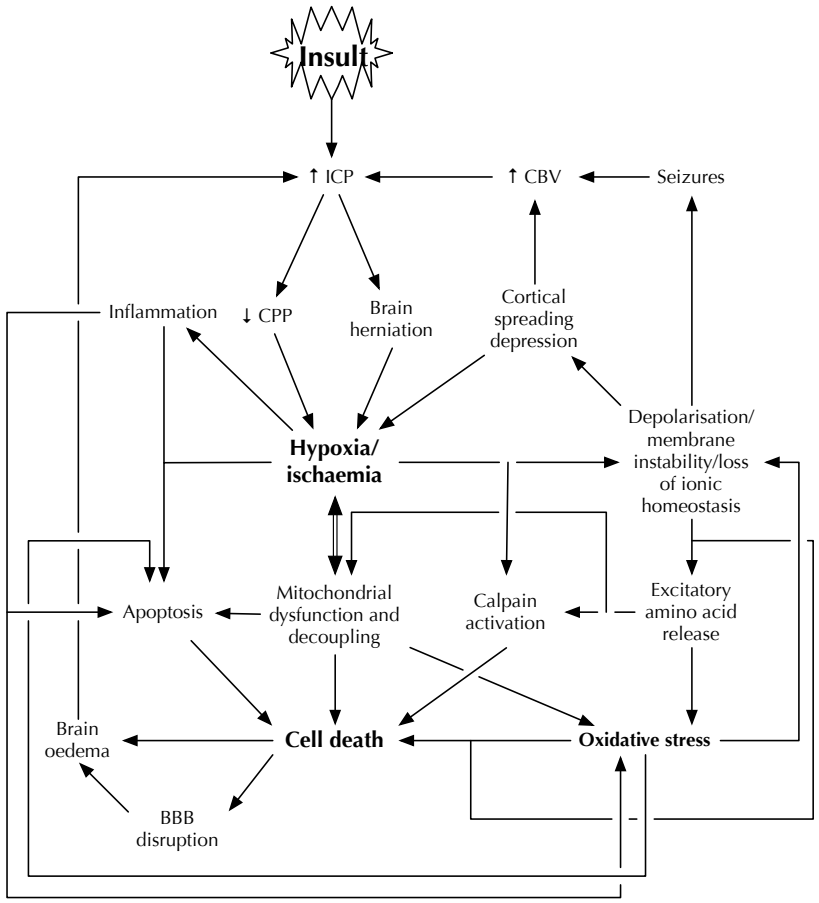

Figure 2.3 – Schematic diagram illustrating principal secondary injury processes. The diagram is not comprehensive, but rather serves to expose the interconnected, recursive nature of secondary injury processes. Cellular hypoxia is a pivotal event that links all secondary injury processes, either directly or indirectly.

between processes of secondary injury that ensue. The mechanisms of secondary injury are described here in more detail, with particular reference to the role of CH-I.

In the 1970s, Miller observed that systemic hypotension and hypoxia had a deleterious effect on functional outcome following TBI [28,29]; these studies – whose findings have been widely replicated subsequently – were the earliest indications of the central role that CH-I plays in the pathophysiology of secondary brain injury. Following SAH, the epidemiological outcome data linking *systemic* hypoxia and hypotension to poor outcome, whilst still congruent, are more sparse [30]; *cerebral* ischaemia is, however, recognised as the major cause of poor outcome [13,31–37]. Several studies have used invasive and non-invasive bedside monitoring techniques, as well as neuroradiological techniques, to confirm both the occurrence of CH-I and its association with poor outcome following ABI (discussed below in Section 2.3.1).

CELLULAR HYPOXIA-ISCHAEMIA Defining CH-I is a non-trivial task. Whilst CH-I can be defined as the state that occurs when CBF and O_2 delivery are inadequate for the continuation of normal cellular and neuronal function, these functions are diverse and vary in their requirements for O_2 and metabolic substrate. Consequently, CH-I does not simply occur as an 'on/off' phenomenon when CBF falls below a certain threshold; rather, there are a *variety* of thresholds for CH-I, which correspond to the physiological functions that are disrupted. Data from ischaemic stroke identifies CBF thresholds for CH-I: below 50 ml.100g^{-1}.min^{-1}, clinical evidence of functional impairment manifests, with corresponding electrophysiological changes, impaired protein synthesis and selective cell loss; below 20 ml.100g^{-1}.min^{-1}, membrane stability is impaired and permanent infarction occurs [38,39].

However, it is unclear the degree to which these thresholds can be applied to the already-injured brain. For example, reduction in $(CMRO)$ *isarecognisedsequelaof TBIandSAH*[40, 41]; *inthiscontext*, *reductionsinCBFmaybepathological*, *thusresultinginCH* $-$ *I*, *butmayalternativelybetheeffectofi* $-$ *consequenttoABI* $-$ $-$ *maycausereduced CBFinthepresenceofnormal CMRO*[42,43], *andthesituationisfurtherco loweringanaestheticagentsasamainstayoftheNCCUmanagementof ABI*. *Thesefactorscombinedmeanthatflowthres relevantischaemia*, *andthereisthusaneedformoresophisticatedmeasuresofinadequatesupplyofmetabolicsubstrateto*

CATEGORY OF CHI CAUSE	EXAMPLE
Decreased O_2 delivery – extracranial cause	Systemic hypoxia/hypotension.
	Can be direct consequence of brain injury (e. g. myocardial dysfunction, neurogenic pulmonary oedema followingeither TBI or SAH), indirectly related to brain injury (e. g. haemorrhagic shock in polytrauma associated with TBI) or unrelated/iatrogenic(e. g. pneumonia, venous thromboembolism).
Decreased O_2 delivery – intracranial cause	Raised ICP causing decreased CPP
	Brain herniation causing large vessel occlusion
	Cerebral vasospasm
	Impaired CA causing hypoperfusion
	Impaired substrate diffusion due to inflammation/oedema
Increased demand for metabolic substrate	Seizures
	Cortical spreading depression
	Excitatory amino acid release
Metabolic failure	Mitochondrial dysfunction/decoupling

Table 2.1 – Categorised causes of cerebral hypoxia-ischaemia

Systemic hypotension/hypoxia can occur in concert with neurological injury – for example, neurogenic myocardial dysfunction and pulmonary oedema are both recognised as complications of TBI and SAH, and cardiorespiratory injury or haemorrhagic shock can result from extracranial injury occurring simultaneously to TBI [44–50]. However,

factors resulting in CH-I are diverse and not limited to systemic hypoxia/hypotension; CH-I can occur as a result of:

- the reduction of cellular O_2 and metabolic substrate *delivery* below critical thresholds;
- an increase in cellular O_2 and metabolic substrate *requirements* because of secondary injury processes such as excitotoxicity;
- an inability to utilise O_2 and metabolic substrate on account of mitochondrial and metabolic dysfunction – i. e. *functional* CH-I;

Systemic hypoxia and hypotension can cause CH-I by overcoming the homeostatic mechanisms described in Section 1.2.1, but CH-I can also occur as a result of disordered CA in the absence of hypoxia/hypotension. Failure of cerebrovascular autoregulation can occur following ABI [51–54], and is associated with poor outcome. A special case of dysautoregulation is cerebral vasospasm, which has the potential to cause delayed cerebral ischaemia (DCI) following SAH. This well-recognised but poorly-understood complication of SAH is discussed separately below. Vasospasm is also increasingly recognised as a complication TBI sustained by blast injuries [55]. Regardless of the cause, CH-I results in the initiation of cascades that can lead to cell death and thus poor outcome. Important processes leading to CH-I are considered here.

INTRACRANIAL HYPERTENSION Inadequate cerebral perfusion can also be the result of intracranial hypertension, which is a key secondary injury process in both SAH and TBI. The role of intracranial hypertension in the brain injury pathogenesis is well-understood as ICP is frequently monitored following ABI (see Section 2.3.1 below).

A key concept in the consideration of ICP in both health and disease is the Monro-Kellie doctrine. This states that the skull is a fixed space which contains non-compressible contents (brain parenchyma, arterial and venous blood and CSF). The expansion of any of these compartments, or the introduction of new contents – in the form of a mass lesion such as a haematoma – can only occur with a resulting compression of the other compartments. The collapse of cerebral venous sinuses and caudal displacement CSF provide limited buffering capacity maintaining ICP at its normal physiological level of 7–15 mmHg, but once this is exhausted, any increase in cerebral content volume results in raised ICP. Intracranial hypertension can result in two serious consequences: reduced cerebral perfusion and brain herniation.

The measurement of ICP allows the determination of CPP, which is defined as the difference between mean arterial pressure (MAP) and ICP, as given by the equation

$$\mathrm{CPP} = \mathrm{MAP} - \mathrm{ICP}. \tag{2.1}$$

CPP represents the pressure gradient that exists across the cerebrovascular bed and is thus a crucial component in determination of CBF and cerebral O_2 delivery [56] and the measurement of CPP forms a cornerstone in the critical care management of TBI.

Aside from causing reduced delivery as a result of decreased CPP, intracranial hypertension can also contribute to secondary brain injury by causing brain herniation [57].

The intracranial vault is incompletely divided in to several compartments: the two cerebral hemispheres are separated by the falx cerebri, and from the cerebellum and brainstem by the tentorium cerebelli. The falx and tentorium are semi-rigid infoldings of the dura mater, one of the meningeal membranes that envelopes the surface of the brain. Pressure gradients from localised mass lesions can cause herniation of cerebral contents and associated vasculature from one compartment to another, leading to shearing strain on brain parenchyma and occlusion of large vessels. Well-recognised patterns of herniation include:

- *trans-falcine hernation*, where the herniation of the cingulate cortex may be associated with the herniation of an ACA, with subsequent ischaemia in that vascular territory;
- *uncal herniation*, where the medial temporal lobe herniates downwards across the tentorium with potential pressure exerted on the midbrain and pons;
- *tonsillar herniation* – also termed "coning" – where the cerebellar tonsils are displaced downwards through the *foramen magnum* in the base of the skull, with pressure exerted on the brainstem. This is almost inevitably a fatal occurrence.

Thus, through brain herniation and reduced cerebral perfusion, intracranial hypertension plays a central role in the pathogenesis of secondary brain injury. It also plays a 'feedback' role in reinforcing pathological cascades, as processes that increase cerebral metabolic demand, through intact neurovascular coupling, can increase cerebral blood volume (CBV) and thus ICP.

DELAYED CEREBRAL ISCHAEMIA AND VASOSPASM delayed cerebral ischaemia (DCI) is a complex and poorly-understood process that is the predominant cause of death and disability following aSAH [10,58,59]. Although a comprehensive review is beyond the scope of this thesis, its high incidence and potentially devastating effects on outcome mandate a more detailed consideration of its pathophysiology.

The first problem encountered in considering DCI is a heterogeneity of nomenclature, with terms such as vasospasm, delayed ischaemic neurological deficit and delayed cerebral ischaemia used seemingly interchangeably. This problem is further complicated by the absence of clear, standardised criteria for the diagnosis of DCI [60]. For the purposes of this thesis, nomenclature proposed by recent consensus guidance from the Neurocritical Care Society is used:

- *delayed cerebral ischaemia* (DCI) refers to any neurological deterioration that is presumed to be ischaemia-related and cannot be attributed to any other cause;
- *delayed neurological deficit* (DND) is a clinical neurological deterioration following SAH that can be attributed to a cause other than re-bleeding, and may be attributed to a wide variety of aetiologies, both extracranial and intracranial; DCI and hydrocephalus are particulary important intracranial causes;
- *vasospasm* describes arterial narrowing, demonstrated either radiologically or by ultrasonography [61].

Whilst arterial vasospasm has historically been considered the predominant aetiological factor in DCI (with the result that the term 'vasospasm' is colloquially used to refer to the clinical diagnosis of DCI), recent discoveries have refuted this assumption. In fact, macrovascular vasospasm has been exposed as only one of many factors that contributes to DCI [33]. There is clearly some link between *ischaemia* and outcome following DCI – for example the administration of nimodipine, the only treatment shown to improve DCI-related outcome following SAH, results in a co-incident reduction in the incidence of poor outcome and radiologically-defined infarction [10]. However, the relationship between clinically-defined DCI, vasospasm observed on digital subtraction angiography (DSA), other measures of vasospasm and ischaemia (such as elevated TCD flow velocities and elevated cerebral microdialysate ischaemic markers, see below) is complex and unclear: patients can show angiographic, TCD, xenon computed tomography (CT) perfusion, positron emission tomography (PET) or microdialysate evidence of 'vasospasm' in the absence of any clinical deficit, or vice versa [62–65]. Furthermore, recent trials of drugs have shown significant reductions in the radiological occurrence of vasospasm without any associated improvement in clinical outcome [66] and more than a quarter of infarcts occur outside areas of angiographically-defined vasospasm [67]; in subsidiary analyses, cerebral infarction has been shown to contribute to poor outcome, but a significant portion of this contribution could be attributed to non-vasospastic processes [68].

DCI, then, is an early complication of aSAH that results in cerebral ischaemia and is associated with evidence of large vessel vasospasm and invasive markers of ischaemia, but not exclusively so. Many other aetiological factors have been associated with DCI: these include microcirculatory vasospasm, microembolism, increased ICP, BBB dysfunction, cortical spreading depression and perihaemorrhagic ischaemia [33]. Whilst these pathophysiological processes are all discussed below in the context of CH-I, what is unclear is how SAH precisely initiates the cascades that leads to their contribution to DCI and impaired outcome.

2.2.3 *Mitochondrial dysfunction*

Under ischaemic conditions, ATP production is the result of anaerobic fermentation, rather than mitochondiral oxidative phosphorylation (see section 1.3.3). However, beyond this expected, substrate-dependent reduction in mitochondrial function, CH-I results in further mitochondrial damage that amplifies cellular bio-energetic failure, apoptotic and necrotic cascades [69]. Mitochondrial dysfunction is considered separately from other processes causing cell death (section 2.2.4 below) not only because of its central importance in the pathogenesis of secondary brain injury, but also because of its role in generating conditions of *functional* ischaemia – that is, the failure of cellular energy generation in the presence of normal cellular oxygen delivery.

Following ABI, mitochondrial injury and dysfunction takes many forms. Structural damage, is observed as mitochondrial swelling and loss of cristal membranes [70,71]; such changes are heterogeneously observed in the brain following experimental TBI [72].

From a pathophysiological perspective, the *functional* impairment of mitochondria following ABI is of more interest. Although many of the injurious processes that occur following CH-I result in a increase in cellular energy requirements, the ability of mitochondria to generate adequate ATP in order to meet these demands is, perversely, reduced.

The intracellular influx of calcium ions (Ca^{2+}) that occurs as a result of excitotoxicity results in Ca^{2+} accumulation within the mitochondrial matrix; this leads to mitochondrial depolarisation and a consequent inability to continue normal oxidative phosphorylation, and leads to the generation of reactive oxygen species (ROS) [69]. Furthermore, intramitochondrial Ca^{2+} accumulation can lead to the opening of the mitochondrial transition pore, an elaborate and poorly understood complex that results in decoupling of oxidative phosphorylation and is the harbinger of cellular apoptosis [73]. Decoupling also occurs as a result of expression of mitochondrial uncoupling protein UCP-2, which may conversely protect against cell death by reducing the formation of ROS [74].

2.2.4 *Other processes causing cell death*

The reduction of CBF and O_2 delivery below critical thresholds puts in motion a set of cascades results in cell death by a variety of mechanisms; these mechanisms – summarised in Figure 2.3 – are considered here.

Under ischaemic conditions, cells must rely on anaerobic respiration to generate ATP. As discussed in Sections 1.3.2 and 1.3.3 , the amount of ATP yielded per glucose molecule by anaerobic respiration is an order of magnitude less than that yielded by aerobic respiration. In severely ischaemic conditions, this leads to an inability to maintain the resting membrane potential (see Section 1.1.1), with subsequent cell

membrane breakdown and tissue necrosis [75]. However, ischaemic insults that do *not* reach the threshold for triggering membrane instability still lead to cell death, by the mechanisms described below.

EXCITOTOXICITY A consequence of sub-lethal membrane depolarisation is the release of excitatory amino acids(EAAs) from presynaptic terminals, particularly glutamate, the primary excitatory neurotransmitter in the CNS. The active re-uptake of released EAAs from the synaptic space requires further energy, but the more deleterious effects of the widespread release of large amounts of glutamate are the result of the postsynaptic activation of α-amino-3-hydroxy-5-methyl-4-isoxazolepropionic acid (AMPA) and N-methyl-D-aspartate (NMDA) receptors channels. The activation of these receptors results in an influx of cations, with many injurious effects. Water passively follows the cations, giving rise to intracellular ("cytotoxic") oedema [76]. Ca^{2+}, the universal second messenger [77], floods in to cells, leading to indiscriminate activation of downstream Ca^{2+}-dependent enzymes. Activation of calpain and caspase proteases initiates apoptotic cascades [78–80]; wholesale activation of other proteases and phospholipases occurs, leading to the lysis of proteins and phospholipids critical to cell structure and survival [81]. Furthermore, the disordered intracellular ionic homeostasis contributes to mitochondrial dysfunction (see below), increases cellular ATP consumption as membrane ion pumps attempt to re-establish homeostasis, and can lead to propagation of depolarisation, as organised pathological neuronal discharge – i. e. seizures – or the more poorly understood process of cortical spreading depression [82,83]. These processes can, as a result of intact neurovascular coupling, be accompanied by large increases in CBF, which can propagate a deleterious cycle of intracranial hypertension and further ischaemia.

INFLAMMATION There is a wealth of experimental evidence, although only limited clinical evidence, that the inflammatory response that accompanies ABI predisposes to, causes and exacerbates injury. Whilst the inflammatory response to brain injury may have some neuroprotective effects, for example the development of ischaemic tolerance and promotion of tissue repair [84], inflammation can also cause cell death as result of oxidative stress, increased BBB permeability leading to oedema and intracranial hypertension, and induction of apoptosis [84–86].

OXIDATIVE STRESS Oxidative stress refers to the cytotoxic effects of ROS. Through both direct and indirect oxidation, peroxidation and nitration of deoxyribonucleic acid (DNA), protein and lipid, ROS are able to cause widespread cellular damage [87,88]. Three important processes generating ROS are as disordered mitochondrial metabolism, induction NO· generation by raised cytosolic Ca^{2+} levels and inflammation (see below).

In health, mitochondria generate ROS as a result of 'leakage' of electrons from the electron transport chain, whereby molecular oxygen is instead oxidised to yield superoxide ($O_2\cdot$). Under ischaemic conditions, factors such as raised intramitochondrial Ca^{2+} levels and mitochondrial decoupling/dysfunction conspire to increase this production [88–90].

NO· is an intriguing molecule; whilst a ROS, it is also a key mediator of cerebrovascular regulation, being involved in the mediation of several vasodilatory processes [91], including hypoxic vasodilation [92,93]. Dysregulation of NO· synthesis is a key component of disordered CA and DCI following SAH [94,95] and TBI [96]. Furthermore, NO· regulates oxidative phosphorylation through CCO inhibition [97,98]. The effects of NO· on CCO activity are complex and incompletely understood, but interactions between NO· and the Cu_B and haem $a_3$result in either inhibition of CCO activity or reduction of NO· to yield to non-reactive nitrite (NO_2^-) [99]; furthermore, these interactions may have spectral significance when using NIRS to measure CCO concentrations.

APOPTOSIS Apoptosis – programmed cell death – is a key cause of cell death following ABI and has been proposed as a therapeutic target [100].

Several of the secondary injury processes described above initiate apoptosis. Caspase activation occurs as a result mitochondrial lysis, opening of the mitochondrial transition pore and translocation of cytochrome *c* in to the cytosol [101–103]. ROS act as 'signalling' molecules, inducing apoptosis by a number of pathways, including by inhibition of DNA repair enzymes [104]. Apoptosis is extrinsically induced through activation of cell membrane 'death receptors' such as the TNF-R (tumour necrosis factor receptor) [84].

After both severe traumatic brain injury (sTBI) and aSAH, evidence for the importance of apoptosis is gleaned primarily from experimental models rather than clinical studies. Following experimental SAH, apoptosis has been implicated as both a key process in the early phase following injury [23] and as a part of DCI [60]. Following experimental TBI, increasing injury severity is associated with an increase in the proportion of cell death caused by necrosis rather than apoptosis [105]. Indeed, it has been suggested that there is a continuum between apoptosis and necrosis, with increasing injury severity predisposing to the latter [106].

2.3 NEUROCRITICAL CARE MANAGEMENT OF ABI

The NCCU management of ABI is a vast subject beset with controversy and widely differing approaches to clinical management. This section is not intended to be a comprehensive review of the clinical management of ABI; recent consensus guidelines for the management of TBI [107, 108] and SAH [61, 109] collate the evidence for

nearly all aspects of clinical management of ABI, from feeding to invasive intracranial monitoring to prophylaxis against thromboembolism. Rather, having established the pivotal role of CH-I in the pathophysiology of ABI, the aim of this section of the thesis is to review strategies for the identification, prevention and correction of CH-I after ABI.

As discussed in Section 2.2.2, cascades leading to cell death are initiated by reductions in cellular O_2 delivery, increases in cellular O_2 utilisation and reductions in the *ability* to utilise the O_2 that *is* delivered. Attempts to treat ABI by targeting the individual injury processes have proved, on the whole, unsuccessful. Examples of failed therapeutic strategies include attempts to prevent excitotoxicity through the use of NMDA antagonists [110–112]; the use of anti-inflammatory glucocorticoids in TBI [113], and the use of anti-oxidant drugs to prevent oxidative stress from ROS [110]. Attempting to attenuate mitochondrial dysfunction forms another therapeutic avenue; ciclosporin has been used in this regard, but is in early stages of human testing, with safety and dose-finding studies complete, but Phase II clinical trials awaited [114,115].

Following aSAH, trials aimed at the prevention of DCI have also proven disappointing, with only nimodipine being of proven benefit [10,116]; it has been suggested that an overemphasis on vasospasm, rather than other causes of secondary brain injury, has hampered attempts to improve outcome following aSAH [117].

In the face of these failures, the approach to neurocritical care management advocated by consensus guidelines is predicated on the *prevention* of CH-I by the maintenance of appropriate systemic physiological conditions like ABP and P_aO_2, the *identification* of CH-I by specific cerebral monitoring, and the *correction* of CH-I by employing clinical manoeuvres to reduce cerebral O_2 utilisation and increase cerebral O_2 delivery.

The epidemiological studies outlined in Section 2.2.2 establish the importance of maintaining systemic parameters such as ABP and P_aO_2 at physiological levels following ABI. However, in some clinical scenarios – e. g. in the case of concomitant cardiopulmonary pathology – it is impossible to do, and thus desirable to establish whether a lower threshold of cerebral oxygen delivery (DO_2) is adequate for the prevention of CH-I and secondary brain injury. Conversely, in some situations, the maintenance of normal physiological levels of parameters such as ABP and P_aO_2 is inadequate for the prevention of CH-I and secondary brain injury. In these situations, it is necessary to monitor the brain for CH-I.

2.3.1 *Detection of CH-I: Cerebral monitoring*

In addition to standard systemic monitoring – invasive ABP, arterial blood gases (ABGs), electrocardiography, inspired/expired gas partial pressures and pulse oximetry – a defining characteristic of neurocritical care is the use of bedside monitoring techniques to minimise secondary injury. Not considered here are the wealth of imaging techniques that are able to characterise cerebral structure, haemodynamics and metabolism with

great spatial resolution [118], but require the transfer of patients to remote radiology suites and are thus inappropriate for the minute-to-minute monitoring of critically-ill patients.

MODALITY	ADVANTAGES	DISADVANTAGES
ICP	Relatively inexpensive	Single RCT shows no superiority to imaging + clinical examination
	Well-established and advocated by consensus guidelines	Not a direct marker of ischaemia – only measures surrogates and epiphenomena
	Continuous	
$P_{br}O_2$	Familiar physiological concept	Likely to represent oxygen delivery, but not necessarily utilisation
	Proven prognostic value	No RCT evidence to support utility
	Focal	Invasive & unable to monitor for remote insults
	Continuous	
Microdialysis	Able to measure parameters of physiological and biochemical importance	Cumbersome
	Focal	Invasive & unable to monitor for remote insults
		Intermittent
TCD	Measurement of CBF	Relative changes only
	Non-invasive, non-ionising	Operator dependent, unable to monitor in 10% of cases
	Continuous	Sensitivity to movement artefact makes ambulatory monitoring difficult

Table 2.2 – Monitoring modalities, their advantages and limitations

INTRACRANIAL PRESSURE Following ABI, ICP is frequently measured. Following sTBI, ICP-monitoring is generally accepted as 'a relatively low-risk, high-yield and value for money intervention' [119]; this evidence has been extrapolated to patients with ICH [120]. Following SAH the role of ICP-monitoring is less well defined [109,121].

ICP can be easily monitored by an implanted intracranial microtransducer catheter or by ventriculostomy , with a relatively low complication rate [119]. The rationale behind ICP monitoring is based on three hypotheses: that uncontrolled intracranial hypertension leads to brain herniation, that intracranial hypertension itself is an epiphenomenon indicating ongoing secondary brain injury, and that therapy aimed at the maintenance of adequate CPP – which depends on ICP measurement – can avoid cerebral ischaemia.

The relationship between intracranial hypertension and poor outcome has been established for over three decades [122], yet the data regarding the clinical benefit of

ICP monitoring following TBI are mixed: studies can be found to support the hypothesis that ICP monitoring is associated with improved, unchanged, or poorer patient survival (e. g. [123–126]. While a large systematic review of 98 studies with a total of >41,000 patients suggests that the use of treatment regimens incorporating ICP monitoring is associated with a reduction in mortality and poor outcome [127], the only RCT evaluating the utility of ICP- and CPP-based management strategies has showed no improvement in a composite outcome of survival and functional recovery [128]. This trial, however, does not refute the notion that ICP-monitoring is a useful exercise, as post-hoc analyses revealed a significant reduction in the required treatment intensity in the ICP-monitored patients [128].

Whilst complex analysis of the measured ICP signal can be used to identify waveforms associated with poor outcome, it is also possible to derive indices describing pathophysiological perturbations in CA and cerebral compliance [51,119,129–131]. However, even such analyses do not explain the consistent finding that many patients with intracranial hypertension go on to achieve a good outcome, whilst many patients *without* intracranial hypertension fail to do so. There must, therefore, be aspects of secondary brain injury that are inadequately reflected in changes in ICP after ABI, and that adequate CPP is an insufficient measure of cerebral perfusion. These realisations that have prompted investigation in to alternative monitoring modalities.

CEREBRAL BLOOD FLOW Despite the difficulty in establishing absolute CBF thresholds for the definition of CH-I (see Section 2.2.2 above), the ability to monitor CBF in order to identify and prevent secondary brain injury remains an attractive prospect. However, while imaging techniques such as single photon emission computed tomography (SPECT), PET and Xenon-enhanced CT imaging can provide snapshots of CBF (SPECT and PET in absolute terms, Xenon-enhanced CT in relative terms), the ability to monitor CBF continuously at the bedside has proved more difficult. Whilst it is possible to estimate or approximate relative changes in CBF indirectly through other monitoring modalities such as jugular venous haemoglobin saturation ($SjvO_2$), NIRS or invasive $P_{br}O_2$ monitoring, the two main modalities that can be used to directly estimate CBF at the bedside are TCD and invasive measurement of CBF by the placement of a proprietary catheter based on thermal diffusion [132,133]. The latter, the Hemedex Bowman Perfusion Monitor® has not found widespread clinical use, so only TCD is considered here in more detail.

TCD is a non-invasive sonographic technique that, in common with all ultrasound Doppler measures, is based on the use of a pulsed-Doppler ultrasonic beam. Ultrasound waves from a combined emitter/transducer are transmitted through a 'window' in the skull. The foramen magnum window is used to insonate the posterior circulation and the orbital (i. e. trans-occular) window is used to insonate the ACAs. However, it is the temporal window, an area found 2cm above by a line drawn from the tragus to the

lateral canthus of the eye that is most frequently used [132]; insonating through this window it is possible to measure flow velocity in the terminal carotid, anterior cerebral, middle cerebral and posterior communicating arteries. The MCA is the most frequently insonated vessel, chiefly as it is the easiest to insonate via the temporal window, and is clinically important, carrying 50-60% of blood from its ipsilateral internal carotid [134].

Normal values for TCD-measured middle cerebral artery flow velocity (V_{MCA}) vary between 35-90 $cm.s^{-1}$, with a high level of intra- and inter-subject variation; this is ascribed to variability in MCA diameter and angle of insonation, rather representing differences in CBF . Following ABI, the use of TCD has been described in a number of scenarios, but the identification of DCI/vasospasm following aSAH is the single scenario where it has found greatest utility. Elevated V_{MCA} values (of above 120–140 $cm.s^{-1}$) are a specific, but not entirely sensitive marker of vasospasm when compared to DSA, and rapid increases in V_{MCA} are associated with outcome. However, the interpretation of V_{MCA} values is difficult, and multifactorial, depending on a number of factors including P_aCO_2, blood haemoglobin levels and levels of sedation, in addition to the issue of large intra/intersubject variability described above [132]. Consequently, it is difficult to interpret single 'spot readings' of V_{MCA}, but ambulatory TCD recording of V_{MCA} can characterise changes in CBF during the length of recording.

BRAIN OXYGENATION The central role of CH-I in the pathophysiology of secondary brain injury underpins the rationale for monitoring brain oxygenation. Two recognised techniques use for the identification of brain tissue hypoxia are jugular venous oximetry and $P_{br}O_2$ measurement [135]; another method of brain oximetry, NIRS, is discussed in detail in Chapter 3.

Jugular venous oximetry is an invasive procedure that measures $SjvO_2$, achieved through the retrograde catheterisation of the dominant internal jugular vein, and subsequent continuous measurement of $SjvO_2$ by fibre optic oximetry [136]. $SjvO_2$ reflects, the global balance between cerebral oxygen utilisation and delivery [137]. Following TBI, the occurrence of jugular venous desaturation is associated with poor outcome [138] and whilst it has been proposed that $SjvO_2$ monitoring may be useful in guiding therapy [136], difficulty in establishing ischaemic thresholds, insensitivity to focal ischaemia and poor reliability have mitigated against its more widespread adoption [139,140].

Conversely, $P_{br}O_2$ monitoring is a means of focal monitoring of cerebral oxygenation that is finding increasingly widespread clinical utility. The LiCox® (Integra Life Sciences, Plainsboro, NJ) system for $P_{br}O_2$ measurement is the commercially available clinical apparatus in most widespread use for the measurement of $P_{br}O_2$ currently. LiCox catheters consist of a Clarke-type electrode [141] that are inserted in to brain parenchyma at craniotomy, via a burr hole or via a "bolt" fixation device. Measurement

in healthy animals has revealed normal $P_{br}O_2$ values between 29–42 mmHg, while human measurements acquired during neurosurgery and from 'normal-appearing' brain following TBI have revealed values between 37–48 mmHg [135].

Various thresholds for the identification of brain tissue hypoxia (BTH) have been proposed. Following TBI, observational studies have linked $P_{br}O_2$ values of <5 mmHg with poor outcome following TBI [142], while one study used regression analysis have associated a higher risk of death with the amount of time spent with $P_{br}O_2$ <20 mmHg, or the occurrence of <6 mmHg at any point [143]. Another study suggested various time-hypoxia thresholds that were associated with a higher (>50%) mortality rate, varying from <5 mmHg x 30 minutes to 10–15 mmHg x 4 hours [144]. Whilst a number of studies have described the use of $P_{br}O_2$ monitoring after SAH, none has proposed a threshold for BTH [145–148]. A recent systematic review identified four cohort studies – using a mixture of historical and non-randomised, prospective controls – that suggest that the $P_{br}O_2$-guided therapy is associated with improved outcome following TBI, when compared to CPP-guided therapy alone [149]; an RCT is currently recruiting to further test this hypothesis [150].

One mixed blessing of $P_{br}O_2$ monitoring, however, is its focal nature. Following both TBI and SAH, patterns of ischaemia are heterogenous; data from cerebral microdialysis (CMD) studies confirms that remote ischaemia can go undetected by focal measurements carried out via an invasive catheter [151]; this heterogeneity is also observed in imaging studies [152]. The invasive nature of $P_{br}O_2$ monitoring necessarily limits the number of sites that can be measured, and thus while focal measurements can identify ischaemia that would go unnoticed by global measures, remote insults can go unnoticed [137]. Furthermore, it is unclear whether $P_{br}O_2$ monitoring adequately represents disorders of oxygen utilisation, as CBF has been shown to be the predominant determinant of $P_{br}O_2$ after ABI [147].

BRAIN TISSUE BIOCHEMISTRY Microdialysis (MD) relies on the principle of dialysis to produce a simulacrum of tissue extracellular fluid. The process, depicted in Figure 2.4, relies on a catheter lined with a semi-permeable membrane – the MD probe – which is implanted within brain tissue at craniotomy via a burr hole or skull bolt and continually infused with isotonic fluid – termed *perfusate*. Small molecules within the brain ECF undergo *recovery* – that is, they diffuse across the probe membrane – and the resulting fluid (*dialysate*) is collected for analysis either at the bedside or frozen for subsequent analysis [153].

The ability to measure the concentration of any molecule that will diffuse across the MD membrane has led to the suggestion that the MD probe is a "universal biosensor" [154]. However, three main groups of molecule are frequently measured after ABI: markers of oxidative metabolism (glucose, lactate and pyruvate), cell membrane damage

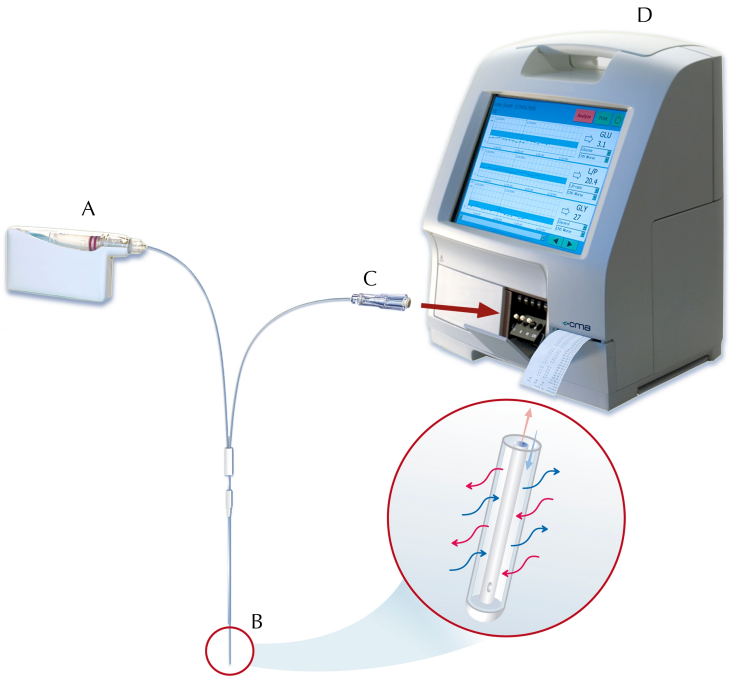

Figure 2.4 – Schematic representation of microdialysis apparatus. A - pump driving perfusate infusion; B - microdialysis catheter, to be implanted within cerebral parenchyma; C - microvial containing dialysate, collected for measurement of relevant D - bedside analyser.

(glycerol) and excitotoxicity (glutamate); only the first group of molecules is considered in more detail here.

Glucose, lactate and pyruvate play a central role in cellular metabolism – discussed in Section 1.3 – and CH-I is reflected by changes in their concentrations. However, as discussed in Section 1.3.2, lactate concentrations can rise in the absence of CH-I. As a consequence, the lactate:pyruvate ratio (LPR) is used as a measure of cellular energy state, as the LPR reflects the balance between (oxidised) NAD^+ and (reduced) NADH in the mitochondrial matrix [155], as given in the equation

$$\frac{[NAD][H+]}{[NAD]} = \frac{[Lactate]}{[Pyruvate]} \times K_{LDH}. \tag{2.2}$$

Frontal lobe measurement in patients undergoing surgery on posterior fossa lesions reveals a normal LPR to be <25 [156]. Following aSAH, LPR thresholds of 20–40 have been suggested for the identification of CH-I, based on correlation with patient clinical

state [157]. The prognostic value of microdialysis is well established: elevated LPR is associated with poor outcome following both TBI [158,159] and aSAH [160–162]. Microdialysis can also provide insights in to the pathophysiology of ABI: one combined PET-microdialysis study in patients following aSAH revealed clinically relevant metabolic derangements with CBF above the classical threshold of 20 $ml.100g^{-1}.min^{-1}$, highlighting the inadequacy of simple flow-based ischaemic thresholds; other studies have shown signs of metabolic crises in the absence of PET-defined ischaemia [163] and independently of CPP [164], both underlining the fact that an inability to utilise delivered substrate is a key feature of ABI.

As in invasive $P_{br}O_2$ monitoring, the position of microdialysis catheter placement is of great importance: placement in normal (as opposed to injured) tissue creates the risk of insensitivity to ischaemia [151]. Furthermore, the interpretation of microdialysate chemistry at the bedside is complex: the clinician is presented with a multitude of biochemical variables and a systematic approach to their interpretation is necessary [154]. However, even when utilising such an approach, current commercial microdialysis apparatus allows a minimum sampling period of 15 minutes, a significantly lower temporal resolution than the other modalities described above. Furthermore, there have been no prospective studies to suggest that clinical management paradigms based on microdialysis are associated with improved outcome. Thus, whilst microdialysis can provide important insights in to the pathophysiology of ABI and be a useful marker of cerebral ischaemia, it has not gained widespread clinical acceptance, despite a consensus meeting in 2002 suggesting that its adoption – and in particular, the measurement of LPR – in patients with aSAH and TBI who require ICP monitoring [165].

2.4 CONCLUSION

Following ABI, there are a multitude of injury processes that conspire to cause cell death, all interlinked in a sometimes recursive fashion; cerebral ischaemia results as a consequence of reductions of substrate delivery below critical thresholds, and yet these thresholds are difficult to define; metabolic dysfunction results functional ischaemia in the presence of otherwise adequate substrate delivery. The ideal clinical management strategies following ABI are unclear: a multitude of monitoring modalities exist and several have proven prognostic value, yet none has been proven to improve outcome. It is against this backdrop that we consider a further monitoring modality: near infrared spectroscopy.

REFERENCES

[1] Tennant, A. Admission to hospital following head injury in England: incidence and socio-economic associations. *BMC public health*, 5:21, 2005.

[2] Tagliaferri, F, Compagnone, C, Korsic, M, Servadei, F & Kraus, J. A systematic review of brain injury epidemiology in Europe. *Acta Neurochirurgica*, 148(3):255–68– discussion 268, 2006.

[3] Faul, M, Xu, L, Wald, MM & Coronado, VG. *Traumatic Brain Injury in the United States: Emergency Department Visits, Hospitalizations and Deaths 2002-2006*. Centers for Disease Control and Prevention, National Center for Injury Prevention and Control, Atlanta, GA, 2010.

[4] Yates, PJ, Williams, WH, Harris, A, Round, A & Jenkins, R. An epidemiological study of head injuries in a UK population attending an emergency department. *Journal of neurology, neurosurgery, and psychiatry*, 77(5):699–701, 2006.

[5] Murray, LS, Teasdale, GM, Murray, GD, Miller, DJ, Pickard, JD & Shaw, MD. Head injuries in four British neurosurgical centres. *British Journal of Neurosurgery*, 13(6):564–569, 1999.

[6] Murray, GD, Teasdale, GM, Braakman, R, Cohadon, F, Dearden, M, Iannotti, F, Karimi, A, Lapierre, F, Maas, A, Ohman, J, Persson, L, Servadei, F, Stocchetti, N, Trojanowski, T & Unterberg, A. The European Brain Injury Consortium survey of head injuries. *Acta Neurochirurgica*, 141(3):223–236, 1999.

[7] Polinder, S, Meerding, WJ, Mulder, S, Petridou, E, van Beeck, E & EUROCOST Reference Group. Assessing the burden of injury in six European countries. *Bulletin of the World Health Organization*, 85(1):27–34, 2007.

[8] Dikmen, SS, Machamer, JE, Powell, JM & Temkin, NR. Outcome 3 to 5 years after moderate to severe traumatic brain injury. *Archives of physical medicine and rehabilitation*, 84(10):1449–1457, 2003.

[9] de Rooij, NK, Linn, FHH, van der Plas, JA, Algra, A & Rinkel, GJE. Incidence of subarachnoid haemorrhage: a systematic review with emphasis on region, age, gender and time trends. *Journal of neurology, neurosurgery, and psychiatry*, 78(12):1365–1372, 2007.

[10] Pickard, JD, Murray, GD, Illingworth, R, Shaw, MD, Teasdale, GM, Foy, PM, Humphrey, PR, Lang, DA, Nelson, R & Richards, P. Effect of oral nimodipine on cerebral infarction and outcome after subarachnoid haemorrhage: British aneurysm nimodipine trial. *British Medical Journal*, 298(6674):636–642, 1989.

[11] Molyneux, A. International Subarachnoid Aneurysm Trial (ISAT) of neurosurgical clipping versus endovascular .... *The Lancet*, 2002.

[12] Feigin, VL, Lawes, CMM, Bennett, DA & Anderson, CS. Stroke epidemiology: a review of population-based studies of incidence, prevalence, and case-fatality in the late 20th century. *Lancet neurology*, 2(1):43–53, 2003.

[13] van Gijn, J, Kerr, RS & Rinkel, GJE. Subarachnoid haemorrhage. *Lancet*, 369(9558):306–318, 2007.

[14] Feigin, VL, Lawes, CM, Bennett, DA, Barker-Collo, SL & Parag, V. Worldwide stroke incidence and early case fatality reported in 56 population-based studies: a systematic review. *The Lancet Neurology*, 8(4):355–369, 2009.

[15] Murray, GD, Butcher, I, McHugh, GS, Lu, J, Mushkudiani, NA, Maas, AIR, Marmarou, A & Steyerberg, EW. Multivariable prognostic analysis in traumatic brain injury: results from the IMPACT study. *Journal of Neurotrauma*, 24(2):329–337, 2007.

[16] Rosen, DS & Macdonald, RL. Subarachnoid hemorrhage grading scales: a systematic review. *Neurocritical Care*, 2(2):110–118, 2005.

[17] Reilly, PL. Brain injury: the pathophysiology of the first hours.'Talk and Die' revisited. *Journal of clinical neuroscience*, 8(5):398–403, 2001.

[18] Werner, C & Engelhard, K. Pathophysiology of traumatic brain injury. *British Journal of Anaesthesia*, 99(1):4–9, 2007.

[19] Ostrowski, RP, Colohan, AR & Zhang, JH. Molecular mechanisms of early brain injury after subarachnoid hemorrhage. *Neurological research*, 28(4):399–414, 2006.

[20] Qureshi, AI, Mendelow, AD & Hanley, DF. Intracerebral haemorrhage. *Lancet*, 373(9675):1632–1644, 2009.

[21] Moustafa, RR & Baron, JC. Pathophysiology of ischaemic stroke: insights from imaging, and implications for therapy and drug discovery. *British journal of pharmacology*, 153 Suppl 1:S44–54, 2008.

[22] Tator, CH & Fehlings, MG. Review of the secondary injury theory of acute spinal cord trauma with emphasis on vascular mechanisms. *Journal of Neurosurgery*, 75(1):15–26, 1991.

[23] Cahill, J, Cahill, WJ, Calvert, JW, Calvert, JH & Zhang, JH. Mechanisms of early brain injury after subarachnoid hemorrhage. *Journal of cerebral blood flow and metabolism*, 26(11):1341–1353, 2006.

[24] Protheroe, RT & Gwinnutt, CL. Early hospital care of severe traumatic brain injury. *Anaesthesia*, 66(11):1035–1047, 2011.

[25] Ercole, A & Menon, DK. Traumatic brain injury. In Matta, BF, Menon, DK & Smith, M, eds., *Core Topics in Neuroanaesthesia and Neurointensive Care*, pp. 315–340. Cambridge University Press, 2011.

[26] Maas, AIR, Stocchetti, N & Bullock, R. Moderate and severe traumatic brain injury in adults. *Lancet neurology*, 7(8):728–741, 2008.

[27] Grote, E & Hassler, W. The critical first minutes after subarachnoid hemorrhage. *Neurosurgery*, 22(4):654–661, 1988.

[28] Miller, JD & Becker, DP. Secondary insults to the injured brain. *Journal of the Royal College of Surgeons of Edinburgh*, 27(5):292–298, 1982.

[29] Miller, JD, Sweet, RC, Narayan, R & Becker, DP. Early Insults to the Injured Brain. *Journal of the American Medical Association*, 240(5):439–442, 1978.

[30] Claassen, J, Vu, A, Kreiter, KT, Kowalski, RG, Du, EY, Ostapkovich, N, Fitzsimmons, BFM, Connolly, ES & Mayer, SA. Effect of acute physiologic derangements on outcome after subarachnoid hemorrhage*. *Critical care medicine*, 32(3):832–838, 2004.

[31] Spiotta, AM, Provencio, JJ, Rasmussen, PA & Manno, E. Brain Monitoring After Subarachnoid Hemorrhage: Lessons Learned. *Neurosurgery*, 69(4):755–766, 2011.

[32] Janjua, N & Mayer, SA. Cerebral vasospasm after subarachnoid hemorrhage. *Current Opinion in Critical Care*, 9(2):113–119, 2003.

[33] Macdonald, RL, Pluta, RM & Zhang, JH. Cerebral vasospasm after subarachnoid hemorrhage: the emerging revolution. *Nature Clinical Practice Neurology*, 3(5):256–263, 2007.

[34] Smith, M. Intensive care management of patients with subarachnoid haemorrhage. *Current Opinion in Anaesthesiology*, 20(5):400–407, 2007.

[35] Rabinstein, AA. Secondary brain injury after aneurysmal subarachnoid haemorrhage: more than vasospasm. *Lancet neurology*, 10(7):593–595, 2011.

[36] Lee, KH, Lukovits, T & Friedman, JA. "Triple-H" Therapy for Cerebral Vasospasm Following Subarachnoid Hemorrhage. *Neurocritical Care*, 4(1):068–076, 2006.

[37] van Gijn, J & Rinkel, G. Subarachnoid haemorrhage: diagnosis, causes and management. *Brain*, 2001.

[38] Hossmann, KA. Viability thresholds and the penumbra of focal ischemia. *Annals of neurology*, 36(4):557–565, 1994.

[39] Zauner, A, Daugherty, WP, Bullock, MR & Warner, DS. Brain oxygenation and energy metabolism: part I-biological function and pathophysiology. *Neurosurgery*, 51(2):289–301; discussion 302, 2002.

[40] Grubb, RL, Raichle, ME, Eichling, JO & Gado, MH. Effects of subarachnoid hemorrhage on cerebral blood volume, blood flow, and oxygen utilization in humans. *Journal of Neurosurgery*, 46(4):446–453, 1977.

[41] Cunningham, AS, Salvador, R, Coles, JP, Chatfield, DA, Bradley, PG, Johnston, AJ, Steiner, LA, Fryer, TD, Aigbirhio, FI, Smielewski, P, Williams, GB, Carpenter, TA, Gillard, JH, Pickard, JD & Menon, DK. Physiological thresholds for irreversible tissue damage in contusional regions following traumatic brain injury. *Brain*, 128(Pt 8):1931–1942, 2005.

[42] Hayashi, T, Suzuki, A, Hatazawa, J, Kanno, I, Shirane, R, Yoshimoto, T & Yasui, N. Cerebral circulation and metabolism in the acute stage of subarachnoid hemorrhage. *Journal of Neurosurgery*, 93(6):1014–1018, 2000.

[43] Jaggi, JL, Obrist, WD, Gennarelli, TA & Langfitt, TW. Relationship of early cerebral blood flow and metabolism to outcome in acute head injury. *Journal of Neurosurgery*, 72(2):176–182, 1990.

[44] Wartenberg, KE & Mayer, SA. Medical complications after subarachnoid hemorrhage: new strategies for prevention and management. *Current Opinion in Critical Care*, 12(2):78–84, 2006.

[45] Solenski, NJ, Haley, EC, Kassell, NF, Kongable, G, Germanson, T, Truskowski, L & Torner, JC. Medical complications of aneurysmal subarachnoid hemorrhage: a report of the multicenter, cooperative aneurysm study. Participants of the Multicenter Cooperative Aneurysm Study. *Critical care medicine*, 23(6):1007–1017, 1995.

[46] Salim, A, Hadjizacharia, P, Brown, C, Inaba, K, Teixeira, PGR, Chan, L, Rhee, P & Demetriades, D. Significance of Troponin Elevation After Severe Traumatic Brain Injury. *The Journal of trauma*, 64(1):46–52, 2008.

[47] Bahloul, M, Chaari, AN, Kallel, H, Khabir, A, Ayadi, A, Charfeddine, H, Hergafi, L, Chaari, AD, Chelly, HE, Ben Hamida, C, Rekik, N & Bouaziz, M. Neurogenic pulmonary edema due to traumatic brain injury: evidence of cardiac dysfunction. *American journal of critical care*, 15(5):462–470, 2006.

[48] Piek, J, Chesnut, RM, Marshall, LF, van Berkum Clark, M, Klauber, MR, Blunt, BA, Eisenberg, HM, Jane, JA, Marmarou, A & Foulkes, MA. Extracranial complications of severe head injury. *Journal of Neurosurgery*, 77(6):901–907, 1992.

[49] Baumann, A, Audibert, G, McDonnell, J & Mertes, PM. Neurogenic pulmonary edema. *Acta anaesthesiologica Scandinavica*, 51(4):447–455, 2007.

[50] Mascia, L & Andrews, PJ. Acute lung injury in head trauma patients. *Intensive Care Medicine*, 24(10):1115–1116, 1998.

[51] Czosnyka, M, Smielewski, P, Kirkpatrick, P, Laing, RJ, Menon, D & Pickard, JD. Continuous assessment of the cerebral vasomotor reactivity in head injury. *Neurosurgery*, 41(1):11–7; discussion 17–9, 1997.

[52] Czosnyka, M, Smielewski, P, Piechnik, S, Steiner, LA & Pickard, JD. Cerebral autoregulation following head injury. *Journal of Neurosurgery*, 95(5):756–763, 2001.

[53] Soehle, M, Czosnyka, M, Pickard, J & Kirkpatrick, P. Continuous Assessment of Cerebral Autoregulation in Subarachnoid Hemorrhage. *Anesthesia & Analgesia*, 2004.

[54] Rasulo, FA, Girardini, A, Lavinio, A, De Peri, E, Stefini, R, Cenzato, M, Nodari, I & Latronico, N. Are optimal cerebral perfusion pressure and cerebrovascular autoregulation related to long-term outcome in patients with aneurysmal subarachnoid hemorrhage? *Journal of Neurosurgical Anesthesiology*, 24(1):3–8, 2012.

[55] Armonda, RA, Bell, RS, Vo, AH, Ling, G, DeGraba, TJ, Crandall, B, Ecklund, J & Campbell, WW. Wartime traumatic cerebral vasospasm: recent review of combat casualties. *Neurosurgery*, 59(6):1215–25; discussion 1225, 2006.

[56] Czosnyka, M & Pickard, JD. Monitoring and interpretation of intracranial pressure. *Journal of neurology, neurosurgery, and psychiatry*, 75(6):813–821, 2004.

[57] Greenberg, MS. Coma. In *Handbook of Neurosurgery*, 6th ed., pp. 154–163. Thieme, New York, 2006.

[58] Kassell, NF, Torner, JC, Haley, EC, Jane, JA, Adams, HP & Kongable, GL. The International Cooperative Study on the Timing of Aneurysm Surgery. Part 1: Overall management results. *Journal of Neurosurgery*, 73(1):18–36, 1990.

[59] Sen, J, Belli, A, Albon, H, Morgan, L, Petzold, A & Kitchen, N. Triple-H therapy in the management of aneurysmal subarachnoid haemorrhage. *Lancet neurology*, 2(10):614–621, 2003.

[60] Al-Tamimi, YZ, Orsi, NM, Quinn, AC, Homer-Vanniasinkam, S & Ross, SA. A review of delayed ischemic neurologic deficit following aneurysmal subarachnoid hemorrhage: historical overview, current treatment, and pathophysiology. *World Neurosurgery*, 73(6):654–667, 2010.

[61] Diringer, MN, Bleck, TP, Claude Hemphill, J, Menon, D, Shutter, L, Vespa, P, Bruder, N, Connolly, ES, Citerio, G, Gress, D, Hänggi, D, Hoh, BL, Lanzino, G, Le Roux, P, Rabinstein, A, Schmutzhard, E, Stocchetti, N, Suarez, JI, Treggiari, M, Tseng, MY, Vergouwen, MDI, Wolf, S & Zipfel, G. Critical Care Management of Patients Following Aneurysmal Subarachnoid Hemorrhage: Recommendations from the Neurocritical Care Society's Multidisciplinary Consensus Conference. *Neurocritical Care*, 2011.

[62] Sarrafzadeh, AS, Sakowitz, OW, Kiening, KL, Benndorf, G, Lanksch, WR & Unterberg, AW. Bedside microdialysis: a tool to monitor cerebral metabolism in subarachnoid hemorrhage patients? *Critical care medicine*, 30(5):1062–1070, 2002.

[63] Frontera, JA, Fernandez, A, Schmidt, JM, Claassen, J, Wartenberg, KE, Badjatia, N, Connolly, ES & Mayer, SA. Defining vasospasm after subarachnoid hemorrhage: what is the most clinically relevant definition? *Stroke*, 40(6):1963–1968, 2009.

[64] Minhas, PS, Menon, DK, Smielewski, P, Czosnyka, M, Kirkpatrick, PJ, Clark, JC & Pickard, JD. Positron Emission Tomographic Cerebral Perfusion Disturbances and Transcranial Doppler Findings among Patients with Neurological Deterioration after Subarachnoid Hemorrhage. *Neurosurgery*, 52(5):1017–22– discussion 1022–4, 2003.

[65] Clyde, BL, Resnick, DK, Yonas, H, Smith, HA & Kaufmann, AM. The relationship of blood velocity as measured by transcranial doppler ultrasonography to cerebral blood flow as determined by stable xenon computed tomographic studies after aneurysmal subarachnoid hemorrhage. *Neurosurgery*, 38(5):896–904– discussion 904–5, 1996.

[66] Macdonald, RL, Kassell, NF, Mayer, S, Ruefenacht, D, Schmiedek, P, Weidauer, S, Frey, A, Roux, S, Pasqualin, A & CONSCIOUS-1 Investigators. Clazosentan to overcome neurological ischemia and infarction occurring after subarachnoid hemorrhage (CONSCIOUS-1): randomized, double-blind, placebo-controlled phase 2 dose-finding trial. *Stroke*, 39(11):3015–3021, 2008.

[67] Brown, RJ, Kumar, A, Dhar, R, Sampson, TR & Diringer, MN. The Relationship Between Delayed Infarcts and Angiographic Vasospasm After Aneurysmal Subarachnoid Hemorrhage. *Neurosurgery*, 2013.

[68] Vergouwen, MDI, Ilodigwe, D & Macdonald, RL. Cerebral infarction after subarachnoid hemorrhage contributes to poor outcome by vasospasm-dependent and -independent effects. *Stroke*, 42(4):924–929, 2011.

[69] Lifshitz, J, Sullivan, PG, Hovda, DA, Wieloch, T & McIntosh, TK. Mitochondrial damage and dysfunction in traumatic brain injury. *Mitochondrion*, 4(5-6):705–713, 2004.

[70] Colicos, MA & Dash, PK. Apoptotic morphology of dentate gyrus granule cells following experimental cortical impact injury in rats: possible role in spatial memory deficits. *Brain research*, 739(1-2):120–131, 1996.

[71] Povlishock, JT. Traumatically induced axonal damage without concomitant change in focally related neuronal somata and dendrites. *Acta neuropathologica*, 70(1):53–59, 1986.

[72] Lifshitz, J, Friberg, H, Neumar, RW, Raghupathi, R, Welsh, FA, Janmey, P, Saatman, KE, Wieloch, T, Grady, MS & McIntosh, TK. Structural and functional damage sustained by mitochondria after traumatic brain injury in the rat: evidence for differentially sensitive populations in the cortex and hippocampus. *Journal of Cerebral Blood Flow & Metabolism*, 23(2):219–231, 2003.

[73] Susin, SA, Zamzami, N & Kroemer, G. Mitochondria as regulators of apoptosis: doubt no more. *Biochimica et biophysica acta*, 1366(1-2):151–165, 1998.

[74] Sullivan, PG, Dubé, C, Dorenbos, K, Steward, O & Baram, TZ. Mitochondrial uncoupling protein-2 protects the immature brain from excitotoxic neuronal death. *Annals of neurology*, 53(6):711–717, 2003.

[75] Zipfel, GJ, Babcock, DJ, Lee, JM & Choi, DW. Neuronal apoptosis after CNS injury: the roles of glutamate and calcium. *Journal of Neurotrauma*, 17(10):857–869, 2000.

[76] Liang, D, Bhatta, S, Gerzanich, V & Simard, JM. Cytotoxic edema: mechanisms of pathological cell swelling. *Neurosurgical focus*, 22(5):E2, 2007.

[77] Berridge, MJ, Lipp, P & Bootman, MD. The versatility and universality of calcium signalling. *Nature Reviews Molecular Cell Biology*, 1(1):11–21, 2000.

[78] Kampfl, A, Posmantur, RM, Zhao, X, Schmutzhard, E, Clifton, GL & Hayes, RL. Mechanisms of calpain proteolysis following traumatic brain injury: implications for pathology and therapy: implications for pathology and therapy: a review and update. *Journal of Neurotrauma*, 14(3):121–134, 1997.

[79] McIntosh, TK, Saatman, KE, Raghupathi, R, Graham, DI, Smith, DH, Lee, VM & Trojanowski, JQ. The Dorothy Russell Memorial Lecture. The molecular and cellular sequelae of experimental traumatic brain injury: pathogenetic mechanisms. *Neuropathology and Applied Neurobiology*, pp. 251–267, 1998.

[80] Eldadah, BA & Faden, AI. Caspase pathways, neuronal apoptosis, and CNS injury. *Journal of Neurotrauma*, 17(10):811–829, 2000.

[81] Kwiatkowski, DJ. Functions of gelsolin: motility, signaling, apoptosis, cancer. *Current opinion in cell biology*, 11(1):103–108, 1999.

[82] Dreier, JP, Major, S, Manning, A, Woitzik, J, Drenckhahn, C, Steinbrink, J, Tolias, C, Oliveira-Ferreira, AI, Fabricius, M, Hartings, JA, Vajkoczy, P, Lauritzen, M, Dirnagl, U, Bohner, G, Strong, AJ & study group, C. Cortical spreading ischaemia is a novel process involved in ischaemic damage in patients with aneurysmal subarachnoid haemorrhage. *Brain*, 132(Pt 7):1866–1881, 2009.

[83] Strong, AJ, Hartings, JA & Dreier, JP. Cortical spreading depression: an adverse but treatable factor in intensive care? *Current Opinion in Critical Care*, 13(2):126–133, 2007.

[84] Kunz, A, Dirnagl, U & Mergenthaler, P. Acute pathophysiological processes after ischaemic and traumatic brain injury. *Best practice & research Clinical anaesthesiology*, 24(4):495–509, 2010.

[85] Denes, A, Thornton, P, Rothwell, NJ & Allan, SM. Inflammation and brain injury: Acute cerebral ischaemia, peripheral and central inflammation. *Brain, Behavior, and Immunity*, 24(5):708–723, 2010.

[86] Ghirnikar, RS, Lee, YL & Eng, LF. Inflammation in traumatic brain injury: role of cytokines and chemokines. *Neurochemical research*, 23(3):329–340, 1998.

[87] Alvarez, B & Radi, R. Peroxynitrite reactivity with amino acids and proteins. *Amino acids*, 25(3-4):295–311, 2003.

[88] Halliwell, B. Oxidative stress and neurodegeneration: where are we now? *Journal of Neurochemistry*, 97(6):1634–1658, 2006.

[89] Turrens, JF. Mitochondrial formation of reactive oxygen species. *The Journal of Physiology*, 552(Pt 2):335–344, 2003.

[90] Lewén, A, Matz, P & Chan, PH. Free radical pathways in CNS injury. *Journal of Neurotrauma*, 17(10):871–890, 2000.

[91] Pacher, P, Beckman, JS & Liaudet, L. Nitric oxide and peroxynitrite in health and disease. *Physiological reviews*, 87(1):315–424, 2007.

[92] Palacios-Callender, M, Hollis, V, Mitchison, M, Frakich, N, Unitt, D & Moncada, S. Cytochrome c oxidase regulates endogenous nitric oxide availability in respiring cells: a possible explanation for hypoxic vasodilation. *Proceedings of the National Academy of Sciences of the United States of America*, 104(47):18508–18513, 2007.

[93] Van Mil, AHM, Spilt, A, Van Buchem, MA, Bollen, ELEM, Teppema, L, Westendorp, RGJ & Blauw, GJ. Nitric oxide mediates hypoxia-induced cerebral vasodilation in humans. *Journal of Applied Physiology*, 92(3):962–966, 2002.

[94] Keyrouz, SG & Diringer, MN. Clinical review: Prevention and therapy of vasospasm in subarachnoid hemorrhage. *Critical care*, 11(4):220, 2007.

[95] Pluta, RM. Delayed cerebral vasospasm and nitric oxide: review, new hypothesis, and proposed treatment. *Pharmacology & therapeutics*, 105(1):23–56, 2005.

[96] Hlatky, R, Goodman, JC, Valadka, AB & Robertson, CS. Role of Nitric Oxide in Cerebral Blood Flow Abnormalities After Traumatic Brain Injury. *Journal of Cerebral Blood Flow & Metabolism*, pp. 582–588, 2003.

[97] Brunori, M. Nitric oxide, cytochrome-c oxidase and myoglobin. *Trends in biochemical sciences*, 26(1):21–23, 2001.

[98] Brunori, M, Giuffrè, A, Forte, E, Mastronicola, D, Barone, MC & Sarti, P. Control of cytochrome c oxidase activity by nitric oxide. *Biochimica et biophysica acta*, 1655(1-3):365–371, 2004.

[99] Cooper, CE. Nitric oxide and cytochrome oxidase: substrate, inhibitor or effector? *Trends in biochemical sciences*, 27(1):33–39, 2002.

[100] Zhang, X, Chen, Y, Jenkins, LW, Kochanek, PM & Clark, RSB. Bench-to-bedside review: Apoptosis/programmed cell death triggered by traumatic brain injury. *Critical care*, 9(1):66–75, 2005.

[101] Kluck, RM, Bossy-Wetzel, E, Green, DR & Newmeyer, DD. The release of cytochrome c from mitochondria: a primary site for Bcl-2 regulation of apoptosis. *Science*, 275(5303):1132–1136, 1997.

[102] Sullivan, PG, Keller, JN, Bussen, WL & Scheff, SW. Cytochrome c release and caspase activation after traumatic brain injury. *Brain research*, 949(1-2):88–96, 2002.

[103] Green, DR & Kroemer, G. The pathophysiology of mitochondrial cell death. *Science*, 305(5684):626–629, 2004.

[104] Chan, PH. Reactive oxygen radicals in signaling and damage in the ischemic brain. *Journal of Cerebral Blood Flow & Metabolism*, 21(1):2–14, 2001.

[105] Raghupathi, R. Cell death mechanisms following traumatic brain injury. *Brain pathology*, 14(2):215–222, 2004.

[106] Ankarcrona, M, Dypbukt, JM, Bonfoco, E, Zhivotovsky, B, Orrenius, S, Lipton, SA & Nicotera, P. Glutamate-induced neuronal death: a succession of necrosis or apoptosis depending on mitochondrial function. *Neuron*, 15(4):961–973, 1995.

[107] Bratton, SL, Chestnut, RM, Ghajar, J, Hammond, FFM, Harris, OA, Hartl, R, Manley, GT, Nemecek, A, Newell, DW, Rosenthal, G, Schouten, J, Shutter, L, Timmons, SD, Ullman, JS, Videtta, W, Wilberger, JE & Wright, DW. Guidelines for the management of severe traumatic brain injury. *Journal of Neurotrauma*, 24 Suppl 1:S1–106, 2007.

[108] Maas, AI, Dearden, M, Teasdale, GM, Braakman, R, Cohadon, F, Iannotti, F, Karimi, A, Lapierre, F, Murray, G, Ohman, J, Persson, L, Servadei, F, Stocchetti, N & Unterberg, A. EBIC-guidelines for management of severe head injury in adults. European Brain Injury Consortium. *Acta Neurochirurgica*, 139(4):286–294, 1997.

[109] Connolly, ES, Rabinstein, AA, Carhuapoma, JR, Derdeyn, CP, Dion, J, Higashida, RT, Hoh, BL, Kirkness, CJ, Naidech, AM, Ogilvy, CS, Patel, AB, Thompson, BG, Vespa, P & on behalf of the American Heart Association Stroke Council, Council on Cardiovascular Radiology and Intervention, Council on Cardiovascular Nursing, Council on Cardiovascular Surgery and Anesthesia, and Council on Clinical Cardiology. Guidelines for the Management of Aneurysmal Subarachnoid Hemorrhage: A Guideline for Healthcare Professionals From the American Heart Association/American Stroke Association. *Stroke*, 43(6):1711–1737, 2012.

[110] Narayan, RK, Michel, ME, Ansell, B, Baethmann, A, Biegon, A, Bracken, MB, Bullock, MR, Choi, SC, Clifton, GL, Contant, CF, Coplin, WM, Dietrich, WD, Ghajar, J, Grady, SM, Grossman, RG, Hall, ED, Heetderks, W, Hovda, DA, Jallo, J, Katz, RL, Knoller, N, Kochanek, PM, Maas, AI, Majde, J, Marion, DW, Marmarou, A, Marshall, LF, McIntosh, TK, Miller, E, Mohberg, N, Muizelaar, JP, Pitts, LH, Quinn, P, Riesenfeld, G, Robertson, CS, Strauss, KI, Teasdale, G, Temkin, N, Tuma, R, Wade, C, Walker, MD, Weinrich, M, Whyte, J, Wilberger, J, Young, AB & Yurkewicz, L. Clinical trials in head injury. In *Journal of neurotrauma*, pp. 503–557. Department of Neurosurgery, Temple University Hospital, Philadelphia, Pennsylvania 19140, USA. Narayan@nimbus.temple.edu, 2002.

[111] Wong, GKC, Poon, WS, Chan, MTV, Boet, R, Gin, T, Ng, SCP, Zee, BCY & Investigators, I. Intravenous magnesium sulphate for aneurysmal subarachnoid hemorrhage (IMASH): a randomized, double-blinded, placebo-controlled, multicenter phase III trial. *Stroke*, 41(5):921–926, 2010.

[112] Ikonomidou, C & Turski, L. Why did NMDA receptor antagonists fail clinical trials for stroke and traumatic brain injury? *Lancet neurology*, 1(6):383–386, 2002.

[113] Roberts, I, Yates, D, Sandercock, P, Farrell, B, Wasserberg, J, Lomas, G, Cottingham, R, Svoboda, P, Brayley, N, Mazairac, G, Laloë, V, Muñoz-Sánchez, A, Arango, M, Hartzenberg, B, Khamis, H, Yutthakasemsunt, S, Komolafe, E, Olldashi, F, Yadav, Y, Murillo-Cabezas, F, Shakur, H, Edwards, P & CRASH Trial Collaborators. Effect of intravenous corticosteroids on death within 14 days in 10008 adults with clinically significant head injury (MRC CRASH trial): randomised placebo-controlled trial. *Lancet*, 364(9442):1321–1328, 2004.

[114] Mazzeo, AT, Brophy, GM, Gilman, CB, Alves, OL, Robles, JR, Hayes, RL, Povlishock, JT & Bullock, MR. Safety and tolerability of cyclosporin a in severe traumatic brain injury patients: results from a prospective randomized trial. *Journal of Neurotrauma*, 26(12):2195–2206, 2009.

[115] Hatton, J, Rosbolt, B, Empey, P, Kryscio, R & Young, B. Dosing and safety of cyclosporine in patients with severe brain injury. *Journal of Neurosurgery*, 109(4):699–707, 2008.

[116] Allen, GS, Ahn, HS, Preziosi, TJ, Battye, R, Boone, SC, Boone, SC, Chou, SN, Kelly, DL, Weir, BK, Crabbe, RA, Lavik, PJ, Rosenbloom, SB, Dorsey, FC, Ingram, CR, Mellits, DE, Bertsch, LA, Boisvert, DP, Hundley, MB, Johnson, RK, Strom, JA & Transou, CR. Cerebral arterial spasm–a controlled trial of nimodipine in patients with subarachnoid hemorrhage. *New England journal of medicine*, 308(11):619–624, 1983.

[117] Cahill, J & Zhang, JH. Subarachnoid hemorrhage: is it time for a new direction? *Stroke*, 40(3 Suppl):S86–7, 2009.

[118] Gallagher, CN, Hutchinson, PJ & Pickard, JD. Neuroimaging in trauma. *Current opinion in neurology*, 20(4):403–409, 2007.

[119] Smith, M. Monitoring intracranial pressure in traumatic brain injury. *Anesthesia & Analgesia*, 106(1):240–248, 2008.

[120] Morgenstern, LB, Hemphill, JC, Anderson, C, Becker, K, Broderick, JP, Connolly, ES, Greenberg, SM, Huang, JN, Macdonald, RL, Messé, SR, Mitchell, PH, Selim,

M, Tamargo, RJ & American Heart Association Stroke Council and Council on Cardiovascular Nursing. Guidelines for the management of spontaneous intracerebral hemorrhage: a guideline for healthcare professionals from the American Heart Association/American Stroke Association. *Stroke*, 41:2108–2129, 2010.

[121] Mack, WJ, King, RG, Ducruet, AF, Kreiter, K, Mocco, J, Maghoub, A, Mayer, S & Connolly, ES. Intracranial pressure following aneurysmal subarachnoid hemorrhage: monitoring practices and outcome data. *Neurosurgical focus*, 14(4):e3, 2003.

[122] Narayan, RK, Kishore, PR, Becker, DP, Ward, JD, Enas, GG, Greenberg, RP, Domingues Da Silva, A, Lipper, MH, Choi, SC, Mayhall, CG, Lutz, HA & Young, HF. Intracranial pressure: to monitor or not to monitor? A review of our experience with severe head injury. *Journal of Neurosurgery*, 56(5):650–659, 1982.

[123] Cremer, OL, van Dijk, GW, van Wensen, E, Brekelmans, GJF, Moons, KGM, Leenen, LPH & Kalkman, CJ. Effect of intracranial pressure monitoring and targeted intensive care on functional outcome after severe head injury. *Critical care medicine*, 33(10):2207–2213, 2005.

[124] Lane, PL, Skoretz, TG, Doig, G & Girotti, MJ. Intracranial pressure monitoring and outcomes after traumatic brain injury. *Canadian journal of surgery Journal canadien de chirurgie*, 43(6):442–448, 2000.

[125] Shafi, S, Diaz-Arrastia, R, Madden, C & Gentilello, L. Intracranial pressure monitoring in brain-injured patients is associated with worsening of survival. *The Journal of trauma*, 64(2):335–340, 2008.

[126] Farahvar, A, Gerber, LM, Chiu, YL, Carney, N, Hartl, R & Ghajar, J. Increased mortality in patients with severe traumatic brain injury treated without intracranial pressure monitoring. *Journal of Neurosurgery*, 117(4):729–734, 2012.

[127] Stein, SC, Georgoff, P, Meghan, S, Mirza, KL & El Falaky, OM. Relationship of aggressive monitoring and treatment to improved outcomes in severe traumatic brain injury. *Journal of Neurosurgery*, 112(5):1105–1112, 2010.

[128] Chesnut, RM, Temkin, N, Carney, N, Dikmen, S, Rondina, C, Videtta, W, Petroni, G, Lujan, S, Pridgeon, J, Barber, J, Machamer, J, Chaddock, K, Celix, JM, Cherner, M & Hendrix, T. A trial of intracranial-pressure monitoring in traumatic brain injury. *The New England journal of medicine*, 367(26):2471–2481, 2012.

[129] Czosnyka, M, Balestreri, M, Steiner, L, Smielewski, P, Hutchinson, PJ, Matta, B & Pickard, JD. Age, intracranial pressure, autoregulation, and outcome after brain trauma. *Journal of Neurosurgery*, 102(3):450–454, 2005.

[130] Czosnyka, M, Smielewski, P, Timofeev, I, Lavinio, A, Guazzo, E, Hutchinson, P & Pickard, JD. Intracranial pressure: more than a number. *Neurosurgical focus*, 22(5):E10, 2007.

[131] Czosnyka, M, Brady, K, Reinhard, M, Smielewski, P & Steiner, LA. Monitoring of cerebrovascular autoregulation: facts, myths, and missing links. *Neurocritical Care*, 10(3):373–386, 2009.

[132] Moppett, IK & Mahajan, RP. Transcranial Doppler ultrasonography in anaesthesia and intensive care. *British Journal of Anaesthesia*, 93(5):710–724, 2004.

[133] Vajkoczy, P, Roth, H, Horn, P, Lucke, T, Thomé, C, Hubner, U, Martin, GT, Zappletal, C, Klar, E, Schilling, L & Schmiedek, P. Continuous monitoring of regional cerebral blood flow: experimental and clinical validation of a novel thermal diffusion microprobe. *Journal of Neurosurgery*, 93(2):265–274, 2000.

[134] Rutgers, DR, Blankensteijn, JD & van der Grond, J. Preoperative MRA flow quantification in CEA patients: flow differences between patients who develop cerebral ischemia and patients who do not develop cerebral ischemia during cross-clamping of the carotid artery. *Stroke*, 31(12):3021–3028, 2000.

[135] Nortje, J & Gupta, AK. The role of tissue oxygen monitoring in patients with acute brain injury. *British Journal of Anaesthesia*, 97(1):95–106, 2006.

[136] Schell, RM & Cole, DJ. Cerebral monitoring: jugular venous oximetry. *Anesthesia & Analgesia*, 90(3):559–566, 2000.

[137] Gopinath, SP, Valadka, AB, Uzura, M & Robertson, CS. Comparison of jugular venous oxygen saturation and brain tissue Po2 as monitors of cerebral ischemia after head injury. *Critical care medicine*, 27(11):2337–2345, 1999.

[138] Gopinath, SP, Robertson, CS, Contant, CF, Hayes, C, Feldman, Z, Narayan, RK & Grossman, RG. Jugular venous desaturation and outcome after head injury. *Journal of neurology, neurosurgery, and psychiatry*, 57(6):717–723, 1994.

[139] Bhatia, A & Gupta, AK. Neuromonitoring in the intensive care unit. II. Cerebral oxygenation monitoring and microdialysis. *Intensive Care Medicine*, 33(8):1322–1328, 2007.

[140] Tisdall, MM & Smith, M. Multimodal monitoring in traumatic brain injury: current status and future directions. *British Journal of Anaesthesia*, 99(1):61–67, 2007.

[141] Clarke, LC, Wolff, R, Granger, D & Taylor, Z. Continuous recording of blood oxygen tensions by polarography. *Journal of Applied Physiology*, 6(3):189–193, 1953.

[142] van Santbrink, H, Maas, AI & Avezaat, CJ. Continuous monitoring of partial pressure of brain tissue oxygen in patients with severe head injury. *Neurosurgery*, 38(1):21–31, 1996.

[143] Valadka, AB, Gopinath, SP, Contant, CF, Uzura, M & Robertson, CS. Relationship of brain tissue PO2 to outcome after severe head injury. *Critical care medicine*, 26(9):1576–1581, 1998.

[144] van den Brink, WA, van Santbrink, H, Steyerberg, EW, Avezaat, CJ, Suazo, JA, Hogesteeger, C, Jansen, WJ, Kloos, LM, Vermeulen, J & Maas, AI. Brain oxygen tension in severe head injury. *Neurosurgery*, 46(4):868–76– discussion 876–8, 2000.

[145] Brawanski, A, Faltermeier, R, Rothoerl, RD & Woertgen, C. Comparison of near-infrared spectroscopy and tissue p(O2) time series in patients after severe head injury and aneurysmal subarachnoid hemorrhage. *Journal of cerebral blood flow and metabolism*, 22(5):605–611, 2002.

[146] Meixensberger, J, Vath, A, Jaeger, M, Kunze, E, Dings, J & Roosen, K. Monitoring of brain tissue oxygenation following severe subarachnoid hemorrhage. *Neurological research*, 25(5):445–450, 2003.

[147] Jaeger, M, Soehle, M, Schuhmann, MU, Winkler, D & Meixensberger, J. Correlation of continuously monitored regional cerebral blood flow and brain tissue oxygen. *Acta Neurochirurgica*, 147(1):51–6, 2005.

[148] Jaeger, M, Schuhmann, MU, Soehle, M, Nagel, C & Meixensberger, J. Continuous monitoring of cerebrovascular autoregulation after subarachnoid hemorrhage by brain tissue oxygen pressure reactivity and its relation to delayed cerebral infarction. *Stroke*, 38(3):981–986, 2007.

[149] Nangunoori, R, Maloney-Wilensky, E, Stiefel, M, Park, S, Andrew Kofke, W, Levine, JM, Yang, W & Le Roux, PD. Brain tissue oxygen-based therapy and outcome after severe traumatic brain injury: a systematic literature review. *Neurocritical Care*, 17(1):131–138, 2012.

[150] Diaz-Arrastia, RR & Moore, CB. Brain tissue oxygen monitoring in traumatic brain injury (TBI) (BOOST 2) [http://clinicaltrials.gov/ct2/show/NCT00974259].

[151] Engström, M, Polito, A, Reinstrup, P, Romner, B, Ryding, E, Ungerstedt, U & Nordström, CH. Intracerebral microdialysis in severe brain trauma: the importance of catheter location. *Journal of Neurosurgery*, 102(3):460–469, 2005.

[152] Coles, JP, Fryer, TD, Smielewski, P, Chatfield, DA, Steiner, LA, Johnston, AJ, Downey, SPMJ, Williams, GB, Aigbirhio, F, Hutchinson, PJ, Rice, K, Carpenter,

TA, Clark, JC, Pickard, JD & Menon, DK. Incidence and mechanisms of cerebral ischemia in early clinical head injury. *Journal of Cerebral Blood Flow & Metabolism*, 24(2):202–211, 2004.

[153] Tisdall, MM & Smith, M. Cerebral microdialysis: research technique or clinical tool. *British Journal of Anaesthesia*, 97(1):18–25, 2006.

[154] Ungerstedt, U & Rostami, E. Microdialysis in neurointensive care. *Current pharmaceutical design*, 10(18):2145–2152, 2004.

[155] Ghosh, A & Smith, M. Brain Tissue Biochemistry. In Matta, BF, Menon, DK & Smith, M, eds., *Core Topics in Neuroanaesthesia and Neurointensive Care*, pp. 85–100. Cambridge University Press, 2011.

[156] Reinstrup, P, Ståhl, N, Mellergård, P, Uski, T, Ungerstedt, U & Nordström, CH. Intracerebral microdialysis in clinical practice: baseline values for chemical markers during wakefulness, anesthesia, and neurosurgery. *Neurosurgery*, 47(3):701–9; discussion 709–10, 2000.

[157] Schulz, MK, Wang, LP, Tange, M & Bjerre, P. Cerebral microdialysis monitoring: determination of normal and ischemic cerebral metabolisms in patients with aneurysmal subarachnoid hemorrhage. *Journal of Neurosurgery*, 93(5):808–814, 2000.

[158] Timofeev, I, Carpenter, KLH, Nortje, J, Al-Rawi, PG, O'Connell, MT, Czosnyka, M, Smielewski, P, Pickard, JD, Menon, DK, Kirkpatrick, PJ, Gupta, AK & Hutchinson, PJ. Cerebral extracellular chemistry and outcome following traumatic brain injury: a microdialysis study of 223 patients. *Brain*, 134(Pt 2):484–494, 2011.

[159] Zauner, A, Doppenberg, EM, Woodward, JJ, Choi, SC, Young, HF & Bullock, R. Continuous monitoring of cerebral substrate delivery and clearance: initial experience in 24 patients with severe acute brain injuries. *Neurosurgery*, 41(5):1082–91; discussion 1091–3, 1997.

[160] Kett-White, R, Hutchinson, PJ, Al-Rawi, PG, Gupta, AK, Pickard, JD & Kirkpatrick, PJ. Adverse cerebral events detected after subarachnoid hemorrhage using brain oxygen and microdialysis probes. *Neurosurgery*, 50(6):1213–21; discussion 1221–2, 2002.

[161] Persson, L, Valtysson, J, Enblad, P, Warme, PE, Cesarini, K, Lewen, A & Hillered, L. Neurochemical monitoring using intracerebral microdialysis in patients with subarachnoid hemorrhage. *Journal of Neurosurgery*, 84(4):606–616, 1996.

[162] Sarrafzadeh, A, Haux, D, Küchler, I, Lanksch, WR & Unterberg, AW. Poor-grade aneurysmal subarachnoid hemorrhage: relationship of cerebral metabolism to outcome. *Journal of Neurosurgery*, 100(3):400–406, 2004.

[163] Vespa, P, Bergsneider, M, Hattori, N, Wu, HM, Huang, SC, Martin, NA, Glenn, TC, McArthur, DL & Hovda, DA. Metabolic crisis without brain ischemia is common after traumatic brain injury: a combined microdialysis and positron emission tomography study. *Journal of cerebral blood flow and metabolism*, 25(6):763–774, 2005.

[164] Vespa, PM, O'Phelan, K, Mcarthur, D, Miller, C, Eliseo, M, Hirt, D, Glenn, T & Hovda, DA. Pericontusional brain tissue exhibits persistent elevation of lactate/pyruvate ratio independent of cerebral perfusion pressure. *Critical care medicine*, 35(4):1153–1160, 2007.

[165] Bellander, BM, Cantais, E, Enblad, P, Hutchinson, P, Nordström, CH, Robertson, C, Sahuquillo, J, Smith, M, Stocchetti, N, Ungerstedt, U, Unterberg, A & Olsen, NV. Consensus meeting on microdialysis in neurointensive care. *Intensive Care Medicine*, 30(12):2166–2169, 2004.

3

NEAR INFRARED SPECTROSCOPY

3.1 INTRODUCTION

The previous chapter established the central role of CH-I in the pathophysiology of ABI, and underlined the role of monitoring for CH-I in its management. Yet despite the existence of a plethora of monitoring modalities to identify CH-I, the limitations of existing monitors mean that time-critical windows to prevent or minimise permanent ischaemic neurological injury may pass silently.

This chapter draws heavily on a review article published in Anesthesia and Analgesia *[1].*

NIRS is a non-invasive optical technique that has the potential to address many of the shortcomings inherent to other cerebral monitoring modalities and is the technique that forms the basis of the experimental studies in this thesis. Although it has been over three decades since its first description, the clinical adoption of NIRS has been limited. There is a wealth of data describing the application of NIRS in neonates, where invasive brain monitoring is not possible [2,3], and NIRS is also widely used in non-brain tissue [4] and during functional brain imaging [5,6]. Whilst there is a burgeoning body of clinical data describing the use of NIRS in the healthy adult brain, data describing its use following ABI are limited.

The aim of this chapter is to review the principles of cerebral NIRS, and its utility and limitations as a monitor of CH-I following ABI. Having considered the limitations of commercially available NIRS apparatus, this is followed by a description of the hybrid optical spectrometer (pHOS), the specialised NIRS apparatus that is used for the experimental studies described in this thesis.

3.2 PRINCIPLES OF NIRS

This section will not exhaustively review the physical principles underlying the clinical use of NIRS – these are comprehensively reviewed elsewhere [7,8] – but rather aims to highlight the capabilities and limitations of, as well as the assumptions underlying different NIRS-based approaches to brain monitoring.

The NIRS technique was first described in 1977 by Franz Jöbsis [9], who made two key observations regarding near infrared (NIR) light. First, light in the NIR spectrum (700-950nm) can traverse biological tissue because of the relative transparency of tissue to light in this wavelength range and, second, several biological molecules, termed chromophores, have distinct absorption spectra in the NIR . From a clinical perspective,

oxyhaemoglobin and deoxyhaemoglobin are the most commonly measured chromophores, although CCO may prove clinically more important [10] and was in fact the target of Jöbsis's initial investigations.

NIRS is based on the transmission and absorption of NIR light as it passes through tissue and there are basic features common to all NIRS devices [8]. Light is generated at specific wavelengths, typically by light-emitting diodes and usually detected by silicon photodiodes [11] . Alternative methods of light detection include photomultiplier tubes in older devices, and CCD, similar to those used in consumer digital cameras, in broadband systems (see Section 3.4 below). The emitting and detecting fibre optics are often referred to as the optodes. Many systems incorporate two or more channels – i. e. optodes and associated detectors capable monitoring of multiple tissue regions of interest simultaneously [12].

3.2.1 *Light absorption, scattering and the Beer-Lambert Law*

ABSORPTION In an idealised situation – shown in Figure 3.1a – where the only cause of light attenuation between a source and its detector is its absorption by chromophores, the attenuation of light which, at a given wavelength, is described by the Beer-Lambert Law (BLL), as given by the equations

$$A = \log_{10}\left(\frac{I}{I_0}\right) \tag{3.1}$$

$$A = \varepsilon.c.d. \tag{3.2}$$

Rearranging to calculate c:

$$c = \frac{A}{\varepsilon.d}. \tag{3.3}$$

This states that, at a given wavelength, attenuation A (which is calculated from emitted light intensity I_0 and measured light intensity I, as shown in Equation 3.1) is dependent to three variables: chromophore concentration c, the source-detector distance d, and the extinction coefficient of the chromophore ε, which describes the absorptive properties of a chromophore at a given wavelength (Equation 3.2). In this hypothetical situation, chromophore concentration can be accurately calculated using the measured degree of light attenuation by the chromophore in association with knowledge of the source-detector separation and relevant absorption coefficient (Equation 3.3).

Conventions vary as to whether base-10 or natural logarithms are used in the definition of attenuation (as well as the absorption and scattering coefficients, described below)

The extinction coefficient ε is a constant defined empirically *a priori* for each chromophore across a desired wavelength range. For a solution containing only a single

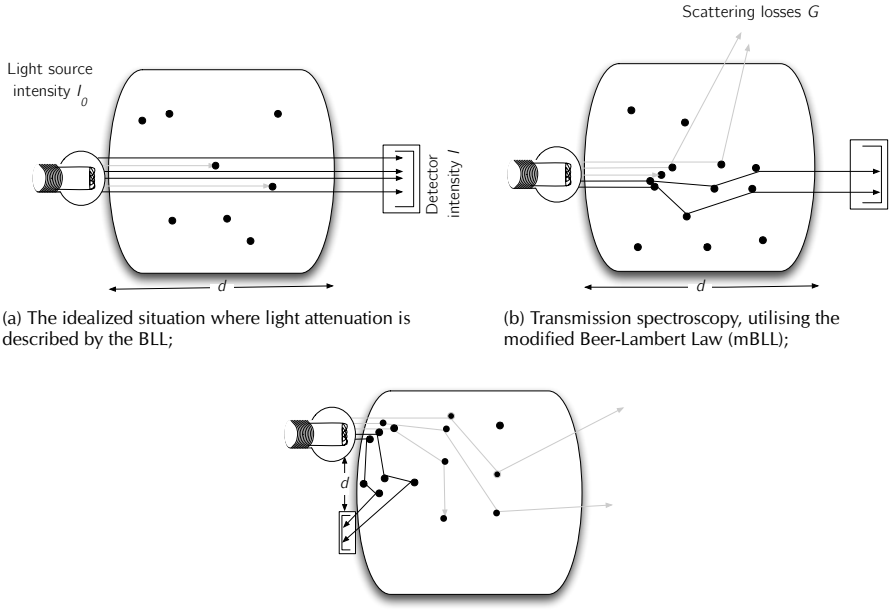

(a) The idealized situation where light attenuation is described by the BLL;

(b) Transmission spectroscopy, utilising the modified Beer-Lambert Law (mBLL);

(c) Reflectance spectroscopy, also using the mBLL.

Figure 3.1 – Schematic depictions of light transport and differential spectroscopy.

chromophore, the is given as the product of the extinction coefficient and the mean optical pathlength:

$$\mu_a = \varepsilon.c.\log_e 10. \tag{3.4}$$

The effect of absorption by multiple chromophores is additive, and thus for a solution containing multiple chromophores, is defined as:

$$\mu_a = (\varepsilon_a.c_a + \varepsilon_b.c_b + \varepsilon_c.c_c + \cdots + \varepsilon_n.c_n).\log_e 10, \tag{3.5}$$

where ε_a and c_a are the extinction coefficient and concentration of chromophore a and so on [13], and the scaling factor $\log_e 10$ included as optical absorption coefficient (μ_a) is defined in natural logarithms. The absorption spectra of several important chromophores are shown in Section 3.2.4 below.

SCATTERING Biological tissue poses a much more complex optical situation than the ideal set out above. Although chromophore concentration is still directly related to light absorption, it is light *scattering* that is the major contributor to attenuation in most biological tissue, including the adult head [14]. Scattering is quantified by means of optical scattering coefficient (μ_s), which is analogous to μ_a, but describes the degree

of attenuation attributable to scattering losses. Where scattering is anisotropic, it can approximately be described using the reduced optical scattering coefficient (μ_s'), which incorporates the anisotropy of such scattering:

$$\mu_s' = \mu_s.(1-g), \tag{3.6}$$

where g is the mean cosine of the scattering angle.

Scattering gives rise to two important consequences. First, not all emitted light reaches the detector because some of it is scattered away from the detector, giving rise to scattering losses (see Figure 3.1b). Second, some of the light that reaches the detector will have been scattered multiple times and therefore the *optical pathlength* is greater in distance than the direct source-detector separation. This increase in pathlength is quantified as the differential pathlength factor (DPF), defined as:

$$DPF = \frac{\text{Mean Optical Pathlength}}{d}, \tag{3.7}$$

so

$$\text{Mean Optical Pathlength} = d.DPF. \tag{3.8}$$

The mBLL incorporates DPF to account for the effect of lengthened pathlength. The DPF must be defined *a priori*, and published values are available for a range of adult human tissues including for the head [15]. Scattering losses (G), by definition, cannot be quantified. However, by assuming that scattering losses are constant, *differential* spectroscopy can be used to derive *changes* in chromophore concentration from attenuation, cancelling out constant G. The mBLL is thus given by the equation

$$A = \varepsilon.c.d.DPF + G. \tag{3.9}$$

Assuming scattering losses G are constant:

$$\begin{aligned} \Delta A &= \Delta c.\varepsilon.d.DPF \\ \Delta c &= \frac{\Delta A}{\varepsilon.d.DPF} \end{aligned} \tag{3.10}$$

In the adult head scattering attenuates NIR light to such an extent that it cannot traverse the whole head so reflectance spectroscopy (Figure 3.1c), where the light source and detector are placed on adjacent areas of the head, must be used.

3.2.2 *NIRS techniques*

All NIRS techniques rely on a measure of optical attenuation, which is the total loss of light due to absorption and scattering. However, chromophore concentrations (which

are the physiologically- and clinically-relevant measures that we wish to know) require knowledge of solely the *absorption spectrum* of tissue, which is then used to construct a series of simultaneous equations based on equation 3.2. Thus one of the major challenges of NIRS is to derive optical *absorption* from measured optical *attenuation*. Several approaches are employed to do so, either by directly measuring optical scattering or accounting for its effects. It should be noted that multi-distance spectroscopy forms the basis of most commercially available clinical devices, in part because of the ability to generate a tissue oxygen saturation (TOS) – a measure that is clinically intuitive – and the majority of other methodologies are used predominantly in a research setting.

DIFFERENTIAL SPECTROSCOPY Differential spectroscopy relies on the mBLL described above and depicted in Figures 3.1b and 3.1c. It is the simplest form of *in vivo* NIRS, although it is now rarely used in adult clinical practice . This technique assumes that light scattering remains constant during the measurement period and that measured changes in attenuation are due only to changes in absorption. Therefore only changes in chromophore concentration from an arbitrary baseline point (i.e. trends) can be measured. The scale of these changes is dependent on the (*a priori* defined) DPF.

MULTI-DISTANCE SPECTROSCOPY This technique, also known as spatially-resolved spectroscopy (SRS), is a technique commonly used in commercial NIRS devices. An array of closely-spaced detectors is used to measure light attenuation as a function of source-detector separation, as depicted in Figure 3.2a.

Commercial devices vary in the algorithm they use to derive the absorption coefficient from multi-distance spectrometers. For example, the INVOS devices (Somanetics®, Troy, MI) apply proprietary algorithms that are not published for scrutiny. The term 'cerebral oximeter' has been coined to describe several commercially available devices, as most report a TOS or equivalent – the nomenclature varies between devices – where

$$\mathrm{TOS} = \frac{[\mathrm{HbO_2}]}{[\mathrm{HbO_2}] + [\mathrm{HHb}]}. \tag{3.11}$$

One widely-used approach to SRS is the use of the Boltzmann diffusion approximation; algorithms based on this model (which considers the transport of photons through a highly-scattering medium as analogous to the diffusion of a particle in a liquid medium) are used in the Hamamatsu NIRO devices (Hamamatsu Photonics KK, Hamamatsu City, Japan), as well as the pHOS (described below in section 3.4). The diffusion approximation states that:

$$\mu_a.\mu_s' \approx \frac{1}{3}\left(\frac{\delta A}{\delta d} - \frac{2}{d}\right)^2. \tag{3.12}$$

The wavelength dependence of scattering (defined *a priori* [16]) is then used to calculate the spectral shape, but not the absolute value, of μ_a. These values are then used to calculate absolute chromophore concentrations, albeit modified by an unknown scaling factor [17]. However, when calculating tissue oxygenation index (TOI, the term coined by Hamamatsu to describe the TOS-equivalent reported by their devices), this scaling factor is cancelled by division.

The use of the diffusion approximation for SRS is subject to certain underlying assumptions [18,19]. These include:

- the tissue being monitored is homogenous in its optical properties and 'semi-infinite'– that is, an infinite medium bound by a flat plane;
- optical scattering is much greater in magnitude than absorption ($\mu_s' \gg \mu_a$) – a situation that is true of most biological tissue
- scattering is nearly isotropic (i. e. $g \approx 1$);
- the source-detector separation is much greater than the diffusion length ($d \gg 1/\mu_s'$)

Whilst the use of SRS serves theoretically to increase the intracranial (or depth-) specificity of NIRS measurements, there is still empirical evidence to suggest a persistent contribution of extracranial haemoglobin concentration changes to TOS measurements [20,21].

FREQUENCY-RESOLVED SPECTROSCOPY Frequency-resolved (or domain) spectroscopy modulates the intensity of light at a known radiofrequency and measures the phase-shift and degree of light attenuation directly (Figure 3.2b). Models of light transport – such as the diffusion approximation detailed above – are then used to derive absolute values of μ_a and μ_s' and therefore absolute chromophore concentration [22].

TIME-RESOLVED SPECTROSCOPY Time-resolved spectroscopy (TRS) uses an ultra-short pulse of light, typically a few picoseconds in duration, emitted by a laser. A histogram of the number of photons detected and their arrival time to the detector is constructed (Figure 3.2c). This is called the temporal point spread function (TPSF) and is interpreted with the aid of a model of light transport (for example, the diffusion approximation shown in Equation 3.12, but solved in the time domain) to calculate absolute values of μ_a and μ_s' , and thereby absolute chromophore concentration [23,24]. There is a relative paucity of TRS-based devices available for use outside of the research arena, but TRS-based techniques may soon overtake 'continuous-wave' techniques such as those three mentioned above [24].

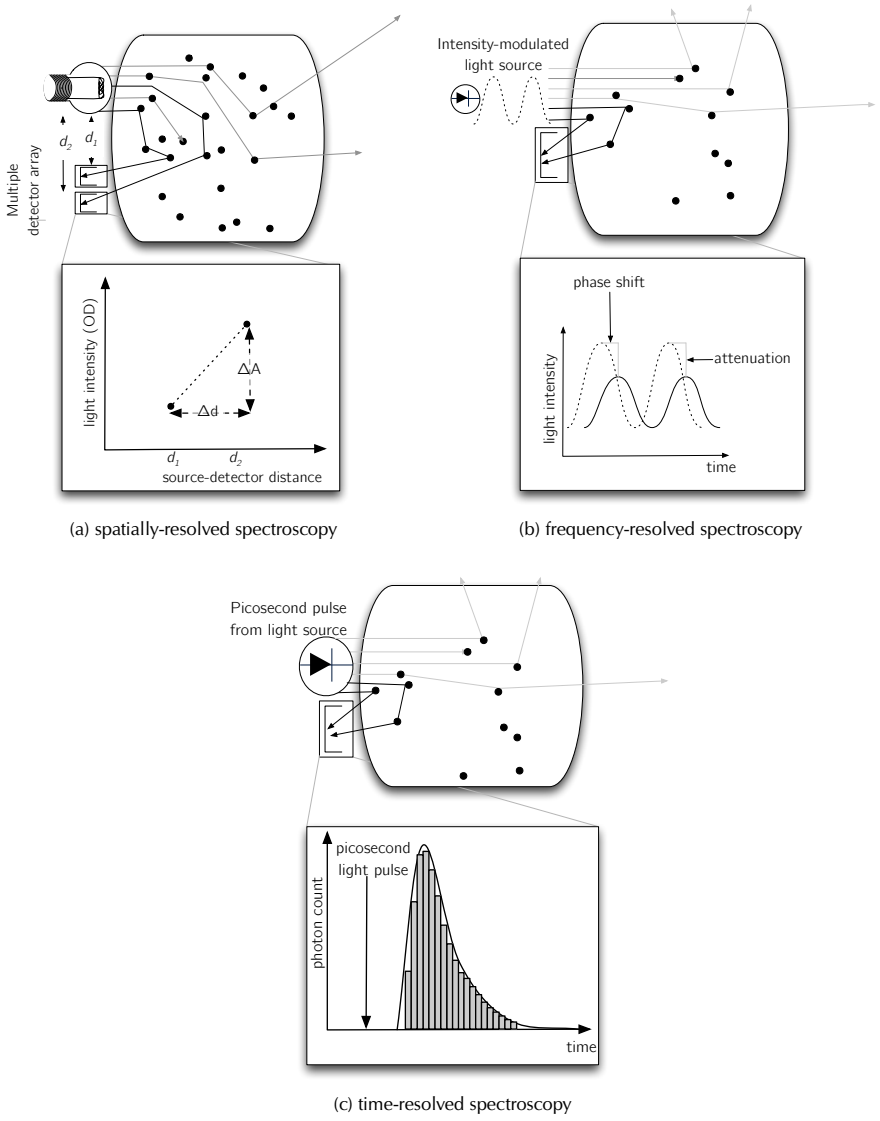

(a) spatially-resolved spectroscopy

(b) frequency-resolved spectroscopy

(c) time-resolved spectroscopy

Figure 3.2 – Schematic depictions of spatially-, frequency-, and time-resolved spectroscopy.

3.2.3 *Spectral resolution*

The accurate derivation of chromophore concentration is tightly linked to the wavelengths of light chosen and optical absorption at one wavelength for each chromophore of interest must be known. The wavelengths of NIR light used in commercial devices are usually selected to be sensitive to haemoglobin and therefore generally utilise wavelengths between 700nm and 850nm where the absorption spectra of oxyhaemoglobin and deoxyhaemoglobin are maximally separated and absorption by water is relatively low (see Figures 3.3 and 3.5) [13]. Many commercial NIRS systems employ two wavelengths, limiting their use to measurement of two chromophores, namely oxyhaemoglobin and deoxyhaemoglobin [8]. The addition of more wavelengths brings improved accuracy and can be achieved through the use of additional laser diodes that emit light at discrete wavelengths, or by using broadband spectroscopy (BBS) systems which utilise a 'white' light source emitting a continuous spectrum of light within the NIR range. The use of multiple wavelengths is of particular importance when measuring CCO [25]; although it is possible to resolve CCO concentration using fewer wavelengths, the selection of these is of paramount importance. However, the task of deciding which wavelengths to use is non-trivial and requires the use of complex algorithms [26].

3.2.4 *Chromophores*

Several chromophores possess characteristic spectra within the NIR range. These include oxyhaemoglobin, deoxyhaemoglobin and the oxidised and reduced forms of CCO, but also lipids, water and melanin.

WATER, MELANIN AND LIPID The human body comprises approximately 70% water by weight, although individual tissue compartments vary from ∼12% water in the case of cortical bone to >99% in the cerebrospinal fluid spaces in the brain [27]. Water is also a weak absorber in the 'near' NIR range, but its strongest absorption is above 1500nm, and in practice this absorption limits photon penetration in this range (see Figure 3.3). Water concentration can be calculated – i. e. cerebral oedema can be quantified – by resolving for its spectrum [28]. Alternatively, if the water concentration is known or assumed *a priori*, the second differential of the water spectrum can be used to estimate pathlength and thus DPF [29].

Melanin is a strong Rayleigh scatterer within the ultraviolet (UV) spectrum, and this is necessary for its primary biological role of protection of cell nuclear material from damage by UV light. Melanin is also a weak absorber within the NIR range. As melanin levels are relatively constant, it is not necessary to account for melanin during differential spectroscopy in most clinical settings. However, the presence of melanin may require consideration when using other absolute quantification methods. Furthermore, the

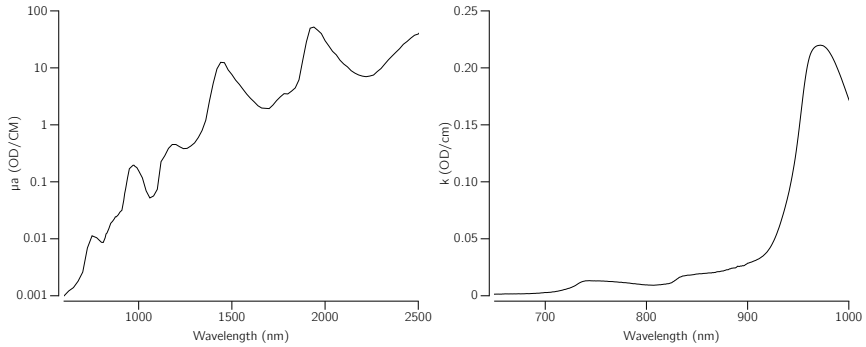

(a) 650-2500nm, measured at 22° C (note logarithmic scale)

(b) 650-1000nm, measured at 37° C

Figure 3.3 – Absorption spectra of water; data from [30,31].

absorptive properties of melanin allow the use of NIRS for the detection of melanin-producing tumours i. e. melanomas [32].

Lipid also possesses a characteristic absorption spectrum within the NIR range (Figure 3.4). However, like melanin, lipid concentration is relatively constant and is not oxygen-dependent, and so it need not be considered for differential spectroscopy, but may be important when using absolute quantification methods. The spectral characteristics of lipid are exploited in the estimation of regional adiposity [4], and also finds utility in the industrial use of NIRS to estimate food lipid and fat content.

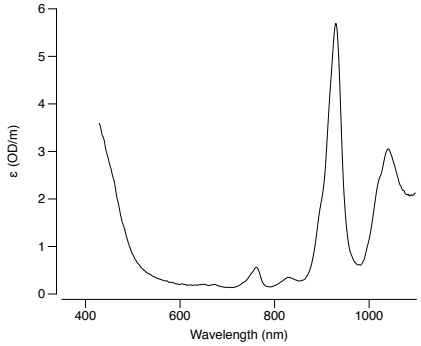

Figure 3.4 – Absorption spectrum of lipid; data from [33].

HAEMOGLOBIN The measurement of haemoglobin (either in its individual forms as oxyhaemoglobin or deoxyhaemoglobin, or as a TOS-like measure) forms the basis of virtually all clinical NIRS studies. Haemoglobin's biological role as oxygen transporter (discussed in Chapter 1.2) is predicated on the binding of oxygen to one of the four iron-containing haeme centres in haemoglobin [34,35]. Just as the oxidation state of haemoglobin causes changes in its absorption spectrum in the visible range (giving rise

to the characteristic violet colour of fully deoxygenated blood and scarlet colour of

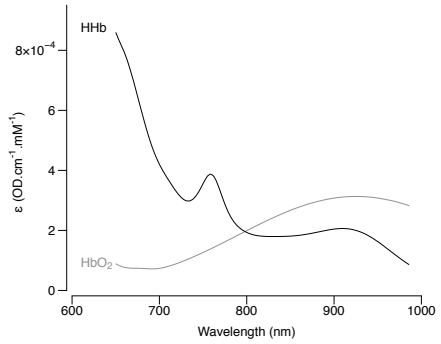

Figure 3.5 – NIR absorption spectra of oxy- and deoxy-haemoglobin. Data from [25,36].

oxygenated blood), haemoglobin's absorption in the NIR range varies with oxidation (Figure 3.5). The measurement of oxyhaemoglobin concentration ($[HbO_2]$) and deoxyhaemoglobin concentration ([HHb]) and derived quantities using the various NIRS techniques described above has reached a relatively mature stage, and many haemoglobin measures and indices are derived using NIRS. Two frequently-encountered measures derived using differential spectroscopy are the total haemoglobin concentration ([HbT]) and the haemoglobin difference concentration ([HbDiff]), defined as:

$$[\text{HbT}] = [\text{HbO}_2] + [\text{HHb}] \tag{3.13}$$

and

$$[\text{HbDiff}] = [\text{HbO}_2] - [\text{HHb}]. \tag{3.14}$$

Other haemoglobin measures frequently encountered are the TOS-equivalents (see above) and total haemoglobin index (THI) – a normalised ratio that is an SRS-derived analogue of [HbT] [13].

CYTOCHROME C OXIDASE Although the measurement of CCO concentration with NIRS was Jöbsis's goal when he first described NIRS [9], subsequent decades have seen an emphasis on the measurement of the haemoglobin species in both clinical and non-clinical NIRS applications [4,8,11,37,38]. The measurement of CCO concentration, however, poses a much greater challenge.

The multiple redox cores of CCO (see section 1.3.3) result in it possessing an oxidation-dependent absorption spectrum within both the visible and NIR ranges (Figure 3.6) – a trait it shares with haemoglobin. However, CCO differs from haemoglobin in two important ways: first, while the individual oxidised and reduced haemoglobin spectra can reliably be measured using whole blood *in vitro*, the purification and

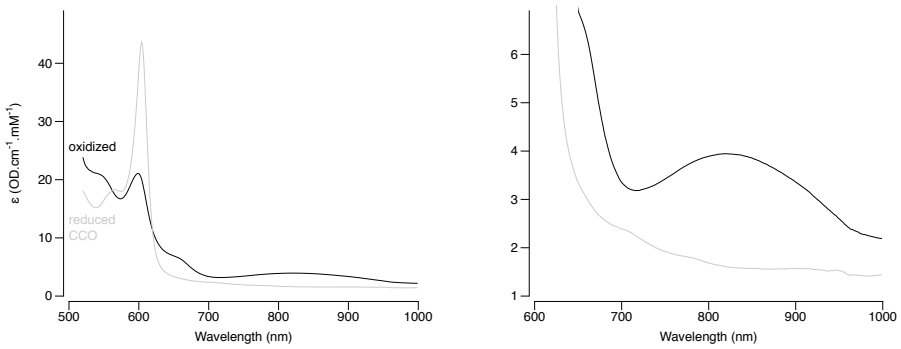

(a) 520-1000nm, including visible peaks (b) 650-1000nm

Figure 3.6 – *In vitro* extinction spectra of oxidised and reduced purified bovine heart CCO, based on data provided by Dr James Moody (Plymouth University) to the Biomedical Optics Research Laboratory, UCL.

preparation of CCO raises concerns regarding the veracity of *in vitro* spectra [39]. Second, CCO concentrations are constant, so it is possible to measure the *in vivo* difference spectrum [i. e. the spectrum of oxidised-reduced cytochrome *c* oxidase (oxCCO), shown in Figure 3.7]. Thus, it is the *in vivo* CCO difference spectrum that is used to resolve for cytochrome in most NIRS studies. The predominant spectral feature of the CCO difference spectrum within the NIR range is the broad peak seen at 830nm. It is generally accepted that the major contributor to this peak is the Cu_B core [41]. While haemoglobin and CCO have similar absorption, *ceteris paribus*, CCO exists in significantly lower concentrations, meaning that that even in conditions of complete anoxia, the absorption signal from CCO is an order of magnitude lower than that from haemoglobin species [39]. The total concentration of CCO within the adult human brain is unknown (it is difficult to measure directly), but it has been suggested that the adult rat CCO concentration – 5.5μM – to be the upper limit of adult human brain concentration [42]. The diminutive size of the CCO absorption signal increases the potential for scattering losses and pathlength changes to confound the accurate

The abbreviation oxCCO is reserved for oxidised-reduced CCO, measured by resolving for the difference spectrum; the oxidised form is always referred to in full.

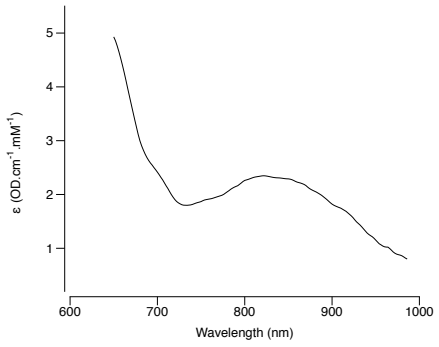

Figure 3.7 – Difference spectrum of CCO measured *in vivo*, based on data from [40].

measurement of CCO changes, although the use of BBS can mitigate somewhat against these confounders [25]. Further difficulties arise in the interpretation of the physiological and clinical relevance of measured CCO oxidation changes. While NIRS can be used to measure the oxidation of the Cu_B core of CCO, the relationship between Cu_B oxidation and electron flux through the enzyme, discussed in Chapter 1.3.3 is complex. These challenges combined have resulted in a relative paucity of NIRS-derived data describing the behaviour of CCO.

3.3 CLINICAL USE OF NIRS

There has been interest in using NIRS to detect CH-I since its first description, but the relatively wide use of the technology in the research setting has not been matched by clinical applications [8]. There are many reasons for this, including limitations inherent to the technique, ambiguity regarding what is actually measured, deficiencies in algorithms, difficult translation of instruments designed for research use to the bedside and data that are not reproducible and specific enough for clinical decision-making.

3.3.1 *Cardiac surgery and carotid endartectomy*

Two clinical scenarios where there is evidence to support the use of NIRS for the identification of CH-I are during carotid endarterectomy (CEA) and cardiac surgery. Following CEA, the decision of whether or not to place an intracarotid shunt during cross-clamping is of key importance: if placed unnecessarily (i.e. when collateral circulation is adequate to perfuse the brain despite cross-clamping), it exposes the patient to the risk of carotid vascular injury; conversely, omission of a shunt in the presence of inadequate collateral circulation can lead to ischaemic brain injury [43].

A number of studies have demonstrated broad equivalence between NIRS and alternative modalities such as TCD, and somatosensory evoked potential measurement to identify CH-I during carotid cross-clamping, but a key difficulty is in the identification of the 'ischaemic threshold' below which shunting should take place. Using a variety of apparatus, TOS threshold values vary between 11-20 percentage point reductions in TOS; an absolute TOS threshold of 59% has also been suggested [44–48]. This ambiguity serves to highlight the inadequacy of purely haemoglobin-based measures in the identification of CH-I, but the relative ease-of-use, temporal resolution and lack of operator-dependence makes NIRS an attractive monitoring option in this context [1].

In the case of cardiac surgery, NIRS-guided 'brain-protection' protocols aimed at optimising cerebral DO_2 during cardiopulmonary bypass (CPB) have generated great interest, in the hope that they may aid in the prevention of stroke, which occurs in 1-3% of patients, and longstanding postoperative cognitive dysfunction, which occurs in more than 50% of patients [49,50]. Whilst the use of protocol based on the maintenance

of normal TOS has not been shown to improve neurological outcome, it is associated with reduced *non-neurological* morbidity [51,52]. Post-hoc analyses suggest that there may exist a 'time-viability' threshold for clinically significant ischaemia, where both the depth and duration of reductions in TOS are of prognostic importance [1].

In summary, there is prospective evidence supporting the use of cerebral NIRS monitoring – in the form of cerebral oximeters – to improve *non-neurological* outcome following CPB, the evidence linking reductions in TOS to poor neurological outcome are limited to retrospective and post-hoc analyses. As with CEA, the question must be asked: could this ambiguity be resolved through the use of NIRS to monitor *metabolism* in addition to haemodynamics and oxygenation?

This was precisely the question posed by the Tamura group, who used NIRS apparatus and associated 'Sapporo' algorithm based largely on the mBLL and designed and validated for the measurement of oxCCO (reviewed in [53]). In an observational study of 66 patients undergoing thoracic arch surgery with CPB, Kakihana and colleagues identified three patterns of oxCCO change in response to CPB (Figure 3.8). Although the algorithm is unable to quantify changes in oxCCO (as it does not correct for pathlength, and thus expresses changes in arbitrary units), the investigators reported a significant association between reductions in concentration of oxidised-reduced cytochrome *c* oxidase ([oxCCO]) and poor neurological outcome: a transient reduction ('Type B') was associated with an 5.7-fold increase and a persistent reduction ('Type C') was associated with a staggering 33.3-fold increase in the occurrence of poor neurological outcome – which was not prospectively defined, but encompassed a range from the occurrence of seizures to coma [54]. Although criticisms have been levelled on the integrity of chromophore changes derived using the Sapporo algorithm [25], this paper is the one of only two studies that associates CCO oxidation status to clinical outcome in man. The other was an observational study of 41 adult patients undergoing cardiac surgery (with bypass), who underwent cerebral NIRS monitoring with a NIRO-500 (Hamamatsu Photonics KK, Hamamatsu City, Japan) device, which reports changes in [oxCCO] using a mBLL-based algorithm. Three patients suffered from a temporary delerium, which resolved within three days; the observed median reduction in [oxCCO] during bypass was as much as 5.5μM greater in these patients than those who did not suffer any neuropsychological sequelae [55]. However, it should be noted that this algorithm, too, has been shown to overestimate the magnitude of [oxCCO] changes [25], a notion corroborated by the fact that an oxCCO reduction of 5.5μM would suggest reduction of the entire enzyme pool.

3.3.2 *Acute brain injury*

ABI presents a more complicated challenge, where CH-I caused by reductions in cerebral substrate delivery *in concert with* increases in cerebral metabolic demand

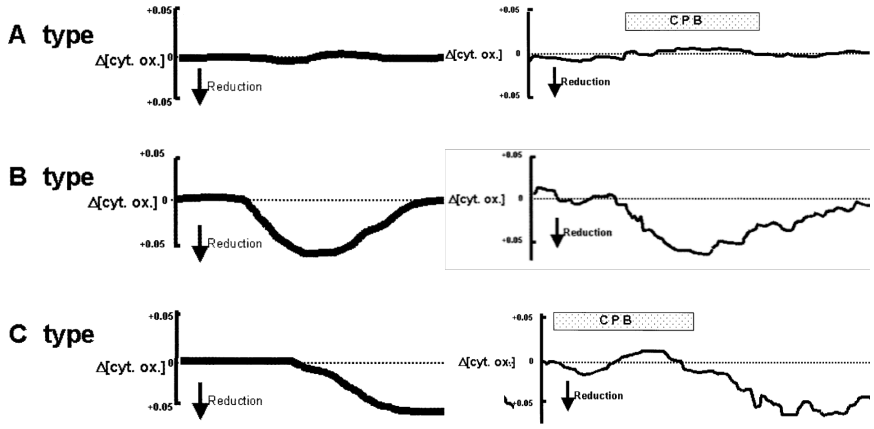

Figure 3.8 – Patterns of oxCCO change seen during cardiopulmonary bypass (schematic on left, actual recordings on right). Reduction in oxCCO (labelled Δ[cyt. ox]) in B type and C type patterns is was associated with poor outcome. Modified from [54].

and mitochondrial dysfunction, leading to an inability to use delivered substrate (see Chapter 2.2). There has been limited investigation of the utility of NIRS in this area, and no outcome studies. Investigations in the adult neurocritical care population have been solely observational and serve to highlight two key difficulties in investigating NIRS-derived variables in this context: the definition of ischaemic thresholds in an injured brain with acutely disordered haemodynamic and metabolic function, and the lack of a gold standard against which to compare NIRS-derived measures [10]. Factors such as the presence of intracranial haematoma, cerebral oedema and subarachnoid blood present further challenges since they may invalidate some of the assumptions upon which NIRS algorithms are based. In fact, this has been utilised to advantage in studies using NIRS to identify intracranial haematomas [56] and cerebral oedema [28].

One small observational study of 18 patients with TBI identified an association between increasing length of time with regional oxygen saturation (rsO_2, the TOS-equivalent reported by INVOS oximeters) values of <60% and mortality, intracranial hypertension and compromised CPP [57]. A more recent study compared $P_{br}O_2$ with regional oxygen saturation (rsO_2) in 22 patients over a 16-hour period following severe TBI [58]. An rsO_2 <60% was moderately accurate for the prediction of 'severe' brain hypoxia ($P_{br}O_2$ < 12 mmHg) but poor at detecting 'moderate' hypoxia ($P_{br}O_2$ 12-15 mmHg) with sensitivities and specificities of 73% and 86%, and 62% and 49% respectively. The authors conclude that rsO_2 is an inadequate substitute for $P_{br}O_2$ for routine monitoring of cerebral oxygenation and, whilst this is reasonable, it fails to consider the different physiological variables and brain regions being monitored by the two techniques.

There has been recent interest in using NIRS to monitor cortical changes during cerebral vasospasm after aSAH. In one study of 32 patients undergoing coil embolisation,

the rate-of-decline of rsO_2 (measured using an INVOS oximeter) was 3.5%.min^{-1} greater in patients who developed vasospasm during the procedure than in those who did not [59]. Yokose and colleagues used TRS (TRS-20, Hamamatsu Photonics) to demonstrate that vasospasm could be predicted with 100% sensitivity and 85.7% specificity in 14 predominantly poor-grade aSAH patients, and that a threshold of a 3.9–6.4% decline in cortical oxygen saturation was optimal for the identification of ischaemia [60]. In this study, the reliability of repeated NIRS measurements over time was ensured by the use of CT image-guidance to position the NIRS optodes. This novel approach allowed consistent measurement of the same cortical area on consecutive days. The introduction of time-resolved devices to the clinical setting brings the prospect of the measurement of multiple chromophore concentrations in absolute terms at the bedside.

Impairment of CA renders the brain more susceptible to ischaemic insults and is thus associated with poor outcome after brain injury (see Chapter 2.2.2). NIRS has recently been used to monitor CA in a variety of clinical settings and, although the therapeutic value of monitoring and managing CA is not clear, this has become an area of intense investigation. In a study of 40 patients with severe TBI, Zweifel and colleagues identified a statistically significant correlation between total haemoglobin reactivity index (THx), a measure of CA based on the moving correlation between THI and arterial blood pressure and pressure reactivity index (PRx), an outcome-validated index of pressure reactivity derived from invasive ICP and arterial blood pressure [61]. The same group also demonstrated a correlation between a TOS-derived measure of CA and Mx, a TCD-based index derived from middle cerebral artery blood flow velocity, in a group of 27 patients following poor-grade SAH [62]. It is suggested that NIRS-derived measures of CA may be able to guide optimisation of cerebral haemodynamics, including cerebral perfusion pressure, although evidence of its clinical utility is currently sparse.

As with CEA and CPB, measurement of CCO oxidation state may provide additional information about metabolic failure and aid in the determination of ischaemic thresholds following brain injury [10]. Using a customised BBS system based on the UCLn algorithm [25], Tisdall and colleagues found that changes in CCO oxidation correlated with measures of cerebral DO_2 in healthy volunteers [63] and subsequently demonstrated an increase in CCO oxidation during normobaric hyperoxia (NBH) in a pilot study of eight patients following TBI [64]. However, as discussed in Section 1.3.3, relationship between CCO oxidation status and metabolic activity is complex, and these complexities combine with the potential confounding effects of scattering and pathlength changes [25] to render the interpretation of observed oxCCO changes very difficult. These difficulties may be addressed by the development of mathematical models of brain haemodynamics and metabolism allows *in silico* derivation of signals which can be compared to measured signals and thereby facilitate their interpretation [65,66].

3.4 THE HYBRID OPTICAL SPECTROMETER

The pHOS is the NIRS apparatus that is used for the experiments described in this thesis. It combines two components: an multidistance broadband spectrometer (MDBBS) and an multidistance frequency domain spectrometer (MDFD) spectrometer. By using these two components, either singly or in concert, it should be possible to investigate, simultaneously, changes in chromophore concentration – in particular changes in oxCCO – as well glean information on factors which may confound the accurate measurement of these chromophore changes. Furthermore, whilst absorption is clearly a biomarker in disease (as it is directly dependent on chromophore concentration), it has also been suggested that scattering may be clinically-relevant biomarker in brain injury [67].

3.4.1 *MDFD instrumentation & technique*

A detailed derivation of the physical and mathematical basis of the MDFD technique is reported by Fantini [18,19] and Hueber [68]; its basic principles are outlined here. The MDFD spectrometer is based on the commercially-available OxyPlexTS™ spectrometer, (ISS Inc, Champaign, IL, USA), but has been modified with LED emitting light at four wavelengths: 690, 750, 790 and 850nm; these are amplitude-modulated at 110MHz. The instrument measures the average light intensity (DC), average wave amplitude (AC) and phase (θ) of the modulated intensity at source-detector separations of 3 and 3.5cm. Using linear regression, the slope (i. e. the change with respect to distance) of each of these variables is calculated. The Boltzmann diffusion approximation (discussed in Section 3.2.2 above) is then used to construct a system of simultaneous equations that relates these six variables (DC amplitude, AC amplitude, phase shift, DC slope, AC slope, phase shift slope) to the μ_a and μ_s'.

The MDFD undergoes a calibration procedure against a tissue-like phantom of known μ_a and μ_s' at the four wavelengths; this is required to account for the fact that the eight different sources (four wavelengths at two source-detector separations) emit light with variable intensity and phase. The original (unmodified) apparatus has been validated using tissue-like optical phantoms [18,19] and for tissue oximetry in adult human muscle [19]; as a tissue oximeter it has found widespread use in a variety of pre-clinical and clinical scenarios that are not considered here. The modified apparatus used for the studies described in this thesis has been validated using tissue-like optical phantoms [69,70], and its use described in use for the measurement of absolute μ_s' in the healthy adult head during a Valsalva manoeuvre and during functional activation [71–73]. This measurement of μ_s' is especially notable as changes in μ_s' have been proposed as cause of spuriously-observed changes in [oxCCO] [42].

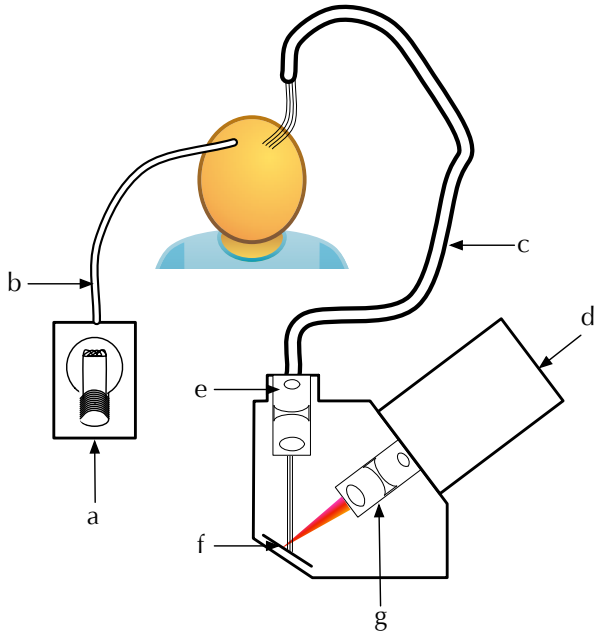

Figure 3.9 – Schematic representation of MDBBS. a-light source; b-source fibre; c-detector fibre bundle, with four detector optodes; d-charge-coupled device (CCD); e-diffraction slit and large-aperture lens; f-diffraction grating; g-large aperture lens.

3.4.2 *MDBBS instrumentation & technique*

The MDBBS component of the pHOS has been described in more detail elsewhere [69,74], it is represented diagramatically in Figure 3.9.

A 50w halogen light source is used with a short-pass filter (to minimise heat effects). The detector assembly comprises four detectors, placed 20/25/30/35mm from the source optical fibre. Detector fibres pass to the lens spectrograph, which is based on large aperture (f/1.2) lenses, a 50x50mm diffusion grating (300 groves per mm, blazed at 1000nm) and a 12.3x12.3mm, 512x512 pixel water-cooled CCD (Pixis 512, Princeton Instruments, Trenton NJ, USA). The spectrometer is calibrated against a mercury-argon laser to ensure accurate wavelength calibration and a spectral resolution of at least 5nm.

The MDBBS thus measures optical attenuation between 512-1024nm at four source-detector separations. These attenuation spectra can be used to measure changes in chromophore concentration using the UCLn algorithm – a broadband algorithm based upon the mBLL [25]– at four distances, potentially measuring chromophore changes in four different tissue layers simultaneously. Alternatively, by combining the four distances to measure the slope of attenuation, broadband SRS can be performed.

3.4.3 *Combined use of MDBBS & MDFD*

In addition to use in isolation, as described above, the two componenents of the pHOS can be used in concert, using novel algorithms. One example of such an algorithm is the use of DPF, derived from the MDFD using the diffusion approximation [71], which states that:

$$DPF = \frac{\sqrt{3\mu_s'}}{2\sqrt{\mu_a}} \tag{3.15}$$

By measuring the DPF in real time and substituting it in to the mBLL (equation 3.10, or its equivalent using the broadband UCLn algorithm). This methodology has been adopted in NIRS studies of functional activation [72,73] and changes in haemoglobin concentrations during a Valsalva manoeuvre [71].

Another novel combined use of the two components of the pHOS is through the use of absolute values of μ_a and μ_s', derived from the MDFD, to accurately scale the value of μ_a derived from multidistance measurements (see Section 3.2.2), providing the absolute values of μ_a across a wide range of wavelengths and thus, potentially, absolute chromophore concentration. This method has been proven in principle, but not validated [75].

3.5 CONCLUSION

Despite a large and ever-increasing number of commercial devices designed for, and clinical studies describing the use of NIRS as a monitor of CH-I, the data from the literature – largely reporting TOS-equivalents – have been largely disappointing. These introductory chapters have made the case for a bedside monitor of not only cerebral haemodynamics and DO_2 but of *metabolism*, on the basis of normal physiology, the pathophysiology of ABI and the clinical data describing the use of NIRS. There is some evidence that oxCCO may fulfil this role, but there are physiological and spectroscopic hurdles to the interpretation of this complex signal. The pHOS is a sophisticated custom-built NIRS apparatus that is designed to clear these hurdles – or at least assess their influence and pertinence. In the next part of this thesis concerns a clinical experimental study describing the use of the pHOS in healthy volunteers and patients with ABI.

REFERENCES

[1] Ghosh, A, Elwell, C & Smith, M. Cerebral near-infrared spectroscopy in adults: a work in progress. *Anesthesia & Analgesia*, 115(6):1373–1383, 2012.

[2] Greisen, G, Leung, T & Wolf, M. Has the time come to use near-infrared spectroscopy as a routine clinical tool in preterm infants undergoing intensive care? *Philosophical transactions of the Royal Society A: Mathematical, physical, and engineering sciences*, 369(1955):4440–4451, 2011.

[3] van Bel, F, Lemmers, P & Naulaers, G. Monitoring neonatal regional cerebral oxygen saturation in clinical practice: value and pitfalls. *Neonatology*, 94(4):237–244, 2008.

[4] Ferrari, M, Muthalib, M & Quaresima, V. The use of near-infrared spectroscopy in understanding skeletal muscle physiology: recent developments. *Philosophical transactions Series A, Mathematical, physical, and engineering sciences*, 369(1955):4577–4590, 2011.

[5] Hoshi, Y. Functional near-infrared spectroscopy: current status and future prospects. *Journal of Biomedical Optics*, 12(6):062106, 2007.

[6] Lloyd-Fox, S, Blasi, A & Elwell, CE. Illuminating the developing brain: the past, present and future of functional near infrared spectroscopy. *Neuroscience and biobehavioral reviews*, 34(3):269–284, 2010.

[7] Rolfe, P. In vivo near-infrared spectroscopy. *Annual review of biomedical engineering*, 2:715–754, 2000.

[8] Wolf, M, Ferrari, M & Quaresima, V. Progress of near-infrared spectroscopy and topography for brain and muscle clinical applications. *Journal of Biomedical Optics*, 12(6):062104, 2007.

[9] Jöbsis, FF. Noninvasive, infrared monitoring of cerebral and myocardial oxygen sufficiency and circulatory parameters. *Science*, 198(4323):1264–1267, 1977.

[10] Smith, M & Elwell, C. Near-infrared spectroscopy: shedding light on the injured brain. *Anesthesia & Analgesia*, 108(4):1055–1057, 2009.

[11] Ferrari, M & Quaresima, V. Review: Near infrared brain and muscle oximetry: from the discovery to current applications. *Journal of Near Infrared Spectroscopy*, 20:1–14, 2012.

[12] Ferrari, M, Mottola, L & Quaresima, V. Principles, techniques, and limitations of near infrared spectroscopy. *Canadian journal of applied physiology = Revue canadienne de physiologie appliquée*, 29(4):463–487, 2004.

[13] Elwell, CE. *A practical users guide to near infrared spectroscopy.* Hamamatsu Photonics KK, Japan, 1995.

[14] Cheong, WF, Prahl, SA & Welch, AJ. A review of the optical properties of biological tissues. *IEEE Quantum Electronics*, 1990.

[15] Delpy, DT, Cope, M, van der Zee, P, Arridge, S, Wray, S & Wyatt, J. Estimation of optical pathlength through tissue from direct time of flight measurement. *Physics in Medicine and Biology*, 33(12):1433–1442, 1988.

[16] Matcher, S, Cope, M & Delpy, D. In vivo measurements of the wavelength dependence of tissue-scattering coefficients between 760 and 900 nm measured with time-resolved spectroscopy. *Applied Optics*, 36(1):386–396, 1997.

[17] Matcher, SJ & Cooper, CE. Absolute quantification of deoxyhaemoglobin concentration in tissue near infrared spectroscopy. *Physics in Medicine and Biology*, 39(8):1295–1312, 1994.

[18] Fantini, S, Franceschini, MA, Fishkin, JB, Barbieri, B & Gratton, E. Quantitative determination of the absorption spectra of chromophores in strongly scattering media: a light-emitting-diode based technique. *Applied Optics*, 33(22):5204–5213, 1994.

[19] Fantini, S, Franceschini-Fantini, MA, Maier, JS, Walker, SA, Barbieri, BF & Gratton, E. Frequency-domain multichannel optical detector for noninvasive tissue spectroscopy and oximetry. *Optical Engineering*, 34:32–42, 1995.

[20] Lam, JM, Smielewski, P, Al-Rawi, P, Griffiths, P, Pickard, JD & Kirkpatrick, PJ. Internal and external carotid contributions to near-infrared spectroscopy during carotid endarterectomy. *Stroke*, 28(5):906–911, 1997.

[21] Davie, SN & Grocott, HP. Impact of extracranial contamination on regional cerebral oxygen saturation: a comparison of three cerebral oximetry technologies. *Anesthesiology*, 116(4):834–840, 2012.

[22] Fantini, S & Francheschini, MA. *Frequency-domain techniques for tissue spectroscopy and imaging*, chap. 7, pp. 405–443. SPIE Publications, 2002.

[23] Patterson, M, Chance, B & Wilson, B. Time resolved reflectance and transmittance for the non-invasive measurement of tissue optical properties. *Applied Optics*, 28(12):2331–2336, 1989.

[24] Torricelli, A, Contini, D, Pifferi, A, Caffini, M, Re, R, Zucchelli, L & Spinelli, L. Time domain functional NIRS imaging for human brain mapping. *NeuroImage*, 2013.

[25] Matcher, SJ, Elwell, CE, Cooper, CE, Cope, M & Delpy, DT. Performance comparison of several published tissue near-infrared spectroscopy algorithms. *Analytical biochemistry*, 227(1):54–68, 1995.

[26] Zhu, T, Faulkner, S, Madaan, T, Bainbridge, A, Price, D, Thomas, D, Cady, E, Robertson, N, Golay, X & Tachtsidis, I. Optimal Wavelength Combinations for Resolving in-vivo Changes of Haemoglobin and Cytochrome-c-oxidase Concentrations with NIRS. In *Biomedical Optics*, p. JM3A.6. OSA, Washington, D.C., 2012.

[27] Woodard, HQ & White, DR. The composition of body tissues. *The British journal of radiology*, 59(708):1209–1218, 1986.

[28] Gill, AS, Rajneesh, KF, Owen, CM, Yeh, J, Hsu, M & Binder, DK. Early optical detection of cerebral edema in vivo. *Journal of Neurosurgery*, 2010.

[29] Cooper, CE, Elwell, CE, Meek, JH, Matcher, SJ, Wyatt, JS, Cope, M & Delpy, DT. The noninvasive measurement of absolute cerebral deoxyhemoglobin concentration and mean optical path length in the neonatal brain by second derivative near infrared spectroscopy. *Pediatric research*, 39(1):32–38, 1996.

[30] Kou, L, Labrie, D & Chylek, P. Refractive indices of water and ice in the 0.65- to 2.5-μm spectral range. *Applied Optics*, 32(19):3531–3540, 1993.

[31] Hale, GM & Querry, MR. Optical Constants of Water in the 200-nm to 200-micron Wavelength Region. *Applied Optics*, 12(3):555–563, 1973.

[32] Zonios, G, Dimou, A, Bassukas, I, Galaris, D, Tsolakidis, A & Kaxiras, E. Melanin absorption spectroscopy: new method for noninvasive skin investigation and melanoma detection. *Journal of Biomedical Optics*, 13(1):014017, 2008.

[33] van Veen, R, Sterenborg, HJ, Pifferi, A, Torricelli, A & Cubeddu, R. Determination of VIS- NIR absorption coefficients of mammalian fat, with time- and spatially resolved diffuse reflectance and transmission spectroscopy. *Biomedical Topical Meetings, OSA Technica Digest (The Optical Society of America)*, 2004.

[34] Perutz, MF. Molecular Anatomy and Physiology of Hemoglobin. In *Disorders of Hemoglobin*, pp. 174–196. Cambridge University Press, 2001.

[35] Perutz, MF. Regulation of oxygen affinity of hemoglobin: influence of structure of the globin on the heme iron. *Annual review of biochemistry*, 48:327–386, 1979.

[36] Matcher, SJ, Cope, M & Delpy, DT. Use of the water absorption spectrum to quantify tissue chromophore concentration changes in near-infrared spectroscopy. *Physics in Medicine and Biology*, 39(1):177–196, 1994.

[37] Smith, M. Shedding light on the adult brain: a review of the clinical applications of near-infrared spectroscopy. *Philosophical transactions of the Royal Society A: Mathematical, physical, and engineering sciences*, 369(1955):4452–4469, 2011.

[38] Elwell, CE & Cooper, CE. Making light work: illuminating the future of biomedical optics. *Philosophical transactions of the Royal Society A: Mathematical, physical, and engineering sciences*, 369:4358–4379, 2011.

[39] Wray, S, Cope, M, Delpy, DT, Wyatt, JS & Reynolds, EO. Characterization of the near infrared absorption spectra of cytochrome aa3 and haemoglobin for the non-invasive monitoring of cerebral oxygenation. *Biochimica et biophysica acta*, 933(1):184–192, 1988.

[40] Cope, M. The application of near infrared spectroscopy to non invasive monitoring of cerebral oxygenation in the newborn infant. *University College London PhD Thesis*, 1991.

[41] Beinert, H, Shaw, RW, Hansen, RE & Hartzell, CR. Studies on the origin of the near-infrared (800-900 nm) absorption of cytochrome c oxidase. *Biochimica et biophysica acta*, 591(2):458–470, 1980.

[42] Cooper, CE, Matcher, SJ, Wyatt, JS, Cope, M, Brown, GC, Nemoto, EM & Delpy, DT. Near-infrared spectroscopy of the brain: relevance to cytochrome oxidase bioenergetics. *Biochemical Society transactions*, 22(4):974–980, 1994.

[43] Howell, SJ. Carotid endarterectomy. *British Journal of Anaesthesia*, 99(1):119–131, 2007.

[44] Moritz, S, Kasprzak, P, Arlt, M, Taeger, K & Metz, C. Accuracy of cerebral monitoring in detecting cerebral ischemia during carotid endarterectomy: a comparison of transcranial Doppler sonography, near-infrared spectroscopy, stump pressure, and somatosensory evoked potentials. *Anesthesiology*, 107(4):563–569, 2007.

[45] Pennekamp, CWA, Bots, ML, Kappelle, LJ, Moll, FL & de Borst, GJ. The value of near-infrared spectroscopy measured cerebral oximetry during carotid endarterectomy in perioperative stroke prevention. A review. *European journal of vascular and endovascular surgery*, 38(5):539–545, 2009.

[46] Samra, SK, Dy, EA, Welch, K, Dorje, P, Zelenock, GB & Stanley, JC. Evaluation of a cerebral oximeter as a monitor of cerebral ischemia during carotid endarterectomy. *Anesthesiology*, 93(4):964–970, 2000.

[47] Mille, T, Tachimiri, ME, Klersy, C, Ticozzelli, G, Bellinzona, G, Blangetti, I, Pirrelli, S, Lovotti, M & Odero, A. Near infrared spectroscopy monitoring during carotid

endarterectomy: which threshold value is critical? *European journal of vascular and endovascular surgery*, 27(6):646–650, 2004.

[48] Al-Rawi, PG & Kirkpatrick, PJ. Tissue oxygen index: thresholds for cerebral ischemia using near-infrared spectroscopy. *Stroke*, 37(11):2720–2725, 2006.

[49] Kellermann, K & Jungwirth, B. Avoiding stroke during cardiac surgery. *Seminars in Cardiothoracic and Vascular Anesthesia*, 14(2):95–101, 2010.

[50] Vohra, HA, Modi, A & Ohri, SK. Does use of intra-operative cerebral regional oxygen saturation monitoring during cardiac surgery lead to improved clinical outcomes? *Interactive cardiovascular and thoracic surgery*, 9(2):318–322, 2009.

[51] Murkin, JM, Adams, SJ, Novick, RJ, Quantz, M, Bainbridge, D, Iglesias, I, Cleland, A, Schaefer, B, Irwin, B & Fox, S. Monitoring brain oxygen saturation during coronary bypass surgery: a randomized, prospective study. *Anesthesia & Analgesia*, 104(1):51–58, 2007.

[52] Slater, JP, Guarino, T, Stack, J, Vinod, K, Bustami, RT, Brown, JM, Rodriguez, AL, Magovern, CJ, Zaubler, T, Freundlich, K & Parr, GVS. Cerebral oxygen desaturation predicts cognitive decline and longer hospital stay after cardiac surgery. *The Annals of thoracic surgery*, 87(1):36–44; discussion 44–5, 2009.

[53] Kakihana, Y, Matsunaga, A, Yasuda, T, Imabayashi, T, Kanmura, Y & Tamura, M. Brain oxymetry in the operating room: current status and future directions with particular regard to cytochrome oxidase. *Journal of Biomedical Optics*, 13(3):033001, 2008.

[54] Kakihana, Y, Matsunaga, A, Tobo, K, Isowaki, S, Kawakami, M, Tsuneyoshi, I, Kanmura, Y & Tamura, M. Redox behavior of cytochrome oxidase and neurological prognosis in 66 patients who underwent thoracic aortic surgery. *European journal of cardio-thoracic surgery*, 21(3):434–439, 2002.

[55] Nollert, G, Möhnle, P, Tassani-Prell, P, Uttner, I, Borasio, GD, Schmoeckel, M & Reichart, B. Postoperative neuropsychological dysfunction and cerebral oxygenation during cardiac surgery. *The Thoracic and cardiovascular surgeon*, 43(5):260–264, 1995.

[56] Robertson, CS, Gopinath, SP & Chance, B. Use of near infrared spectroscopy to identify traumatic intracranial hematomas. *Journal of Biomedical Optics*, 2(1):31–41, 1997.

[57] Dunham, CM, Ransom, KJ, Flowers, LL, Siegal, JD & Kohli, CM. Cerebral hypoxia in severely brain-injured patients is associated with admission Glasgow Coma

Scale score, computed tomographic severity, cerebral perfusion pressure, and survival. *The Journal of trauma*, 56(3):482–9; discussion 489–91, 2004.

[58] Leal-Noval, SR, Cayuela, A, Arellano-Orden, V, Marín-Caballos, A, Padilla, V, Ferrándiz-Millón, C, Corcia, Y, García-Alfaro, C, Amaya-Villar, R & Murillo-Cabezas, F. Invasive and noninvasive assessment of cerebral oxygenation in patients with severe traumatic brain injury. *Intensive Care Medicine*, 36(8):1309–1317, 2010.

[59] Bhatia, R, Hampton, T, Malde, S, Kandala, NB, Muammar, M, Deasy, N & Strong, A. The application of near-infrared oximetry to cerebral monitoring during aneurysm embolization: a comparison with intraprocedural angiography. *Journal of Neurosurgical Anesthesiology*, 19(2):97–104, 2007.

[60] Yokose, N, Sakatani, K, Murata, Y, Awano, T, Igarashi, T, Nakamura, S, Hoshino, T & Katayama, Y. Bedside monitoring of cerebral blood oxygenation and hemodynamics after aneurysmal subarachnoid hemorrhage by quantitative time-resolved near-infrared spectroscopy. *World Neurosurgery*, 73(5):508–513, 2010.

[61] Zweifel, C, Castellani, G, Czosnyka, M, Helmy, A, Manktelow, A, Carrera, E, Brady, KM, Hutchinson, PJA, Menon, DK, Pickard, JD & Smielewski, P. Noninvasive monitoring of cerebrovascular reactivity with near infrared spectroscopy in head-injured patients. *Journal of Neurotrauma*, 27(11):1951–1958, 2010.

[62] Zweifel, C, Castellani, G, Czosnyka, M, Carrera, E, Brady, KM, Kirkpatrick, PJ, Pickard, JD & Smielewski, P. Continuous assessment of cerebral autoregulation with near-infrared spectroscopy in adults after subarachnoid hemorrhage. *Stroke*, 41(9):1963–1968, 2010.

[63] Tisdall, MM, Tachtsidis, I, Leung, TS, Elwell, CE & Smith, M. Near-infrared spectroscopic quantification of changes in the concentration of oxidized cytochrome c oxidase in the healthy human brain during hypoxemia. *Journal of Biomedical Optics*, 12(2):024002, 2007.

[64] Tisdall, MM, Tachtsidis, I, Leung, TS, Elwell, CE & Smith, M. Increase in cerebral aerobic metabolism by normobaric hyperoxia after traumatic brain injury. *Journal of Neurosurgery*, 109(3):424–432, 2008.

[65] Banaji, M, Mallet, A, Elwell, CE, Nicholls, P & Cooper, CE. A model of brain circulation and metabolism: NIRS signal changes during physiological challenges. *PLoS computational biology*, 4(11):e1000212, 2008.

[66] Jelfs, B, Banaji, M, Tachtsidis, I, Cooper, CE & Elwell, CE. Modelling Noninvasively Measured Cerebral Signals during a Hypoxemia Challenge: Steps towards Individualised Modelling. *PloS one*, 7(6):e38297, 2012.

[67] Thiagarajah, JR, Papadopoulos, MC & Verkman, AS. Noninvasive early detection of brain edema in mice by near-infrared light scattering. *Journal of Neuroscience Research*, 80(2):293–299, 2005.

[68] Hueber, DM, Franceschini, MA, Ma, HY, Zhang, Q, Ballesteros, JR, Fantini, S, Wallace, D, Ntziachristos, V & Chance, B. Non-invasive and quantitative near-infrared haemoglobin spectrometry in the piglet brain during hypoxic stress, using a frequency-domain multidistance instrument. *Physics in Medicine and Biology*, 46(1):41–62, 2001.

[69] Tachtsidis, I, Leung, T, Tahir, B & Elwell, C. A Hybrid Multi-Distance Phase and Broadband Spatially Resolved Algorithm for Resolving Absolute Concentrations of Chromophores in the Near-Infrared Light Spectrum: Results from Studies in Dynamic Phantoms. *Biomedical Topical Meetings (The Optical Society of America), BSuE76, Florida, USA*, 2008.

[70] Tachtsidis, I, Gao, L, Leung, TS, Kohl-Bareis, M, Cooper, CE & Elwell, CE. A hybrid multi-distance phase and broadband spatially resolved spectrometer and algorithm for resolving absolute concentrations of chromophores in the near-infrared light spectrum. *Advances in Experimental Medicine and Biology*, 662:169–175, 2010.

[71] Gao, L, Elwell, CE, Kohl-Bareis, M, Gramer, M, Cooper, CE, Leung, TS & Tachtsidis, I. Effects of assuming constant optical scattering on haemoglobin concentration measurements using NIRS during a Valsalva manoeuvre. *Advances in Experimental Medicine and Biology*, 701:15–20, 2011.

[72] Ghosh, A, Tachtsidis, I, Kolyva, C, Cooper, CE, Smith, M & Elwell, CE. Use of a hybrid optical spectrometer for the measurement of changes in oxidized cytochrome c oxidase concentration and tissue scattering during functional activation. *Advances in Experimental Medicine and Biology*, 737:119–124, 2012.

[73] Kolyva, C, Tachtsidis, I, Ghosh, A, Moroz, T, Cooper, CE, Smith, M & Elwell, CE. Systematic investigation of changes in oxidized cerebral cytochrome c oxidase concentration during frontal lobe activation in healthy adults. *Biomedical optics express*, 3(10):2550–2566, 2012.

[74] Soschinski, J, Mine, LB, Geraskin, D, Bennink, G & Kohl-Bareis, M. Cerebral Oxygenation Monitoring during Cardiac Bypass Surgery in Infants with Broad Band Spatially Resolved Spectroscopy. In *European Conference on Biomedical Optics*, pp. 6629–30. OSA, Washington, D.C., 2007.

[75] Tachtsidis, I, Leung, T, Elwell, CE, Ghosh, A, Smith, M & Cooper, CE. Multi-Wavelength, Depth Resolved, Scattering and Pathlength Corrected in vivo Near-

Infrared Spectroscopy of Brain Tissue. *Biomedical Optics (BIOMED), OSA Technical Digest*, p. BTuB, 2010.

Part II

EXPERIMENTAL STUDIES

4

CYTOCHROME *C* OXIDASE DURING MANIPULATION OF CEREBRAL OXYGEN DELIVERY IN HEALTHY VOLUNTEERS

This chapter draws heavily on a paper published in NeuroImage *[1].*

This chapter describes the use of the hybrid optical spectrometer (pHOS) in a cohort of healthy volunteers. We manipulated cerebral oxygen delivery (cDO_2) by controlling the volunteers' gas mix and minute volume. The pHOS was used in a single-channel, four-distance configuration to measure changes in oxyhaemoglobin concentration ($[HbO_2]$), deoxyhaemoglobin concentration ([HHb]) and concentration of oxidised-reduced cytochrome *c* oxidase ([oxCCO]) at four source-detector separations, and also to perform spatially-resolved spectroscopy (SRS) to measure tissue oxygen saturation (TOS). We describe the changes in these chromophores and explore the anatomical and physiological basis of the observed [oxCCO] changes.

4.1 INTRODUCTION

TOS and its proprietary equivalents are frequently described as potential targets for brain monitoring in clinical contexts, yet the evidence to support such use is limited to a handful of specific clinical scenarios (as described in Section 3.3 and [2]). Whilst the concept behind TOS – that proportion of tissue haemoglobin that is oxidised – is simple, interpretation of this measure in the context of acute brain injury (ABI) is complex. Brain injury entails a number of interlinking pathophysiological cascades that may serve to limit the utility of TOS-like measures because differing pathophysiological perturbations may result in the same change in TOS. This results in difficulty deconvoluting the underlying contributing processes and thus appropriate clinical interventions [3]. Furthermore, haemoglobin from extra-cranial tissues makes a significant contribution to near infrared spectroscopy (NIRS)-derived haemoglobin measures [4–6]. The use of SRS-derived measures like TOS decreases this extracranial contribution [7,8], but lack of 'depth-specificity' remains a significant concern [9].

The measurement of changes in cytochrome *c* oxidase (CCO) oxidation state – as the NIRS-measured [oxCCO] – is thus an attractive alternative prospect for the detection and avoidance of secondary brain injury. It has been suggested that [oxCCO] is a 'brain-specific' signal because the higher mitochondrial number in brain compared to extracranial tissue gives rise to a higher CCO concentration in the former [3,10,11], but this postulate has never been proven experimentally. Before moving to clinical studies measuring [oxCCO] in patients with ABI, we sought to address specific concerns

regarding the veracity and robustness of the [oxCCO] signal [12]. Specifically, we wished to establish whether [oxCCO] is a more brain-specific signal than the concentration of haemoglobin species, by using the multidetector broadband array of the pHOS to measure simultaneously at multiple source-detector separations. We also sought to establish whether changes in optical scattering or differential pathlength factor (DPF) could be potentially confounding the accurate measurement of CCO oxidation in vivo.

Because reductions in cDO_2 are a key aspect of ABI pathophysiology, we sought to investigate the CCO response across a wide range of cDO_2 – ideally wider than one would encounter during clinical practice, for example during significant ischaemia, hypoxia or large changes in cerebral blood flow (CBF). Reduction in cDO_2, however, carries significant risks in patients with ABI; incrementing cDO_2 by means of inducing increases in CBF carries the risk of concomitantly increasing cerebral blood volume (CBV), thus increasing intracranial pressure (ICP) in patients who are liable to have decreased cerebral compliance and thus potentially inducing secondary injury. Increasing cDO_2 by means of normobaric hyperoxia (NBH), however, carries no such risk and thus forms the basis of the experiment described in Chapter 5.

The aims of this study were to investigate the utility of measurement of CCO oxidation status, measured with NIRS as Δ[oxCCO]. In particular, we wish to confirm the veracity of the measurements and the 'brain-specificity' of the Δ[oxCCO] measure. Furthermore, we wish to investigate whether measurement of Δ[oxCCO] has any additional benefit over the measurement of more commonly-used NIRS chromophores, both as a result of brain-specificity and its physiological basis. The experiment thus aims to systematically investigate the NIRS measured haemoglobin and CCO redox responses to isovolaemic and hypo- and hypervolaemic manipulations in cDO_2.

The hypotheses were that:

- changes in chromophore concentration in response to hypoxia, hyperoxia, hypocapnia and hypercapnia would be consistent with basic physiological principles and with those previously reported in the literature;
- CCO concentration changes would show a greater depth-specificity than haemoglobin species concentration. This would manifest as:
  - a greater magnitude of CCO oxidation changes observed in longer source-detector separations and
  - no difference in haemoglobin species concentration between the different source-detector separations.
- Optical scattering would show no change during the course of the cDO_2 manipulations.

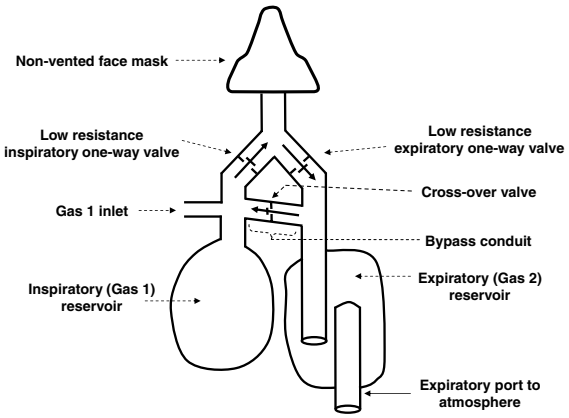

Figure 4.1 – Schematic diagram of sequential gas delivery circuit used for the hypoxia, hyperoxia and hypercapnia challenges (from [13]).

4.2 METHODS

This study was approved by the Joint Research Ethics Committee of the National Hospital for Neurology & Neurosurgery and Institute of Neurology. All subjects provided written informed consent.

4.2.1 *Physiological challenges*

Cerebral oxygen delivery was manipulated by four separate physiological challenges: hypoxia, hyperoxia, hypocapnia and hypercapnia. Before each challenge, a 5-minute period of baseline recording, inhaling room air, was carried out. A sequential gas delivery circuit, shown in Figure 4.1 was constructed and used for the hypoxia, hyperoxia and hypercapnia challenges [13], and throughout these challenges, the overall gas flow rate titrated to maintain the desired end tidal CO_2 ($etCO_2$) (i. e. constant in the hypoxia/hyperoxia studies and increased, as described below, during the hypercapnia studies).

HYPOXIA Hypoxia was induced through the delivery of a hypoxic mix, achieved through the addition of nitrogen to room air. Following the initial 5-minute 'baseline' period of recording, a mix with an inspired fraction of oxygen (FiO_2) of 8% was introduced – the 'induction' period, where the FiO_2 was titrated to achieve a reduction in pulse haemoglobin oxygen saturation (SpO_2) to 80%. Once this desired level of hypoxia was achieved, SpO_2 was maintained at 80% for a period of 5 minutes – the 'plateau' period. Following this, the inspired gas was returned to room air – the 'recovery' period, which ended when the end tidal O_2 (etO_2) had returned to baseline

values. A further 5 minutes of baseline recording was then carried out to complete the return-to-baseline period.

HYPEROXIA After the initial 5-minute baseline period of recording, hyperoxia was induced by increasing the FiO_2 to >90%. This was maintained for 5 minutes – the 'challenge' period – before returning the inspired gas to room air. The period between this re-introduction of room air inspiration to the normalisation of etO_2 to baseline levels was the recovery period, which was followed by a further 5 minutes of baseline recording.

HYPERCAPNIA The hypercapnia protocol was analogous to that used for hyperoxia in timing, with the inspired gas mix comprising an FiO_2 of 21% with the addition of 8% carbon dioxide (CO_2) for the challenge period, titrated to achieve an $etCO_2$ increase of $\sim$2kPa and the recovery period considered complete when $etCO_2$ had returned to baseline values.

HYPOCAPNIA The sequential gas delivery circuit was not used for the hypocapnia studies; rather, the subjects were given a mouthpiece incorporating the $etCO_2$ and etO_2 sensors/sidestreams and were breathing room air. Following the 5-minute baseline recording, subjects were instructed to hyperventilate to achieve an $etCO_2$ reduction of $\sim$2kPa, which was maintained for 5 minutes.

4.2.2 *NIRS monitoring*

Instrumentation

The pHOS (described previously [14,15] and Section 3.4) comprises multidistance broadband spectrometer (MDBBS) and multidistance frequency domain spectrometer (MDFD) components. The MDBBS component was used to measure chromophore concentration and TOS; all four distances (20, 25, 30 and 35mm) of MDBBS component were used. The MDFD component was used to measure optical absorption coefficient (μ_a) and reduced optical scattering coefficient (μ_s'). The pHOS optode – shown in Figure 4.2 – was applied in the mid-pupillary line on the forehead, high enough to avoid the expected position of the frontal sinus using elastic bandages, with extra light-shielding applied if the initial reflectance spectrum showed signs of external light contamination. The sampling period of the pHOS was 3.2 seconds - comprising a 2 second window for MDBBS data acquisition and 1.2 seconds for MDFD acquisition, shown schematically in Figure 4.3. MDBBS exposure adjusted to achieve a photon count of 6-65,000 photons per sample) and MDFD collected four samples in a 1.2 second period and with mean of these four samples recorded as the MDFD reading for this period. The processing

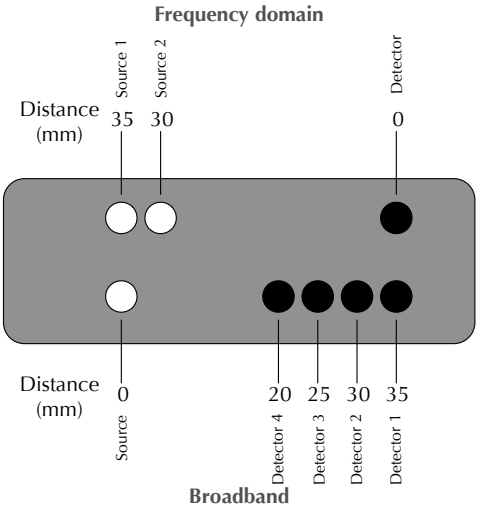

Figure 4.2 – Schematic diagram showing hybrid system optode, incorporating two MDFD light sources with a single detector (top half) and single MDBBS light source with four detectors (bottom half).

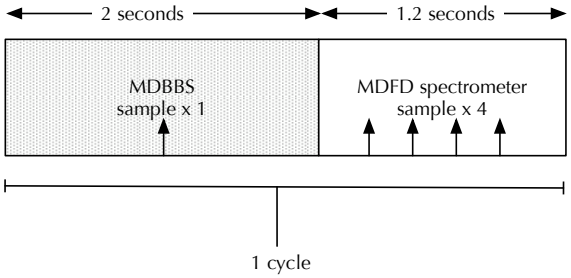

Figure 4.3 – pHOS sampling period with sequential MDBBS and MDFD acquisition.

of NIRS data to derive chromophore concentration was performed in Matlab (version R2010b, MathWorks, Natick MA).

NIRS algorithms

FREQUENCY DOMAIN SPECTROSCOPY The MDFD component was used to measure the μ_a and μ_s' using the technique described in Section 3.4.1; μ_a and μ_s' were derived from the measured average wave amplitude (AC) amplitude and phase shift [16–18]. We report μ_s' and DPF measured at 790nm and 850nm, as these were the wavelengths that lie within the resolving wavelength used for broadband spectroscopy (see below).

DIFFERENTIAL SPECTROSCOPY The modified Beer-Lambert Law (mBLL) was used to derive $\Delta[HbO_2]$, Δ[HHb] and Δ[oxCCO] using the UCLn algorithm (described previously [15,19] and Sections 3.2.1 and 3.2.2), incorporating a correction for the

wavelength dependence of DPF [20] and resolving over the wavelength range 780-900nm. Chromophore concentration changes were calculated individually for each source-detector separation. For the proximal two detectors (20 and 25mm), the DPF was assumed to be 6.26 [21]. For the distal two detectors (30 and 35mm), an individual-specific DPF was calculated from the mean DPF as measured with the MDFD during the first minute of recording, as previously described [22,23]. After $\Delta[HbO_2]$ and Δ[HHb] were derived, changes in Δhaemoglobin difference concentration ([HbDiff]) and Δtotal haemoglobin concentration ([HbT]) were calculated as described in Equations 3.14 and 3.13.

SPATIALLY RESOLVED SPECTROSCOPY TOS was calculated using the SRS methodology [24]. Using the measurements of light attenuation (A) across the four source-detector separations (d), linear regression was performed to yield an attenuation slope ($\delta A/\delta d$). This was repeated for every wavelength (λ) across the range 740-900nm for each time point. The diffusion approximation was then used to derive a relative μ_a spectrum as given by the equation

$$k\mu_a(\lambda) = \frac{1}{3(1-h\lambda)}\left(\ln 10.\frac{\delta A(\lambda)}{\delta p} - \frac{2}{\overline{\rho}}\right)^2. \tag{4.1}$$

where $(1-h\lambda)$ is a correction factor for the wavelength dependency of optical scattering [25] and $\overline{\rho}$ is the mean source-detector separation. A 70% water concentration was assumed, and the consequent spectrum was subtracted from the $k\mu_a(\lambda)$ spectrum; this spectrum was used to derive the relative concentrations of $[HbO_2]$ and [HHb], and the TOS then derived as described in Equation 3.11.

FURTHER PROCESSING All concentrations calculated using the mBLL as well as the TOS were processed with a linear detrend to remove baseline drifts and subject to a low-pass filter with a 5th order Butterworth filter with a cut-off frequency of 0.08 Hz as previously described [22,26].

4.2.3 *Other physiological monitoring*

Other physiological monitoring comprised SpO_2 measurement, using beat-to-beat pulse oximetry (modified Oxypleth, NovaMetrix, MA); continuous non-invasive arterial blood pressure (PortaPres, Finapres Medical Systems, The Netherlands); heart rate monitoring, using electrocardiography (IntelliVue MP50, Philips Healthcare, The Netherlands); inspired/expired oxygen partial pressure (IntelliVue Anaesthetic Gas Module, Philips Healthcare); $etCO_2$ measurement by capnography (CO2SMO, NovaMetrix) and middle cerebral artery flow velocity (VMCA) measurement, using transcranial Doppler (TCD) ultrasonography ipsilateral to the pHOS optode (DWL Doppler Box, Compumedics,

Germany). Data from the IntelliVue monitors was collected using Trendface (Ixellence, Wildau, Germany) at 125hz. Capnography and blood pressure waveforms and SpO_2 connected via analogue interface and analogue-to-digital convertor (ADC) to the TCD software (QL, Compumedics, Germany) and oversampled at 50hz.

4.2.4 *Derivation of other brain metabolic indices*

Changes in estimated cerebral oxygen delivery ($ecDO_2$) were calculated from the measured V_{MCA} and SpO_2. CDO_2, in units of ml/100g tissue/minute can be calculated as follows:

$$\begin{aligned} cDO_2 &= CBF \times (\text{Haemoglobin-bound } O_2 + \text{dissolved } O_2) \\ &= CBF \times (1.39 \times [Hb] \times SpO_2 + 0.0025 \times pO_2). \end{aligned} \tag{4.2}$$

where CBF is in ml/100g tissue/minute, 1.39 is the oxygen carrying-capacity of haemoglobin in ml/g, [Hb] is the concentration of haemoglobin in g/dL, 0.0025 is the solubility of oxygen in blood in ml/kPa/dL and partial pressure of oxygen (pO_2) is in kPa. Assuming constant TCD insonation angle and middle cerebral artery (MCA) artery diameter, V_{MCA} correlates with CBF [27], and ignoring dissolved fraction of O_2, which is small in comparison to the haemoglobin-bound component, changes $ecDO_2$ can be estimated as:

$$\Delta ecDO_2 \approx \Delta V_{MCA} \times \Delta SpO_2. \tag{4.3}$$

$ecDO_2$ was calculated in this fashion for the hypoxia, hypocapnia and hypercapnia challenges. It was not calculated during the hyperoxia challenge as the increase in cDO_2 achieved during hyperoxia is typically as a result of an increase in water-dissolved O_2, assuming – as it is in health – that haemoglobin is at full or near-full saturation.

An estimation of $(CMRO)$ *was also derived in a similar fashion, using a NIRS – approximation of the Kety – Schmidt / Fick equation* [28] :

$$\Delta \text{Relative CMRO} = \frac{V_{MCA}}{V_{MCA_0}} \cdot \left(\frac{SpO_2 - TOS}{SpO_{2_0} - TOS_0} \right), \tag{4.4}$$

where V_{MCA}, SpO_2 and TOS for any given timepoint are compared to their respective baseline values, V_{MCA_0}, SpO_{2_0} and TOS_0.

4.2.5 *Further processing and epoch selection*

All further processing was carried out in MatLab (version R210b, MathWorks, Natick MA). Synchronisation between the various systems was achieved by means of a constant potential output by the MDFD component of the pHOS, which was recorded by the

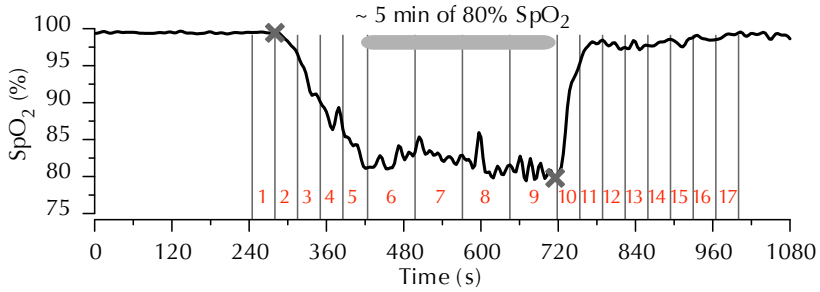

Figure 4.4 – Illustrative example of epoch selection during hypoxia challenge in a single volunteer.

TCD software via ADC and Trendface via a modified pressure monitor interfaced with the IntelliVue monitor. After synchronisation of all measured signals, the measured oxygen (O_2) and CO_2 partial pressure waveforms were processed by selecting the mean of the maximum and minimum 5% of readings to yield the inspired and end-tidal gas partial pressures. The TCD-measured velocity envelope, SpO_2, heart rate and arterial blood pressure were all averaged over 3.2-second periods to coincide with the sampling period of the pHOS and the resulting data synchronised with the NIRS data yielded from the pHOS, resulting in a single combined dataset for each subject.

Each subject varied in their physiological responses to the individual challenges. In order to allow averaging across subjects despite this, for each challenge in each subject, the recorded data were split in to 17 epochs on the basis of the observed (systemic) physiological response to the challenge.

For the hyperoxia, hypercapnia and hypocapnia challenges, the beginning and end of the challenge periods were identified from the corresponding inspired or end-tidal gas partial pressures. This challenge period was split in to 8 epochs of equal length (termed Epochs 2–9); Epoch 1 was defined as the time period immediately preceding the commencement of the challenge; Epochs 10–17 were defined as those epochs immediately following the completion of the challenge period. All epochs were of equal length, that length being defined in the initial split of the challenge period. Examples

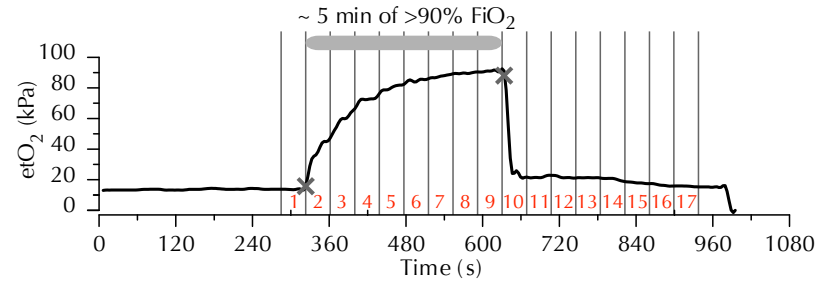

Figure 4.5 – Illustrative example of epoch selection during hyperoxia challenge in a single volunteer.

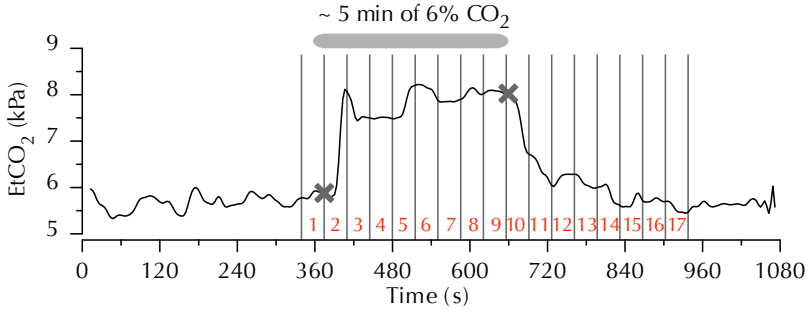

Figure 4.6 – Illustrative example of epoch selection during hypercapnia challenge in single volunteer.

illustrating this process in individual subjects' datasets are shown in Figures 4.5, 4.6 and 4.7.

The hypoxia challenge differed from the others in that it contained an induction phase – that is, the time between the commencement of hypoxic gas mix inhalation and reduction of SpO_2 to 80% – which varied in length from individual to individual; this mandated a different approach to epoch selection. First, the onset of the induction period and end of the plateau period were identified by inspection of the measured FiO_2. The onset of the plateau period was identified from the measured SpO_2. The induction and plateau period were then each split in to 4 epochs of equal length (termed Epochs 2–5 for induction and Epochs 6–9 for plateau). The period following the plateau was split in to eight epochs (Epochs 10–17), each the same in length as Epochs 2–5. An illustrative example of this process as carried out in an experimental subject is shown in Figure 4.4.

In each of epochs in each of the challenges, representative NIRS and systemic physiological data were derived by averaging the values final 9×3.2s.

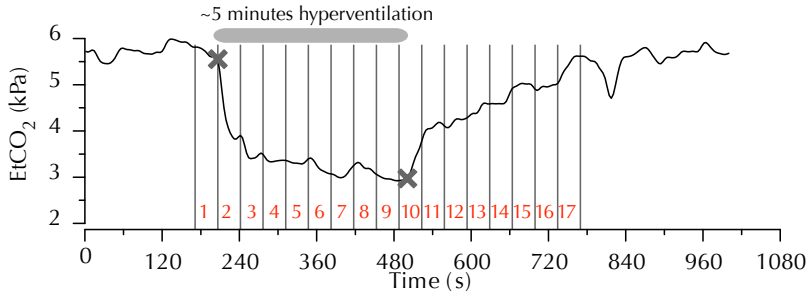

Figure 4.7 – Illustrative example of epoch selection during hypocapnia challenge in single volunteer.

Figure 4.8 – Photograph of volunteer with all monitoring *in situ* (reproduced with permission of subject).

4.2.6 *Statistical analysis*

Statistical analysis was carried out in SPSS (PASW Statistics for Windows, version 18.0, SPSS Inc, Chicago, IL) and R [29]. Normality was assessed through the use of Q-Q plots. For each of the four challenges, two sets of comparisons were made.

First a comparison of group means (for each measured variable) between the baseline epoch (Epoch 1) and each subsequent epoch in the challenge protocol was performed. This was achieved by first using repeated measures analysis of variance (ANOVA) with a Greenhouse-Geisser correction for sphericity. If this showed a significant change, post-hoc tests with Bonferroni corrections were used to calculate the statistical significance of the observed mean changes in Epochs 2–17 compared to baseline Epoch 1.

Second, a comparison was made between the mBLL-derived chromophore concentration changes between the four source-detector separations at each time point. A repeated-measures ANOVA with Greenhouse-Geisser correction was again used to determine whether there was a significant difference between the varying source-detector separations; if this showed statistically significant variation, then post hoc tests with Bonferroni corrections were used determine the statistical significance of changes when compared to the neighbouring detectors.

Unless otherwise stated, all data are expressed as mean ± standard error of mean (SEM). Statistical significance was inferred at $p<0.05$.

4.3 RESULTS

Each challenge was completed in 15 subjects (22 subjects took part in total, but not all completed every challenge). Demographic data is shown in Table 4.1. With regard to statistical significance, p-values reported in the text below are those derived from the repeated-measures ANOVA; where statistical significance is indicated in Figures 4.9–4.16, these were derived from the post-hoc testing comparing either individual Epochs to the baseline Epoch, or adjacent detectors during the same epoch. We were unable to resolve SRS-derived chromophore measures for 3 volunteers in hypoxia and hypocapnia studies, and for 2 volunteers in the hyperoxia and hypercapnia studies – the TOS figures quoted are thus for 12 and 13 volunteers, respectively.

4.3.1 *Hypoxia*

PHYSIOLOGICAL VARIABLES Reduction of FiO_2 resulted in a reduction in SpO_2 to 80 ± 1.3 % ($p<0.001$) by the end of the challenge period. Changes in physiological variables are shown in Table 4.2 and Figure 4.9. Statistically significant increases in heart rate and V_{MCA} were also seen (both $p<0.001$), as was a statistically significant reduction in $etCO_2$ ($p<0.01$). Baseline V_{MCA} was 61.6±3.5 $cm.s^{-1}$.

Of note, throughout the experiments, the baseline SpO_2 was approximately 97.5%, rather than the 99-100% that would be expected for a set of healthy volunteers. We ascribe this to an equipment-related error pertaining to the interfacing between the pulse oximeter, which outputted an analogue signal which required re-digitisation for recording. This discrepancy was noted during the experiments, but after several volunteers had already completed the experiments, and a decision taken to continue without applying an extra scaling factor to all experiments to correct for this.

CHROMOPHORE CONCENTRATION Figure 4.9 shows changes in [oxCCO], [HbT] and [HbDiff] during hypoxia and recovery at the 35mm source-detector separation. Reductions in [oxCCO] and [HbDiff] were seen, accompanied by an increase in [HbT] ($p<0.001$ for all). Changes for each source-detector combination are shown in Figure 4.13. The direction of change was consistent – i. e. a reduction in mean [oxCCO] and [HbDiff] and increase in [HbT] – was seen in each Epoch of the challenge period for each of the source-detector separations. A statistically significant difference in mean [oxCCO] between one detector and its neighbour was observed in 10/30 post-hoc comparisons between a detector and its neighbour during the induction or challenge Epochs; such a change was observed in 12/30 comparisons in the case of [HbDiff] and

only 1/30 in the case of [HbT]. A significant reduction in TOS was seen ($p<0.001$), as shown in Figure 4.17a.

VASOVAGAL SYNCOPE One subject suffered from a vasovagal syncope during the hypoxia challenge. He was excluded from the group for analysis, but the findings from his study are discussed below in Section 4.4.6.

4.3.2 *Hyperoxia*

PHYSIOLOGICAL VARIABLES Increase in FiO_2 resulted in an increase in mean etO_2 from 14.3 $\pm$ to 89.2 $\pm$ 1.4 kPa ($p<0.001$) with a corresponding increase in SpO_2 ($p<0.01$). Changes in measured physiological variables are shown in Table 4.2 and Figure 4.10. Statistically significant reductions in $etCO_2$ ($p<0.01$) and heart rate ($p<0.05$) were also seen. No statistically significant change was observed in VMCA, with a baseline flow of 60.7$\pm$3.1 cm.s^{-1}.

CHROMOPHORE CONCENTRATION Figure 4.10 shows changes in chromophore concentration at the 35mm source-detector separation; the changes observed were the inverse of those seen during hypoxia, with increases in [oxCCO] and [HbDiff] and a reduction in [HbT] (all $p<0.001$). Changes for each source-detector combination are shown in Figure 4.14. As was the case with the hypoxic challenge, there was a consistent direction of change was consistent, with an increase in mean [oxCCO] and [HbDiff] and reduction in mean [HbT] seen for each of the source-detector separations during the induction and challenge Epochs of the study. A statistically significant difference in mean [oxCCO] between one detector and its neighbour was observed in 8/30 post-hoc comparisons between a detector and its neighbour during the induction or challenge Epoch, but only in 3/30 comparisons in the case of [HbDiff] and no significant difference was seen between detectors in for [HbT]. A significant increase in TOS was seen ($p<0.05$), as shown in Figure 4.17b.

4.3.3 *Hypocapnia*

PHYSIOLOGICAL VARIABLES Changes in measured physiological variables are shown in Table 4.2 and Figure 4.11. Hyperventilation resulted in a reduction in $etCO_2$ from 5.3 $\pm$ 0.2 to 3.0 $\pm$ 0.1 kPa, with a corresponding reduction in VMCA by 30 $\pm$ 2.3% from a baseline flow rate of 56.6$\pm$4.1 cm.s^{-1}; both changes were statistically significant ($p<0.001$). A statistically significant increase in heart rate was also seen. An increase in mean arterial pressure (MAP) was observed ($p<0.05$), although post-hoc testing revealed no change during the challenge period, but there was a statistically significant increase observed in a single Epoch during the recovery period. Heart rate showed a significant increase ($p<0.001$).

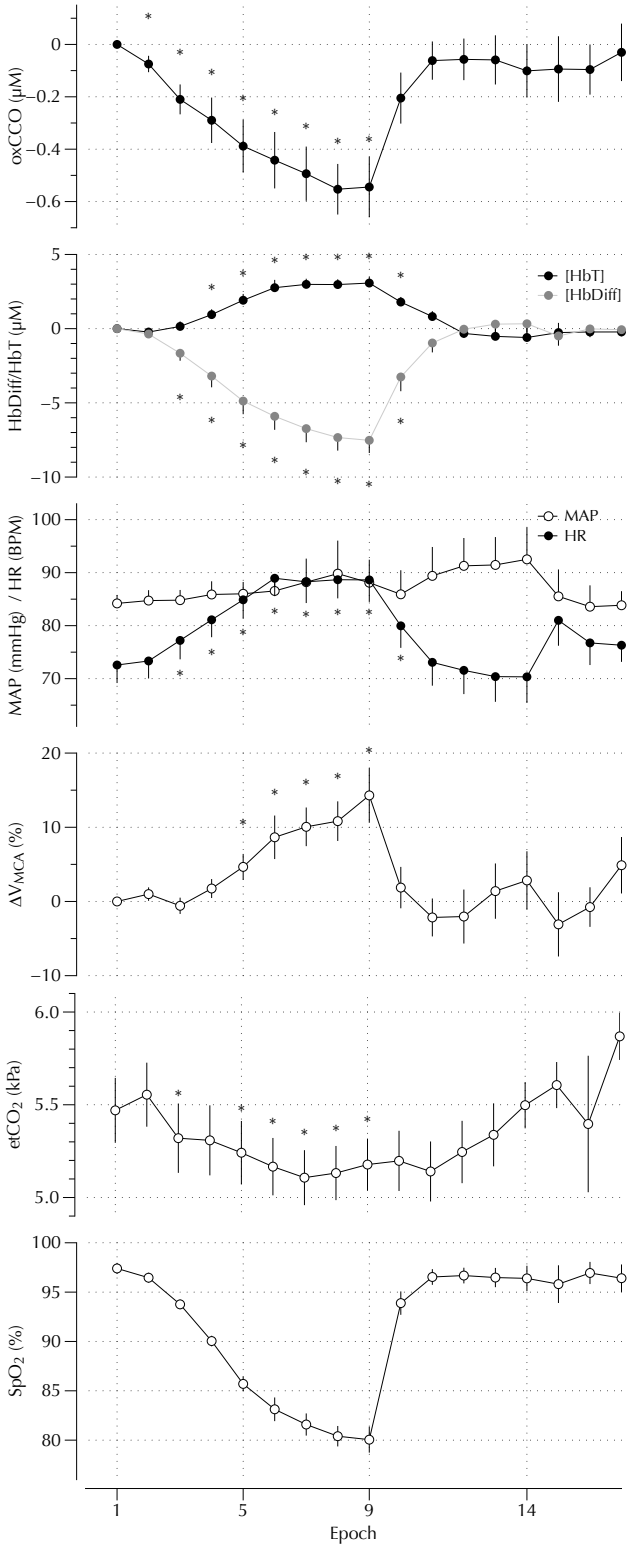

Figure 4.9 – Physiological variables and chromophore concentration with 35mm detector during hypoxia challenge. All figures are mean with error bars showing SEM. * - statistically significant ($p<0.05$) difference when compared to baseline Epoch (Epoch 1).

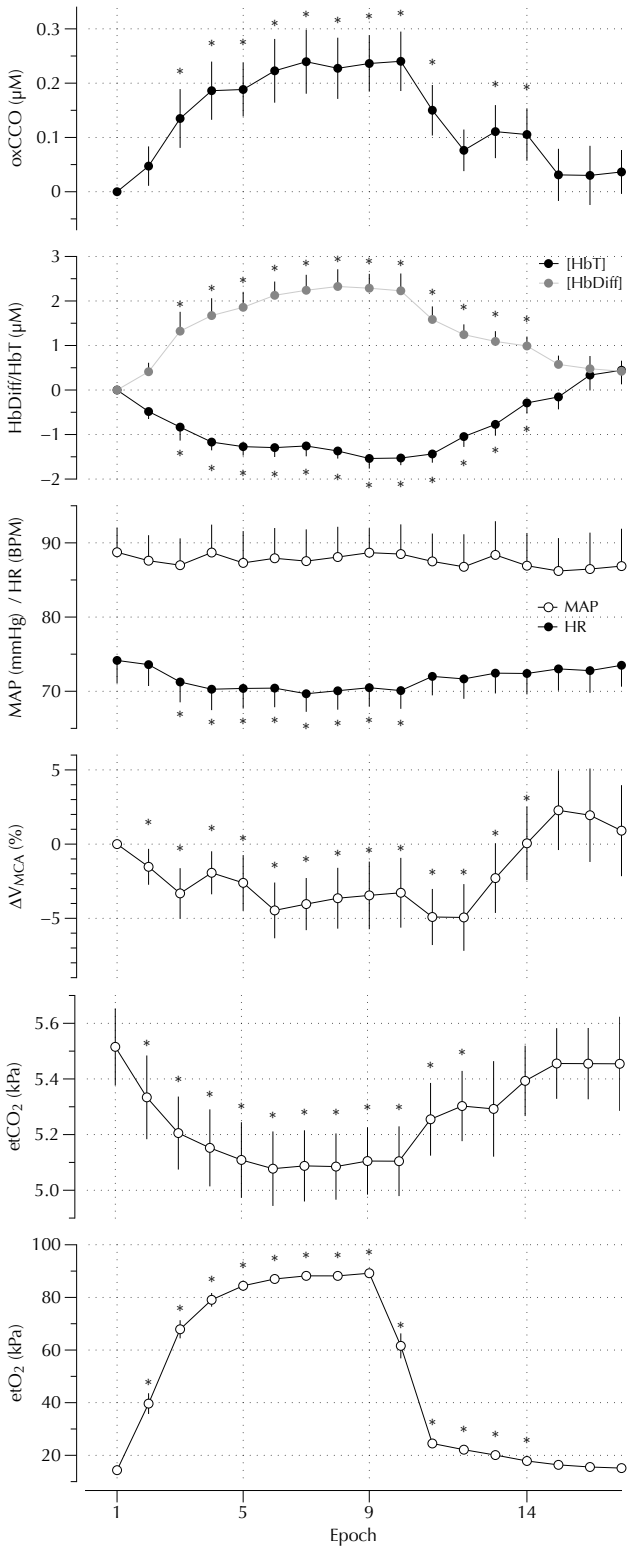

Figure 4.10 – Physiological variables and chromophore concentration with 35mm detector during hyperoxia challenge. All figures are mean with error bars showing SEM. * - statistically significant ($p<0.05$) difference when compared to baseline Epoch (Epoch 1).

CHROMOPHORE CONCENTRATION As shown in Figure 4.11, hyperventilation was associated with reductions in concentrations all chromophores ($p<0.01$ for [oxCCO] and [HbT]; $p<0.05$ for [HbDiff]). Changes for each source-detector combination are shown in Figure 4.15. While the direction of change was consistent – i. e. there was a reduction in each of the chromophores seen in in each Epoch of the challenge period for each of the source-detector separations during the induction and challenge periods. A statistically significant difference in mean oxidised-reduced cytochrome *c* oxidase (oxCCO) between one detector and its neighbour was observed in 8/30 post-hoc comparisons between a detector and its neighbour during the induction or challenge Epochs; this was the case in 13/30 comparisons of [HbT], but with smaller magnitude changes seen at the most distal (35mm) detector. There was no significant difference between detectors in [HbDiff] measurements. A significant reduction in TOS was seen ($p<0.05$), as shown in Figure 4.17c.

4.3.4 *Hypercapnia*

PHYSIOLOGICAL VARIABLES The delivery of a hypercapnic mix resulted in an increase in $etCO_2$ from 5.1 $\pm$ 0.1 to 7.7 $\pm$ 0.2 kPa, with a corresponding increment in VMCA by 59.1$\pm$6.0% from a baseline flow rate of 60.6$\pm$7.6 $cm.s^{-1}$; both changes were statistically signficant ($p<0.001$). Significant increases in MAP ($p<0.01$) and heart rate ($p<0.05$) were also seen, as shown in Table 4.2 and Figure 4.12.

CHROMOPHORE CONCENTRATION As shown in Figure 4.12, changes in chromophore concentration during hypercapnia were the inverse of those seen during hypocapnia, with reductions in [oxCCO] and [HbDiff] ($p<0.001$) as well as [HbT] ($p<0.01$). Changes for each source-detector combination are shown in Figure 4.16. The direction of change was consistent with an increase in chromophore concentration seen in each Epoch of the challenge period for each of the source-detector separations. Larger increases in [oxCCO] were seen in more distal detectors, whereas [HbT] showed smaller changes in the more distal detectors; there was no clear pattern with [HbDiff]. A statistically significant difference in mean [oxCCO] between one detector and its neighbour was observed in 22/30 post-hoc comparisons between a detector and its neighbour during the induction or challenge Epochs; such a change was observed in 7/30 comparisons in the case of [HbDiff] and only 2/30 in the case of [HbT]. A significant increase in TOS was seen ($p<0.001$), as shown in Figure 4.17d.

4.3.5 *Comparison of changes in $ecDO_2$ with estimated CMRO and chromophore concentration changes*

Plots comparing $ecDO_2$ to changes in Δ[HbDiff], Δ[oxCCO], both absolute and individual-changes in TOS and estimated CMRO are shown in Figures 4.20 and 4.21.

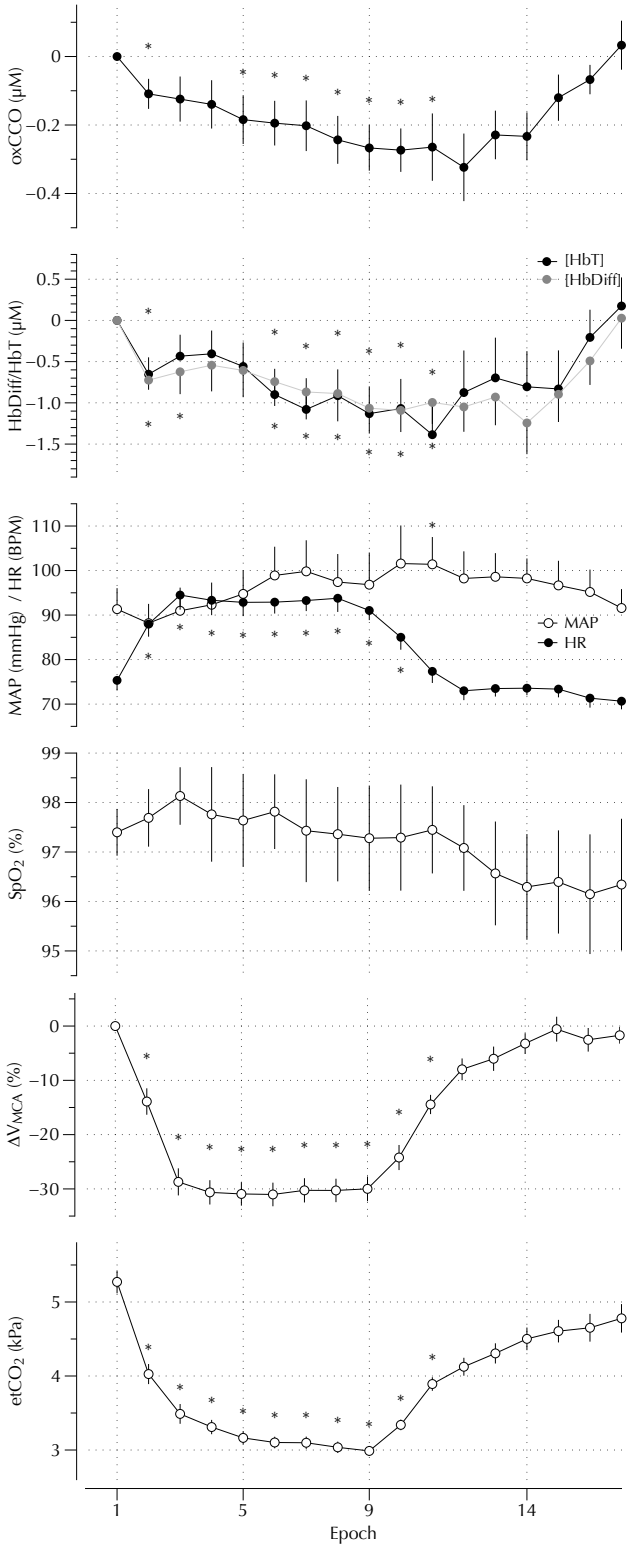

Figure 4.11 – Physiological variables and chromophore concentration with 35mm detector during hypocapnia challenge. All figures are mean with error bars showing SEM. * - statistically significant ($p<0.05$) difference when compared to baseline Epoch (Epoch 1).

	HYPOXIA	HYPEROXIA	HYPOCAPNIA	HYPERCAPNIA
n	15	15	15	15
Age (years)	30±4	30±4	31±4	30±3
Gender (m:f)	10:5	10:5	9:6	11:4

Table 4.1 – Demographic data for volunteers.

4.3.6 *DPF and scattering*

Mean baseline values for DPF used for the 30 and 35mm detectors, as well as μ_s' for each experiment, are shown in Table 4.3. There was no change in μ_s' for any of the experiments at any wavelength.

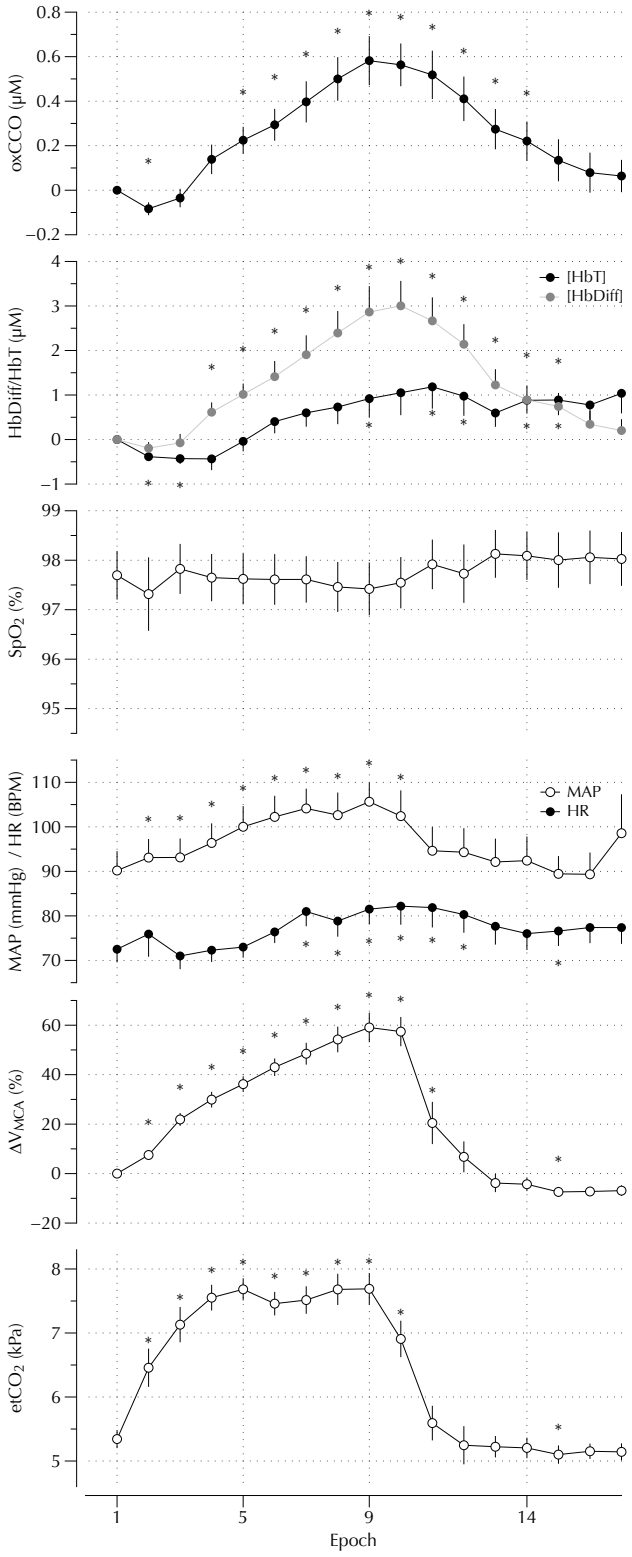

Figure 4.12 – Physiological variables and chromophore concentration with 35mm detector during hypercapnia challenge. All figures are mean with error bars showing SEM. * - statistically significant ($p<0.05$) difference when compared to baseline Epoch (Epoch 1).

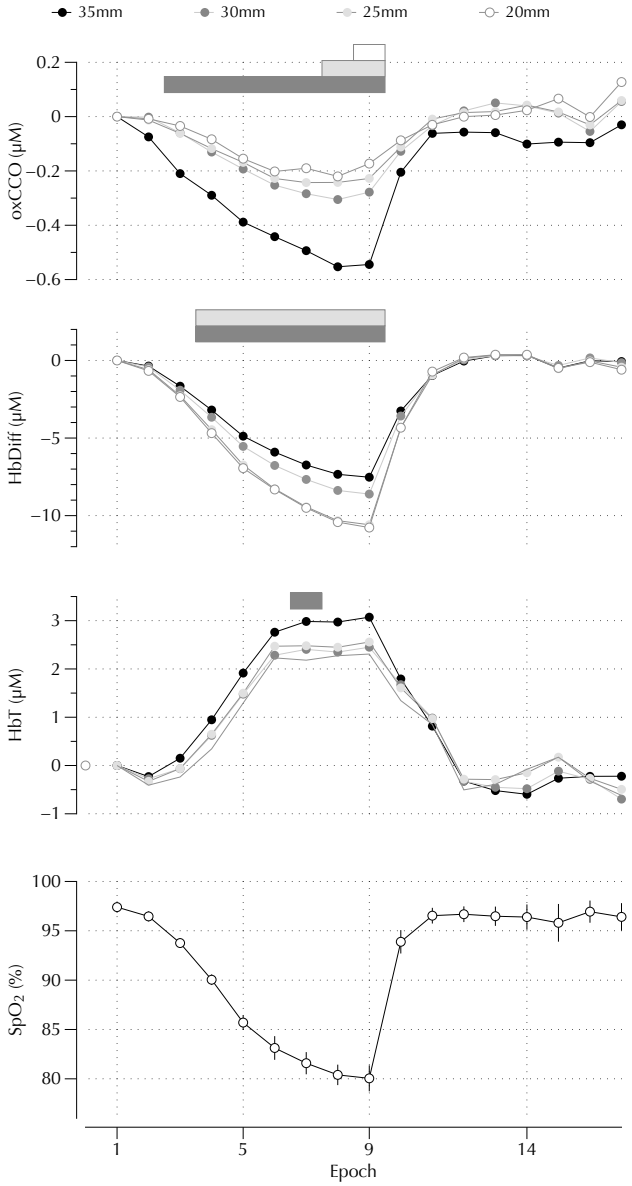

Figure 4.13 – Chromophore concentration for each detector during hypoxia challenge. All figures are mean, with SEM error bars shown for the SpO_2. The bars placed over the chromophore plots indicate a statistically significant ($p<0.05$) difference in chromophore concentration between a detector and its neighbour, where the dark grey box indicates a difference between the 35-30mm pair, light grey indicates a difference between the 30-25mm pair and the white box indicates a difference between the 25-20mm pair.

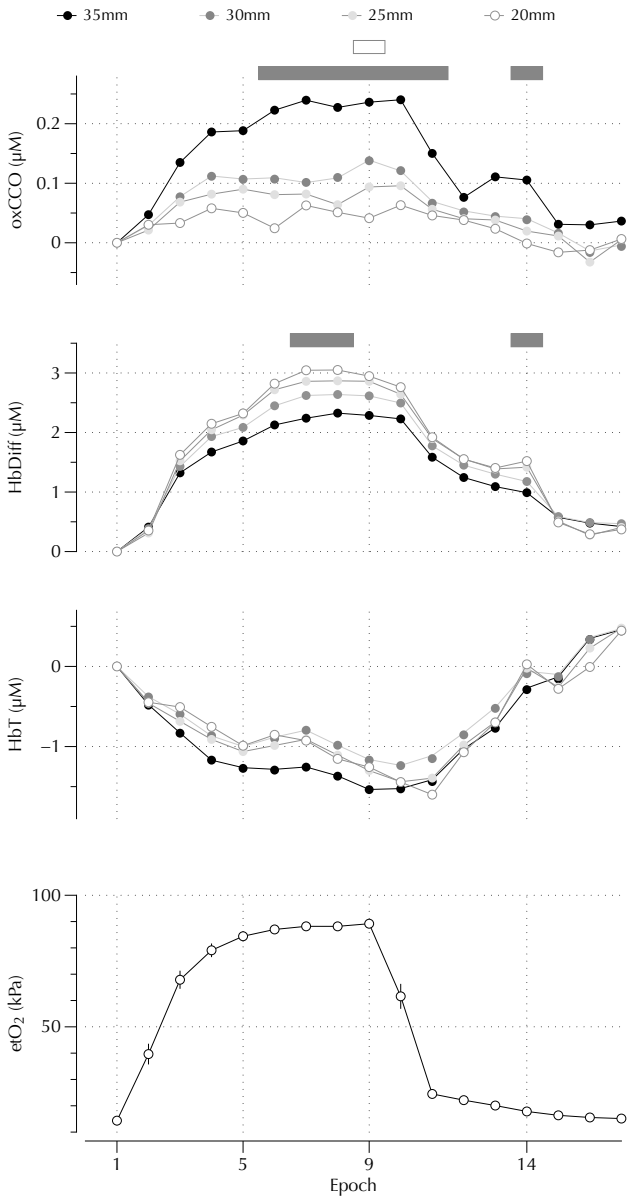

Figure 4.14 – Chromophore concentration for each detector during hyperoxia challenge. All figures are mean, with SEM error bars shown for the etO_2. Statistically significant differences between detectors are indicated by the overlying bars as in Figure 4.13.

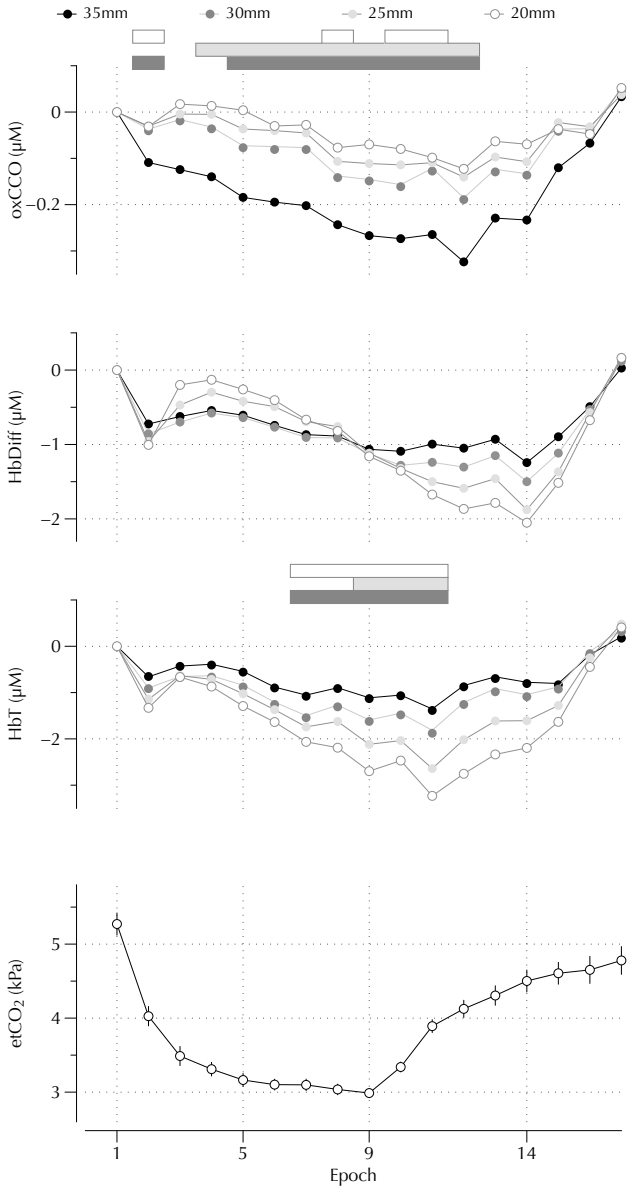

Figure 4.15 – Chromophore concentration for each detector during hypocapnia challenge. All figures are mean, with SEM error bars shown for the $etCO_2$. Statistically significant differences between detectors are indicated by the overlying bars as in Figure 4.13.

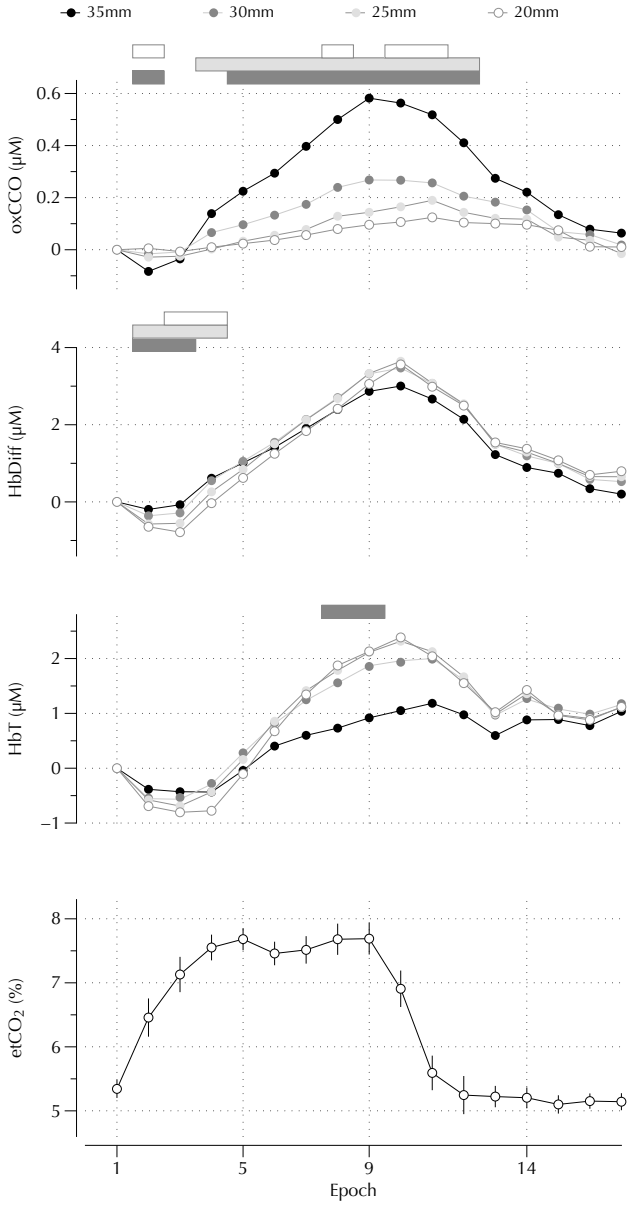

Figure 4.16 – Chromophore concentration for each detector during hypercapnia challenge. All figures are mean, with SEM error bars shown for the $etCO_2$. Statistically significant differences between detectors are indicated by the overlying bars as in Figure 4.13.

		Epoch 1	Epoch 9	
HYPOXIA	MAP (mmHg)	84.2 ± 1.6	88.1 ± 4.3	
	HR (BPM)	72.6 ± 3.4	88.6 ± 4.1	*
	SpO_2 (%)	97.4 ± 0.6	80.0 ± 1.3	*
	$etCO_2$ (kPa)	5.5 ± 0.2	5.2 ± 0.1	*
	ΔV_{MCA}(%)	0	14.3 ± 3.7	*
HYPEROXIA	MAP (mmHg)	88.7 ± 3.3	88.7 ± 3.3	
	HR (BPM)	74.2 ± 3.1	70.5 ± 2.5	*
	SpO_2 (%)	97.2 ± 0.5	98.2 ± 0.6	*
	etO_2 (kPa)	14.3 ± 0.3	89.2 ± 1.4	*
	$etCO_2$ (kPa)	5.5 ± 0.1	5.1 ± 0.1	*
	ΔV_{MCA}(%)	0	−3.5 ± 2.3	
HYPOCAPNIA	MAP (mmHg)	91.3 ± 4.7	96.8 ± 7.2	
	HR (BPM)	75.3 ± 2.3	91.0 ± 2.2	*
	SpO_2 (%)	97.4 ± 0.5	97.3 ± 1.1	
	$etCO_2$ (kPa)	5.3 ± 0.2	3.0 ± 0.1	*
	ΔV_{MCA}(%)	0	−30.0 ± 2.3	
HYPERCAPNIA	MAP (mmHg)	90.2 ± 4.3	105.6 ± 4.2	*
	HR (BPM)	72.5 ± 3.0	81.5 ± 3.4	*
	SpO_2 (%)	97.7 ± 0.5	97.4 ± 0.5	
	$etCO_2$ (kPa)	5.3 ± 0.1	7.7 ± 0.2	*
	ΔV_{MCA}(%)	0	59.1 ± 6.0	*

Table 4.2 – Changes, expressed as mean ± SEM, in physiological variables for volunteers at baseline (Epoch 1) and at the end of each challenge (Epoch 9).

	HYPOXIA	HYPEROXIA	HYPOCAPNIA	HYPERCAPNIA
DPF	7.45 ± 1.19	6.98 ± 1.04	6.93 ± 0.97	7.17 ± 0.96
μ_s' (cm^{-1})	8.98 ± 0.37	8.91 ± 0.43	9.26 ± 0.41	8.87 ± 0.41

Table 4.3 – DPF used and μ_s' at baseline (i. e. Epoch 1).

		Epoch 1	Epoch 9
HYPOXIA	Δ[HbDiff] (μM)	0	-7.50 ± 0.52*
	Δ[HbT] (μM)	0	3.10 ± 0.50*
	Δ[oxCCO] (μM)	0	-0.55 ± 0.09*
	TOS (%)	69.6 ± 2.5	61.6 ± 1.9 *
	ΔTOS (%)	0	-8.0 ± 2.0 *
HYPEROXIA	Δ[HbDiff] (μM)	0	2.29 ± 0.33*
	Δ[HbT] (μM)	0	-1.54 ± 0.23*
	Δ[oxCCO] (μM)	0	0.24 ± 0.05*
	TOS (%)	64.5 ± 3.5	66.9 ± 4.2
	ΔTOS (%)	0	2.4 ± 1.1 *
HYPOCAPNIA	Δ[HbDiff] (μM)	0	-1.06 ± 0.31*
	Δ[HbT] (μM)	0	-1.13 ± 0.33*
	Δ[oxCCO] (μM)	0	-0.27 ± 0.07*
	TOS (%)	64.6 ± 4.2	62.8 ± 3.8
	ΔTOS (%)	0	-1.8 ± 0.7 *
HYPERCAPNIA	Δ[HbDiff] (μM)	0	2.86 ± 0.58*
	Δ[HbT] (μM)	0	0.92 ± 0.42*
	Δ[oxCCO] (μM)	0	0.58 ± 0.11*
	TOS (%)	64.3 ± 4.1	69.3 ± 3.9
	ΔTOS (%)	0	5.0 ± 1.2 *

Table 4.4 – Changes, expressed as mean $\pm$ SEM, in chromophore concentration and TOS for volunteers at baseline (Epoch 1) and the end of each challenge (Epoch 9). * - $p < 0.05$ compared to baseline. Note both absolute values for TOS and changes from baseline are shown, but statistical comparison only reported for the latter.

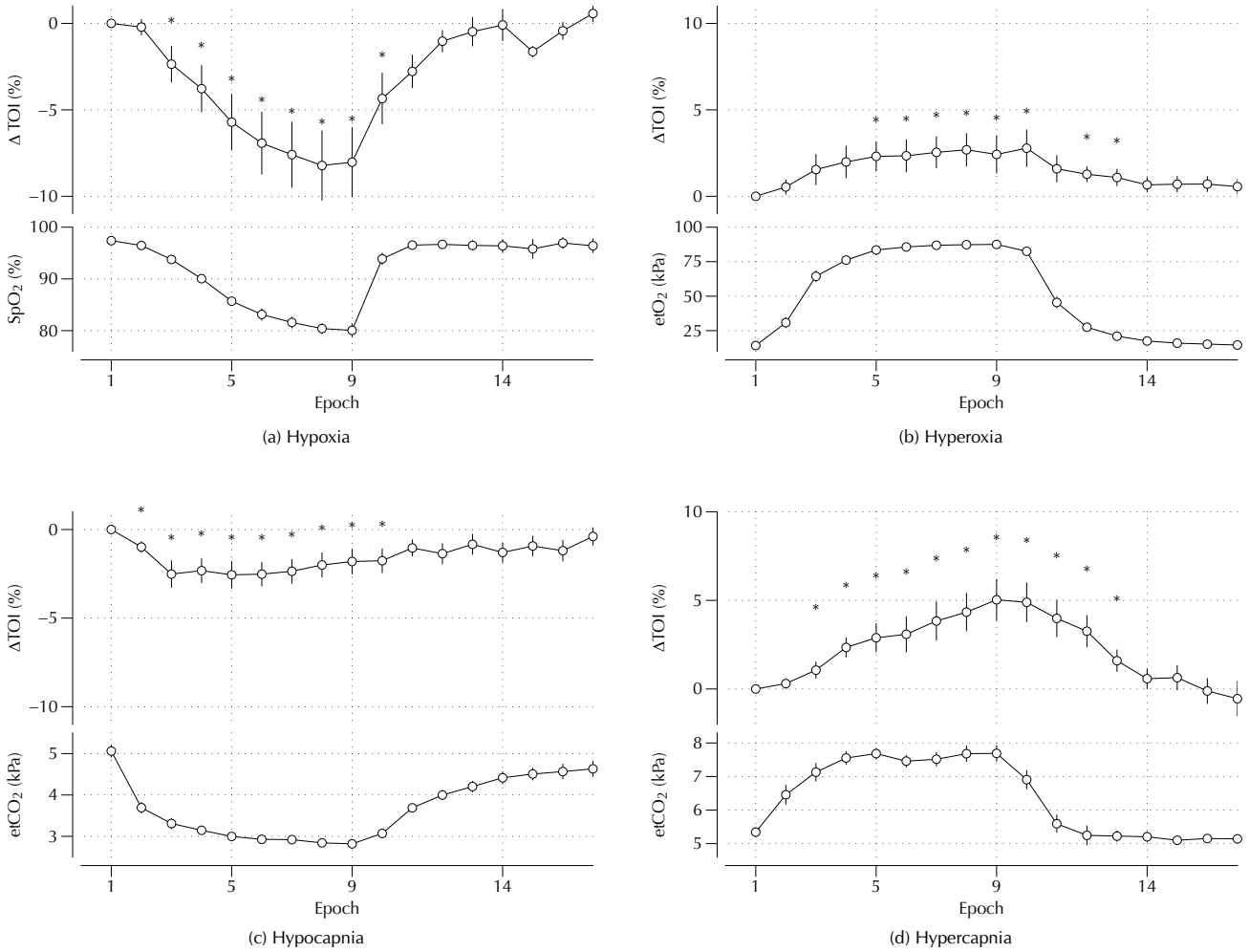

Figure 4.17 – Mean TOS four each of the four challenges.

4.4 DISCUSSION

We manipulated CBF and $ecDO_2$ in 15 healthy volunteers whilst measuring chromophore concentration at 4 source-detector separations and TOS. Analysis of the relationships between change in chromophore concentration, source-detector separations and changes in $ecDO_2$ – summarised in Table 4.5 discussed in detail below – confirms that Δ[oxCCO] is the most 'brain-specific' NIRS-derived measure of brain oxygen delivery. Further qualitative examination suggests that Δ[oxCCO] measurement more closely reflects changes in $ecDO_2$ and thus may be a superior biomarker of cellular energy status.

4.4.1 *Physiological changes induced by challenges*

All challenges induced the expected changes in measures of systemic oxygenation and CBF, although some changes in potentially confounding systemic physiological variables did occur.

The sequential gas delivery circuit did not succeed in completely stabilising $etCO_2$, and we observed a reduction in $etCO_2$ from 5.5 to 5.2 kPa comparing baseline to end-of-challenge epochs, likely caused by an increase in minute volume as a result of hypoxic drive [30]. Despite this, V_{MCA} showed a mean increase of 14.3%, which could be explained by the occurrence of hypoxic vasodilation [31,32] but also may have been driven by the increase in heart rate, which increased from 72.6 to 88.6 BPM, comparing baseline to end-of-challenge epochs. The combined effect of the reduction in SpO_2 and increment in V_{MCA} was to produce a change in $ecDO_2$ to 93.6±2.6% (mean±SEM) of baseline values.

The increase in etO_2 that was observed following hyperoxia, with an increase from 14.3 to 89.2 kPa was associated with modest reductions in HR, V_{MCA} and $etCO_2$.

Hyperventilation induced a reduction in $etCO_2$ from 5.3±0.2 kPa to 3.0±0.1 kPa. There was an associated increase in HR from 75.3±2.3 to 91.0±2.2 BPM, which we speculate was caused by the increased work of breathing and reduction in intrathoracic pressure/preload that hyperventilation entailed. Despite these increments in HR and MAP, there was an overall reduction in V_{MCA} of 30%; as SpO_2 was stable, this reduction in V_{MCA} was the main cause for the observed reduction in $ecDO_2$ to 69.8% of baseline values.

The delivery of a hypercapnic mix for the hypercapnia challenge was associated with an increment in $etCO_2$ from 5.3±0.1 to 7.7±0.2 kPa, inducing an increase in V_{MCA} by 59.1±6.0% from baseline levels. There were associated increases in HR and BPM, both well-recognised effects of hypercapnia [33]. As with the hypocapnia challenge, SpO_2 remained unchanged, so the change in $ecDO_2$ mirrored that of V_{MCA}, with an increase to 158.6% of baseline values.

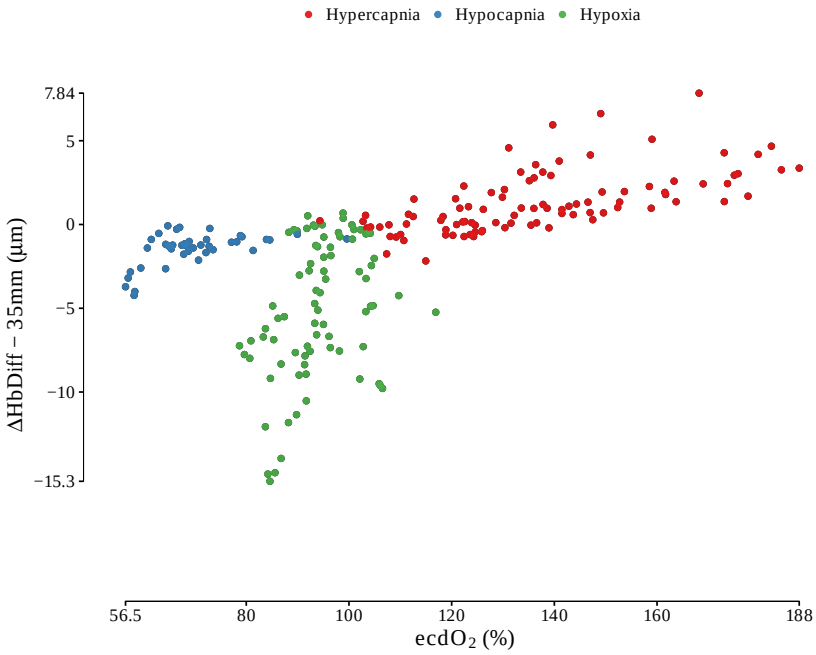

(a) 35mm

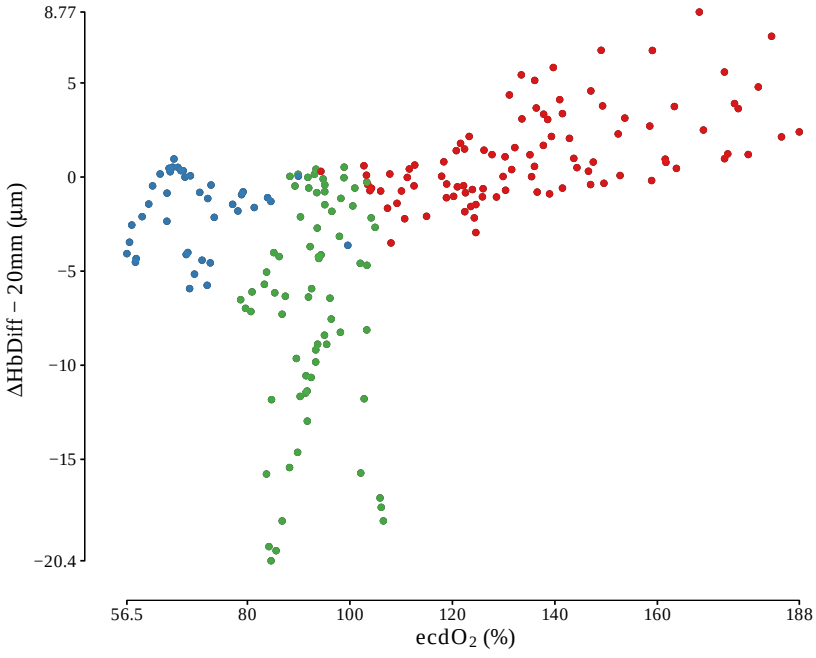

(b) 20mm

Figure 4.18 – Graphs comparing $ecDO_2$ and changes in Δ[HbDiff] at 20 and 35mm; changes in Δ[HbDiff] shown to same scale

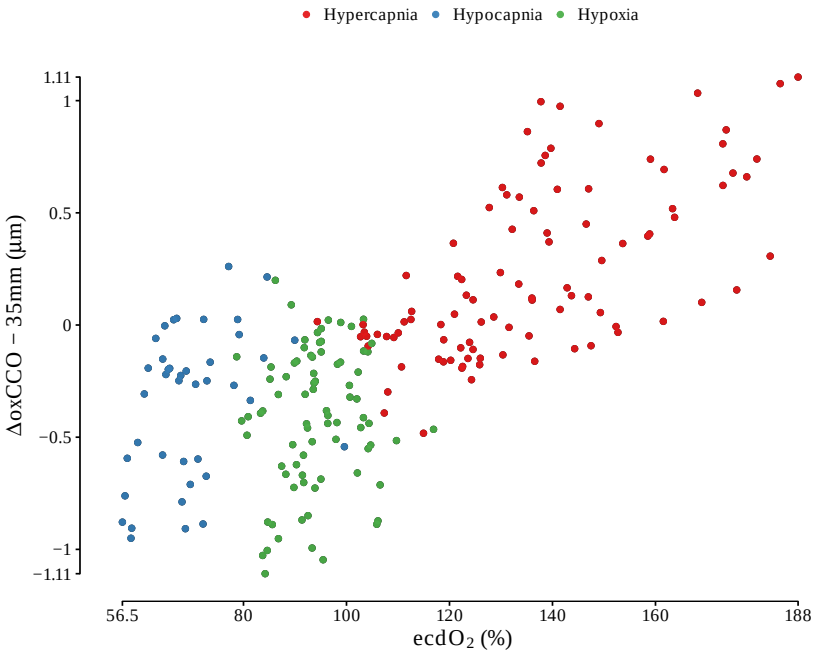

(a) 35mm

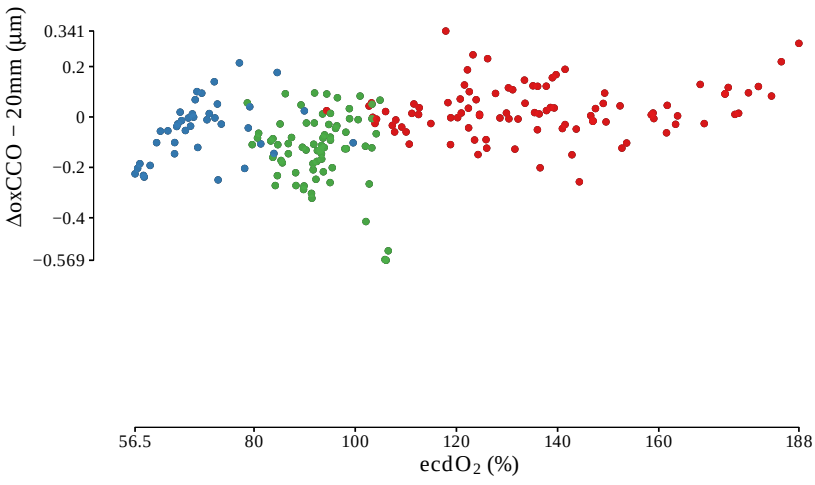

(b) 20mm

Figure 4.19 – Graphs comparing $ecDO_2$ and changes in Δ[oxCCO] at 20 and 35mm; changes in Δ[oxCCO] shown to same scale

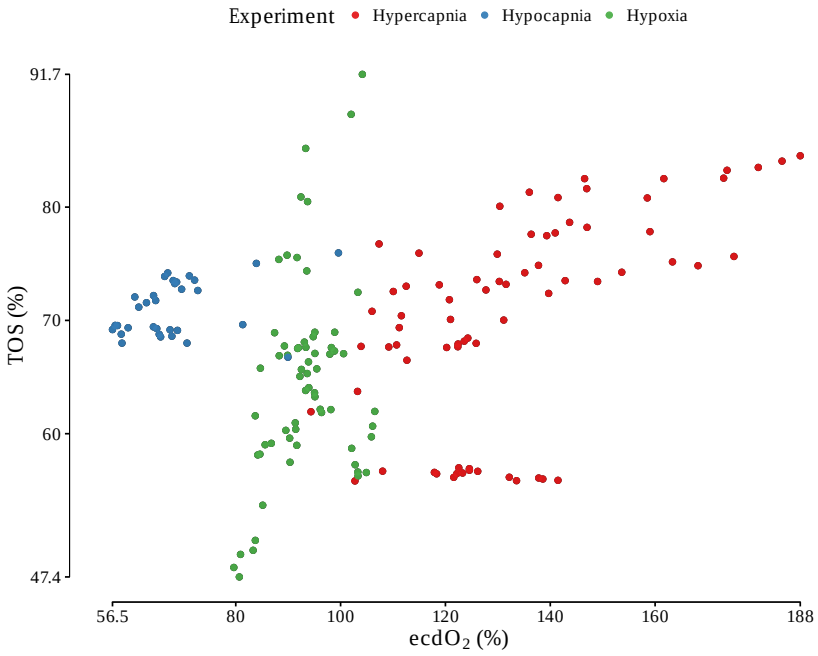

(a) Absolute TOS

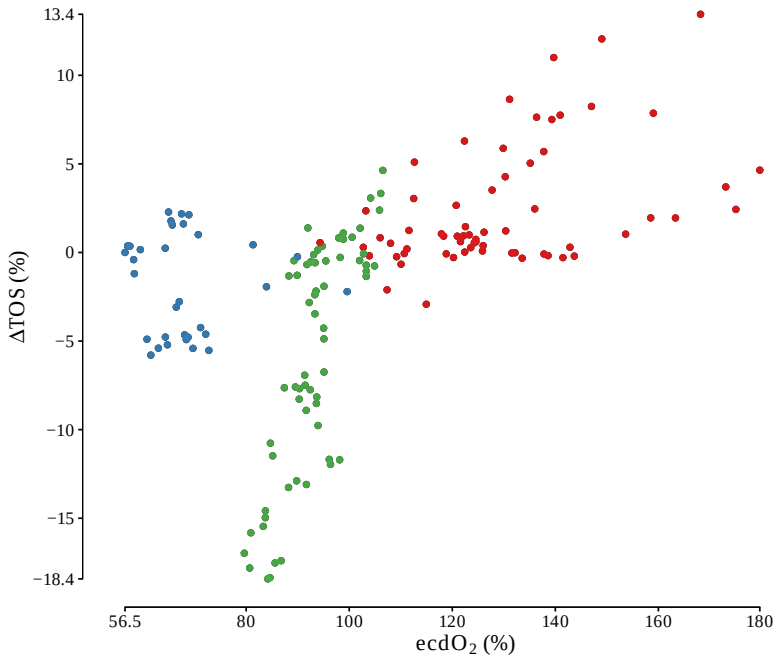

(b) Change in TOS

Figure 4.20 – Graphs comparing ecDO$_2$, absolute TOS and changes in TOS

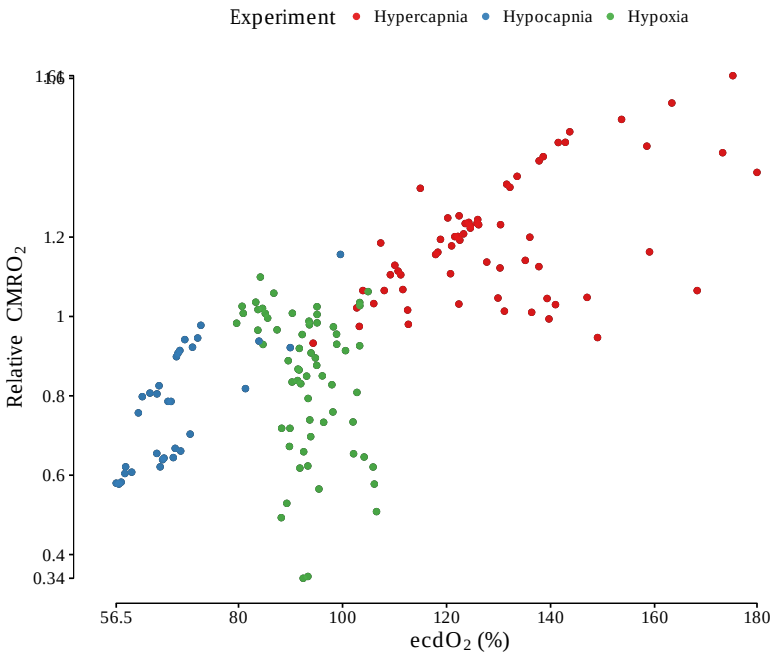

Figure 4.21 – Graph comparing $ecDO_2$ to estimated CMRO

4.4.2 *Changes in UCLn-derived chromophore concentration at 35mm*

Chromophore changes at the 35mm source-detector separation ought to be the most reflective of true changes in *brain* chromophore concentration, as discussed below; we consider these first. The changes observed in haemoglobin measures at 35mm were consistent with those expected by basic physiological principles outlined in Chapter 1. Hypocapnia was associated with a reduction [HbT], hypercapnia conversely associated with increase, consistent with the vasodilatory effect of carbon dioxide and consistent with the observed changes in VMCA. In both these challenges, changes in [HbDiff] mirrored those in [HbT], which would be consistent an increase in CBV caused by vasodilation. Hypoxia was associated with an increase in [HbT] and hyperoxia a decrease. In the case of the hypoxia challenge, the reduction in arterial oxygenation was enough to cause a reduction in [HbDiff], with the converse being true during the hyperoxia challenge. In summary: the direction of group mean changes in [HbT] mirrored CBF, and group mean changes in [HbDiff] mirrored those in cDO_2 measures. The pattern of [oxCCO] changes at 35mm similarly mirrored changes in $ecDO_2$.

The pattern of chromophore change is entirely concordant with those previously reported in the literature [10,34]. There were differences in magnitude of chromophore change – in a hypoxia study Tisdall and colleagues [10] found different median changes in [HbDiff] and [oxCCO] compared to this study; they reported [HbDiff] changes of -

12.7μM compared to our change of -7.5μM and [oxCCO] changes of -0.24μM compared to our finding of -0.55μM. Tachtsidis and colleagues investigated the effects of hyperoxia and hypercapnia on haemoglobin and CCO oxidation/concentration [34]. They found hyperoxia resulted in larger [HbDiff] changes (+4.6μM) but larger changes in [HbT] and [oxCCO] (-1.3μM and +0.09μM, respectively) compared to our study. They also found that hypercapnia resulted in much larger changes in [HbDiff] and [HbT] (+7.4μM and +2.6μM, respectively), although oxCCO changes were smaller (+0.25μM). The hyperoxia/hypercapnia paradigms used by Tachtsidis *et al*. were broadly comparable to those used in our current study, although surprisingly, we achieved a significantly higher increase in VMCA (+59.1% in our study, compared to +14.9%).

One explanation for the differences in magnitude of chromophore is that the previous studies have used the second differential of water for calculation of DPF. During the hypoxia studies carried out by Tisdall *et al*. (reported in his MD Thesis [35] but not in the literature), the use of second water differential gave rise to a pathlength of 12.5cm, equating to a DPF of 3.6. This compares to a DPF of between 6.93 and 7.46 in our study; this might explain some of the significantly smaller chromophore concentration changes in our study (see Equation 3.10). It is also possible that differences in experimental paradigm could explain these differences, as our study used a prolonged hypoxic challenge, whereas Tisdall and colleagues used a brief 'swing' with the maximum hypoxic period only sustained for a few seconds, as opposed to several minutes in our experiment.

4.4.3 *Changes in TOS*

The broadband SRS methodology we used to derive TOS is novel, and to our knowledge, the first use of broadband SRS to measure TOS in the adult human head – although such methodology has been reported for skin recording [36]. The aim of this study was not, however, to develop an improved SRS methodology, but rather to concurrently measure TOS whilst measuring chromophore concentration with the UCLn algorithm at different source-detector separations, using the same optode array. Comparison with previous studies using established NIRS apparatus revealed that the baseline values and changes that we observed in TOS were consistent with those reported in the literature. Mean baseline values of TOS were approximately 65–70%, depending on experiment, although there was a high degree of intersubject variability and an overall (individual subject) baseline range of 55.0–88.6%. Changes in TOS mirrored those in oxygen delivery (DO_2), as shown in Table 4.4 and Figures 4.20a & 4.20b.

Tisdall *et al*. found similar magnitude TOS changes with a two-distance, 3-wavelength commercially available apparatus (Hamamatsu NIRO-300), finding median TOS changes of -7.0% during hypoxia, +2.3% during hyperoxia, -2.1% during hypocapnia and +2.6% during hypercapnia – all changes that are markedly similar in magnitude to

those we report in this study, despite the differences in SRS algorithms, suggesting that this methodology of broadband SRS TOS measurement is relatively veracious.

One aspect that warrants further investigation is the wavelength range used to derive chromophore concentration with the SRS methodology. For SRS-derived measures, we used the wavelength range 740–900nm, whereas for the UCLn-derived chromophore concentrations, we used the wavelength range 780–900nm. Our original intention was to use the latter range for both methodologies for the sake of consistency. For the University College London *n*-wavelength (UCLn)-derived measures, our intention was to investigate oxCCO, and we thus wished to include the 830nm peak (as shown in Figure 3.6), but wished to avoid distortion induced by the prominent 760nm peak of deoxyhaemoglobin (shown in Figure 3.5). Furthermore, this is consistent with previous studies we have reported using both this and other broadband spectrometers [10,34,37, 38]. We initially used this wavelength resolution range for broadband SRS, but signals appeared to have significant levels of noise and some results were physiologically implausible, including negative absolute concentrations of deoxyhaemoglobin and subsequently TOS figures in excess of 100%. This prompted us to undertake a systematic approach to debugging the algorithm; when analysis was repeated using the wavelength range 740-900nm, far more plausible figures resulted. It is possible that the extra noise induced by the use of 4 separate detectors is the cause for these physiologically impossible figures, and perhaps the use of the broader wavelength resolution range has allowed for an improved signal-to-noise ratio and thus more realistic results. We have previously compared the use of the 740-900nm and 780-900nm wavelength resolution ranges when using differential (i. e. UCLn) spectroscopy and found no significant differences between the two methods [15]. Systematic investigation of this aspect of the broadband SRS algorithm is required to affirm its robustness.

	OBSERVED CHANGE IN:					
	SYSTEMIC PHYSIOLOGY	CBF	ecDO$_2$	Δ[oxCCO]	Δ[HBDIFF] & Δ[HBT]	TOS
HYPOXIA	SpO_2 ↓ to 80.0%; HR ↑; BP ↔	VMCA ↑ by 14.3%	↓ to 93.6% baseline level	↓ with larger reduction with longer source-detector separation	[HbDiff] ↓, [HbT] ↑. Larger changes with longer source-detector separation for [HbDiff] but not [HbT]	Absolute ↓ 8%
HYPEROXIA	etO_2 and SpO_2 ↑ ; $etCO_2$ ↓; HR ↓	↔	Unable to determine	↑, with larger increases with longer source-detector separation	[HbDiff] ↑ & [HbT] ↓; no any clear association between source-detector separation & magnitude	Absolute ↑ 2.4%
HYPOCAPNIA	$etCO_2$ ↓ to 3.0 kPa; BP & HR ↑	VMCA ↓ by 30%	↓ to 69.8% baseline level	↓ with larger ↓ with longer source-detector separations	Δ[HbDiff] and Δ[HbT] ↓; significantly larger changes with longer source-detector separation for Δ[HbT] but not Δ[HbDiff]	Absolute ↓ 2.3%
HYPERCAPNIA	$etCO_2$ ↑ from 5.1 to 7.7 kPa; HR and MAP ↑	VMCA ↑ by 59.1%	↑ to 158.6% baseline level	↑, with larger increases in longer source-detector separations	[HbDiff] and [HbT] ↑; smaller [HbT] changes at longer source-detector separations; no clear relationship between source-detector separation and magnitude of Δ[HbDiff]	Absolute ↑ 4.5%

Table 4.5 – Summary of observed changes in systemic physiology, CBF, ecDO$_2$ and NIRS parameters during different challenges

4.4.4 *Depth sensitivity and brain-specificity*

Longer source-detector separations are associated with an increased partial pathlength in brain – that is, a larger proportion of backscattered photons will have passed through brain tissue [39,40] – thus chromophore concentrations derived from longer source-detector separations reflect changes in brain chromophore concentration to a larger extent than shorter ones, which reflect skin changes [41]. Despite this, even at longer source-detector separations, extracranial 'contamination' of NIRS signals is an acknowledged issue (as discussed in Chapter 3.2.2 and [2]). Whilst the use of SRS has served to mitigate this somewhat, extracranial tissues have still been proven to contribute significantly to changes in TOS [4,42].

A key aim of this experiment was to investigate the difference in observed chromophore concentration change at different source-detector separations in response to the four experimental challenges. Figures 4.13–4.16 show the response of different chromophores at each source-detector separation in response to each of these challenges. Our results show changes in Δ[oxCCO] were consistently larger for longer source-detector separations than changes in Δ[HbDiff] and Δ[HbT].

Δ[HbT] showed no difference between detectors for the hyperoxia challenge, and only a modest difference between detectors for the hypoxia and hypercapnia challenges. Interestingly, a significantly larger reduction in *shorter* source-detector separations were shown during the hypocapnia challenge, perhaps suggesting that the extracranial tissues have a higher CO_2 reactivity than brain (in response to hypocapnia, at least), although there are no data in the literature supporting this notion.

Changes in [HbDiff] too generally showed larger changes at shorter distances than longer ones in response to most of the challenges. This was particularly pronounced in the response to hypoxia, as shown in Figure 4.13. A statistically significant difference between a detector and its neighbour was also seen for a number of observations in response to hyperoxia and hypercapnia.

In contrast, Δ[oxCCO] consistently showed larger changes for the longer source-detector separations than the shorter ones. This was the case for each of the four experimental challenges. This suggests that Δ[oxCCO] is the most brain-specific of the UCLn-derived chromophore measures we report. This notion is also supported by comparison between the 35mm and 20mm source-detector separations when comparing chromophore concentration change to changes in $ecDO_2$. Comparing Figures 4.18a & 4.18b the pattern of Δ[HbDiff] response is substantially similar in between the two source-detector separations, whereas comparing changes in Δ[oxCCO], as shown in Figures 4.19a & 4.19b, the gradient of the curve of the line of best fit comparing Δ[oxCCO] to changes in $ecDO_2$ is clearly shallower in the 20mm detector than the 35mm detector, which would be consistent with a significantly lower concentration of CCO within the tissue volume interrogated at 20mm than 35mm.

	Δ[oxCCO]	Δ[HBDIFF]	Δ[HBT]
HYPOXIA	85%	17%	67%
HYPEROXIA	81%	33%	67%
HYPOCAPNIA	93%	63%	8%
HYPERCAPNIA	94%	48%	30%

Table 4.6 – Scores of brain-specificity for each chromophore for each challenge

CCO has previously been suggested a brain-specific chromophore by virtue of its posited high brain concentration compared to that in extracerebral tissues [3,10–12], although there are no experimental data proving this notion. This in part because the direct measurement of tissue CCO concentrations is technically challenging; CCO *activity* can be measured through biochemical methods [43], but this only allows relative measurement of enzyme concentration and function. Absolute measurements have been described in rat brain, using differential spectroscopy with the [oxCCO] spectrum in the presence of oxidising and reducing agents – Brown *et al*. found concentrations of 5.5μM in the adult rat brain [44] – but such measurements have never been carried out in the adult human brain or other tissue. An extracranial:cerebral concentration ratio of 1:10 ratio of CCO has been posited [CE Cooper, personal communication], but this has never been proven experimentally.

In order to clearly summarise the brain-specificity of each chromophore, we contrived a supplementary score of brain specificity – shown in Table 4.6. This was derived by individually inspecting each of the 15 datasets for each challenge and identifying the point of maximum Δ[oxCCO] change. Subsequently, for each of the 60 datasets, we assigned a score to the Δ[oxCCO], Δ[HbDiff] and Δ[HbT] based on whether a larger change was seen in the longer detector source-detector pair comparisons. Scores were summed for each of the challenges, and a final score of brain-specificity was calculated as a percentage of the maximum possible score. This analysis again corroborates the higher brain-specificity of Δ[oxCCO]. The higher brain specificity scores of [HbT] for the hypocapnia and hypercapnia challenges may be reflective of the fact that these challenges induce larger changes in CBV, whereas the hypoxia and hyperoxia challenges resulted in larger brain specificity scores for Δ[HbDiff], which is considered to better reflect changes in arterial oxygenation [2].

It should be note that the methodology used to create this score of brain specificity uses the point of maximal CCO (as opposed to maximal [HbT] or [HbDiff]) change as the point of comparison, and there is thus potential for this score to introduce bias overstating the relative brain specificity of CCO when compared to the haemoglobin measures.

4.4.5 *Physiological interpretation*

We aimed to establish the utility of Δ[oxCCO] as a marker of cerebral energy status. The physiological plausibility of the changes observed in this study, as well as the reproducibility of Δ[oxCCO] measurement (i. e. consistency with previously reported literature) serve to bolster the notion that these measurements are robust and not artefactual. This notion is further reinforced through the observation that optical scattering, a significant potential confounder, has shown no significant change during the challenges.

A qualitative examination of our results – in particular, when compared to $ecDO_2$ as shown in figures 4.18–4.21 – reveals several other features that suggest that Δ[oxCCO] more closely represents changes in cDO_2 than other NIRS-based measures. Comparing changes in $ecDO_2$ to changes in Δ[HbDiff], there appears to be a relatively linear relationship between $ecDO_2$ and Δ[HbDiff] for the hypocapnia/hypercapnia challenges, whereas the the hypoxia challenge leads to a clearly distinct cluster of readings. The same pattern is apparent on examining the relationship between changes in TOS and $ecDO_2$, as shown in Figure 4.20b. Examining the equivalent graph showing the relationship between $ecDO_2$ and Δ[oxCCO], shown in Figure 4.19a, the distinction between the hypocapnia/hypercapnia challenges and the hypoxia challenges is far less distinct. Two possible explanations for this are changes in the arterial:venous blood volume ratio (A:V ratio) and physiological considerations specific to each challenge.

NIRS measures such as [HbDiff] and TOS will, in part, reflect changes in A:V ratio, but such changes are not necessarily a matter of clinical interest. For example, hypocapnia induced significant reductions in $ecDO_2$, but only modest reductions in [HbDiff]. Conversely, the reductions in $ecDO_2$ induced by hypoxia were much smaller, but the reduction in [HbDiff] was much larger. The A:V ratio is typically approximately 1:3 [45], and some studies of NIRS-measured TOS have suggested that the ratio contributing to the TOS signal can be as low a 1:6 [46]. Thus, the reductions in *arterial* $[HbO_2]$ induced by hypocapnic arterial vasoconstriction may be masked by the much larger *venous* volume within the head – that is, hypocapnia resulted in a decrease in A:V ratio. Although one would expect for a reduction in arterial $[HbO_2]$ to eventually result in a reduction in venous $[HbO_2]$ (assuming constant CMRO), this analysis is unable to account for the time it would take for this to occur. The distinction between the hypoxia and hypocapnia/hypercapnia challenges, whilst still present, is far less apparent for the relationship Δ[oxCCO], suggesting that oxCCO more closely reflects oxygen delivery.

Nevertheless, despite the fact that the individual data points are far more closely grouped for the hypoxia and hypocapnia challenges for Δ[oxCCO], they do not overlap – or rather, the same reduction in $ecDO_2$ resulted in a larger Δ[oxCCO] reduction during hypoxia challenges than for the hypocapnia challenges. There are potential physiological explanations for this. For example, increases in pH are known to reduce the affinity of haemoglobin for oxygen (discussed in Chapter 1.2 and shown in Figure

1.1). Furthermore, hypocapnia resulted in reduced cDO_2 by reducing CBF; as SpO_2 remained constant, partial compensation could occur through an increase in oxygen extraction fraction (OEF), thus attenuating the reduction in cellular and mitochondrial oxygen delivery. Such a compensation would be less possible during the hypoxia challenges, where the affinity of haemoglobin for oxygen would be increased as a result of lower pO_2. Increased CO_2 is also known to reduce CCO activity in plants [47], although similar data in mammals do not exist. pH is also known to influence CCO oxidation, with increases in pH known to induce reduction of CCO [48]; however, predicting the effect of modulations in either arterial partial pressure of carbon dioxide (PCO_2) or pO_2 on mitochondrial pH is non-trivial. Mathematical models of cerebral circulation and metabolism [49–52] have been proposed to aid in the interpretation of these complex changes [53], and such models have been used to explore the physiological basis of changes in NIRS signals during hypoxia [51,54], and such models have been used to look at changes of V_{MCA} and intracranial pressure during changes in arterial PCO_2 [55], but no modelled data to explain the changes that we report in this study exist.

The relationship between this estimated CMRO and $ecDO_2$ is shown in Figure 4.21. However, this was calculated primarily as a contrast to the analysis to be described in 5, as the measurement is likely to be subject to confounding. We estimated CMRO using a previously described approximation of the Fick equation [28]. The original Fick equation states that:

$$CMRO = CBF \times AVDO_2. \tag{4.5}$$

where $AVDO_2$ is the arterio-venous oxygen concentration difference [56]. However, the NIRS approximation uses the difference between SpO_2 and TOS to estimate arterio-venous oxygen concentration difference ($AVDO_2$). As discussed above, changes in A:V ratio can have a significant effect on TOS, and such changes can occur in the absence of changes in $AVDO_2$. This notion is bolstered by the fact that CMRO has previously been shown to be independent of reductions in SpO_2 to 70% in a cohort of healthy volunteers, with the arguably more robust method of CMRO estimating, by calculating CBF from ultrasound-measured internal carotid artery and vertebral artery cross sectional areas and velocities, and arterial and jugular venous sampling to calculate the $AVDO_2$. The changes observed in Figure 4.21 are thus likely affected by this confounding by changes in A:V ratio. The originators of NIRS-CMRO approximation, interestingly, do not comment on the importance of ensuring that A:V ratios remain stable in order to prevent such confounding.

4.4.6 *Illustrative case: vasovagal syncope during volunteer hypoxia*

During these experiments, one subject suffered from a vasovagal pre-syncope, providing a further opportunity to demonstrate the relationship between Δ[oxCCO] and cerebral

This case has been reported in a case report in Advances in Experimental Medicine and Biology [57].

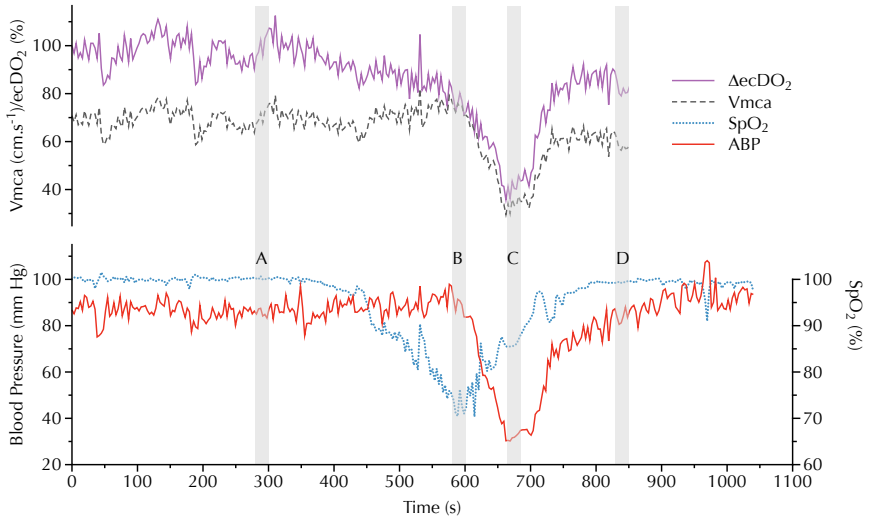

Figure 4.22 – Changes in physiological variables during vasovagal syncope, with data averaging windows indicated A – baseline; B – hypoxia; C – hypoxia-ischaemia; D – recovery. .

		BASELINE	HYPOXIA	HYPOXIA-ISCHAEMIA	RECOVERY
ABP (mmHg)		85.4	88.9	32.1	83.5
HR (bpm)		78.0	117	41.3	101
VMCA ($cm.s^{-1}$)		70.4	73.9	34.1	57.8
SPO_2 (%)		100	72.6	86.3	99.4
$ECDO_2$ (mmHg)		99.8	75.8	41.5	81.2
ΔoxCCO (μM)	3.5cm	0	−0.74	−1.56	−0.13
	3.0cm	0	−0.38	−0.62	0.008
	2.5cm	0	−0.30	−0.55	0.045
	2.0cm	0	−0.14	−0.16	0.23

Table 4.7 – Changes in systemic and cerebral physiology and CCO oxidation before, during and after vasovagal syncope, with data averaging windows as indicated in Figure 4.22.

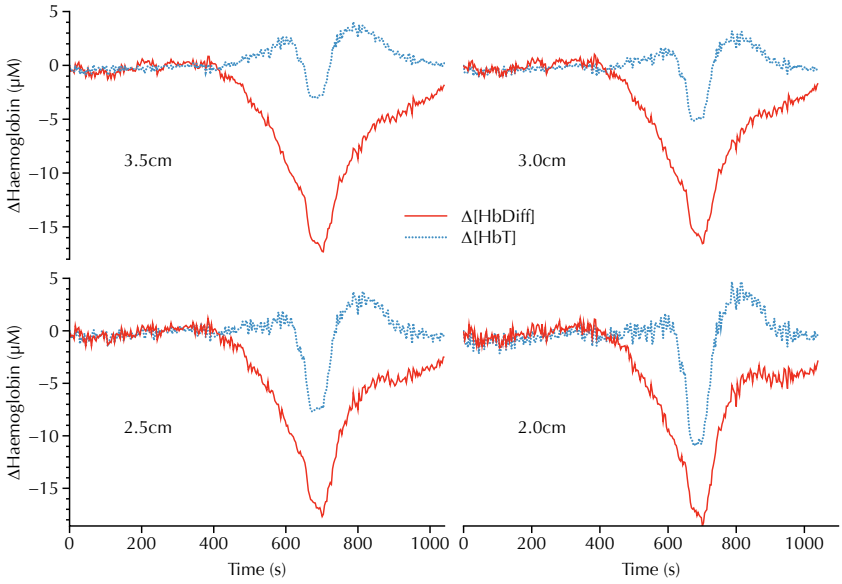

Figure 4.23 – Changes in [HbDiff] and [HbT] during vasovagal syncope.

oxygen delivery during an episode of cerebral ischaemia more severe than one would usually encounter in clinical practice. The 31 year-old male subject, who had been screened for pre-existing medical conditions, suffered from vasovagal pre-syncope during the hypoxia challenge. Approximately 600s after the commencement of recording, during the nadir of hypoxia, the subject suffered from sudden onset bradycardia and hypotension (a typical vasovagal episode[58]), resulting in a reduction in ecDO2 to 41.5% of baseline values. During this time, the subject became briefly unresponsive. The planned experimental protocol and monitoring was otherwise as described in Chapter 4.2. The changes in blood pressure, heart rate, V_{MCA} and $ecDO_2$ are shown in Figure 4.22, with values over the specified data averaging windows shown in Table 4.7.

Individual time courses of [HbDiff]/[HbT] and Δ[oxCCO] are shown in Figures 4.23 and 4.24. The relationship between $ecDO_2$ and Δ[oxCCO] is shown in Figure 4.25.

Whilst hypoxia is a recognised cause of syncope, the occurrence of bradycardia and hypotension indicate a vasovagal aetiology [58], in this case, provoked by – as the subject reported – the shock of seeing his reduced SpO_2 reading. This vasovagal response resulted in a profound reduction in cerebral blood flow (evidenced by both reduced [HbDiff] and V_{MCA}), and this led to a significant reduction in $ecDO_2$.

The other experiments have achieved only modest reductions in $ecDO_2$, leaving questions unanswered about the relationship between $ecDO_2$ and Δ[oxCCO] [10]. In particular, it was unclear whether the relationship between $ecDO_2$ and Δ[oxCCO] is linear, or whether there was a threshold below which rapid reduction occurs. However,

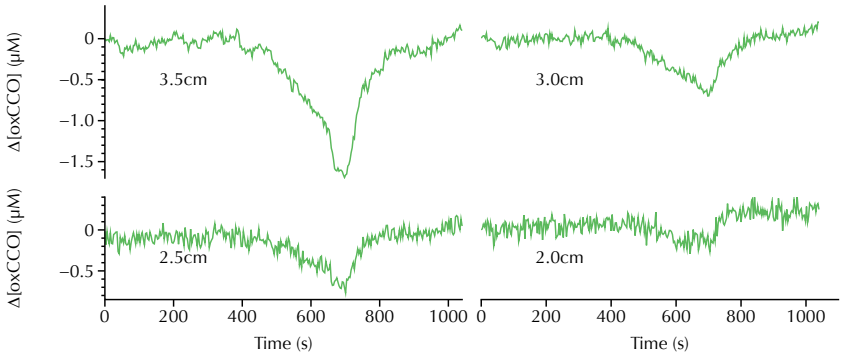

Figure 4.24 – Changes in [HbDiff] and [HbT] during vasovagal syncope.

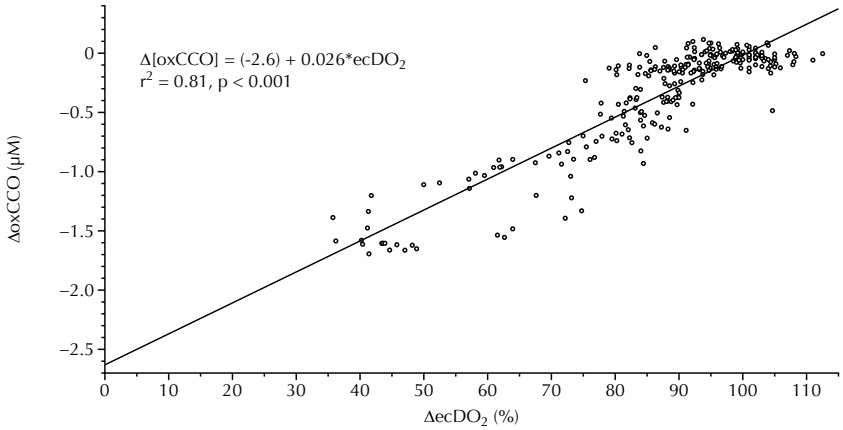

Figure 4.25 – Relationship between $ecDO_2$ and Δ[oxCCO] during vasovagal syncope

our data in Figure 4.25 suggest a linear relationship between Δ[oxCCO] and $ecDO_2$ ($r^2 = 0.81$, p < 0.001). From this, the extrapolated value of Δ[oxCCO] of -2.6 μM with zero cerebral oxygen delivery is suggestive of a resting oxidised $ecDO_2$ concentration of around 2.6 μM. Although no reduction of this size has been reported in humans – understandably as a reduction in $ecDO_2$ to zero is impractical in humans – these values are consistent with those reported in animal anoxia models [12,59].

This single case, when considered in conjunction with the results of the larger cohort of (uncomplicated!) studies, further underlines confidence in the ability to use NIRS to measure Δ[oxCCO] as a marker of cellular energy status.

4.4.7 *Optical scattering*

We measured optical scattering at 790nm and found no significant change in optical scattering for any of the four challenges. The scale of changes in oxCCO are an order of magnitude lower than those seen in haemoglobin species, and thus the potential for 'cross-talk', whereby changes in optical scattering are misrepresented as changes in chromophore concentration, is thus a significant concern in the measurement of Δ[oxCCO] [12]. The range of cerebral oxygenation and blood flow during these challenges lies far outside those routinely encountered in clinical practice, confirming that Δ[oxCCO] will not be confounded by scattering under normal clinical conditions.

4.4.8 *Limitations & Future work*

Because we did not measure blood haemoglobin concentration, we could not accurately calculate cDO_2 and instead had to estimate it; measurement of haemoglobin concentration would allow the estimation of absolute, rather than relative, cDO_2, as well as allowing for calculation of $ecDO_2$ for the hyperoxia studies.

The major limitation to this study is, however, that the analysis and interpretation of the data were qualitatively described. The statistical models for interrogating such a wealth of data are limited; simple linear models would be inappropriate to apply (due to the repeated measures and non-independence of measurements) and repeated statistical testing on the same data set re-presented in different convolutions, as has been performed in this study, runs the risk of inducing type I errors. Rather, a far more fruitful approach to understanding the physiological basis of the observed changes is likely to be through *physiological* rather than statistical analysis, through the use of mathematical models of cerebral haemodynamics and metabolism as previously described [49–52,55].

4.5 CONCLUSION

This study has shown a clear relationship between Δ[oxCCO] and changes in cDO_2 induced through both changes in CBF and arterial oxygenation in a cohort of healthy volunteers. The results suggest that Δ[oxCCO] is a robust and useful biomarker of cerebral energy status. In the next chapter, we describe the measurement of changes in Δ[oxCCO] in a cohort of patients with acute brain injury.

REFERENCES

[1] Kolyva, C, Ghosh, A, Tachtsidis, I, Highton, D, Cooper, CE, Smith, M & Elwell, CE. Cytochrome c oxidase response to changes in cerebral oxygen delivery in the adult brain shows higher brain-specificity than haemoglobin. *NeuroImage*, 85(1):234–244, 2014.

[2] Ghosh, A, Elwell, C & Smith, M. Cerebral near-infrared spectroscopy in adults: a work in progress. *Anesthesia & Analgesia*, 115(6):1373–1383, 2012.

[3] Smith, M & Elwell, C. Near-infrared spectroscopy: shedding light on the injured brain. *Anesthesia & Analgesia*, 108(4):1055–1057, 2009.

[4] Lam, JM, Smielewski, P, Al-Rawi, P, Griffiths, P, Pickard, JD & Kirkpatrick, PJ. Internal and external carotid contributions to near-infrared spectroscopy during carotid endarterectomy. *Stroke*, 28(5):906–911, 1997.

[5] Lee, CK, Sun, CW, Lee, PL, Lee, HC, Yang, C, Jiang, CP, Tong, YP, Yeh, TC & Hsieh, JC. Study of photon migration with various source-detector separations in near-infrared spectroscopic brain imaging based on three-dimensional Monte Carlo modeling. *Optics express*, 13(21):8339–8348, 2005.

[6] Sørensen, H, Secher, NH, Siebenmann, C, Nielsen, HB, Kohl-Bareis, M, Lundby, C & Rasmussen, P. Cutaneous vasoconstriction affects near-infrared spectroscopy determined cerebral oxygen saturation during administration of norepinephrine. *Anesthesiology*, 117(2):263–270, 2012.

[7] Kirkpatrick, PJ, Smielewski, P, Lam, JM & Al-Rawi, P. Use of near infrared spectroscopy for the clinical monitoring of adult brain. *Journal of Biomedical Optics*, 1(4):363, 1996.

[8] Al-Rawi, PG, Smielewski, P & Kirkpatrick, PJ. Evaluation of a near-infrared spectrometer (NIRO 300) for the detection of intracranial oxygenation changes in the adult head. *Stroke*, 32(11):2492–2500, 2001.

[9] Elwell, CE & Cooper, CE. Making light work: illuminating the future of biomedical optics. *Philosophical transactions of the Royal Society A: Mathematical, physical, and engineering sciences*, 369:4358–4379, 2011.

[10] Tisdall, MM, Tachtsidis, I, Leung, TS, Elwell, CE & Smith, M. Near-infrared spectroscopic quantification of changes in the concentration of oxidized cytochrome c oxidase in the healthy human brain during hypoxemia. *Journal of Biomedical Optics*, 12(2):024002, 2007.

[11] Kakihana, Y, Matsunaga, A, Yasuda, T, Imabayashi, T, Kanmura, Y & Tamura, M. Brain oxymetry in the operating room: current status and future directions with particular regard to cytochrome oxidase. *Journal of Biomedical Optics*, 13(3):033001, 2008.

[12] Cooper, CE & Springett, R. Measurement of cytochrome oxidase and mitochondrial energetics by near-infrared spectroscopy. *Philosophical Transactions of the Royal Society B: Biological Sciences*, 352(1354):669–676, 1997.

[13] Slessarev, M, Han, J, Mardimae, A, Prisman, E, Preiss, D, Volgyesi, G, Ansel, C, Duffin, J & Fisher, JA. Prospective targeting and control of end-tidal CO2 and O2 concentrations. *The Journal of Physiology*, 581(3):1207–1219, 2007.

[14] Tachtsidis, I, Leung, T, Elwell, CE, Ghosh, A, Smith, M & Cooper, CE. Multi-Wavelength, Depth Resolved, Scattering and Pathlength Corrected in vivo Near-Infrared Spectroscopy of Brain Tissue. *Biomedical Optics (BIOMED), OSA Technical Digest*, p. BTuB, 2010.

[15] Kolyva, C, Tachtsidis, I, Ghosh, A, Moroz, T, Cooper, CE, Smith, M & Elwell, CE. Systematic investigation of changes in oxidized cerebral cytochrome c oxidase concentration during frontal lobe activation in healthy adults. *Biomedical optics express*, 3(10):2550–2566, 2012.

[16] Fantini, S, Franceschini, MA, Fishkin, JB, Barbieri, B & Gratton, E. Quantitative determination of the absorption spectra of chromophores in strongly scattering media: a light-emitting-diode based technique. *Applied Optics*, 33(22):5204–5213, 1994.

[17] Fantini, S, Franceschini-Fantini, MA, Maier, JS, Walker, SA, Barbieri, BF & Gratton, E. Frequency-domain multichannel optical detector for noninvasive tissue spectroscopy and oximetry. *Optical Engineering*, 34:32–42, 1995.

[18] Hueber, DM, Franceschini, MA, Ma, HY, Zhang, Q, Ballesteros, JR, Fantini, S, Wallace, D, Ntziachristos, V & Chance, B. Non-invasive and quantitative near-infrared haemoglobin spectrometry in the piglet brain during hypoxic stress, using a frequency-domain multidistance instrument. *Physics in Medicine and Biology*, 46(1):41–62, 2001.

[19] Matcher, SJ, Elwell, CE, Cooper, CE, Cope, M & Delpy, DT. Performance comparison of several published tissue near-infrared spectroscopy algorithms. *Analytical biochemistry*, 227(1):54–68, 1995.

[20] Essenpreis, M, Elwell, CE, Cope, M, van der Zee, P, Arridge, SR & Delpy, DT. Spectral dependence of temporal point spread functions in human tissues. *Applied Optics*, 32(4):418–425, 1993.

[21] Duncan, A, Meek, JH, Clemence, M, Elwell, CE, Tyszczuk, L, Cope, M & Delpy, DT. Optical pathlength measurements on adult head, calf and forearm and the head of the newborn infant using phase resolved optical spectroscopy. *Physics in Medicine and Biology*, 40(2):295–304, 1995.

[22] Gao, L, Elwell, CE, Kohl-Bareis, M, Gramer, M, Cooper, CE, Leung, TS & Tachtsidis, I. Effects of assuming constant optical scattering on haemoglobin concentration measurements using NIRS during a Valsalva manoeuvre. *Advances in Experimental Medicine and Biology*, 701:15–20, 2011.

[23] Ghosh, A, Tachtsidis, I, Kolyva, C, Cooper, CE, Smith, M & Elwell, CE. Use of a hybrid optical spectrometer for the measurement of changes in oxidized cytochrome c oxidase concentration and tissue scattering during functional activation. *Advances in Experimental Medicine and Biology*, 737:119–124, 2012.

[24] Suzuki, S, Takasaki, S, Ozaki, T & Kobayashi, Y. Tissue oxygenation monitor using NIR spatially resolved spectroscopy. In *Proceedings of the SPIE*. 1999.

[25] Matcher, S, Cope, M & Delpy, D. In vivo measurements of the wavelength dependence of tissue-scattering coefficients between 760 and 900 nm measured with time-resolved spectroscopy. *Applied Optics*, 36(1):386–396, 1997.

[26] Tachtsidis, I, Tisdall, MM, Pritchard, C, Leung, TS, Ghosh, A, Elwell, CE & Smith, M. Analysis of the changes in the oxidation of brain tissue cytochrome-c-oxidase in traumatic brain injury patients during hypercapnoea: a broadband NIRS study. *Advances in Experimental Medicine and Biology*, 701:9–14, 2011.

[27] Valdueza, JM, Balzer, JO, Villringer, A, Vogl, TJ, Kutter, R & Einhäupl, KM. Changes in blood flow velocity and diameter of the middle cerebral artery during hyperventilation: assessment with MR and transcranial Doppler sonography. *AJNR American journal of neuroradiology*, 18(10):1929–1934, 1997.

[28] Roche-Labarbe, N, Fenoglio, A, Aggarwal, A, Dehaes, M, Carp, SA, Franceschini, MA & Grant, PE. Near-infrared spectroscopy assessment of cerebral oxygen metabolism in the developing premature brain. *Journal of cerebral blood flow and metabolism : official journal of the International Society of Cerebral Blood Flow and Metabolism*, 32(3):481–488, 2012.

[29] R Core Team. *R: A Language and Environment for Statistical Computing*. R Foundation for Statistical Computing, Vienna, Austria, 2012.

[30] Weil, JV, Byrne-Quinn, E, Sodal, IE, Friesen, WO, Underhill, B, Filley, GF & Grover, RF. Hypoxic ventilatory drive in normal man. *The Journal of clinical investigation*, 49(6):1061–1072, 1970.

[31] Palacios-Callender, M, Hollis, V, Frakich, N, Mateo, J & Moncada, S. Cytochrome c oxidase maintains mitochondrial respiration during partial inhibition by nitric oxide. *Journal of cell science*, 120(Pt 1):160–165, 2007.

[32] Palacios-Callender, M, Hollis, V, Mitchison, M, Frakich, N, Unitt, D & Moncada, S. Cytochrome c oxidase regulates endogenous nitric oxide availability in respiring cells: a possible explanation for hypoxic vasodilation. *Proceedings of the National Academy of Sciences of the United States of America*, 104(47):18508–18513, 2007.

[33] Sechzer, PH, Egbert, LD, Linde, HW, Cooper, DY, Dripps, RD & Price, HL. Effect of carbon dioxide inhalation on arterial pressure, ECG and plasma catecholamines and 17-OH corticosteroids in normal man. *Journal of applied physiology (Bethesda, Md : 1985)*, 15(3):454–458, 1960.

[34] Tachtsidis, I, Tisdall, MM, Leung, TS, Pritchard, C, Cooper, CE, Smith, M & Elwell, CE. Relationship between brain tissue haemodynamics, oxygenation and metabolism in the healthy human adult brain during hyperoxia and hypercapnea. *Advances in Experimental Medicine and Biology*, 645:315–320, 2009.

[35] Tisdall, MM. *Non-invasive near infrared spectroscopy: a tool for measuring cerebral oxygenation and metabolism in patients with traumatic brain injury*. UCL MD Thesis, 2008.

[36] Liu, H, Kohl-Bareis, M & Huang, X. Design of a tissue oxygenation monitor and verification on human skin. In Ramanujam, N & Popp, J, eds., *Proceedings of the SPIE*, p. 80871Y. Moor Instruments, Ltd., United Kingdom, SPIE, 2011.

[37] Tisdall, MM, Tachtsidis, I, Leung, TS, Elwell, CE & Smith, M. Increase in cerebral aerobic metabolism by normobaric hyperoxia after traumatic brain injury. *Journal of Neurosurgery*, 109(3):424–432, 2008.

[38] Tisdall, MM, Taylor, C, Tachtsidis, I, Leung, TS, Elwell, CE & Smith, M. The effect on cerebral tissue oxygenation index of changes in the concentrations of inspired oxygen and end-tidal carbon dioxide in healthy adult volunteers. *Anesthesia & Analgesia*, 109(3):906–913, 2009.

[39] Okada, E & Delpy, DT. Near-infrared light propagation in an adult head model. I. Modeling of low-level scattering in the cerebrospinal fluid layer. *Applied Optics*, 42(16):2906–2914, 2003.

[40] Okada, E & Delpy, DT. Near-infrared light propagation in an adult head model. II. Effect of superficial tissue thickness on the sensitivity of the near-infrared spectroscopy signal. *Applied Optics*, 42(16):2915–2922, 2003.

[41] Germon, TJ, Evans, PD, Barnett, NJ, Wall, P, Manara, AR & Nelson, RJ. Cerebral near infrared spectroscopy: emitter-detector separation must be increased. *British Journal of Anaesthesia*, 82(6):831–837, 1999.

[42] Davie, SN & Grocott, HP. Impact of extracranial contamination on regional cerebral oxygen saturation: a comparison of three cerebral oximetry technologies. *Anesthesiology*, 116(4):834–840, 2012.

[43] Wong-Riley, MT. Cytochrome oxidase: an endogenous metabolic marker for neuronal activity. *Trends in neurosciences*, 12(3):94–101, 1989.

[44] Brown, GC, Crompton, M & Wray, S. Cytochrome oxidase content of rat brain during development. *Biochimica et biophysica acta*, 1057(2):273–275, 1991.

[45] An, H & Lin, W. Cerebral venous and arterial blood volumes can be estimated separately in humans using magnetic resonance imaging. *Magnetic resonance in medicine : official journal of the Society of Magnetic Resonance in Medicine / Society of Magnetic Resonance in Medicine*, 48(4):583–588, 2002.

[46] Watzman, HM, Kurth, CD, Montenegro, LM, Rome, J, Steven, JM & Nicolson, SC. Arterial and venous contributions to near-infrared cerebral oximetry. *Anesthesiology*, 93(4):947–953, 2000.

[47] Gonzàlez-Meler, MA & Siedow, JN. Direct inhibition of mitochondrial respiratory enzymes by elevated CO2: does it matter at the tissue or whole-plant level? *Tree Physiology*, 1999.

[48] Thörnström, PE, Brzezinski, P, Fredriksson, PO & Malmström, BG. Cytochrome c oxidase as an electron-transport-driven proton pump: pH dependence of the reduction levels of the redox centers during turnover. *Biochemistry*, 27(15):5441–5447, 1988.

[49] Banaji, M, Tachtsidis, I, Delpy, D & Baigent, S. A physiological model of cerebral blood flow control. *Mathematical biosciences*, 194(2):125–173, 2005.

[50] Banaji, M. A generic model of electron transport in mitochondria. *Journal of theoretical biology*, 243(4):501–516, 2006.

[51] Banaji, M, Mallet, A, Elwell, CE, Nicholls, P & Cooper, CE. A model of brain circulation and metabolism: NIRS signal changes during physiological challenges. *PLoS computational biology*, 4(11):e1000212, 2008.

[52] Ursino, M & Lodi, CA. Interaction among autoregulation, CO2 reactivity, and intracranial pressure: a mathematical model. *The American journal of physiology*, 274(5Pt2):H1715–28, 1998.

[53] Smith, M. Shedding light on the adult brain: a review of the clinical applications of near-infrared spectroscopy. *Philosophical transactions of the Royal Society A: Mathematical, physical, and engineering sciences*, 369(1955):4452–4469, 2011.

[54] Jelfs, B, Banaji, M, Tachtsidis, I, Cooper, CE & Elwell, CE. Modelling Noninvasively Measured Cerebral Signals during a Hypoxemia Challenge: Steps towards Individualised Modelling. *PloS one*, 7(6):e38297, 2012.

[55] Ursino, M, Ter Minassian, A, Lodi, CA & Beydon, L. Cerebral hemodynamics during arterial and CO(2) pressure changes: in vivo prediction by a mathematical model. *American journal of physiology Heart and circulatory physiology*, 279(5):H2439–55, 2000.

[56] Kety, SS & Schmidt, CF. THE EFFECTS OF ALTERED ARTERIAL TENSIONS OF CARBON DIOXIDE AND OXYGEN ON CEREBRAL BLOOD FLOW AND CEREBRAL OXYGEN CONSUMPTION OF NORMAL YOUNG MEN 1. *The Journal of clinical investigation*, 27(4):484–492, 1948.

[57] Ghosh, A, Kolyva, C, Highton, D, Tachtsidis, I, Elwell, CE & Smith, M. Reduction of Cytochrome *c* Oxidase During Vasovagal Hypoxia-Ischaemia in Human Adult Brain: a Case Study. *Advances in Experimental Medicine and Biology*, 789:21–27, 2013.

[58] Chen-Scarabelli, C & Scarabelli, TM. Neurocardiogenic syncope. *BMJ (Clinical research ed)*, 329(7461):336–341, 2004.

[59] Cooper, CE, Cope, M, Springett, R, Amess, PN, Penrice, J, Tyszczuk, L, Punwani, S, Ordidge, R, Wyatt, J & Delpy, DT. Use of Mitochondrial Inhibitors to Demonstrate That Cytochrome Oxidase Near-Infrared Spectroscopy Can Measure Mitochondrial Dysfunction Noninvasively in the Brain. *Journal of Cerebral Blood Flow & Metabolism*, 19(1):27–38, 1999.

5

EFFECTS OF NORMOBARIC HYPEROXIA ON CYTOCHROME *C* OXIDASE IN PATIENTS WITH ACUTE BRAIN INJURY

This chapter draws heavily on a paper published in the Journal of Cerebral Blood Flow and Metabolism *[1].*

This chapter describes the use of the hybrid optical spectrometer (pHOS) in a cohort of patients who had suffered from acute brain injury (ABI). The pHOS was used in a single-channel, single-distance configuration to measure changes in oxyhaemoglobin concentration ([HbO_2]), deoxyhaemoglobin concentration ([HHb]) and concentration of oxidised-reduced cytochrome *c* oxidase ([oxCCO]) at 3.5cm, and also four distances to perform spatially-resolved spectroscopy (SRS) to measure tissue oxygen saturation (TOS). A multimodal monitoring array was used to measure variables related to cerebral oxygen delivery and metabolism, and the relationship between these variables and the pHOS-measured Δ[oxCCO] explored in order to better understand the pathophysiology of ABI and establish the utility of Δ[oxCCO] as a clinical biomarker of hypoxia/ischaemia.

5.1 INTRODUCTION

The high metabolic demand of the brain make it critically dependent on oxidative metabolism to generate adequate energy – in the form of adenosine 5'-triphosphate (ATP) – to sustain function and survival. As discussed in Chapter 2, there are a wide variety of primary ABI processes, including trauma, thrombotic/embolic ischaemia, subarachnoid haemorrhage (SAH) and intracerebral haemorrhage (ICH), but hypoxia/ischaemia is a central pathogenic process – either as the primary injury or as a secondary injury process. The consequent lapses in oxygen and substrate supply can result in failure of cellular energy generation, an event that sets in motion a variety of inflammatory, excitotoxic, oxidant, apoptotic, and necrotic cascades that lead to cell death and thus poor functional outcome, as summarised in Figure 2.3 [2–4].

The avoidance of hypoxia/ischaemia is thus critical to the neurocritical care management of ABI and, as described in Chapter 2, this requires the use of clinical monitors that are able to identify hypoxia/ischaemia. Monitors such as transcranial Doppler (TCD)-based measures of cerebral blood flow (CBF) and brain partial pressure of oxygen ($P_{br}O_2$) describe cellular substrate delivery, but mitochondrial dysfunction also plays a significant role in the pathophysiology of ABI [2,5], with two important consequences: first, cellular energy failure – that is, an inability to generate sufficient ATP to sustain normal function and repair – can occur in the presence of adequate substrate delivery

[6] and second, the leak of electrons from a dysfunctional mitochondrial electron transport chain (ETC) leads to the dual effects of cytotoxic reactive oxygen species (ROS) generation and decoupling of substrate oxidation from ATP generation [7–10].

For these reasons, the ideal clinical monitor would encompass a measure of oxygen *utilisation* as well as delivery, yet, there are no ideal means of identifying impaired oxidative metabolism following ABI. The (*CMRO*) *canbemeasuredusingpositronemissiontomography* (*PET*) [11], *butth illbrain* − *injuredpatientstotheradiologysuite* − − *itselfariskyprocedure*; *alternatively*, *relativechangescanbeestimat venousoxygendifferences* [12] *or nearinfraredspectroscopy* (*NIRS*) − *derivedmeasurementof TOS* [13]. *Microdialysa pyruvateratio* (*LPR*) *isanothersurrogateofintracellularenergystatus*, *beinglinkedtointracellular nicotinamideadenine* and microdialysate LPR has allowed the investigation of the relationship between oxygen (O_2) delivery, tissue oxygenation and surrogates of oxidative metabolism following traumatic brain injury (TBI), SAH and ICH [6,15–18]. The relationship between brain tissue hypoxia or raised LPR and poor neurological outcome – reviewed in depth in Chapter 2.3.1 – is well-recognised and while this has led to the widespread adoption of treatment strategies focused on the maintenance of cerebral substrate delivery [19,20], the clinical benefit of these strategies is unproven [5].

In this context, the measurement of Δ[oxCCO] is an attractive prospect, for both practical and physiological reasons. From a practical perspective, NIRS-measured Δ[oxCCO] has the potential to be a non-invasive, bedside monitor of cellular energy status. Its noninvasive nature allows for the interrogation of multiple regions of interest. From a physiological perspective, cytochrome c oxidase (CCO)'s role as the final electron acceptor in the mitochondrial electron transport chain means that the maintenance of normal CCO function is central to normal oxidative metabolism, and pathophysiological first principles dictate that an inability to generate adequate ATP should be reflected in reduced CCO oxidation, as discussed in previous chapters.

In Chapter 4, we used the pHOS to measure chromophore concentration and TOS in a variety of challenges manipulating cerebral oxygen delivery in the healthy adult brain. Our findings confirmed that Δ[oxCCO] was the most brain-specific of modified Beer-Lambert Law (mBLL)-derived chromophore measures and was superior to TOS as it was not prone to confounding by changes in arterial:venous ratio. We also found that optical scattering coefficient (μ_s) and differential pathlength factor (DPF) showed no change during physiological challenges that were more extreme than those that would routinely be encountered in clinical practice.

The aim of this study was to investigate mitochondrial oxidative metabolism in vivo following ABI, and in particular investigate the feasibility and veracity of the NIRS-measured Δ[oxCCO] in patients with ABI. We hypothesised that increasing cerebral oxygen delivery by means of normobaric hyperoxia (NBH) would elicit an increase in CCO oxidation and CMRO and a reduction in microdialysate LPR. We also hypothesised that there would be no significant change in μ_s that could potentially confound accurate measurement of Δ[oxCCO].

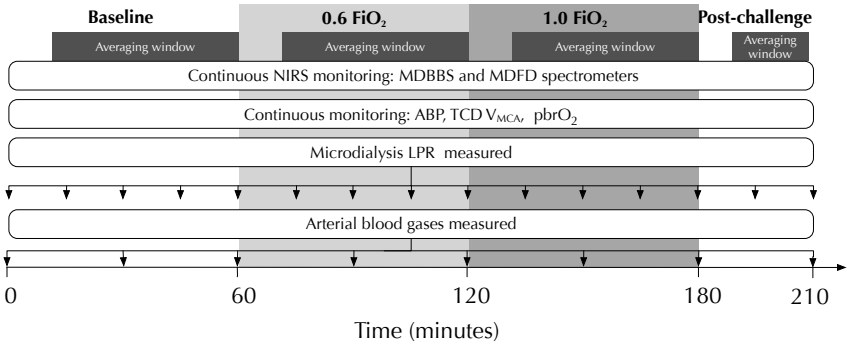

Figure 5.1 – Schematic representation of NBH protocol and data averaging windows

5.2 METHODS

5.2.1 *Study participants and protocol*

After approval by the institutional Research Ethics Committee (reference 04/Q0512/67) and representative consent, recordings were carried out in 16 sedated, mechanically ventilated patients requiring invasive neuromonitoring as part of the clinical management of ABI. Inclusion criteria also included baseline inspired fraction of oxygen (FiO_2) less than 0.5. The patients were subject to the NBH protocol shown in Figure 5.1. It consisted of a 60-minute epoch of baseline recording followed by two 60-minute epochs in which FiO_2 was increased to 0.6 and then 1.0. In a final 30-minute epoch FiO_2 was returned to baseline values. Patients' electronic clinical records were reviewed to ascertain Glasgow Outcome Score (GOS) at 1 year post-study.

5.2.2 *Monitored variables*

Systemic monitoring included continuous arterial blood pressure (ABP) and intermittent measurement of arterial blood gases (ABGs), including arterial partial pressure of oxygen (P_aO_2) and arterial partial pressure of carbon dioxide (P_aCO_2) and pulse haemoglobin oxygen saturation (SpO_2). Middle cerebral artery flow velocity (V_{MCA}) was measured ipsilateral to the other cranial monitoring by TCD ultrasonography (DWL Doppler Box, Compumedics, Singen, Germany). Invasive cerebral monitoring comprised $P_{br}O_2$ (Licox, Integra Neurosciences, Plainsboro, USA) and measurement of LPR by cerebral microdialysis (M Dialysis AB, Stockholm, Sweden), with catheters implanted via a cranial access device (Technicam, Newton Abbot UK or Licox IP2, Integra Neurosciences) or surgically at time of craniotomy. In accordance with consensus guidelines [21], catheters were placed in peri-lesional tissue in patients with focal TBI or ICH, in the right frontal lobe in patients with diffuse TBI, or tissue thought

to be at risk of ischaemia from vasospasm in patients with aneurysmal subarachnoid haemorrhage (aSAH).

5.2.3 *NIRS instrumentation and processing*

The NIRS apparatus used in this study is described in more detail in Chapter 3.4 and elsewhere [22]. We previously established in Chapter 4 that the 35mm source-detector separation is the most brain-specific, and we thus report findings for this distance only. We used the University College London *n*-wavelength (UCLn) algorithm to derive [HbO_2], [HHb] and oxidised-reduced cytochrome *c* oxidase (oxCCO) at the 35mm distance. The multidistance frequency domain spectrometer (MDFD) component of the spectrometer was used to derive absolute optical absorption coefficient (μ_a) and μ_s at 790nm and these were used to calulate the DPF using the diffusion approximation [23]. We report changes in μ_s recorded at 790nm, and an individual DPF was calculated for each patient, based on the μ_a and μ_s measured by the MDFD spectrometer during the initial minute of recording of the baseline epoch.

The TOS – as defined in Equation 3.11 – was calculated using SRS [24]. As in Chapter 4, the wavelength range 740–900nm was used to resolve for [HbO_2], [HHb] and water, combined with scattering values from the MDFD system as previously described [25] in Chapter 4.2.2.

NIRS data analysis was performed in Matlab 2010b (Mathworks, Natick MA). Differential concentrations of [HbO_2], [HHb] and Δ[oxCCO] were calculated using the UCLn algorithm [26,27]. Changes in total haemoglobin concentration ([HbT]) and haemoglobin difference concentration ([HbDiff]) were calculated as described in Equations 3.13 and 3.14.

5.2.4 *Data processing, epoch selection, averaging*

After manual identification and linear interpolation to remove NIRS signal artefacts, mean values for each monitored variable were calculated for individual epochs for each patient. The continuously monitored systemic and cerebral variables (including NIRS) were synchronized and a mean value from a noise-free window, comprising $\geq$ 50% of the entire epoch was used for subsequent analysis. For intermittently sampled variables (i. e. ABGs and microdialysate LPR), the mean of all readings per epoch (minimum 2 per epoch) were used as the summary variable for that epoch.

Relative CMRO was calculated for the post-challenge epoch, as compared to the baseline epoch – as described in Chapter 4.2.4 and Equation 4.4 [13].

5.2.5 *Statistical analysis*

We used GLIMMPSE, a validated model for power calculation in linear mixed models [28] to conduct a sample-size calculation. Assuming a Δ[oxCCO] standard deviation of

0.2 μM in each epoch, a total of 16 patients would be required in order to provide a power of 90% in detecting Δ[oxCCO] changes of +0.1, +0.2 and +0.05 μM during the 0.6 FiO_2, FiO_2 = 100% and post-challenge epochs.

Statistical analyses were carried out in R [29]. Parameters of interest were analysed using a mixed effects model [30], modelling individual subjects as random and epochs as fixed effects. The significance of the fixed epoch effect for each variable (i. e. the probability that the variable was the same across all 4 epochs) was then estimated using the Likelihood Ratio Test (LRT), comparing the mixed effects model to a null model comprising only random effects. In variables with an epoch effect probability of <0.05, subsequent pairwise comparison between baseline and subsequent epochs (0.6 FiO_2, 1.0 FiO_2, and post-challenge) was performed using Bonferroni-corrected Wilcoxon signed-rank tests; the Hodges-Lehman estimate was used to calculate the (pseudo)median and per-epoch 95% confidence intervals; relative changes in CMRO similarly treated, with only the baseline and post-challenge epochs compared and thus no Bonferonni correction was necessary.

The associations between Δ[oxCCO] and microdialysate LPR & $P_{br}O_2$ were similarly analysed using a mixed effects model, with patients modelled as random effects and $P_{br}O_2$ or LPR modelled as fixed effects for their respective analyses. The probability that the variance of the fixed effects was equal to zero was calculated using the LRT; the probability that the variance of the random effect was equal to zero was derived from simulation of the restricted likelihood ratio test (RLRT) [31].

In order to establish whether there was a relationship between baseline hypoxia/ischaemia and subsequent changes in LPR, a Spearman correlation was used to assess the relationship between baseline $P_{br}O_2$ and LPR and the ΔLPR response to hyperoxia.

All data are expressed as (pseudo)median (95% confidence interval) unless otherwise stated. Statistical significance was inferred at $p < 0.05$.

5.3 RESULTS

The full study protocol was completed in 16 patients; technical failure resulted in the loss of ABP and $P_{br}O_2$ recordings for one patient – this patient was still included in all analyses. The demographic data of the 16 patients included in the analysis are shown in Table 5.1. Baseline levels for the physiological variables are shown in Table 5.2, the epoch effect for each variable in Table 5.3, and changes in measured variables in Table 5.4 and Figure 5.2.

No change in Δ[HbT] was observed. Hyperoxia caused an increase in Δ[HbDiff]] (Δ[HbDiff]] +1.18 μM and +2.17 during the 0.6 FiO_2 and 1.0 FiO_2 epochs respectively, both p<0.001) with no significant change observed during the post-challenge epoch. No significant changes were observed in optical scattering measured at 790nm (epoch

AGE	46.5 (39.3–51.5)	
SEX	6 male, 10 female	
PRIMARY DIAGNOSIS	TBI	7
	SAH	8
	ICH	1
TIME TO STUDY (HOURS)	25.5–45	
ADMISSION GCS	4–9	
OUTCOME	GOS 1	6
	GOS 4	7
	GOS 5	1
	Unknown	2

Table 5.1 – Patient demographic and outcome data

VARIABLE	BASELINE VALUE (IQR)	
FiO_2 (%)	0.325	(0.28–0.35)
P_aO_2 (kPa)	15.7	(12.5–18.0)
P_aCO_2 (kPa)	4.85	(4.65–4.97)
SpO_2 (%)	99	(98–99)
MAP (mmHg)	91.5	(83.2–96.8)
V_{MCA} ($cm.s^{-1}$)	52.1	(48.7–71.8)
$P_{br}O_2$ (mmHg)	17.5	(12.0–24.4)
Microdialysate LPR	25.3	(23.5–33.5)
TOS (%)	72.8	(65.5–77.0)
DPF	9.33	(6.75–10.8)
μ_s (cm^{-1})	11.1	(6.76–12.4)

Table 5.2 – Values of physiological and optical variabes at baseline.

VARIABLE	χ^2	*p*
P_aO_2	171	<0.001
P_aCO_2	5.63	0.131
SpO_2	64.8	<0.001
LPR	9.28	0.026
$P_{br}O_2$	44.6	<0.001
VMCA	8.31	0.04
Δ[HbDiff]	27.0	<0.001
Δ[HbT]	4.5	0.21
Δ[oxCCO]	15.1	0.002
TOS	22.3	<0.001
μ_s	1.06	0.787

Table 5.3 – Effect of epoch on specified variable from likelihood ratio test

effect p = 0.786). TOS showed a significant increase during the 0.6 FiO_2 and 1.0 FiO_2 epochs, with ΔTOS 2.8% and 6.0%, respectively (both p<0.001), with no significant change observed during the post-challenge epoch.

Hyperoxia was associated with statistically significant increases in P_aO_2, SpO_2 and $P_{br}O_2$. There was no change seen in P_aCO_2 during the study. While a significant overall epoch effect for VMCA was observed, post hoc testing identified no single epoch as being different to baseline.

Statistically significant increases in Δ[oxCCO] and reductions in microdialysate LPR during the NBH challenge were seen. Δ[oxCCO] increased by +0.18 (p<0.01) and +0.32 (p<0.001) during the 0.6 FiO_2 and 1.0 FiO_2 epochs respectively. ΔLPR showed a change of -1.16 (p<0.01) and -3.07 (p<0.01) during the 0.6 FiO_2 and 1.0 FiO_2 epochs respectively. These changes persisted in to the post-challenge epoch (Δ[oxCCO] +0.22 [p <0.01] and ΔLPR -0.254 [p<0.01]); CMRO was higher in the post-challenge epoch compared to the baseline epoch [CMRO 107.5% of baseline (95% CI 100.3% - 119.0%, p = 0.039)]

Scatterplots showing the relationship between Δ[oxCCO] and $P_{br}O_2$ or LPR are shown in Figures 5.3 and 5.4, respectively. Comparison between Δ[oxCCO] and $P_{br}O_2$ revealed both significant fixed effects (χ^2 21.4, p < 0.0001) and random effects (RLRT statistic 21.5, p < 0.0001). Comparison between Δ[oxCCO] and microdialysate LPR revealed no significant fixed effect (χ^2, p = 0.194) and a significant random effect (RLRT statistic 19.9, p < 0.0001); however, after post-hoc exclusion of a single patient who had evidence of critical ischaemia in their microdialysate (baseline microdialysate glucose 0.04mM, LPR 65), a significant association between Δ[oxCCO] and LPR was observed (χ^2 8.72, p = 0.003)

	0.6 FiO_2	FiO_2 = 100%	POST-CHALLENGE
Δ[HbDiff] (μM)	1.18 (0.59 – 2.12)	1.13 (1.17 – 4.13)	0.30 (-0.22 – 1.28)
Δ[HbT] (μM)	-0.13 (-0.52 – 0.22)	-0.46 (-1.16 – 0.13)	0.44 (-0.01 – 0.90)
Δ[oxCCO] (μM)	0.18 (0.08 – 0.47)	0.32 (0.11 – 0.76)	0.22 (0.06 – 0.62)
ΔTOS (%)	2.8 (1.8 – 5.6)	6.0 (3.4 – 10.9)	3.1 (-2.6 – 2.8)
Relative CMRO (%)	—	—	107.5 (100.3 – 119.0)
ΔLPR	-1.16 (-1.93 – -0.475)	-3.07 (-4.38 – -1.61)	-2.54 (-4.38 – -0.475)
Δ$P_{br}O_2$ (mmHg)	8.44 (5.19 – 12.2)	30.9 (21.6 – 43.4)	2.72 (-1.76 – 9.46)
ΔMAP (mmHg)	1.19 (-2.32 – 4.92)	1.48 (-3.73 – 8.8)	-0.56 (-7.83 – 7.38)
ΔP_aCO_2 (kPa)	0.15 (0.033 – 0.26)	0.114 (-0.05 – 0.258)	0.203 (-0.1 – 0.425)
ΔP_aO_2 (kPa)	14.1 (11.3 – 17)	38.7 (35 – 42.3)	-1.21 (-1.99 – -0.1)
ΔSpO_2	1.5 (1.00 – 2.00)	1.5 (1.01 – 2.00)	-0.831 (-1.16 – -0.778)
Δ V_{MCA} ($cm.s^{-1}$)	2.19 (-1.23 – 5.62)	2.64 (-2.09 – 7.47)	5.19 (-0.45 – 11)
μ_s (cm^{-1})	5.19 (-0.45 – 11)	-0.0201 (-0.394 – 0.297)	0.0785 (-0.423 – 0.354)

Table 5.4 – Changes in measured physiological and optical variables for each epoch. All figures (pseudo)-median (95% confidence interval from Hodges-Lehman estimate in brackets).

5.4 DISCUSSION

We have demonstrated an increase in mitochondrial oxidative metabolism – evidenced by an increase in Δ[oxCCO] and reduction in microdialysate LPR – in a cohort of critically-ill brain-injured patients during an NBH challenge. Furthermore, these changes persisted in to the post-challenge phase of the study, where they were accompanied by an increase in relative CMRO in the post-challenge compared the initial baseline epoch. These findings imply that there is an impairment of cerebral oxidative metabolism at baseline and that this is partially and persistently reversed by hyperoxia. The potential mechanisms for these observed changes include impaired substrate availability – potentially as a result of impaired oxygen diffusion – at baseline, alterations in NO· metabolism and dysfunction of the mitochondrial electron transport chain,

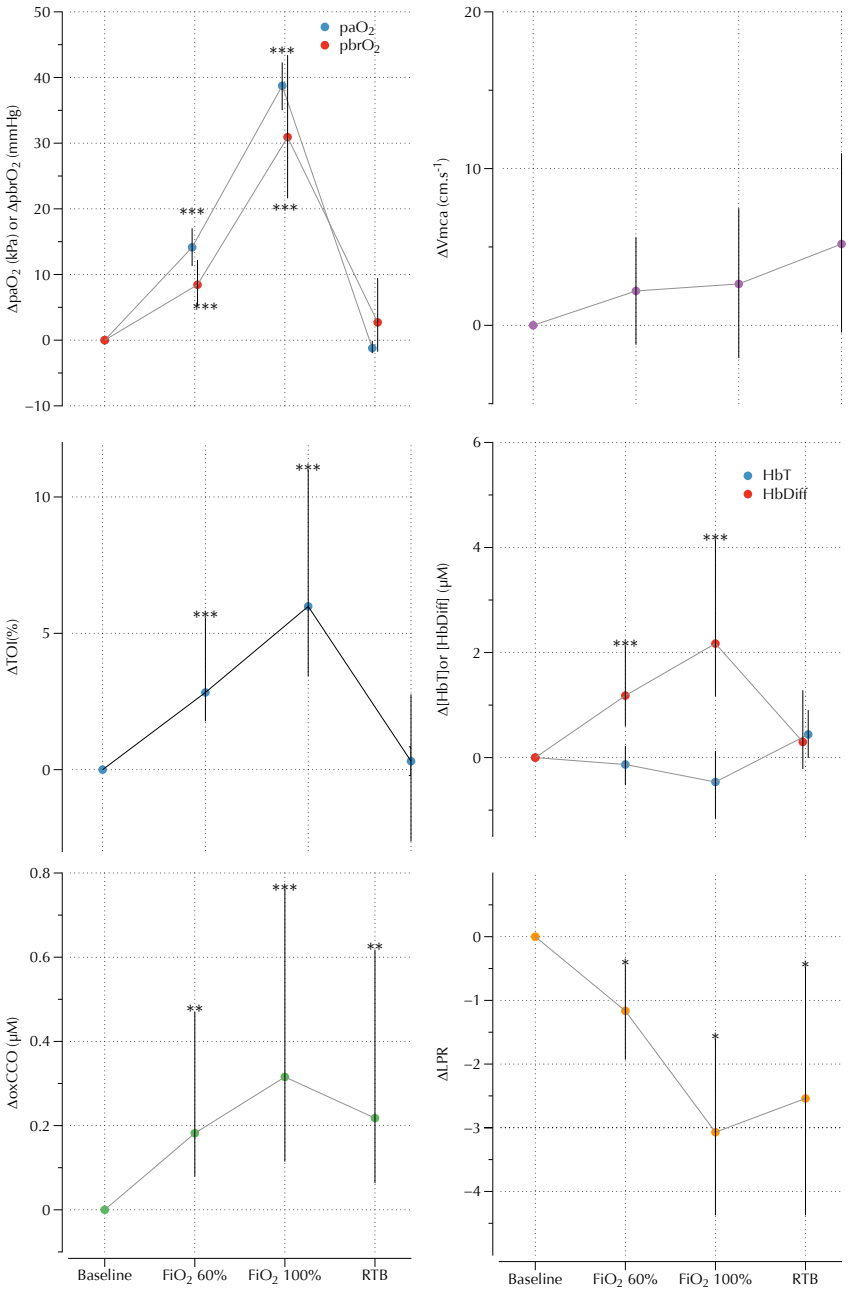

Figure 5.2 – Median changes (with error bars signifying 95% confidence intervals) in systemic and cerebral physiological variables and markers of cerebral aerobic metabolism during NBH from all 16 patients.

all of which are discussed below. Furthermore, we found no significant change in μ_s measured at 790nm, suggesting that changes in scattering do not confound the accurate measurement of Δ[oxCCO].

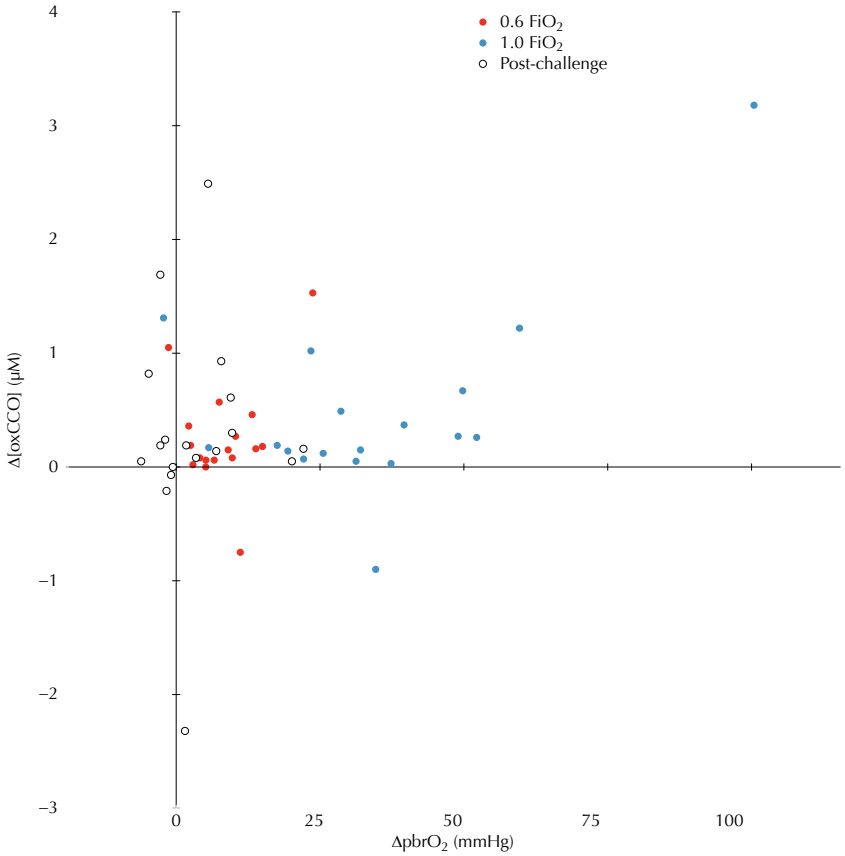

Figure 5.3 – Comparison between $\Delta P_{br}O_2$ and Δ[oxCCO] across all (non-baseline) epochs

Our findings of concomitant, congruent changes in brain LPR, CMRO and CCO oxidation in response to the physiological challenge of hyperoxia on a group level, as well as our findings of a clear association between $\Delta P_{br}O_2$ and Δ[oxCCO] on an individual-observation level underline the notion that CCO oxidation is a valid marker of cerebral oxidative metabolism.

5.4.1 *Comparison with previous studies*

The hyperoxia-induced changes in $P_{br}O_2$, LPR and CCO oxidation that we have shown are consistent with those reported in a previous pilot study [32]. Our results build on existing work in that they demonstrate not only increased oxygen delivery in response to hyperoxia but also an increase in aerobic metabolism evidenced by three modalities, namely reduction in microdialysate LPR, increase in Δ[oxCCO] oxidation and persistent increase in CMRO in a mixed population of patients with severe ABI requiring neurocritical care.

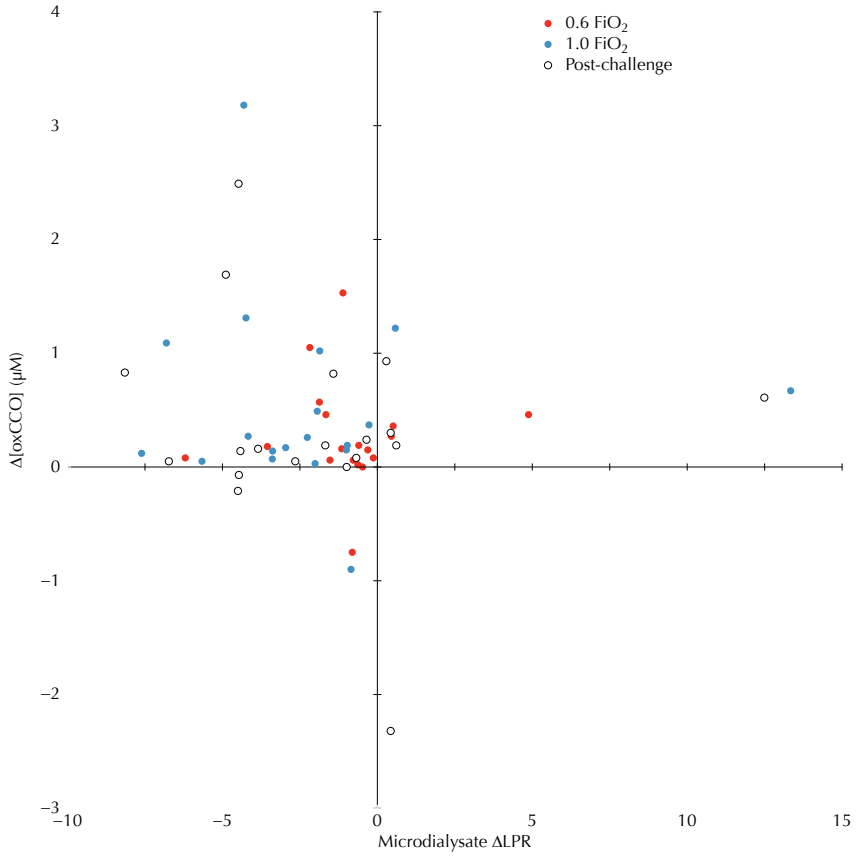

Figure 5.4 – Comparison between ΔLPR and Δ[oxCCO] across all (non-baseline) epochs

The literature contains conflicting evidence regarding the effects of hyperoxia on cerebral pathophysiology following ABI, but with the majority of studies suggesting no metabolic benefit. These include one that reported a reduction in microdialysate lactate but not LPR during hyperoxia [33], and another demonstrating no reduction in LPR [34]. One small PET study also showed no increase in CMRO during hyperoxia, but this was small and likely underpowered [35] . Furthermore, a study in 83 patients with severe TBI found that the effect of hyperoxia on $P_{br}O_2$ was partially correlated with regional CBF, with a greater relative increase in $P_{br}O_2$ observed with higher CBF in the region of interest [36]. In a study combining PET and microdialysis in 11 patients with TBI, Nortje *et al*. found that hyperoxia increased CMRO in areas of brain that showed evidence of ischaemia – that is in areas with already reduced CMRO – but not in areas of 'normal' brain, or in whole-brain studies [37].

The reduction in microdialysate LPR (median reduction -3.07) that we observed in this study during hyperoxia is small, but consistent with that previously reported [32,37]. Such reductions in LPR reflect an increased intracellular NADH:NAD^+ ratio

[14], and are likely to represent increased aerobic metabolism [32,38], although LPR elevatations can reflect mitochondrial dysfunction rather than ischaemia [6] .

The changes that we observed in CCO oxidation are physiologically plausible and, when compared to measurements taken in different contexts, credible in magnitude. The total concentration of CCO in the adult human brain is unknown, but has been found to be approximately 5 μM in rats [39]; on the basis of mitochondrial number and CMRO, this has been speculated to be the upper limit of adult brain CCO concentration [40]. In this context, the changes of 0.18–0.32 μM that we have observed are modest, but plausible, and similar in magnitude to those observed in healthy volunteers during increments in cerebral oxygen delivery and functional activation [22,25,41,42].

The increase in Δ[oxCCO] during hyperoxia is consistent with an increase in electron throughput through the enzyme, and thus through the entire mitochondrial electron transport chain [43–45]. This likely represents increased aerobic metabolism. This change was dose-dependent, with larger changes observed during the 1.0 FiO_2 compared to the 0.6 FiO_2 Epoch. The median changes were $+0.18\mu$M and $+0.32\mu$M during 0.6 FiO_2 and 1.0 FiO_2 epochs respectively, and these are comparable to those previously reported in patients with severe TBI [32] . Interestingly, both microdialysate LPR and Δ[oxCCO] did not return to baseline values following a return to the initial baseline FiO_2, despite the fact that $P_{br}O_2$ and P_aO_2 did, again mirroring the results of our previous work [32]. Baseline drift is an unlikely explanation for this change, as LPR is routinely measured over the course of several days within the clinical setting without any reported concerns of drift in the literature; the other chromophores measured using the NIRS apparatus showed returned to pre-challenge levels, suggesting that drift is an unlikely explanation for these observed changes. Furthermore CMRO showed an increase in the post-challenge when compared to baseline epoch. This raises the prospect that hyperoxia induces an increase in cerebral oxidative metabolism that persists beyond the hyperoxic challenge – although our data collection only carried on for 30 minutes post-challenge and thus the length of time for which this phenomenon persists is unknown.

5.4.2 *Pathophysiological explanations for observed changes*

In health, robust methods of CMRO measurement have shown CMRO to be independent of moderate modulations cerebral oxygen delivery, but following ABI, a range of disturbances to oxygen transport and its utilisation may complicate the relationship between $P_{br}O_2$ and metabolism. Ischaemia is classically described as a situation in which there is insufficient blood-borne substrate delivery. Studied with PET, a characteristic combination of increased OEF, reduced CBF and depressed CMRO is well-recognised following ABI [46]. However, metabolic dysfunction has been identified in the presence of apparently acceptable tissue oxygenation, where both diffusion impaired oxygen

diffusion and mitochondrial dysfunction have been implicated as alternative forms of restriction to oxidative metabolism in the presence of a normal $P_{br}O_2$ or OEF [6].

Protocols for the management of patients with ABI typically seek to maintain $P_{br}O_2$ above a 'critical' threshold for anaerobic metabolism [47]. Although anaerobic metabolism has typically been described when $P_{br}O_2$ falls below 10mmHg, NBH and hyperbaric hyperoxia may improve LPR and CMRO after TBI in the presence of $P_{br}O_2$ values that lie within or above the normal physiological range [32,37,48]. Taken as a whole, this suggests that mitochondrial aerobic metabolism is in some way impaired in brain-injured patients, whether as a result of decreased substrate delivery or an inability to use the delivered substrate. Furthermore, these studies were unable to distinguish between impaired oxygen diffusion and mitochondrial dysfunction as a cause for metabolic impairment – this distinction is not solely academic, but may have clinical consequences, as impaired oxygen diffusion could potentially be overcome by means of hyperoxia.

The mitochondrial matrix, where oxidative phosphorylation occurs, is virtually anoxic, giving rise to a diffusion gradient for oxygen transport from the microvasculature, and offering protection from oxidant damage. CCO has low Michaelis-Menton constant (K_m) for oxygen, meaning that oxidative phosphorylation may continue unimpeded in isolated mitochondria with a partial pressure of oxygen (pO_2) less than 1mmHg [49]. Below a critical ischaemic threshold, CCO is reduced and impaired oxygen availability then becomes a rate-limiting factor resulting in decreased oxidative phosphorylation [50,51].

In this context, potential explanations for the persistent increase in Δ[oxCCO] and CMRO and reduction in LPR observed in the post-challenge period are the presence of either oxygen diffusion limitation or mitochondrial dysfunction and hypoxia-ischaemia despite 'normal' values for $P_{br}O_2$. Importantly, while the [oxCCO] and LPR changes are sustained into the post-challenge period while the markers of microvascular and brain tissue oxygenation (TOS, [HbDiff], [HbT] & $P_{br}O_2$) return to baseline values. This suggests that hyperoxia-induced improvement in cellular metabolism persists beyond the immediate period of normobaric hyperoxia, a supposition supported by the elevation in estimated CMRO during this epoch.

Although the mean baseline $P_{br}O_2$ of 17.5mmHg in our study would be defined as hypoxic (<20 mmHg) by some [52], the majority of previous studies highlight <10mmHg as the threshold at which LPR and PET markers indicate ischaemia [53,54] . However, since both phases of the hyperoxia protocol resulted in elevation of $P_{br}O_2$ to 'normal' physiological levels and a stepwise increase in Δ[oxCCO] and reduction in LPR was observed in the 1.0 FiO_2 epoch, our findings are inconsistent with classical hypoxia-ischaemia.

Both diffusion oxygen abnormalities and mitochondrial dysfunction have been proposed to elicit this phenomenon [6,37,55], but our findings of sustained metabolic

improvement on post-challenge FiO_2, and predicted oxygenation gradients (see below), are not completely consistent with isolated diffusion limitation. Concerning the oxygenation measurements, we found a baseline TOS of 73%, which lies within a physiologically 'normal' range for NIRS-derived regional cerebral saturation [56] . Assuming one quarter of blood volume is saturated arterial blood, this predicts a venous saturation of 64% and approximate venous pO_2 of 33mmHg (using the calculation from Nortje *et al*. [37]), and thus an average difference of 15.5mmHg between venous blood (33mmHg) and $P_{br}O_2$ (17.5mmHg). Similar comparisons using PET and $P_{br}O_2$ have described gradients of 10mmHg and 27mmHg in normal and impaired brain regions [37], so our observations are consistent with a moderate diffusion distance between the microvasculature and tissue interstitium.

One explanation for these results is the occurrence of cerebral oedema, which is typically maximal at 24–72 hours after acute brain injury [57,58]. Limitations to oxygen diffusion are the main barriers to oxygen delivery following TBI [55] and it is thus possible that hyperoxia increases the capillary-mitochondrial diffusion gradient sufficiently to drive oxygen in to the hypoxic mitochondrion. Alternatively, hyperoxia may have a direct effect on cerebral oedema itself, a hypothesis that could be tested in the future through the use of diffusion magnetic resonance or NIRS-measurement of water concentration.

CCO oxidation increased by 0.32 μM during a mean $P_{br}O_2$ change of 30.9mmHg, and returned to 0.22 μM in the post-challenge epoch. Assuming a total concentration of approximately 5μM [40], the CCO changes that we observed are therefore likely to reflect an approximate 6% change in its oxidation and is higher than that observed in healthy volunteers during increases in cerebral oxygen delivery in Chapter 4 and previously [25, 42] or during functional activation [22,41], but equivalent to that described previously in TBI [32]. The oxidation status of CCO is modified by both mitochondrial pO_2 and metabolic factors (such as adenosine 5'-diphosphate (ADP) concentration and the NADH:nicotinamide adenine dinucleotide (NAD^+) ratio), and our findings are consistent with both an increase in aerobic metabolism and/or increased mitochondrial pO_2. Earlier studies and our findings in Chapter 4 have shown an association between cerebral oxygen delivery and CCO oxidation in healthy volunteers [25,59] and, in animal models, with brain ATP concentrations [40] and brain lactate [60]. Likewise, the persistent CCO oxidation in the post-challenge epoch suggests either increased aerobic metabolism (consistent with the measured LPR and estimated CMRO) and/or an altered K_m for O_2.

Furthermore, perturbations of nitric oxide (NO·) metabolism could partially explain the observed changes. NO· is subject to complex perturbations following ABI, with both increases and reductions in NO· reported after TBI and SAH [61]; these have been implicated in the development of delayed cerebral ischaemia and vasospasm after SAH [62]. NO· competes with oxygen to bind CCO, and can also inhibit CCO

activity [63,64] and has been shown to do so after experimental TBI [65]. The CCO-NO· interaction is the proposed basis of hypoxic vasodilation and its obverse, hyperoxic vasoconstriction [66,67] . Competitive reversal of this effect has been proposed as the basis of the therapeutic action of hyperoxia following ABI, with NBH leading to increased ATP generation and paradoxically increased CBF because of pre-existing NO· excess [37] . This would also explain absence of hyperoxic vasoconstriction seen in our study and several others (Diringer et al., 2007; Nortje et al., 2008; Tisdall et al., 2008), as oxygen displaces otherwise-bound NO· and prevents its degradation. Further evidence of a dose-responsive hyperaemia induced by hyperoxia was found by Rockswold and colleagues who showed that hyperbaric hyperoxia induced a larger increase in both arterial oxygen partial pressure and CBF than NBH [68]. Furthermore, NO· is known to increase the K_m of CCO, and the proposed mechanism of action for normobaric and hyperbaric hyperoxia is the reversal of this nitric oxide effect. Thus our results could theoretically represent the hyperoxia-induced breakdown of NO· rather than a direct effect of elevated mitochondrial pO_2 [69], although the effect of NO· on the CCO response to hyperoxia is more difficult to predict, as NO· can cause the CCO complex to remain in both oxidised- and reduced-inhibited forms [70].

A further means by which normobaric hyperoxia may have increased aerobic metabolism may have been by means of upregulation of pyruvate dehydrogenase complex (PDHC) function. PDHC is responsible for the conversion of pyruvate to acetyl-coenzyme A (discussed in Chapter 1.3.3), and is thus a rate-limiting step for substrate entry in to Kreb's cycle and thus oxidative metabolism. In hypoxic conditions, PDHC is deactivated by downstream effects of hypoxia-inducible factor 1α (HIF-1α); this has been proposed as a protective mechanism that minimises the generation of reactive oxygen species during hypoxic conditions [71]. The reversal of hypoxia/ischaemia induced HIF-1α expression by hyperoxia has been proposed to reduce both lactate and pyruvate concentrations [37]. This would thus explain observed increases in CMRO and Δ[oxCCO], but not the reduction in LPR.

One final aspect of brain injury pathophysiology is that of 'electron leak' from the electron transport chain and consequent generation of ROS. Whilst this study builds on an increasing body of evidence and opinion [72–74] regarding the beneficial effects of hyperoxia, there is widespread and increasing concern regarding the potentially deleterious effects of hyperoxia, in particular with the potential for generation of cytotoxic mitochondrial reactive oxygen species [75–77]. ROS are generated as a result of normal metabolism but in particular during periods of mitochondrial hypoxia [78]; there are a wide variety of inbuilt mechanisms for their neutralisation[79,80]. When these protections are overcome, mitochondrial elimination and/or apoptosis ensue [80,81]. The generation of ROS occurs as the result of 'leak' from electrons from the electron transport chain, with the consequence that their potential is not harnessed to generate the mitochondrial chemosmotic gradient required for ATP generation, thus

decoupling substrate oxidation from ATP generation, a phenomenon seen in animal models of TBI [82]. One would expect this to result in a reduction in the oxidised fraction of CCO (as fewer electrons are delivered to the end of electron transport chain) and an increase in LPR (as the leak of electrons prevents the generation of NADH with consequent effects on lactate dehydrogenase). If hypoxia-induced electron leak [78] were reduced by hyperoxia, it could explain the increase in CCO oxidation and reduction in LPR we observed.

These findings highlight the difficulties in establishing thresholds for hypoxia and ischaemia in the injured brain. The wide variation in CCO oxidation and LPR responses to hyperoxia suggests the need for individualised patient-specific targets for the avoidance of secondary brain injury. The deconvolution of the variously measured signals to establish appropriate interventions to minimise secondary brain injury – for example, to establish measures of CBF, arterial and venous volumes and true CMRO – may be possible through the use of mathematical models of cerebral circulation and metabolism may assist in this regard [83–85].

5.4.3 *Relationship between measures of hypoxia/ischaemia and metabolism*

A significant proportion of our patient cohort had either brain-tissue hypoxia (defined as $P_{br}O_2$<20 mmHg) or ischaemia (defined as microdialysate LPR > 25) [38,52] at baseline. In order to examine whether the occurrence of baseline hypoxia or ischaemia influenced the response of LPR, Δ[oxCCO] and CMRO to hyperoxia, we split the patients into two groups on the basis of these hypoxic & ischaemic thresholds, as shown in Tables 5.5 & 5.6 and conducted post-hoc correlation analysis between the baseline $P_{br}O_2$ or LPR and Δ[oxCCO] during the 1.0 FiO_2 Epoch and CMRO during the post-challenge epoch. Post hoc correlation analysis (using Spearman's rank-sum) showed no correlation between the $P_{br}O_2$ or LPR at baseline and Δ[oxCCO] at 1.0 FiO_2 or CMRO during the post-challenge Epochs. However, our study was not powered to carry out such analyses, and inspection of Tables 5.5 & 5.6 suggest that a larger effect in terms of changes in LPR and CMRO is seen in hypoxic/ischaemic patients. Δ[oxCCO] showed a larger change in patients with baseline brain hypoxia, but not in patients with baseline brain ischaemia.

Given the concordance between the various measures of oxidative metabolism on a group level, it was surprising that we did not find a stronger relationship between the variables when comparisons were made between the variables. There was a significant relationship between $P_{br}O_2$ and Δ[oxCCO] ($p<0.0001$), but the relationship between LPR and Δ[oxCCO] was not statistically significant ($p = 0.19$). On further examination of the data, it was apparent that one patient had microdialysate evidence of critical ischaemia, with a baseline LPR of 65 and glucose concentration of 0.04 mM. Furthermore, this patient displayed significant increase in LPR with hyperoxia, with LPR rising

VARIABLE	BASELINE NORMOXIC		BASELINE HYPOXIC	
n	9		6	
Baseline LPR	23.5	(22.2–24.6)	25.8	(24.5–33.9)
Baseline $P_{br}O_2$	25.8	(23.8–27.0)	12.2	(10.9–16.6)
ΔLPR at 1.0 FiO_2 Epoch	-1.4	(-2.2 – -1.9)	-2.7	(-3.9 – -1.8)
Δ[oxCCO] at 1.0 FiO_2 Epoch (μM)	0.13	(0.09–0.34)	0.18	(0.08–0.62)
CMRO during post-challenge Epoch (%)	104.3	(100.8–113.2)	109.4	(98.0 – 115.8)

Table 5.5 – Comparison of changes in measures of oxidative metabolism between patients with brain tissue normoxia (i. e. . $P_{br}O_2$>20mmHg) and hypoxia ($P_{br}O_2$<20) at post-challenge. All figures median (interquartile range (IQR))

.

VARIABLE	BASELINE NOT ISCHAEMIC		BASELINE ISCHAEMIC	
n	8		7	
Baseline LPR	23.4	(21.7–24.0)	33.5	(31.4–38.4)
Baseline $P_{br}O_2$	24.4	(16.3–26.4)	12.2	(11.4–18.2)
ΔLPR at 1.0 FiO_2 Epoch	-1.6	(-3.3 – -1.3)	-2.3	(-3.2 – -0.5)
Δ[oxCCO] at 1.0 FiO_2 Epoch (μM)	0.28	(0.09–0.92)	0.15	(0.06–0.39)
CMRO during post-challenge Epoch (%)	100.9	(96.6–114.3)	109.8	(103.4 – 116.0)

Table 5.6 – Comparison of changes in measures of oxidative metabolism between patients with signs of ischaemia (i.e. LPR>25) without signs of ischaemia (LPR<25) at baseline. All figures median (IQR)

.

to 71 and 79 during the 0.6 FiO_2 and 1.0 FiO_2 epochs, respectively. We speculate that in this patient the microdialysis catheter was placed in critically ischaemic brain and was thus non-responsive to hyperoxia. After post-hoc exclusion of this single patient, a statistically significant association between LPR and Δ[oxCCO] was demonstrated ($\chi^2 = 32.9$, $p = 0.003$).

Comparisons between Δ[oxCCO] & $P_{br}O_2$ and Δ[oxCCO] & LPR with mixed model analysis revealed significant *random* effects in both cases. This suggests that the relationships that exist between Δ[oxCCO] and $P_{br}O_2$ or LPR show significant inter-individual variation. This is compatible with the clear heterogeneity of brain injury pathophysiology; each of the pathophysiological phenomena described above could exist in varying degrees in different brain injuries, and each should influence the relationship between Δ[oxCCO] & $P_{br}O_2$ and Δ[oxCCO] and LPR.

Taken as a whole, these findings suggest that Δ[oxCCO] is a valid marker of cerebral oxidative metabolism, showing a distinct relationship with $P_{br}O_2$ and microdialysiate LPR, but that this relationship cannot be linearly defined on a group basis, but shows significant variation between individual patients. As discussed above, the pathophysiological basis of these variations could be further elucidated though the use of cerebral haemodynamic and metabolic models [83–85] .

5.4.4 *Strengths and limitations*

This study is, to our knowledge, the first report of broadband SRS in clinical use in the adult human brain. The use of broadband SRS as opposed to the discrete-wavelength methodologies employed by most commercially available NIRS apparatus [56] allowed us to resolve for changes in cerebral water content, which could feasibly have confounded accurate measurement of chromophore concentration. Another significant strength is the size of the cohort included in the study: other similar studies have typically included numbers of patients in the single-figures [32,35–37].

In the absence of a single 'gold-standard' measurement of cerebral oxidative metabolism, it was necessary for us to utilise multiple measurement modalities and corroborate the changes between these multiple modalities in order to construct inferences about the pathophysiological basis of the observed changes. A significant strength of this study is that the multimodal monitoring array covered the entire cascade of oxygen metabolism from the microvasculature (measured with TOS and [HbDiff], through to the tissue interstitium ($P_{br}O_2$), to mitochondria (Δ[oxCCO] and composite measures of oxidative metabolism (CMRO and LPR). Considered as a whole, this array might allow the differentiation between limitation of oxygen diffusion and mitochondrial dysfunction.

Each of the individual monitoring modalities used in our study is subject to their own limitations. Differential spectroscopy NIRS methodologies, such as the one we used

to measure haemoglobin concentrations and Δ[oxCCO] in this study, are subject to significantly more extracranial 'contamination' than SRS methodologies [56]. However, we have shown in Chapter 4 that CCO is a brain-specific chromophore, with negligible changes seen in extracranial tissues, overcoming this concern [25]. Furthermore, we used an individual-specific DPF and found no significant changes in optical scattering, excluding these potential confounders of accurate CCO oxidation measurement [40]. The differential spectroscopy methodology we used to measure changes in CCO oxidation is based upon the modified Beer-Lambert law and is only able to quantify relative changes in chromophore concentration from an unknown baseline, as opposed to providing absolute concentrations of oxidised and reduced CCO or a CCO 'saturation' analogous to that of haemoglobin described by TOS [56]. To our knowledge, there are no apparatus that are currently able to provide such measures, but time-resolved spectrometers capable of doing so are on the horizon [56,86].

Microdialysate LPR is an imperfect measure of cerebral aerobic metabolism. It reflects the activity of cytosolic lactate dehydrogenase, which is in large part reflective of intracellular NADH:NAD^+ ratio and thus related to the ability of mitochondria to produce ATP; there are circumstances, including electron leak from the electron transport chain (discussed below), during which LPR can remain unchanged in the face of an inability for cells to generate energy [87].

It is also likely that our different monitoring modalities each interrogated a different area of tissue. In order to minimise this effect, we placed the microdialysis catheters peri-lesionally, or in the case of patients with SAH, in the tissue most likely to develop delayed cerebral ischaemia, in line with consensus guidelines [21,88], and attached NIRS optodes in the frontal region as close as possible to this site. Similarly, it is difficult to know exactly what tissue volume is represented by our CMRO measure. CMRO was derived from V_{MCA} – itself a relatively global measure of hemispheric CBF [89–91] – and TOS, a regional measure of tissue oxygenation [56].

5.5 CONCLUSION

We have demonstrated an increase in several invasively and non-invasively measured markers of cerebral aerobic metabolism during NBH in patients with ABI. The changes observed underline the potential utility of measurement of CCO oxidation as a clinically relevant marker of energy metabolism following ABI.

Furthermore, the changes observed in the various markers of cerebral metabolism provide further confirmation for the existence of mitochondrial dysfunction as a consequence of brain injury and suggest that limitations to oxidation diffusion may play a key role in brain injury pathophysiology. Standard clinical therapy following ABI fundamentally aims to avoid mitochondrial hypoxia in order to minimise secondary

tissue ischaemia and worse clinical outcomes, and while $P_{br}O_2$ and microdialysate LPR have been used as surrogates of mitochondrial oxygen availability and its effect on mitochondrial redox status at the bedside, clinical application and interpretation of such techniques requires clearly defined thresholds for 'ischaemia'.

Our results demonstrate an increase in Δ[oxCCO], reduction in LPR and increase in estimated CMRO during and following normobaric hyperoxia. These findings are consistent with increased aerobic metabolism at $P_{br}O_2$ levels higher than those typically recognised as 'ischaemic' thresholds. Such oxygen-limited metabolism suggests that hypoxia-ischaemia secondary to oxygen diffusion limitation or mitochondrial dysfunction might be prevalent after acute brain injury, and complicate assessment of ischaemia using measurement of $P_{br}O_2$ in isolation. Simultaneous measurement of microvascular, tissue and cellular oxygenation and metabolism has potential to redefine our understanding of ischaemia after acute brain injury. Measurement of the oxidation status of CCO as a bedside, continuous assessment of mitochondrial energetics over multiple regions of interest has considerable potential to guide treatment after acute brain injury.

REFERENCES

[1] Ghosh, A, Highton, D, Kolyva, C, Tachtsidis, I, Elwell, CE & Smith, M. Hyperoxia results in increased aerobic metabolism following acute brain injury. *Journal of cerebral blood flow and metabolism*, p. 271678X16679171, 2016.

[2] Cahill, J, Cahill, WJ, Calvert, JW, Calvert, JH & Zhang, JH. Mechanisms of early brain injury after subarachnoid hemorrhage. *Journal of cerebral blood flow and metabolism*, 26(11):1341–1353, 2006.

[3] Kunz, A, Dirnagl, U & Mergenthaler, P. Acute pathophysiological processes after ischaemic and traumatic brain injury. *Best practice & research Clinical anaesthesiology*, 24(4):495–509, 2010.

[4] Qureshi, AI, Mendelow, AD & Hanley, DF. Intracerebral haemorrhage. *Lancet*, 373(9675):1632–1644, 2009.

[5] Loane, DJ & Faden, AI. Neuroprotection for traumatic brain injury: translational challenges and emerging therapeutic strategies. *Trends in pharmacological sciences*, 31(12):596–604, 2010.

[6] Vespa, P, Bergsneider, M, Hattori, N, Wu, HM, Huang, SC, Martin, NA, Glenn, TC, McArthur, DL & Hovda, DA. Metabolic crisis without brain ischemia is common after traumatic brain injury: a combined microdialysis and positron emission tomography study. *Journal of cerebral blood flow and metabolism*, 25(6):763–774, 2005.

[7] Brookes, PS. Mitochondrial H(+) leak and ROS generation: an odd couple. *Free radical biology & medicine*, 38(1):12–23, 2005.

[8] Adam-Vizi, V. Production of reactive oxygen species in brain mitochondria: contribution by electron transport chain and non-electron transport chain sources. *Antioxidants & redox signaling*, 7(9-10):1140–1149, 2005.

[9] Merenda, A & Bullock, R. Clinical treatments for mitochondrial dysfunctions after brain injury. *Current Opinion in Critical Care*, 12(2):90–96, 2006.

[10] Jastroch, M, Divakaruni, AS, Mookerjee, S, Treberg, JR & Brand, MD. Mitochondrial proton and electron leaks. *Essays in biochemistry*, 47:53–67, 2010.

[11] Jones, T, Rabiner, EA & PET Research Advisory Company. The development, past achievements, and future directions of brain PET. *Journal of cerebral blood flow and metabolism : official journal of the International Society of Cerebral Blood Flow and Metabolism*, 32(7):1426–1454, 2012.

[12] Ainslie, PN, Shaw, AD, Smith, KJ, Willie, CK, Ikeda, K, Graham, J & Macleod, DB. Stability of cerebral metabolism and substrate availability in humans during hypoxia and hyperoxia. *Clinical science (London, England : 1979)*, 126(9):661–670, 2014.

[13] Roche-Labarbe, N, Fenoglio, A, Aggarwal, A, Dehaes, M, Carp, SA, Franceschini, MA & Grant, PE. Near-infrared spectroscopy assessment of cerebral oxygen metabolism in the developing premature brain. *Journal of cerebral blood flow and metabolism : official journal of the International Society of Cerebral Blood Flow and Metabolism*, 32(3):481–488, 2012.

[14] Veech, RL. The metabolism of lactate. *NMR in biomedicine*, 4(2):53–58, 1991.

[15] Chen, HI, Stiefel, MF, Oddo, M, Milby, AH, Maloney-Wilensky, E, Frangos, S, Levine, JM, Kofke, WA & Leroux, PD. Detection of cerebral compromise with multimodality monitoring in patients with subarachnoid hemorrhage. *Neurosurgery*, 69(1):53–63– discussion 63, 2011.

[16] Sarrafzadeh, AS, Sakowitz, OW, Kiening, KL, Benndorf, G, Lanksch, WR & Unterberg, AW. Bedside microdialysis: a tool to monitor cerebral metabolism in subarachnoid hemorrhage patients? *Critical care medicine*, 30(5):1062–1070, 2002.

[17] Belli, A, Sen, J, Petzold, A, Russo, S, Kitchen, N & Smith, M. Metabolic failure precedes intracranial pressure rises in traumatic brain injury: a microdialysis study. *Acta Neurochirurgica*, 150(5):461–9; discussion 470, 2008.

[18] Schmidt, JM, Ko, SB, Helbok, R, Kurtz, P, Stuart, RM, Presciutti, M, Fernandez, L, Lee, K, Badjatia, N, Connolly, ES, Claassen, J & Mayer, SA. Cerebral Perfusion Pressure Thresholds for Brain Tissue Hypoxia and Metabolic Crisis After Poor-Grade Subarachnoid Hemorrhage. *Stroke*, 42(5):1351–1356, 2011.

[19] Connolly, ES, Rabinstein, AA, Carhuapoma, JR, Derdeyn, CP, Dion, J, Higashida, RT, Hoh, BL, Kirkness, CJ, Naidech, AM, Ogilvy, CS, Patel, AB, Thompson, BG, Vespa, P & on behalf of the American Heart Association Stroke Council, Council on Cardiovascular Radiology and Intervention, Council on Cardiovascular Nursing, Council on Cardiovascular Surgery and Anesthesia, and Council on Clinical Cardiology. Guidelines for the Management of Aneurysmal Subarachnoid Hemorrhage: A Guideline for Healthcare Professionals From the American Heart Association/American Stroke Association. *Stroke*, 43(6):1711–1737, 2012.

[20] Bratton, SL, Chestnut, RM, Ghajar, J, Hammond, FFM, Harris, OA, Hartl, R, Manley, GT, Nemecek, A, Newell, DW, Rosenthal, G, Schouten, J, Shutter, L, Timmons, SD, Ullman, JS, Videtta, W, Wilberger, JE & Wright, DW. Guidelines for the

management of severe traumatic brain injury. *Journal of Neurotrauma*, 24 Suppl 1:S1–106, 2007.

[21] Hutchinson, PJ, Jalloh, I, Helmy, A, Carpenter, KLH, Rostami, E, Bellander, BM, Boutelle, MG, Chen, JW, Claassen, J, Dahyot-Fizelier, C, Enblad, P, Gallagher, CN, Helbok, R, Hillered, L, Le Roux, PD, Magnoni, S, Mangat, HS, Menon, DK, Nordström, CH, O'Phelan, KH, Oddo, M, Perez Barcena, J, Robertson, C, Ronne-Engström, E, Sahuquillo, J, Smith, M, Stocchetti, N, Belli, A, Carpenter, TA, Coles, JP, Czosnyka, M, Dizdar, N, Goodman, JC, Gupta, AK, Nielsen, TH, Marklund, N, Montcriol, A, O'Connell, MT, Poca, MA, Sarrafzadeh, A, Shannon, RJ, Skjøth-Rasmussen, J, Smielewski, P, Stover, JF, Timofeev, I, Vespa, P, Zavala, E & Ungerstedt, U. Consensus statement from the 2014 International Microdialysis Forum. *Intensive Care Medicine*, 41(9):1517–1528, 2015.

[22] Kolyva, C, Tachtsidis, I, Ghosh, A, Moroz, T, Cooper, CE, Smith, M & Elwell, CE. Systematic investigation of changes in oxidized cerebral cytochrome c oxidase concentration during frontal lobe activation in healthy adults. *Biomedical optics express*, 3(10):2550–2566, 2012.

[23] Fantini, S, Hueber, D, Franceschini, MA, Gratton, E, Rosenfeld, W, Stubblefield, PG, Maulik, D & Stankovic, MR. Non-invasive optical monitoring of the newborn piglet brain using continuous-wave and frequency-domain spectroscopy. *Physics in Medicine and Biology*, 44(6):1543–1563, 1999.

[24] Suzuki, S, Takasaki, S, Ozaki, T & Kobayashi, Y. Tissue oxygenation monitor using NIR spatially resolved spectroscopy. *BiOS '99 International Biomedical Optics Symposium*, 3597:582–592, 1999.

[25] Kolyva, C, Ghosh, A, Tachtsidis, I, Highton, D, Cooper, CE, Smith, M & Elwell, CE. Cytochrome c oxidase response to changes in cerebral oxygen delivery in the adult brain shows higher brain-specificity than haemoglobin. *NeuroImage*, 85(1):234–244, 2014.

[26] Matcher, SJ, Elwell, CE, Cooper, CE, Cope, M & Delpy, DT. Performance comparison of several published tissue near-infrared spectroscopy algorithms. *Analytical biochemistry*, 227(1):54–68, 1995.

[27] Duncan, A, Meek, JH, Clemence, M, Elwell, CE, Tyszczuk, L, Cope, M & Delpy, DT. Optical pathlength measurements on adult head, calf and forearm and the head of the newborn infant using phase resolved optical spectroscopy. *Physics in Medicine and Biology*, 40(2):295–304, 1995.

[28] Guo, Y, Logan, HL, Glueck, DH & Muller, KE. Selecting a sample size for studies with repeated measures. *BMC medical research methodology*, 13(1):100, 2013.

[29] R Core Team. *R: A Language and Environment for Statistical Computing*. R Foundation for Statistical Computing, Vienna, Austria, 2012.

[30] Laird, NM & Ware, JH. Random-effects models for longitudinal data. *Biometrics*, 38(4):963–974, 1982.

[31] Scheipl, F, Greven, S & Küchenhoff, H. Size and power of tests for a zero random effect variance or polynomial regression in additive and linear mixed models. *Computational statistics & data ...*, 2008.

[32] Tisdall, MM, Tachtsidis, I, Leung, TS, Elwell, CE & Smith, M. Increase in cerebral aerobic metabolism by normobaric hyperoxia after traumatic brain injury. *Journal of Neurosurgery*, 109(3):424–432, 2008.

[33] Tolias, CM, Reinert, M, Seiler, R, Gilman, C, Scharf, A & Bullock, MR. Normobaric hyperoxia–induced improvement in cerebral metabolism and reduction in intracranial pressure in patients with severe head injury: a prospective historical cohort-matched study. *Journal of Neurosurgery*, 101(3):435–444, 2004.

[34] Magnoni, S, Ghisoni, L, Locatelli, M, Caimi, M, Colombo, A, Valeriani, V & Stocchetti, N. Lack of improvement in cerebral metabolism after hyperoxia in severe head injury: a microdialysis study. *Journal of Neurosurgery*, 98(5):952–958, 2003.

[35] Diringer, MN, Aiyagari, V, Zazulia, AR, Videen, TO & Powers, WJ. Effect of hyperoxia on cerebral metabolic rate for oxygen measured using positron emission tomography in patients with acute severe head injury. *Journal of Neurosurgery*, 106(4):526–529, 2007.

[36] Hlatky, R, Valadka, AB, Gopinath, SP & Robertson, CS. Brain tissue oxygen tension response to induced hyperoxia reduced in hypoperfused brain. *Journal of Neurosurgery*, 108(1):53–58, 2008.

[37] Nortje, J, Coles, JP, Timofeev, I, Fryer, TD, Aigbirhio, FI, Smielewski, P, Outtrim, JG, Chatfield, DA, Pickard, JD, Hutchinson, PJ, Gupta, AK & Menon, DK. Effect of hyperoxia on regional oxygenation and metabolism after severe traumatic brain injury: preliminary findings. *Critical care medicine*, 36(1):273–281, 2008.

[38] Ungerstedt, U & Rostami, E. Microdialysis in neurointensive care. *Current pharmaceutical design*, 10(18):2145–2152, 2004.

[39] Brown, GC, Crompton, M & Wray, S. Cytochrome oxidase content of rat brain during development. *Biochimica et biophysica acta*, 1057(2):273–275, 1991.

[40] Cooper, CE & Springett, R. Measurement of cytochrome oxidase and mitochondrial energetics by near-infrared spectroscopy. *Philosophical Transactions of the Royal Society B: Biological Sciences*, 352(1354):669–676, 1997.

[41] Heekeren, HR, Kohl, M, Obrig, H, Wenzel, Rd, von Pannwitz, W, Matcher, SJ, Dirnagl, U, Cooper, CE & Villringer, A. Noninvasive Assessment of Changes in Cytochrome-c Oxidase Oxidation in Human Subjects During Visual Stimulation. *Journal of Cerebral Blood Flow & Metabolism*, 19(6):592–603, 1999.

[42] Tachtsidis, I, Tisdall, MM, Leung, TS, Pritchard, C, Cooper, CE, Smith, M & Elwell, CE. Relationship between brain tissue haemodynamics, oxygenation and metabolism in the healthy human adult brain during hyperoxia and hypercapnea. *ADVANCES IN EXPERIMENTAL MEDICINE AND BIOLOGY*, 645(Chapter 47):315–320, 2009.

[43] Cooper, CE, Matcher, SJ, Wyatt, JS, Cope, M, Brown, GC, Nemoto, EM & Delpy, DT. Near-infrared spectroscopy of the brain: relevance to cytochrome oxidase bioenergetics. *Biochemical Society transactions*, 22(4):974–980, 1994.

[44] Richter, OMH & Ludwig, B. Cytochrome c oxidase–structure, function, and physiology of a redox-driven molecular machine. *Reviews of physiology, biochemistry and pharmacology*, 147:47–74, 2003.

[45] Saraste, M. Oxidative phosphorylation at the fin de siècle. *Science*, 283(5407):1488–1493, 1999.

[46] Coles, JP, Fryer, TD, Smielewski, P, Rice, K, Clark, JC, Pickard, JD & Menon, DK. Defining Ischemic Burden After Traumatic Brain Injury Using 15O PET Imaging of Cerebral Physiology. *Journal of Cerebral Blood Flow & Metabolism*, pp. 191–201, 2004.

[47] Geukens, P & Oddo, M. Brain Tissue Oxygen Monitoring in Neurocritical Care. In *Annual Update in Intensive Care and Emergency Medicine 2012*, pp. 735–745. Springer Berlin Heidelberg, Berlin, Heidelberg, 2012.

[48] Kumaria, A & Tolias, CM. Normobaric hyperoxia therapy for traumatic brain injury and stroke: a review. *British Journal of Neurosurgery*, 23(6):576–584, 2009.

[49] Krab, K, Kempe, H & Wikström, M. Explaining the enigmatic K(M) for oxygen in cytochrome c oxidase: a kinetic model. *Biochimica et biophysica acta*, 1807(3):348–358, 2011.

[50] Rolett, EL, Azzawi, A, Liu, KJ, Yongbi, MN, Swartz, HM & Dunn, JF. Critical oxygen tension in rat brain: a combined (31)P-NMR and EPR oximetry study. *American journal of physiology Regulatory, integrative and comparative physiology*, 279(1):R9–R16, 2000.

[51] Scheufler, KM, Lehnert, A, Rohrborn, HJ, Nadstawek, J & Thees, C. Individual value of brain tissue oxygen pressure, microvascular oxygen saturation, cytochrome redox level, and energy metabolites in detecting critically reduced cerebral energy state during acute changes in global cerebral perfusion. *Journal of Neurosurgical Anesthesiology*, 16(3):210–219, 2004.

[52] Longhi, L, Pagan, F, Valeriani, V, Magnoni, S, Zanier, ER, Conte, V, Branca, V & Stocchetti, N. Monitoring brain tissue oxygen tension in brain-injured patients reveals hypoxic episodes in normal-appearing and in peri-focal tissue. *Intensive Care Medicine*, 33(12):2136–2142, 2007.

[53] Johnston, AJ, Steiner, LA, Coles, JP, Chatfield, DA, Fryer, TD, Smielewski, P, Hutchinson, PJ, O'Connell, MT, Al-Rawi, PG, Aigbirihio, FI, Clark, JC, Pickard, JD, Gupta, AK & Menon, DK. Effect of cerebral perfusion pressure augmentation on regional oxygenation and metabolism after head injury. *Critical care medicine*, 33(1):189–95; discussion 255–7, 2005.

[54] van den Brink, WA, van Santbrink, H, Steyerberg, EW, Avezaat, CJ, Suazo, JA, Hogesteeger, C, Jansen, WJ, Kloos, LM, Vermeulen, J & Maas, AI. Brain oxygen tension in severe head injury. *Neurosurgery*, 46(4):868–76– discussion 876–8, 2000.

[55] Menon, DK, Coles, JP, Gupta, AK, Fryer, TD, Smielewski, P, Chatfield, DA, Aigbirhio, F, Skepper, JN, Minhas, PS, Hutchinson, PJ, Carpenter, TA, Clark, JC & Pickard, JD. Diffusion limited oxygen delivery following head injury. *Critical care medicine*, 32(6):1384–1390, 2004.

[56] Ghosh, A, Elwell, C & Smith, M. Cerebral near-infrared spectroscopy in adults: a work in progress. *Anesthesia & Analgesia*, 115(6):1373–1383, 2012.

[57] Marmarou, A, Fatouros, PP, Barzó, P, Portella, G, Yoshihara, M, Tsuji, O, Yamamoto, T, Laine, F, Signoretti, S, Ward, JD, Bullock, MR & Young, HF. Contribution of edema and cerebral blood volume to traumatic brain swelling in head-injured patients. *Journal of Neurosurgery*, 93(2):183–193, 2000.

[58] Marmarou, A, Signoretti, S, Fatouros, PP, Portella, G, Aygok, GA & Bullock, MR. Predominance of cellular edema in traumatic brain swelling in patients with severe head injuries. *Journal of Neurosurgery*, 104(5):720–730, 2006.

[59] Tisdall, MM, Tachtsidis, I, Leung, TS, Elwell, CE & Smith, M. Near-infrared spectroscopic quantification of changes in the concentration of oxidized cytochrome c oxidase in the healthy human brain during hypoxemia. *Journal of Biomedical Optics*, 12(2):024002, 2007.

[60] Bainbridge, A, Tachtsidis, I, Faulkner, SD, Price, D, Zhu, T, Baer, E, Broad, KD, Thomas, DL, Cady, EB, Robertson, NJ & Golay, X. Brain mitochondrial oxidative metabolism during and after cerebral hypoxia-ischemia studied by simultaneous phosphorus magnetic-resonance and broadband near-infrared spectroscopy. *NeuroImage*, 102:173–183, 2013.

[61] Cherian, L, Hlatky, R & Robertson, CS. Nitric oxide in traumatic brain injury. *Brain pathology (Zurich, Switzerland)*, 14(2):195–201, 2004.

[62] Provencio, JJ & Vora, N. Subarachnoid hemorrhage and inflammation: bench to bedside and back. *Seminars in neurology*, 25(4):435–444, 2005.

[63] Brunori, M, Giuffrè, A, Forte, E, Mastronicola, D, Barone, MC & Sarti, P. Control of cytochrome c oxidase activity by nitric oxide. *Biochimica et biophysica acta*, 1655(1-3):365–371, 2004.

[64] Cooper, CE. Nitric oxide and cytochrome oxidase: substrate, inhibitor or effector? *Trends in biochemical sciences*, 27(1):33–39, 2002.

[65] Hüttemann, M, Lee, I, Kreipke, CW & Petrov, T. Suppression of the inducible form of nitric oxide synthase prior to traumatic brain injury improves cytochrome c oxidase activity and normalizes cellular energy levels. *Neuroscience*, 151(1):148–154, 2008.

[66] Palacios-Callender, M, Hollis, V, Mitchison, M, Frakich, N, Unitt, D & Moncada, S. Cytochrome c oxidase regulates endogenous nitric oxide availability in respiring cells: a possible explanation for hypoxic vasodilation. *Proceedings of the National Academy of Sciences of the United States of America*, 104(47):18508–18513, 2007.

[67] Unitt, DC, Hollis, VS, Palacios-Callender, M, Frakich, N & Moncada, S. Inactivation of nitric oxide by cytochrome c oxidase under steady-state oxygen conditions. *Biochimica et biophysica acta*, 1797(3):371–377, 2010.

[68] Rockswold, SB, Rockswold, GL, Zaun, DA, Zhang, X, Cerra, CE, Bergman, TA & Liu, J. A prospective, randomized clinical trial to compare the effect of hyperbaric to normobaric hyperoxia on cerebral metabolism, intracranial pressure, and oxygen toxicity in severe traumatic brain injury. *Journal of Neurosurgery*, 112(5):1080–1094, 2010.

[69] Cooper, CE. Competitive, reversible, physiological? Inhibition of mitochondrial cytochrome oxidase by nitric oxide. *IUBMB Life*, 55(10-11):591–597, 2003.

[70] Cooper, CE & Giulivi, C. Nitric oxide regulation of mitochondrial oxygen consumption II: Molecular mechanism and tissue physiology. *American journal of physiology Cell physiology*, 292(6):C1993–2003, 2007.

[71] Circu, ML & Aw, TY. Reactive oxygen species, cellular redox systems, and apoptosis. *Free radical biology & medicine*, 48(6):749–762, 2010.

[72] Bullock, MR. Hyperoxia. *Journal of Neurosurgery*, 109(3):421–3; author reply 423, 2008.

[73] Diringer, MN. Hyperoxia: good or bad for the injured brain? *Current Opinion in Critical Care*, 14(2):167–171, 2008.

[74] Longhi, L & Stocchetti, N. Hyperoxia in head injury: therapeutic tool? *Current Opinion in Critical Care*, 10(2):105–109, 2004.

[75] Lee, PJ & Choi, AMK. Pathways of cell signaling in hyperoxia. *Free radical biology & medicine*, 35(4):341–350, 2003.

[76] Bayir, H & Kagan, VE. Bench-to-bedside review: Mitochondrial injury, oxidative stress and apoptosis–there is nothing more practical than a good theory. *Critical care (London, England)*, 12(1):206, 2008.

[77] Altemeier, WA & Sinclair, SE. Hyperoxia in the intensive care unit: why more is not always better. *Current Opinion in Critical Care*, 13(1):73–78, 2007.

[78] Guzy, RD & Schumacker, PT. Oxygen sensing by mitochondria at complex III: the paradox of increased reactive oxygen species during hypoxia. *Experimental physiology*, 91(5):807–819, 2006.

[79] Andreyev, AY, Kushnareva, YE & Starkov, AA. Mitochondrial metabolism of reactive oxygen species. *Biochemistry (Moscow)*, 70(2):200–214, 2005.

[80] Venditti, P, Di Stefano, L & Di Meo, S. Mitochondrial metabolism of reactive oxygen species. *Mitochondrion*, 13(2):71–82, 2013.

[81] Susin, SA, Zamzami, N & Kroemer, G. Mitochondria as regulators of apoptosis: doubt no more. *Biochimica et biophysica acta*, 1366(1-2):151–165, 1998.

[82] Kilbaugh, TJ, Karlsson, M, Byro, M, Bebee, A, Ralston, J, Sullivan, S, Duhaime, AC, Hansson, MJ, Elmér, E & Margulies, SS. Mitochondrial bioenergetic alterations after focal traumatic brain injury in the immature brain. *Experimental neurology*, 271(C):136–144, 2015.

[83] Banaji, M, Mallet, A, Elwell, CE, Nicholls, P & Cooper, CE. A model of brain circulation and metabolism: NIRS signal changes during physiological challenges. *PLoS computational biology*, 4(11):e1000212, 2008.

[84] Moroz, T, Banaji, M, Robertson, NJ, Cooper, CE & Tachtsidis, I. Computational modelling of the piglet brain to simulate near-infrared spectroscopy and magnetic resonance spectroscopy data collected during oxygen deprivation. *Journal of the Royal Society, Interface / the Royal Society*, 9(72):1499–1509, 2012.

[85] Jelfs, B, Banaji, M, Tachtsidis, I, Cooper, CE & Elwell, CE. Modelling Noninvasively Measured Cerebral Signals during a Hypoxemia Challenge: Steps towards Individualised Modelling. *PloS one*, 7(6):e38297, 2012.

[86] Dunne, L, Hebden, J & Tachtsidis, I. Development of a near infrared multi-wavelength, multi-channel, time-resolved spectrometer for measuring brain tissue haemodynamics and metabolism. *ADVANCES IN EXPERIMENTAL MEDICINE AND BIOLOGY*, 812:181–186, 2014.

[87] Gjedde, A & Marrett, S. Glycolysis in neurons, not astrocytes, delays oxidative metabolism of human visual cortex during sustained checkerboard stimulation in vivo. *Journal of Cerebral Blood Flow & Metabolism*, 21(12):1384–1392, 2001.

[88] Bellander, BM, Cantais, E, Enblad, P, Hutchinson, P, Nordström, CH, Robertson, C, Sahuquillo, J, Smith, M, Stocchetti, N, Ungerstedt, U, Unterberg, A & Olsen, NV. Consensus meeting on microdialysis in neurointensive care. *Intensive Care Medicine*, 30(12):2166–2169, 2004.

[89] Bishop, CC, Powell, S, Rutt, D & Browse, NL. Transcranial Doppler measurement of middle cerebral artery blood flow velocity: a validation study. *Stroke; a journal of cerebral circulation*, 17(5):913–915, 1986.

[90] Dahl, A, Lindegaard, KF, Russell, D, Nyberg-Hansen, R, Rootwelt, K, Sorteberg, W & Nornes, H. A comparison of transcranial Doppler and cerebral blood flow studies to assess cerebral vasoreactivity. *Stroke; a journal of cerebral circulation*, 23(1):15–19, 1992.

[91] Weyland, A, Stephan, H, Kazmaier, S, Weyland, W, Schorn, B, Grüne, F & Sonntag, H. Flow velocity measurements as an index of cerebral blood flow. Validity of transcranial Doppler sonographic monitoring during cardiac surgery. *Anesthesiology*, 81(6):1401–1410, 1994.

Part III

CONCLUSIONS AND FUTURE WORK

6

CYTOCHROME *C* OXIDASE IN ACUTE BRAIN INJURY: WHERE ARE WE NOW, WHERE TO GO NEXT?

The overarching goal of the work reported in this thesis is to establish the potential for near infrared spectroscopy (NIRS)-based measurement of cytochrome *c* oxidase (CCO) to be a useful biomarker of cerebral energy status in order to detect and thus guide the prevention or treatment cerebral ischaemia

In this final chapter, we consider whether the experiments described in chapters 4 and 5 support this notion, as well as considering what obstacles remain to developing a practical bedside CCO monitor.

6.1 DEVELOPMENT OF CLINICAL MONITORS

Unlike drugs, which have a recognised regulatory pathway and framework for development, the development of biomarkers by necessity follows more heterogenous paths [1]. In this context, it is useful to consider the USA National Institutes of Health Research definition of a biomarker, which is 'a characteristic that is objectively measured and evaluated as an indicator of normal biological processes, pathogenic processes, or pharmacologic responses to a therapeutic intervention' [2]. Thus, once technical development of specific instrumentation is complete, it is necessary to define the behaviour of the biomarker in normal function, in response to disease and in response to treatment – a schema for doing so is shown in Figure 6.1.

6.2 CCO AS A BIOMARKER: WHERE ARE WE NOW?

In the case of CCO, I believe the work presented in this thesis now places us squarely within the 'Clinical Development' phase shown in Figure 6.1. Why has it taken four decades to move here from Jöbsis's initial description of NIRS-measured CCO oxidation in cat brain to the potential for use of this measurement in the clinical arena? The current status and future directions of CCO as a biomarker of brain oxidative metabolism have been recently reviewed elsewhere [3]; the obstacles that I have identified are related to technical aspects of measurement, the practicalities of running studies in complex clinical environments and finally, the challenge of interpreting the (patho)physiological relevance of results.

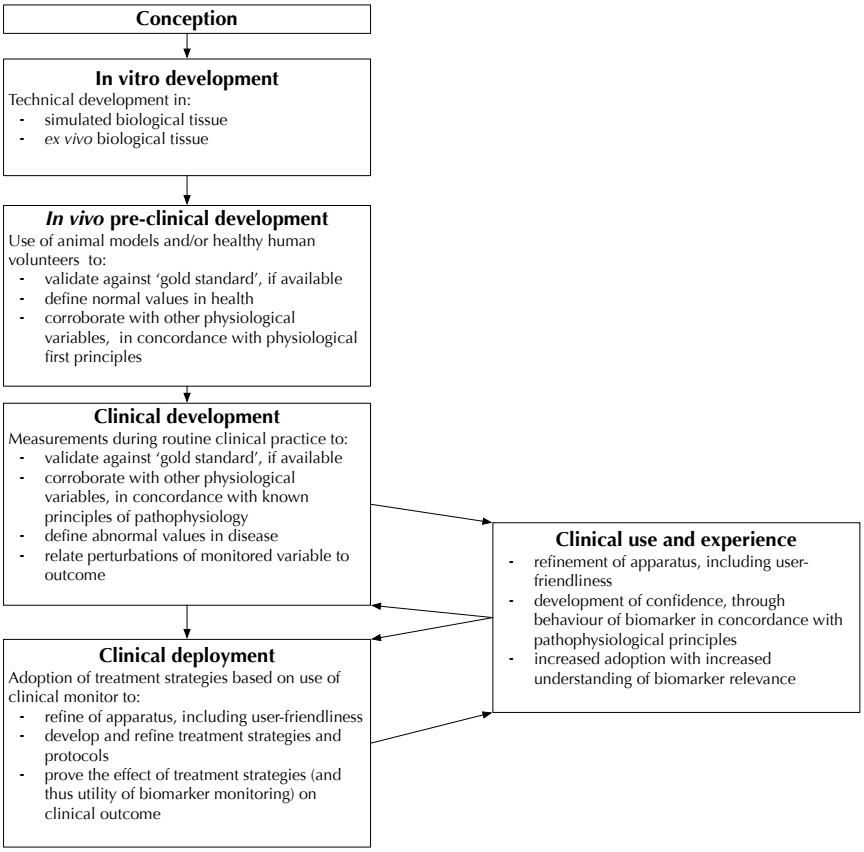

Figure 6.1 – Proposed schema for biomarker monitor development

6.2.1 *Technical challenges*

The relatively indistinct spectral characteristics of CCO, as discussed in Chapter 3.2.4, combined with the submicromolar changes that we have been seeking to demonstrate, in the context of haemoglobin concentrations that are an order of magnitude higher, has presented a significant challenge to the accurate measurement CCO oxidation [4] . Our use of a charge-coupled device (CCD) based system has allowed 2-dimensional measurement in both spectral and spatial dimensions [5]. As CCD size has reduced and resolution has increased in line with Moore's Law [6], we have been able to achieve the signal-to-nose ratios necessary to accurately measure CCO oxidation in the adult human head.

Having achieved the ability to resolve the minuscule spectral changes induced by submicromolar changes in CCO oxidation, the following challenge has been establishing the *veracity* of the observed changes. There is a relatively poor understanding of CCO physiology *in vivo*, because the only means of directly measuring its oxidation state is through light spectroscopy. Although CCO oxidation can be measured with visible

light spectroscopy, the poor penetration of visible light through biological tissue means that this must be performed invasively in the human brain, or via exposed cortex. A key challenge facing the validation of CCO-measuring apparatus like the hybrid optical spectrometer (pHOS) is the circular argument that CCO physiology can only be defined through measurements by unvalidated apparatus, and yet we seek to use these CCO measurements in order to validate this very apparatus!

This 'validation' of the biomarker has thus involved corroboration with other measures of cerebral metabolism and evaluating whether observed changes in CCO oxidation state are consistent with those that are seen in these other measures, based on our understanding of cerebral physiology. This has been performed in a number of animal models [4,7–9] and healthy volunteers [10,11]. The studies we report in Chapter 4 confirm these findings, as well as excluding the important confounders of pathlength and scattering changes on the NIRS-measured variables. I believe that this weight of evidence is sufficient for us to accept the CCO oxidation state measured with the pHOS as largely veracious.

6.2.2 *Practical challenges*

From a practical perspective, the apparatus are large and cumbersome. The pHOS – shown in Figure 6.2 – used in the studies described in this thesis was as large as a domestic fridge (and thus only deployable in the neurocritical care unit in the early hours of the night without causing significant disruption to clinical activities). Although this was approximately one third the size of the previous generation of broadband systems used by our group [11], I believe that significant further miniaturisation is necessary for more widespread use to be feasible. Other practical impediments include a need for reference spectrum recording for the broadband spectrograph and susceptibility of recordings to significant artefact from any optode movement – for example through patient repositioning or coughing, with the need for manual identification and decontamination of data.

In order to conduct the experiments described in this thesis, we have been required to construct breathing circuits to manipulate inspiratory gas mixes, site invasive intracranial monitoring, educate staff in the use of this monitoring, conduct ultrasound recording of cerebral blood flow, package the NIRS apparatus into a form suitable for use in a clinical environment, and interface and synchronise the various devices. Although each individual patient experiment reported in Chapter 5 recorded data for only 210 minutes, I estimate that at least 15 hours of preparation, followed by 15 hours of data analysis and manipulation was also required. In addition, for both patient and volunteer studies, approximately 25% of experiments failed due to the equipment malfunction – not only the NIRS apparatus, but also in particular pumps and analysers. Overall, *after* the data had been summarised in to single points for each variable in each Epoch,

the study in Chapter 4 yielded over 80,000 and the study in Chapter 5 yielded over 6000 individual data points for statistical analysis. This volume of data was necessary to provide corroboration to 'validate' the CCO oxidation measure that could not be directly measured by other means.

6.2.3 *Challenges in interpretation*

The technical and practical challenges described above will, in my view, inevitably be overcome, as advances in electronics manufacture and the ubiquity of consumer electronics filters through to medical devices, with resulting increases in ease-of-use and miniaturisation. However, understanding the physiological meaning of observed changes in CCO oxidation remains a major obstacle to clinical development and deployment of this biomarker. This is also intertwined with the technological limitations of current equipment. The use of continuous wave, modified Beer-Lambert Law-based algorithms means that observed CCO changes can only be reported from a necessarily unknown baseline, as discussed in 3.2.2, rather than being able to provide an absolute measure. In Chapters 4.4.5 and 5.4.3, we limited ourselves to using either qualitative explorations or statistical models to explore the (patho)physiological basis of the CCO changes we observed. Yet, the relationships that exist between differently observed physiological variables are not defined by statistical models, but rather by physiological cascades. Nevertheless, our findings in Chapter 4 confirm that CCO oxidation state is a brain-specific and noninvasive measure of cerebral oxidative metabolism and our findings in Chapter 5 confirm the notion that the measurement of CCO oxidation state provides insights into acute brain injury (ABI) pathophysiology that are not apparent from other monitoring modalities.

6.3 CLINICAL ADOPTION OF CCO AS A BIOMARKER: WHERE NEXT?

The work I have undertaken in this thesis leads me to conclude that NIRS-based CCO oxidation monitoring can be a useful part of an array of clinical monitors to guide the treatment of patients with ABI in order to guide prevention of secondary brain injury and thus improve functional outcome. There is a parallel between measurement of CCO and haemoglobin oxidation state, in that the advent of spatially-resolved spectroscopy (SRS)-based monitors for haemoglobin oxidation state gave rise to measurement of tissue oxygen saturation (TOS) and its equivalents, a simple measure that is easily understood by clinicians. When, in an exploratory analysis not reported in this thesis, we attempted to perform broadband SRS in order to resolve for a 'CCO oxygen saturation' (COS) on a number of the volunteer datasets reported in Chapter 4, we found that the noise introduced from the use of multiple detectors overwhelmed the underlying signal. Improvements in CCD technology or the deployment of time-resolved spectroscopy

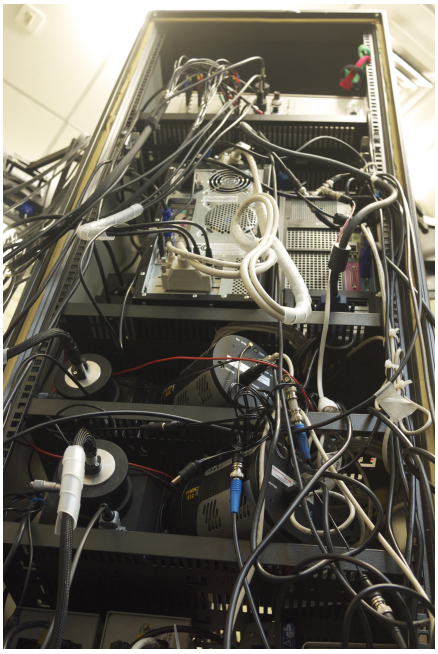

(a) Viewed from rear

(b) In use on neurocritical care unit

Figure 6.2 – Hybrid system

(TRS)-based apparatus may overcome this important hurdle and turn CCO oxidation in to a 'approachable' measure for clinicians. It would also, as an absolute measure, overcome the issue of reporting changes from an unknown baseline, and that of reproducibility, with the potential for intermittent, rather than continuous recordings, as has been previously been performed for TOS in ABI [12]. The simultaneous incorporation of a diffuse correlation spectroscopy array [13] allows the simultaneous measurement of cerebral blood flow and TOS, with derivation of $(CMRO)asperformedin Chapter 5$[14, 15].

I believe that when COS can be reliably measured, providing apparatus can be miniaturised to the extent that it is easily deployable in the neurocritical care unit by regular clinicians, rather than dedicated researchers, the next stage will be to conduct outcome studies, aiming to relate outcome after ABI to COS. The heterogeneity of injury pattern and outcome following ABI mandates large studies in order to achieve adequate statistical power, and this in turn mandates that the apparatus are simple enough to be used by clinicians without specialist expertise in NIRS.

If perturbations in COS are shown to be associated with outcome following ABI, the ultimate goal must be the formulation of treatment strategies incorporating the use of COS, but also other brain monitoring modalities. It is notable that the only randomised, controlled trial involving the use of NIRS – that of a treatment strategy based on the maintenance of TOS above 75% [16] during cardiopulmonary bypass – involved interventions guided by other physiological variables including respiratory and haemodynamic variables. The incorporation of mathematical models of cerebral haemodynamics and metabolism [17, 18] in addition to computer aided decision support systems will, I anticipate, be necessary to assist clinicians in interpreting and acting upon what is already a potentially overwhelming amount of physiological data. For example, in Chapter 5, we considered simultaneous changes in multiple physiological variables from across a broad-based monitoring array to make inferences about the pathophysiological processes at play. A real-time model might, for example, be able to distinguish between mitochondrial dysfunction, classical ischaemia and impaired oxygen diffusion as a cause for reduced oxidative metabolism, allowing for the institution of appropriate corrective measures. Importantly, the work in this thesis provides a corpus of data with which these models can be refined and validated in the future.

A significant advantage of NIRS-measured CCO oxidation over invasively measured biomarkers of cerebral metabolism is the potential for multichannel arrays of monitoring. Whilst rates of complication following invasively-placed catheters are low [19], they cannot be placed in eloquent cortex or in close proximity. ABI pathophysiology shows significant spatial heterogeneity [20]. Multichannel NIRS arrays capable of simultaneous chromophore measurement in multiple regions are now being developed, with the potential to reveal new aspects of ABI pathophysiology, as shown in Figure 6.3.

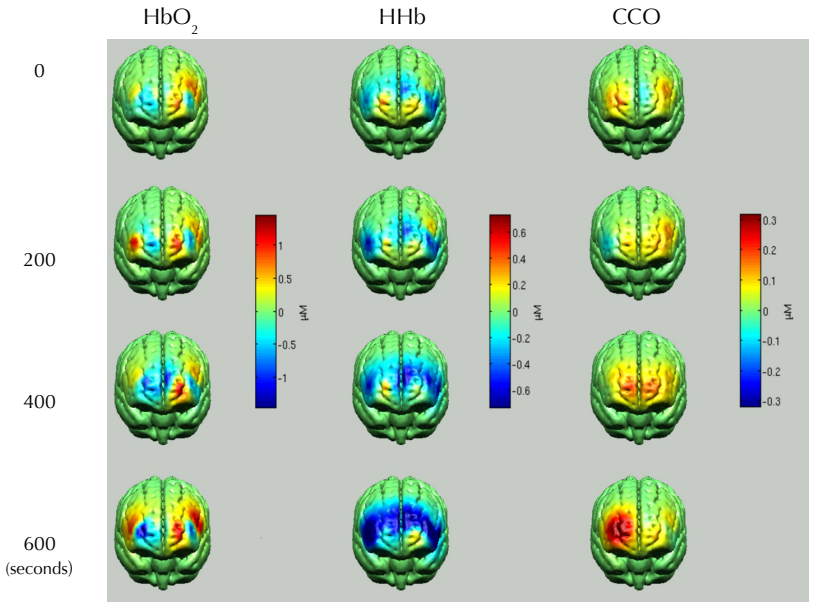

Figure 6.3 – Reconstructed images showing a time series of spontaneous slow oscillations of , [HHb] and Δ[oxCCO] at four time points over a 600-second period in a patient with a right frontal intracerebral haemorrhage. The changes inΔ[oxCCO] are spatially and temporally distinct from those of haemoglobin. D Highton, personal communication.

6.4 CONCLUSION

This thesis describes current understanding of the pathophysiology of ABI and the current state of the art of NIRS. We have conducted experiments in healthy volunteers that confirm that observed CCO changes are physiologically plausible – from which we infer that the CCO oxidation measure is veracious –and are better localised to brain, when compared to other NIRS-measured chromophores. Experiments in patients with ABI have shown the feasibility of CCO measurement in a clinical setting, with the measurement of CCO oxidation allowing us to infer additional insights that would not be apparent with state-of-the-art brain clinical monitors. The findings underline the potential for measurement of CCO oxidation to be a valuable adjunct to accepted brain monitoring modalities in the treatment of acute brain injury.

REFERENCES

[1] Becker, K. Fundamentals of Clinical Study Design and Evaluation. In Becker, K & White, J, eds., *Clinical Evaluation of Medical Devices: Principles and Case Studies*, chap. 1, pp. 3–20. Springer Science Business Media, New York, 2007.

[2] Biomarkers Definitions Working Group. Biomarkers and surrogate endpoints: preferred definitions and conceptual framework. *Clinical pharmacology and therapeutics*, 69(3):89–95, 2001.

[3] Bale, G, Elwell, CE & Tachtsidis, I. From Jöbsis to the present day: a review of clinical near-infrared spectroscopy measurements of cerebral cytochrome-c-oxidase. *Journal of Biomedical Optics*, 21(9):091307–19, 2016.

[4] Cooper, CE & Springett, R. Measurement of cytochrome oxidase and mitochondrial energetics by near-infrared spectroscopy. *Philosophical Transactions of the Royal Society B: Biological Sciences*, 352(1354):669–676, 1997.

[5] Scholkmann, F, Kleiser, S, Metz, AJ, Zimmermann, R, Mata Pavia, J, Wolf, U & Wolf, M. A review on continuous wave functional near-infrared spectroscopy and imaging instrumentation and methodology. *NeuroImage*, 85 Pt 1:6–27, 2014.

[6] Schaller, RR. Moore's law: past, present and future. *IEEE spectrum*, 34(6):52–59, 1997.

[7] Cooper, CE, Delpy, DT & Nemoto, EM. The relationship of oxygen delivery to absolute haemoglobin oxygenation and mitochondrial cytochrome oxidase redox state in the adult brain: a near-infrared spectroscopy study. *The Biochemical journal*, 332 (Pt 3)(Pt 3):627–632, 1998.

[8] Cooper, CE, Cope, M, Springett, R, Amess, PN, Penrice, J, Tyszczuk, L, Punwani, S, Ordidge, R, Wyatt, J & Delpy, DT. Use of Mitochondrial Inhibitors to Demonstrate That Cytochrome Oxidase Near-Infrared Spectroscopy Can Measure Mitochondrial Dysfunction Noninvasively in the Brain. *Journal of Cerebral Blood Flow & Metabolism*, 19(1):27–38, 1999.

[9] Bainbridge, A, Tachtsidis, I, Faulkner, SD, Price, D, Zhu, T, Baer, E, Broad, KD, Thomas, DL, Cady, EB, Robertson, NJ & Golay, X. Brain mitochondrial oxidative metabolism during and after cerebral hypoxia-ischemia studied by simultaneous phosphorus magnetic-resonance and broadband near-infrared spectroscopy. *NeuroImage*, 102:173–183, 2013.

[10] Tisdall, MM, Tachtsidis, I, Leung, TS, Elwell, CE & Smith, M. Near-infrared spectroscopic quantification of changes in the concentration of oxidized cytochrome

c oxidase in the healthy human brain during hypoxemia. *Journal of Biomedical Optics*, 12(2):024002, 2007.

[11] Tisdall, MM. *Non-invasive near infrared spectroscopy: a tool for measuring cerebral oxygenation and metabolism in patients with traumatic brain injury*. UCL MD Thesis, 2008.

[12] Yokose, N, Sakatani, K, Murata, Y, Awano, T, Igarashi, T, Nakamura, S, Hoshino, T & Katayama, Y. Bedside monitoring of cerebral blood oxygenation and hemodynamics after aneurysmal subarachnoid hemorrhage by quantitative time-resolved near-infrared spectroscopy. *World Neurosurgery*, 73(5):508–513, 2010.

[13] Durduran, T, Choe, R, Baker, WB & Yodh, AG. Diffuse optics for tissue monitoring and tomography. *Reports on Progress in Physics*, 73(7):076701, 2010.

[14] Roche-Labarbe, N, Fenoglio, A, Aggarwal, A, Dehaes, M, Carp, SA, Franceschini, MA & Grant, PE. Near-infrared spectroscopy assessment of cerebral oxygen metabolism in the developing premature brain. *Journal of cerebral blood flow and metabolism : official journal of the International Society of Cerebral Blood Flow and Metabolism*, 32(3):481–488, 2012.

[15] Dehaes, M, Aggarwal, A, Lin, PY, Rosa Fortuno, C, Fenoglio, A, Roche-Labarbe, N, Soul, JS, Franceschini, MA & Grant, PE. Cerebral oxygen metabolism in neonatal hypoxic ischemic encephalopathy during and after therapeutic hypothermia. *Journal of cerebral blood flow and metabolism : official journal of the International Society of Cerebral Blood Flow and Metabolism*, 34(1):87–94, 2014.

[16] Murkin, JM, Adams, SJ, Novick, RJ, Quantz, M, Bainbridge, D, Iglesias, I, Cleland, A, Schaefer, B, Irwin, B & Fox, S. Monitoring brain oxygen saturation during coronary bypass surgery: a randomized, prospective study. *Anesthesia & Analgesia*, 104(1):51–58, 2007.

[17] Banaji, M, Mallet, A, Elwell, CE, Nicholls, P & Cooper, CE. A model of brain circulation and metabolism: NIRS signal changes during physiological challenges. *PLoS computational biology*, 4(11):e1000212, 2008.

[18] Jelfs, B, Banaji, M, Tachtsidis, I, Cooper, CE & Elwell, CE. Modelling Noninvasively Measured Cerebral Signals during a Hypoxemia Challenge: Steps towards Individualised Modelling. *PloS one*, 7(6):e38297, 2012.

[19] Hutchinson, PJ, Hutchinson, DB, Barr, RH, Burgess, F, Kirkpatrick, PJ & Pickard, JD. A new cranial access device for cerebral monitoring. *British Journal of Neurosurgery*, 14(1):46–48, 2000.

[20] Vespa, PM, O'Phelan, K, Mcarthur, D, Miller, C, Eliseo, M, Hirt, D, Glenn, T & Hovda, DA. Pericontusional brain tissue exhibits persistent elevation of lactate/pyruvate ratio independent of cerebral perfusion pressure. *Critical care medicine*, 35(4):1153–1160, 2007.

COLOPHON

This thesis was typeset with LaTeX 2_ε using *URW Classico*, an approximation of Herman Zapf's *Optima* provided under the Aladdin Free Public Licence by URW Design and Development; mathematical formulae are set in *Computer Modern Bright*, a LaTeX 2_ε core font. *URW Palladio*, an approximation of Zapf's *Palatino* also released by URW under the Alladdin Free Public Licence, was also used.

The typographic style was inspired by Bringhurst as presented in *The Elements of Typographic Style* [1]. The package upon which this thesis is based is available for LaTeX via CTAN as "`classicthesis`".

REFERENCES

[1] Bringhurst, R. *The Elements of Typographic Style*. 2nd ed. Hartley & Marks Publishers, 2002.

Final Version as of 15th March 2017 at 23:43.